Proceedings

International Conference on Nuclear Science and Technology

Nuclear Society Of Iran | Atomic Energy Organization of Iran | Nuclear Sciences and Technologies Research Institute

Papers on:

Nuclear Governance

Stable & Radiactive Isotopes

*In this booklet, you will find the selected papers presented at the **First International Conference on Nuclear Science and Technology**, held from May 6-8, 2024, in Isfahan, Iran.*
We hope you find it informative and enjoyable!

ICNST 2024

Contact and Accessibility
icnst2024.com
registration@icnst2024.com


بسم الله الرحمن الرحیم

The Conference President's Message
ICNST 2024

Attendees, guests, and colleagues

I would like to warmly welcome you to the first International Conference on Nuclear Science and Technology (ICNST 2024). It has been a real honor and privilege to serve as the president of this conference. The conference this year has brought together an incredible diversity of authors and speakers from universities, government, and industry to share ideas and new perspectives on a wide range of radiation applications, nuclear reactors, particle accelerators, radiation measurements, fusion and plasma, stable and radioactive isotopes, radiation safety and security, nuclear agriculture, fuel cycle, lasers, education and training and nuclear governance.

Climate change, a new topic which has been added to this year's agenda as an important worldwide issue. a matter that has been brought up as a critical concern at the majority of IAEA conferences and nuclear scientific assemblies in recent years.

Panel discussions and exhibitions are being introduced as side activities in an attempt to keep this scientific meeting from becoming one-dimensional and increase its effectiveness.

More than 520 complete papers have been approved for this conference; when combined with the additional panels, get-togethers, and side activities, it is anticipated that over 1000 people will attend in person in the historical and touristic city of Isfahan. We look forward to welcoming participants to share their practical ideas and to enjoy an academical and cultural three days in Isfahan.

I'll close by wishing you everyone an incredible, instructive, and transformative experience during ICNST2024 and I hope that this conference can pave the route for academic materials to be used in industry and everyday life.

Prof. Javad Karimi-Sabet
President of ICNST2024
Javad Karimi-Sabet

welcome statment of scientific secretary
ICNST 2024

"In the name of God, the Merciful,

Prior to giving the stage to address this distinguished forum, let me take this opportunity to express our deep gratitude, on behalf of all attendees, for His Excellency Mr. Islami's scientific, educational, and motivational remarks, as well as for his excellent organization of this conference.

I would also like to express our appreciation to His Excellency Dr. Mortazavi, Governor-General of Isfahan Province, for his constructive and useful support in enabling this meeting to take place.

This is a great pleasure and honor to extend a warm greeting to each and every one of you for the International Conference on Nuclear Science and Technology, scheduled from May 6th to May 8th, 2024, in the historic city of Isfahan, Iran.

With the aim of advancing our knowledge of nuclear science and technology, this conference is a major global convergence of experts, researchers, and practitioners. It is a platform for the sharing of creative concepts, the presentation of state-of-the-art research, and the formation of cooperative alliances.

As the scientific secretary of this prestigious event, I am particularly excited about the diverse array of participants expected to grace us with their presence. From the esteemed scientists and engineers of Russian universities and research centers to representatives from Islamic countries, friendly nations, and beyond, this conference promises to be a melting pot of perspectives, experiences, and expertise.

The extensive coverage of this conference is another aspect of its uniqueness. We have nearly 900 participants representing 22 countries around the world. Of the 900 participants, 620 are authors covering 13 major topics. There are 421 papers for oral and poster presentations, with additional documents for publication in ISC journals. There will be 3 plenary sessions, 16 panel discussions, 20 parallel oral presentation sessions, and 3 poster sessions.

Prof. Hosein Afarideh
Scientific Secretariat of ICNST2024

Organizers

Nuclear Society Of Iran (NSI)

Atomic Energy Organization of Iran (AEOI)

Nuclear Science and Technology Research Institute (NSTRI)

Scientific Partnership

International Atomic Energy Agency (IAEA)

Isfahan University

Sharif University

Kurchatov Institute

Amirkabir University of Technology (Tehran Polytechnique)

Shahid Beheshti University

Isfahan University of Technology

Shiraz University

Islamic Azad University

K. N. Toosi University of Technology

Ferdowsi University of Mashhad

Kerman Graduate University of Technology

Sahand University of Technology

University of Tabriz

Islamic World Scieence Citation Center

Journal of Nuclear Science and Technology (JonSat)

Radiation Physics and Engineering journal

Nuclear Watch

Cooperative Organization

Isfahan Governorate

Isfahan Municipality

Abbasi Hotel

Iran Atomic Energy Production & Development Co.

Iran's Nuclear Raw Materials & Fuel Production Co.

Radiation Application Development Co.

Ofogh Consulting Engineers Co.

Nuclear Power Plant Safety Development & Promotion Co.

Nuclear Power Plant Engineering & Construction Co.

Engineering & Design of Industrial Simulator Co.

Energy Industry Development Engineering Co

Atomic Power Plant Pepair & support

Nuclear Reactors Fuel Co.

Iran Radioactive Waste Management Co.

Mesbah Energy Co.

Iran Gharb Industrial, Mining and Energy Co.

Pars Isotope Co.

Center for Laser Science & Technology of Iran

Centrifuge Production of Iran Co.

Plasma Technology Development Co.

Rasa Technology and Innovation Center

Behyaar Sanaat Sepahan Co.

Nuclear Data Base of Iran (NDB)

Parto think tank (strategic studies of nuclear industry development)

International Conference Alerts

Local Scientific Board

RAW	NAME	ROLE	AFFILIATION
1	**Prof. Hossein Afarideh**	**Chairman of Local Scientific Board**	**Amirkabir University of Technology (Tehran Polytechnique)(AUT)**
2	**Prof. Mohammad Ghanadi Maragheh**	**Member of The Local Scientific Board**	**Nuclear Science and Technology Research Institute of Iran (NSTRI)**
3	**Prof. Mohammad Lamei Rashti**	**Member of The Local Scientific Board**	**Nuclear Science and Technology Research Institute of Iran (NSTRI)**
4	**Prof. Mohammad Bagher Ghofrani**	**Member of The Local Scientific Board**	**Sharif University of Technology (SUT)**
5	**Prof. Hosein Faghihian**	**Member of The Local Scientific Board**	**University of Isfahan (UI)**
6	**Prof. Javad Rahighi**	**Member of The Local Scientific Board**	**Institute for Research in Fundamental Sciences (IPM)**
7	**Prof. Seyed Amirhossein Feghhi**	**Member of The Local Scientific Board**	**Shahid Beheshti University (SBU)**

Scientific Committee

RAW	NAME	ROLE	AFFILIATION
1	**Prof. Ali Akbar Salehi**	**Member of The Scientific Committe**	**Sharif University of Technology (SUT)**
2	**Prof. Seyyed Javad Ahmadi**	**Member of The Scientific Committe**	**Nuclear Science and Technology Research Institute of Iran (NSTRI)**
3	**Prof. Farhoud Ziaee**	**Member of The Scientific Committe**	**Nuclear Science and Technology Research Institute of Iran (NSTRI)**
4	**Prof. Saeed Hamidi**	**Member of The Scientific Committe**	**University of Arak**
5	**Prof. Seyedzafarollah Kalantari**	**Member of The Scientific Committe**	**Isfahan University of Technology (IUT)**
6	**Prof. Naser Bagheri Moghaddam**	**Member of The Scientific Committe**	**National Research Institute for Science Policy (NRISP)**
7	**Prof. Naser Vosoghi**	**Member of The Scientific Committe**	**Sharif University of Technology (SUT)**
8	**Prof. Seied Rabi Mahdavi**	**Member of The Scientific Committe**	**Iran University of Medical Sciences**
9	**Prof. Meisam Torab Mostaedi**	**Member of The Scientific Committe**	**Nuclear Science and Technology Research Institute of Iran (NSTRI)**
10	**Prof. Fereydoun Abbasi Davani**	**Member of The Scientific Committe**	**Shahid Beheshti University (SBU)**
11	**Prof. Seyed Farhad Masoudi**	**Member of The Scientific Committe**	**K.N.Toosi University of Technology**
12	**Prof. Rasool Ruknizadeh**	**Member of The Scientific Committe**	**University of Isfahan (UI)**
13	**Prof. Gholamreza Raeesali**	**Member of The Scientific Committe**	**Nuclear Science and Technology Research Institute of Iran (NSTRI)**
14	**Prof. Asghar Sedighzadeh**	**Member of The Scientific Committe**	

15	**Prof. Hossein Kazeminejad**	**Member of The Scientific Committe**	**Nuclear Science and Technology Research Institute of Iran (NSTRI)**
16	**Prof. Seyyed Jaber Safdari**	**Member of The Scientific Committe**	**Nuclear Science and Technology Research Institute of Iran (NSTRI)**
17	**Prof. Omid Reza Kakuee**	**Member of The Scientific Committe**	**Nuclear Science and Technology Research Institute of Iran (NSTRI)**
18	**Prof. Alireza Keshtkar**	**Member of The Scientific Committe**	**Nuclear Science and Technology Research Institute of Iran (NSTRI)**
19	**Prof. Fereshte Haj esmail Beigi**	**Member of The Scientific Committe**	**Nuclear Science and Technology Research Institute of Iran (NSTRI)**
20	**Prof. Masoud Mahjour-shafiei**	**Member of The Scientific Committe**	**Nuclear Science and Technology Research Institute of Iran (NSTRI)**
21	**Prof. Mahmoud Payami Shabestar**	**Member of The Scientific Committe**	**Nuclear Science and Technology Research Institute of Iran (NSTRI)**
22	**Prof. Ali Bahrami Samani**	**Member of The Scientific Committe**	**Nuclear Science and Technology Research Institute of Iran (NSTRI)**
23	**Dr. Farhanaz Motamedi**	**Member of The Scientific Committe**	**Nuclear Science and Technology Research Institute of Iran (NSTRI)**
24	**Dr. Faezeh Rahmani**	**Member of The Scientific Committe**	**K.N.Toosi University of Technology**
25	**Dr. Ebrahim Moghiseh**	**Member of The Scientific Committe**	**Nuclear Science and Technology Research Institute of Iran (NSTRI)**
26	**Dr. Iraj Jabari**	**Member of The Scientific Committe**	**University of Isfahan (UI)**
27	**Dr. Nima Ghal-Eh**	**Member of The Scientific Committe**	**Ferdowsi University of Mashhad**
28	**Dr. Mitra Athari Alaf**	**Member of The Scientific Committe**	**Islamic Azad University Science and Research Branch**
29	**Dr. Gholamreza Etaati**	**Member of The Scientific Committe**	
30	**Dr. Amir Movafeghi**	**Member of The Scientific Committe**	**Nuclear Science and Technology Research Institute of Iran (NSTRI)**

Executive Committee

RAW	NAME	ROLE
1	Dr. Farshad Ghasemi	Chairman of the Executive Committee
2	Dr. Ehsan Molazadeh	Member of The Executive Committee
3	Dr. Seyyed Ghasem Biniaz	Member of The Executive Committee
4	Mr. Aliakbar Aminidoust	Member of The Executive Committee
5	Ms. Fatemeh Zamani	Member of The Executive Committee
6	Ms. Mahya Pazoki	Member of The Executive Committee
7	Mr. Hosein Maleki	Member of The Executive Committee
8	Mr. Maziar Dalili	Member of The Executive Committee
9	Mr. Shojaei	Member of The Executive Committee
10	Ms. Fatemeh Rezaei	Member of The Executive Committee
11	Mr. Reza Rafiei	Member of The Executive Committee
12	Ms. Seyyedeh Elham Ebrahimi	Member of The Executive Committee

Nuclear Governance

Stable & Radioactive Isotopes

Nuclear Governance

ICNST 2024
International Conference on Nuclear Science and Technology
6- 8 MAY 2024 | Isfahan, Iran

The Importance of Studying Nuclear Thermal Propulsion (NTP) Systems From the Political Viewpoint, Scientific Authority Creation, And The Development Of Iran's Nuclear Infrastructure (Paper ID : 1118)

Naghavi dizaji[1]*. D, Nikoosefat[2], M

[1] *Department of Energy Engineering, Sharif University of Technology, Tehran, Iran*

[2] *Nuclear Physics Group, Faculty of Basic Science, Comprehensive University of Imam Hossein, Tehran, Iran*

Abstract

Nuclear fission-thermal propulsion systems are currently one of the world's emerging scientific and technological advancements. NASA and the United States Department of Energy (DOE) have projected the use of these systems in the upcoming decade of 2030 for deep space exploration and travel to Mars. In these systems, the energy required to generate thrust is supplied by the heat from nuclear reactions, primarily nuclear fission. In addition to good maneuverability, these systems have a much higher specific impulse than chemical propulsion systems. This allows for higher speeds for aerospace systems with less thrust. Additionally, these systems have a significantly lower mass ratio and weight compared to conventional chemical propulsion, making it easy to deploy them in space orbits. Given the increasing significance of space exploration and activities beyond Earth's atmosphere for nations worldwide, and in light of the country's space-related documents such as the Comprehensive Aerospace Development Document, which emphasizes the need for the development of efficient, reliable technologies with national security implications and broader impacts on science, technology, and industry, as well as the substantial research and investment by advanced nations in these systems, we have chosen to focus on the study of thermal-nuclear propulsion systems. This research aims to underscore the political importance of investigating and advancing these systems and to assess Iran's scientific capabilities and development of nuclear infrastructure.

Keywords: Nuclear Thermal Propulsion (NTP), Aerospace Systems, Specific Impulse, Nuclear Infrastructure.

Introduction

The utilization of space, including outer space, is crucial for countries, particularly their military capabilities[1]. In addition to being a pristine field for scientific research, space is also a highly suitable environment for the economic and military activities of countries[2]. These factors have contributed to

the increasing competition in space among countries. In light of this, and to address the potential scientific lag in the country's aerospace industry, it is essential to explore systems currently at the forefront of global scientific and technological advancements. One of these systems is nuclear thermal propulsion (NTP), which will have many applications in the field of space travel in the future[3]. These systems benefit from high reliability, high specific impulse, and lower weight than chemical propellants[4]. These factors ensure high maneuverability, reduce travel duration in space, and minimize the amount of radiation astronauts receive from harmful cosmic rays[5, 6]. So, this technology has been the focus of extensive research by international experts in countries such as the United States and the Soviet Union since the 1960s[7]. With advancements in material science, equipment ground testing, and the design and construction of nuclear reactors, the United States, including NASA, has once again made significant progress in this field. NASA has identified this technology as crucial for uncovering the mysteries of the solar system[8].

The operation of NTPs involves the direct transfer of heat generated by nuclear fission to the propellant, which increases the enthalpy of the working fluid through heat absorption at nearly constant pressure. Then, the propellant is expanded through a nozzle to generate the propulsive force necessary for spacecraft propulsion[9]. This technology has attracted global scientific interest for over six decades, especially in the United States, where NASA and the US Department of Energy have laid out plans to achieve this technology by the 2030s. NASA's focus on advancing this system is driven by the potential for its repeated use in missions to explore Mars, as nuclear fuel has one of the highest energy densities among known man-made fuels. Notably, NASA's main goal is to facilitate a two-year round-trip mission to Mars, a challenge that can only be accomplished with the implementation of these systems[10].

To develop these systems, NASA collaborates with a range of organizations and companies, such as the US Department of Energy (including Idaho National Laboratory, Oak Ridge National Laboratory, and Los Alamos National Laboratory), Massachusetts Institute of Technology, University of Alabama Huntsville, Aerojet Rocketdyne, BWX Technologies, UltraSafe Nuclear Corporation, the Aerospace Corporation, Analytical Mechanics Associates, and Geocent[10].

Considering the cases mentioned, we have decided to introduce NTPs and examine the importance of studying and developing these systems from various perspectives, including political implications, scientific advancements, and the development of the country's nuclear infrastructure.

In the following section 2, NTP systems and their historical background are briefly summarized, followed by an analysis of the technical importance of these systems in section 3. Subsequently, sections 4 to 6 explore the main focus of the article, which relates to the significance of studying and developing NTPs in enhancing politics and national security, establishing scientific authority, and advancing nuclear infrastructures. Finally, section 7 provides conclusions derived from the compilation of materials presented in the preceding sections.

Ntp Systems

Space travel is still very challenging for humanity. The primary requirement for space travel is fast and efficient transportation, enabling humans to reach planets like Mars within the constraints of space[8, 9]. Among the various propulsion systems, thermal propulsion is more efficient because it reduces one step of energy conversion (e.g., from thermal to electric), leading to a significant increase in the output thrust force[11]. Also, due to the energy density of conventional fuels, nuclear energy creates a special opportunity to produce a low-weight propulsion system, which is possible through NTP systems.

Table 1 presents the specific energy and power of common fuels utilized in space propulsion. According to this table, it is evident that fusion systems have the highest energy and production power per unit of mass. However, these systems have not yet been economically exploited on a global scale. The second option, which is related to nuclear fission, currently represents advanced technology in the world. The nuclear industry has a significant background in this field, making it the best option for the development of NTP systems. In addition, based on previous scientific and industrial efforts in the field of these propellants, particularly the existence of the NERVA[1] reactor design and test data in the United States[12], nuclear fission is considered the closest and most optimal option for achieving NTP systems.

Table 1. Specific energy and power of common fuels of space propulsion systems[8].

[1] Nuclear Engine for Rocket Vehicle Application (NERVA)

Energy source	Mass specific energy (kJ/kg)	Mass specific power (kW/kg)
Nuclear Fusion	4×10^{11}	10^{11}
Nuclear Fission	8×10^{10}	2×10^{10}
Radioactive Decay	$2 \times 10^{8} - 3 \times 10^{9}$	$7 \times 10^{6} - 7 \times 10^{8}$
Chemical Sources	$4 \times 10^{2} - 2 \times 10^{4}$	$2 \times 10^{1} - 10^{3}$

According to the above explanations and Table 1, this research exclusively focuses on NTP systems utilizing nuclear fission as the fuel source, among the various technologies for space propulsion shown in Fig.1. Nuclear fission thermal propulsion systems are equipped with a critical fission reactor core that supplies the necessary energy to heat the expanding propellant gas[13]. These reactors can use solid, liquid, or gaseous nuclear fuel structures[8].

As a fact, NTP is a specific type of thermal propulsion, categorized as a subset of Newtonian reaction engines designed for space propulsion. This system operates on the principle of momentum conservation and, due to the variation in mass during the thrust process, can also be classified as a type of rocket system[9].

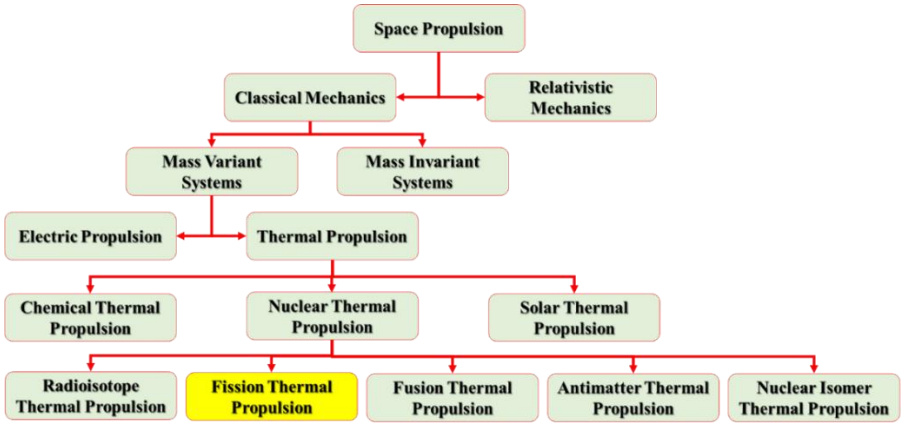

Fig. 1. Classification of space propulsion[8].

A schematic diagram of NTP systems is depicted in Fig.2. As illustrated in this figure, an NTP typically comprises a nuclear power source (nuclear reactor core), a heat exchange system, a nozzle at the end, a radiation shield, a cargo container (with transport capacity and a bio-chamber), a propellant (hydrogen) tank, and a heat sink. This heat sink is known as the thermal power processing unit. It collects the leaked heat of the core in thrust mode and also gathers the residual heat of the core when the reactor core is shut

down. Depending on the spacecraft's needs, it either discharges the heat into space or uses it to produce and supply electricity[3, 8, 14].

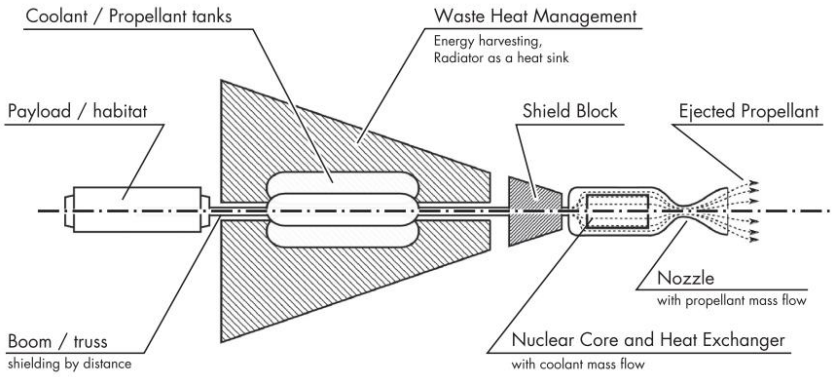

Fig. 2. A typical NTP[8].

History of NTPs

The concept of utilizing nuclear energy for space propulsion has been a longstanding idea, dating back to the early stages of rocket design and the development of nuclear energy. As early as 1913, Robert Esnault-Pelterie proposed the use of radium for interplanetary propulsion. While there were other suggestions in this area, it was the Manhattan Project that made significant strides in the development of nuclear thermal rockets (NTRs)[7].

In fact, the United States of America was the first country to allocate substantial resources to the development of NTRs rockets as a practical technology, rather than just a promising concept. This effort began as part of the Nuclear Energy for the Propulsion of Aircraft (NEPA) in 1946 [15]. This extensive research program was divided into various more focused programs, eventually leading to the development of NTRs, which became known as Project Rover in 1955. The original facility for developing these rockets was situated at the Los Alamos National Laboratory, which later evolved into the Nuclear Engine for Rocket Vehicle Application (NERVA) program in the 1960s[12].

The advancement of a nuclear thermal rocket necessitates an extensive research and development initiative encompassing system efficiency, nuclear reactors, engine control, fluid dynamics, high-temperature testing of engine components, heat transfer techniques, and nuclear fuel elements. The initial phase involved an examination of a 1500 MW reactor utilizing uranium-graphite fuel. The primary

objective of this program was to concentrate on the nuclear reactor and fundamental engine components, with no practical tests conducted at this stage. It was anticipated that practical tests of the reactor would be conducted in 1958[16]. The report also highlights a significant finding: if the system can elevate the exhaust temperature to 2500-2700°C and utilize a low molar mass working fluid, such as hydrogen, it has the potential to supplant chemical systems and transport larger payloads over a greater operating radius. Furthermore, the report outlines a feasible roadmap and identifies the subsequent steps, including the design and testing of the reactor core, development of a suitable heat exchanger, and underscores the pivotal factor of nuclear energy's high thermal density.

In the 1960s, the United States continued its efforts with the NERVA project (Fig.3), building on previous endeavors. This project, led by the Los Alamos National Laboratory, aimed to advance reactor fuel and systems capable of operating with hydrogen at temperatures exceeding 2200°C. NERVA project represented a significant effort in the development of NTP, laying the groundwork for many future research projects[12, 17].

The reactor's design and construction, typical of many nuclear and space projects, were executed incrementally. The reactor underwent tests at each stage to achieve maturity. These tests were conducted on various reactors, collectively referred to as the NERVA family, as detailed in Table 2. The table outlines key features, design objectives, and outcomes. The research and development spanned from 1956 to 1973, during which the reactor neared readiness for deployment. However, due to economic challenges faced by the US government, the project was terminated, despite an investment of approximately $1.5 billion (equivalent to $7 to $8 billion in today's currency)[18, 19].

It is important to note that there are numerous conceptual designs for reactors utilized in NTP systems. However, this section focuses solely on the examination of the most significant design, the NERVA family, which is the only design that has undergone testing.

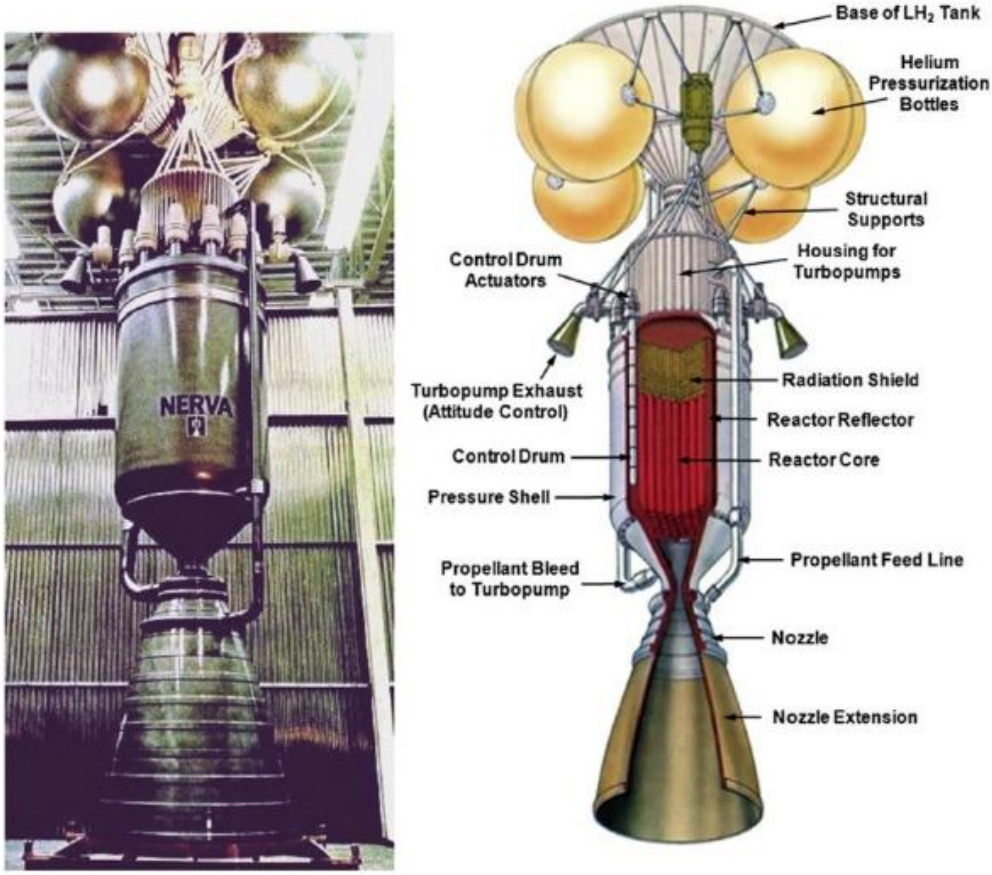

Fig. 3. Prototype of the NERVA project[17].

Table 2. A summary of the most important tests conducted on NERVA family of reactors[20-26].

Reactor under test	Objective of the test	Features and conclusions
KIWI-A	The first test of a NTP system reactor	1- The possibility of using the reactor in NTPs was proved. 2- Vibrations in the reactor core caused structural damage, erosion, and melting of some fuel rods. 3- Uranium oxide plates (UO_2) were used without cladding, which melted in some areas of the core, rendering them unusable for the next experiments. 4- This reactor achieved a thermal power of 70 MW_{th} and a maximum temperature of 2683°K.
KIWI-B	1- Considering the lessons learned from the KIWI-A series; 2- Restarting the reactor; 3- eliminating vibrations; 4-Operation in zero power (critical) and non-zero power.	1- Vibrations resulted in the ejection of seven fuel elements. 2- The zero-power experiment was executed effectively.

NRX	1- Testing the upgraded reactor based on the lessons learned from the previous two tests. 2- Restarting the reactor.	Successful
PHOEBUS	1- Achieving a higher specific impulse; 2- Long-term exploitation; 3- Constructing and testing a larger reactor.	1- The reactor fuel was depleted during the test. 2- This reactor was the most powerful, with a design thermal power of 5000 MW_{th}. 3- Niobium carbide (NbC) was used for the cladding. 4- The test was limited to 4000 MW_{th} due to overheating of the aluminum parts that hold the pressure vessels. 5- The total duration of the test, including start-up and operation, was 12.5 minutes, and the resulting temperature was 2310°K.
PEWEE	1-testing a small reactor with the highest power density. 2-Fuel test with zirconium carbide (ZrC) and niobium carbide (NbC) cladding.	1- Achieved success. 2- Zirconium carbide (ZrC) demonstrates superior cladding performance compared to niobium carbide (NbC). 3- The compact design of the reactor was a result of financial limitations and served as a prototype reactor for testing purposes. 4- The reactor achieved a maximum thermal power output of 503 MW_{th} and reached a peak temperature of 2550 °K. 5- The core exhibited an average power density of 2340 MW_{th}/m^3, with a peak state power density of 5200 MW_{th}/m^3. 6- The specific impulse was approximately 845 seconds.
XE	A prototype reactor in down firing mode	Successful
NF-1	1- Testing on fuel and recyclable structural materials; 2- Refinement of fission products	Only one test was conducted and some equipment was recyclable.
KIWI-TNT	Validation of Analytical Models for Power Changes	Successful

Technical Importance of NTPs

Astronauts face numerous health challenges due to their exposure to moderate levels of energetic galactic cosmic rays during space missions. These rays typically include alpha particles, protons, and **H**igh atomic number (Z) and **E**nergy ions (HZE), which can penetrate shields and pose significant risks to the skin, various tissues, and particularly the nervous system[6].

In addition to radiation, zero gravity can also have serious health effects. For instance, astronauts on long-duration space missions have experienced serious physiological effects on their bones, muscles, and cardiovascular systems due to extended periods of zero gravity. For example, returning from zero relative gravity ($g/g_0 \approx 0$) to one ($g/g_0 = 1$) results in an inability to maintain proper blood pressure in the upright position and insufficient blood flow to the brain. Furthermore, other cardiovascular effects, such as cardiac arrhythmia, have been observed and should be further investigated. Osteoporosis and muscle wasting are also long-term effects of low gravity[5, 6]. The impacts of space radiation and reduced gravity on human health are outlined in Fig. 4. In light of the aforementioned adverse impacts, the most efficient approach to mitigating the harm to astronauts is to minimize the duration of space travel[27]. Terry Kamash[28], a former professor at the University of Michigan, has proposed the round-trip duration for astronauts based on Eq.(1).

$$\tau_{RT} = \frac{4D}{gI} + 4\sqrt{\frac{DW_f}{gF}} \quad (1)$$

In this equation, D represents the linear distance of the target point from the Earth, g denotes the acceleration of Earth's gravity, W_f signifies the net weight of the spacecraft (excluding crew, fuel, and cargo), I stands for the specific impulse, and F represents the thrust force. According to Eq.(1), the duration of the trip decreases as the weight of the spacecraft decreases and as the specific impulse and thrust force increase. A comparison of the specific impulse and the round-trip time to Mars is shown in Fig.5.

In addition to the importance of travel time, the ability to power spacecraft and reach distant destinations is also crucial. To achieve this, the presence of two crucial systems in every space mission is essential: (1) the power generation system and, (2) the propulsion system. The power generation system is essential for the operation of the subsystems, including sensors, computers, and the exchange of information and messages with the mission center. The propulsion system is responsible for moving the spacecraft, reaching its destination, changing its position, and altering its direction[3].

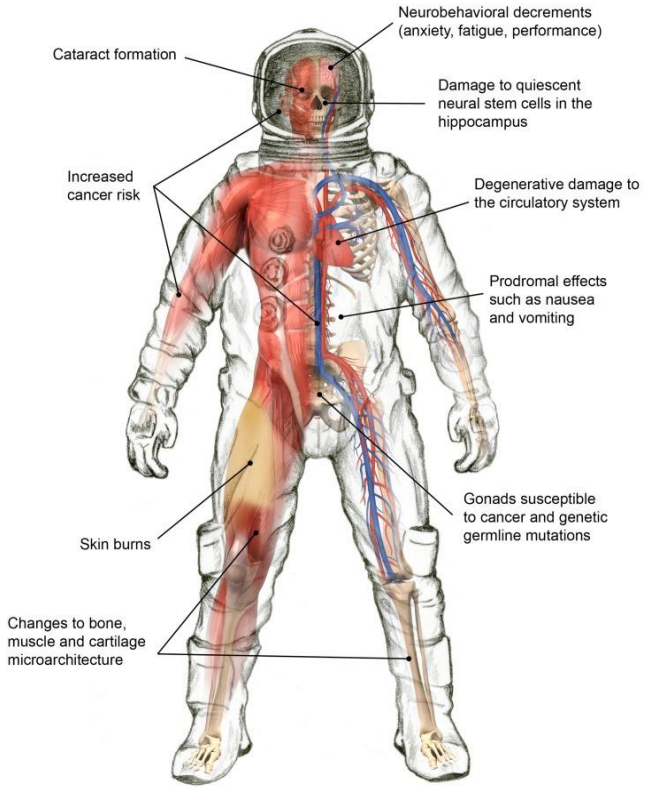

Fig. 4. Important health effects of space radiations[5].

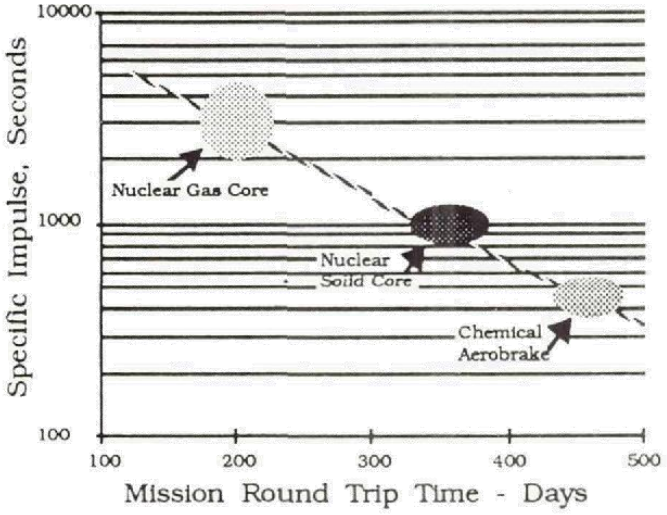

Fig. 5. Performance of the different propulsion systems for a manned mission to Mars[12].

NTP generally offers higher energy density and approximately double the specific impulse compared to chemical propulsion, which is currently used by humans. The increased energy density of nuclear fuel leads to reduced spacecraft weight, while the higher specific impulse allows the spacecraft to travel greater distances with less fuel consumption [29, 30].

Political Importance of NTPs

Nuclear energy is distinct from other forms of energy due to its significant military implications, particularly in relation to the development and proliferation of nuclear weapons. Within the framework of international relations, the use of nuclear energy for peaceful purposes is governed by the international nuclear nonproliferation regime[31]. The peaceful utilization of nuclear technology can be categorized into two primary groups: one for the production of electricity, and the other for non-electricity generation purposes. The former is commonly referred to as power applications, while the latter is known as non-power applications[32]. Therefore, NTPs can be considered as a non-power peaceful technology. The advancement of nuclear technology has consistently been overseen and supported by governmental entities, owing to its intricate characteristics and substantial financial investment[33]. The emphasis on nuclear technology is evident not only in developing countries but also in developed ones, indicating that the future of nuclear power extends beyond being solely a matter of science and technology, and is fundamentally a political issue[34]. It should be mentioned that the primary aim of the development of NTPs is focused on advancing deep space exploration, a pursuit characterized by peaceful intentions that align with established international agreements, notably those overseen by the Committee on the Peaceful Uses of Outer Space (COPUOS)[35, 36]. By providing a thorough elucidation of this objective, it is improbable that significant adverse responses from global organizations would arise.

Given its delicate strategic and geopolitical location, the Islamic Republic of Iran must prioritize and enhance multiple dimensions of hard power, including military and economic capabilities, while also bolstering its soft power[37]. In the present era, the influence of scientific and technological advancements has significantly impacted all facets of national power, particularly the political aspect. Nuclear science and technology serve as a crucial cornerstone for advancement and a formidable instrument for competition across diverse domains. The field of nuclear technology exerts a far-reaching influence on various other scientific disciplines. The acquisition of nuclear technology has fundamentally

altered Iran's geopolitical boundaries and transformed the geopolitical and political dynamics in Southwest Asia and the Persian Gulf. These changes have been closely linked to fluctuations in Iran's national power and geopolitical influence over the past few decades[38].

In recent years, Iran has demonstrated its commitment to eschewing the pursuit of nuclear weapons, instead emphasizing the utilization of peaceful nuclear technology as a key component of its soft power and, consequently, national security. The assertion is evident in the Joint Comprehensive Plan of Action (JCPOA), indicating that this agreement serves as a significant substantiation of the peaceful nature of nuclear activities[39]. However, the drafting process of this document underscores the imperative for global powers to engage in negotiations with Iran rather than resorting to coercive and military tactics, thereby underscoring the pivotal role of nuclear technology in deterrence. Based on these explanations, Iran should progress by enhancing its existing peaceful technological capabilities while also advancing its nuclear scientific expertise to achieve a competitive edge.

Iran's capacity to develop a diverse range of missiles with both military and aerospace utility serves as one of the main factors in its deterrent capabilities. In addition to their military applications, aerospace missiles enable Iran to establish itself as a proficient spacefaring nation, fostering independence in telecommunications, navigation, meteorology, and related domains. In the aftermath of the United States' withdrawal from the JCPOA, the primary requirement for rejoining the agreement was the negotiation aimed at constraining Iran's missile program[40]. This condition underscores the U.S. objective of diminishing Iran's deterrent capabilities, particularly its missile program. In this context, it can be inferred that if Iran were not utilizing nuclear technology under these circumstances, it would have engaged in direct negotiations focused on imposing limitations on its missile program. This further underscores the political significance of nuclear technology for Iran.

Now, let us contemplate a technology such as NTPs, which harnesses both nuclear and aerospace technologies concurrently[11]. The successful development of this technology not only showcases the scientific prowess of the nation but also serves as a catalyst for inspiring other countries, particularly those in the process of development, positioning Iran as a role model for their advancement. Furthermore, this technology will facilitate Iran's foray into deep space, elevating the nation from possessing orbiting satellite capabilities to being equipped for long-range space exploration.

Furthermore, the exploration and examination of NTPs align with the scientific and technical objectives outlined in the preceding official documents of the Islamic Republic of Iran. This is evident in the nation's development initiatives[41], which aim to coordinate and harness its resources and capabilities to enhance its global scientific contributions and obtain advanced technologies, such as microtechnology, biotechnologies, information and communication, environmental, aerospace, and nuclear technologies. Another significant document in this context is the comprehensive document of the country's aerospace development[42], which outlines the following vision: With reliance on divine assistance and the advancement of science and technology, the aerospace sector of the Islamic Republic of Iran aims to pursue technologies characterized by their authoritative and effective contribution to national security, efficiency and reliability in meeting strategic and societal needs, inspirational expansion of knowledge frontiers and aerospace technology development, driving advancements in other scientific, technological, industrial, and service sectors, and application of the latest scientific, research, and technological discoveries. Additionally, the fourth chapter of the document[42], which delineates the overarching aerospace policies, emphasizes the maximization of internal resources and capacity activation, equitable opportunities for individual, corporate, and institutional participation in aerospace sector development, leveraging aerospace technology advancements in other sectors, and prioritizing the enhancement of human capital and the attraction of skilled individuals as the primary drivers of technological progress.

Hence, attaining NTPs can serve as a novel means of enhancing diplomatic leverage, scientific and technological capabilities, and ultimately bolstering national security. Additionally, it can offer valuable support to the government in the execution of strategic initiatives.

Importance Of NTPs in Scientific Authority Creation

Currently, there is a prevalent discourse on the topic of scientific authority within academic institutions, research facilities, and policy-making organizations. This matter was initially brought to attention by Ayatollah Khamenei at the upper echelons of the political leadership of Iran, as he perceives science to be a fundamental component of a nation's power in the contemporary global landscape[43].

Establishing scientific authority involves the establishment of an independent scientific institution that garners global recognition and influence. This entails positioning oneself as a leading scientific hub,

thereby earning distinction and credibility in the international scientific community. The realization of scientific authority necessitates a comprehensive and enduring strategy, which encompasses various prerequisites. These include fostering a cultural shift, bolstering self-assurance, and promoting a collaborative ethos. Additionally, it involves formulating a forward-looking vision to underpin a substantive scientific movement, devising detailed strategies, and establishing requisite infrastructure. Emphasis is also placed on theoretical discourse and the development of intellectual frameworks. Furthermore, the compilation of a comprehensive roadmap delineating the responsibilities of all stakeholders, demarcating the boundaries of each authority, and outlining the interplay of diverse elements is imperative[44].

The concept of scientific authority encompasses various levels, one of which pertains to thematic authority. This level involves the advancement and establishment of expertise in a specific subject area, with the aim of becoming a significant reference point on a global scale. This developmental process is commonly observed in many advanced nations. Typically, at this level of authority, there is a swift progression through philosophical discussions and theoretical foundations, with a predominant focus on the creation of knowledge-based and economically valuable products. It is inherent that the optimal utilization of existing human knowledge and the acknowledgment of technical and scientific constraints are essential for the establishment of such a scientific reference. It is important to note that achieving this type of authority requires sustained effort over a period of at least several decades, as resources are often limited and the scope is not all-encompassing, but rather concentrated on a specific aspect of science and technology[45, 46].

The endeavor to research and master the NTP systems is a sustained undertaking and a long-term program that has the potential to establish scholarly expertise and authority in the fields of nuclear science and technology, as well as space science and technology. This is due to the utilization of nuclear energy for spacecraft propulsion within these systems, which serves as a pivotal intersection between the two aforementioned technologies.

The inquiry arises as to how this extended program can establish the country as a leading scientific authority. The answer to this question is actually at the core of the challenges in this program. Historically, humanity has struggled to develop a dependable propulsion system with a high specific

impulse and an appropriate operational range for human voyages to Mars. The realization of this aspiration would establish the nation as the primary producer of such systems, thereby conferring scientific prestige.

The second point pertains to the multidisciplinary aspect of accessing NTP systems. This characteristic necessitates experts from various fields to confront and address challenges concurrently. These fields encompass:

The production of nuclear fuel capable of withstanding extreme temperatures ranging from 2500 to 3000°K[47] involves a complex process that encompasses various critical disciplines, including the extraction, enrichment, and manufacturing of the necessary fuel (referred to as nuclear fuel cycle engineering). This is essential to ensure that the structural materials do not undergo melting at elevated temperatures, requiring expertise in materials science and engineering as well as metallurgy.

The design of the reactor structure for a Nuclear Thermal Rocket (NTR) is notably distinct from other types of reactors. In NTR reactors, there is a notable contrast in temperature between the very hot fuel, which can reach temperatures of 2500-3000°K, and the very cold fluid, which is approximately 200°K. This temperature differential can fluctuate during the startup and shutdown of the reactor. These varying thermal conditions can result in a complex interplay of stresses arising from material expansion and contraction, posing a significant challenge to the structural integrity of the materials. These challenges may stem from the diminished strength of materials at extremely high temperatures or their reduced ductility at very low temperatures. Additionally, the simultaneous impact of hydrogen and neutrons has the potential to render structural materials brittle, further testing their resilience[4]. Addressing this significant challenge necessitates the collaboration of specialists from diverse disciplines, including nuclear engineering, mechanical engineering, material engineering and etc.

The instrumentation and control of reactors, particularly those operating with NTPs, pose significant challenges due to their heightened complexity and uncertainty. NTP reactors exhibit higher neutron flux and temperature levels compared to other reactor types, necessitating instrumentation that can withstand these conditions with minimal uncertainty. For instance, accurately measuring internal temperatures within the reactor core may prove impractical, posing challenges for systems reliant on complex reactive

feedback. Additionally, the emphasis on low mass in NTP development may limit the practical use of diagnostic tools. Precision instruments must also function in vacuum environments, endure extreme temperatures and launch vibrations, and perform reliably during the vibrations generated by NTP thrust[4]. Addressing these challenges requires expertise from various scientific and engineering disciplines, including nuclear, mechanical, aerospace, electrical, electronic, and instrumentation engineering.

The potential for accidents during the launch or re-entry from orbit presents a distinctive challenge for nuclear thermal reactors (NTRs) and aerospace reactors. While the technical assessment indicates minimal radiation risks to the public[48], societal and political apprehensions and sensitivities towards nuclear materials can pose a substantial barrier. This issue encompasses various disciplines within the realms of science and engineering, including project management, sociology, safety engineering, and aerospace engineering.

Based on the cited instances, studying and achieving NTPs has the potential to establish scientific credibility and authority within the aerospace and nuclear sectors, as well as facilitate the transfer of technology to other domains of sciences and engineering.

Importance oF NTPs in The Development of Nuclear

Infrastructure

Studying, striving to develop, and safe operation of nuclear systems always necessitates a fundamental infrastructure that addresses the essential needs for managing all aspects of a nuclear project. Once in place, this framework can be gradually expanded to support a comprehensive, sustainable, and domestic nuclear industry in the nation. This foundational framework encompasses[49]:

Creation and official approval of government policy on nuclear power.

Verification of the practicality of carrying out a nuclear initiative.

Formation of the necessary institutional framework, such as a nuclear regulatory body (NRB).

Creation of the physical elements required for the infrastructure.

Planning, contracting, and funding of the nuclear initiative.

Building the nuclear facility by safety, quality, and financial standards.

Ensuring the safe, secure, and effective operation of the nuclear project.

When formulating a strategy for the development of NTP, it is essential to consider both programmatic and engineering factors[50], as they have the potential to yield significant advancements in infrastructure development within the nuclear and aerospace sectors.

Several programmatic factors need to be taken into account, such as project authority and governance, people and organizations, cooperation, funding and schedule, acquisition approach, past program lessons learned, safety, environmental protection, and education and public engagement.

Establishing NTP requires the collaboration of various entities, including the Space Agency, the Atomic Energy Organization, the Ministry of Defense and Armed Forces Logistics, research centers, and universities. This process mirrors the approach taken in the United States[50], where NASA, the Department of Energy(DOE), and the Department of Defense (DOD) are involved in providing the necessary tools and infrastructure. The responsibility for financing the final system should lie with the organization utilizing it, with other centers serving as contractors and supporters. This element contributes to the establishment of a robust managerial infrastructure, facilitating collaboration among various organizations to cultivate a sophisticated and scientific edge system. Furthermore, the knowledge gained from this initiative can be applied to comparable and forthcoming projects.

In addition to programmatic factors, it is essential to evaluate various engineering considerations when formulating the development approach. These engineering considerations encompass technology readiness, the conventional rocket engineering development approach, the conventional nuclear reactor engineering development approach, insights from previous program experiences, safety measures, environmental protection, and the development of infrastructure or facilities.

The main challenge faced by the NTPs development is anticipated to be the execution of a nuclear ground test at nominal power, due to the significant financial investment required and the complexities associated with obtaining safety, environmental, and aerospace clearances. Additionally, the establishment of facilities capable of conducting these tests entails substantial costs. solving these challenges can prove to be highly beneficial as they compel regulatory bodies to thoroughly examine nuclear energy matters, and the laboratory infrastructures created for these instances can also be applied to other endeavors. These advantages were evident during the NERVA project[12], as substantial equipment from its experimental infrastructure continues to be utilized in the national laboratories of the United States, including the Idaho National Laboratory (INL), Oak Ridge National Laboratory (ORNL), and Los Alamos National Laboratory (LANL).

Some of the necessary test facilities, with a focus on the nuclear or nuclear-related structural components of NTP, include[50, 51]:

Fuel Fabrication Facilities: Infrastructure for the advancement and eventual manufacturing of enriched uranium nuclear fuel materials and fuel elements.

Test Facilities for Unirradiated Fuel Materials: Material testing and characterization infrastructure capable of handling unirradiated, uranium fuel materials.

Test Facilities for Unirradiated Materials: Infrastructures for testing and characterizing nonradioactive materials intended for use in structural components, such as pressure vessels.

Hot Hydrogen Flow Test Facilities: Infrastructures that use materials or subsystems in an environment of flowing hot hydrogen without nuclear heating. There should be two types of hot hydrogen flow test facilities: (1) Fuels and Materials/Low flow rate, which primarily uses pure H_2 for material and fuel tests, and (2) High flow rate equipment, which uses H_2/O_2 gas generator or electrically heated H_2 for testing turbopumps, nozzles, and propellant management systems.

Fuel Irradiation Test Facilities: Facilities housing reactors or radiation sources that expose uranium fuel material to gamma or neutron fluence for testing purposes.

Material Irradiation Test Facilities: Facilities housing reactors or radiation sources that expose test specimens of structural or non-fuel-bearing materials to gamma or neutron fluence.

Fuel Element Loops in Existing Reactors: Test loops for nuclear-heated fuel element experiments in existing reactors.

Low-Power Critical Assemblies Facilities: A reactor facility with low power, adaptable geometry, and variable material volume fraction for conducting physics benchmarking, confirming designs, and safety tests.

Prototypic Fuel Element Test Reactor: A test reactor capable of simultaneously achieving various performance parameters such as time, temperature, and power density for one or more prototype fuel elements. This facility is commonly referred to as the "Nuclear Furnace," as it shares similar test objectives with the Nuclear Furnace operated in the early 1970s.

Reactor Test Cell: A section of a Reactor/Engine Test Facility designed for the ground-based testing of early "engine-like" reactors at high power levels.

Engine Ground Test Cell: A section of a reactor/engine test facility designed for the ground-based testing of nuclear rocket engines operating at high power levels, simulating conditions similar to those experienced during flight.

Remote Inspection/Post-Irradiation Examination Facilities: Hot cell facilities where post-test examinations of radioactive fuel, reactor, and engine components will be conducted

Component Test Facilities without Hot Hydrogen or Irradiation Environment: Facilities that are capable of simulating the structural, thermal, and cycling conditions experienced by system components during startup, continuous operation, and shutdown. It is important to note that these environments do not encompass irradiation or exposure to hot hydrogen.

Control System Test Facilities: Laboratory for simulation aimed at the development and evaluation of reactor and engine systems.

Component Safety Test Facilities: Facilities capable of simulating realistic malfunctions and extreme or accident scenarios on system components through testing.

System-Level Safety Test Facilities: Test facilities that can simulate on the complete engine all realistic malfunctions and severe or accident environments.

Training and Simulator Test Facilities: Training facilities for operators and astronauts to simulate emergency sequences for instructional purposes.

Engine Integration Test Facility: A cold flow test facility for the comprehensive evaluation of an entire engine system. The facility will utilize hot gas, specifically H_2/O_2 gas, to simulate reactions and assess potential pre-flight and in-flight issues. It is important to note that the operations of this facility will not involve any nuclear critical operations or nuclear heating.

Flight Test Facilities: Infrastructure at the launch site or operations control center necessary to provide support for launch or operations, particularly due to the presence of nuclear propulsion systems.

In Fig. 6, a visual representation is provided to outline the systematic procedure for conducting mentioned tests.

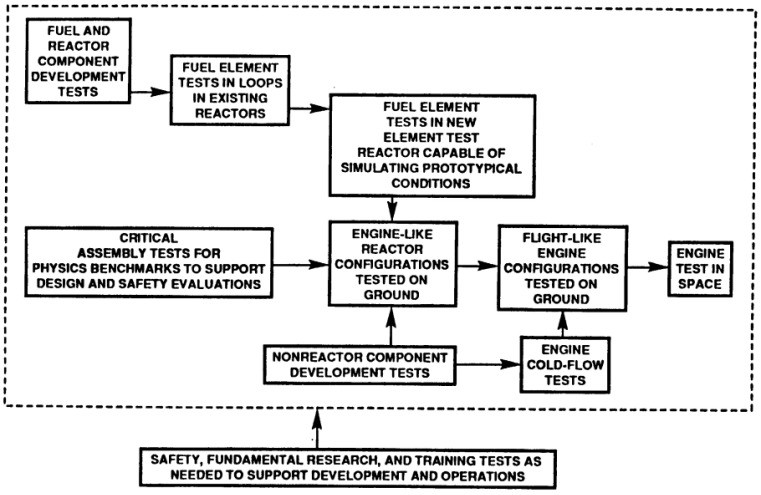

Fig. 6. Logical summary of tests for NTP development[51].

Based on the aforementioned information, it can be asserted that the efforts to implement the NTP system offer numerous advantages for the nuclear industry, including the establishment of various laboratories, facilities, and equipment. These infrastructures can significantly contribute to the advancement and dissemination of scientific knowledge and nuclear technologies, thereby exerting a substantial impact on the nuclear and space industries.

Conclusion

Indeed, in addition to serving as an unspoiled domain for scientific inquiry, space also provides a favorable environment for economic and military activities by nations. Consequently, this has led to an increase in competition among countries for dominance in space. To overcome potential scientific stagnation in the aerospace and nuclear industries, it is crucial to investigate systems that are currently leading the global scientific and technological discussions. One such system is nuclear thermal propulsion (NTP), which offers significant promise for various applications in space travel due to its high reliability, high specific impulse, and reduced weight compared to chemical propellants. These attributes can improve maneuverability, reduce travel time in space, and minimize astronauts' exposure to harmful cosmic radiation. Consequently, this article examines the importance of studying and achieving these systems, while introducing nuclear thermal propulsion to the aerospace and nuclear research community of the country.

As indicated in various sections of the article, the advancement and realization of NTPs hold significance from multiple standpoints. Primarily, this technology holds the potential to shape the future of the country's space endeavors and missions involving human space travel. Additionally, these systems bolster national security through the utilization of cutting-edge and strategic technologies, namely nuclear and aerospace, thereby showcasing the scientific prowess of the nation and enhancing its influence over other developing countries. Furthermore, the establishment of such a system, unprecedented on a global scale, enhances the scientific reputation of the nation and establishes scientific authority. Moreover, the development of these systems and the implementation of lessons derived from them can propel advancements in various other fields of science and engineering, enabling the efficient utilization of resulting technological advancements.

Also, the advancement of Nuclear Thermal Propulsion (NTP) technology presents numerous programmatic and engineering challenges, necessitating the establishment of laboratories, facilities, equipment, and diverse strategies. These resources, once in place, can be leveraged for the advancement of other fields within the nuclear and aerospace sciences. The successful development of NTP systems would equip the country with valuable and multidisciplinary infrastructures in the nuclear industry, which could also be applied to the development of other peaceful nuclear technology sectors.

References

[1] Howe, J.C., Atomic Space A history and analysis of U.S. policy for the development of nuclear space propulsion and power technologies. 2023, University of Leicester.

[2] Gholami, M., Assessment of Socio-economic Impacts of Investments in Space Industry. Technology in Aerospace Engineering, 2020. 4(1): p. 35-44.

[3] Bennett, G.L., Introduction to space nuclear power and propulsion, in Encyclopedia of Nuclear Energy. 2021.

[4] Poston, D.I., Nuclear Thermal Propulsion: Benefits and Challenges, in Encyclopedia of Nuclear Energy. 2021.

[5] Chancellor, J.C., G.B. Scott, and J.P. Sutton, Space Radiation: The Number One Risk to Astronaut Health beyond Low Earth Orbit. Life (Basel), 2014. 4(3): p. 491-510.

[6] Onorato, G., E. Di Schiavi, and F. Di Cunto, Understanding the effects of deep space radiation on nervous system: the role of genetically tractable experimental models. Frontiers in Physics, 2020. 8: p. 362.

[7] Cassandra, G., The History of Nuclear Thermal Rocket Development, in Encyclopedia of Nuclear Energy, G. Ehud, Editor. 2021, Elsevier: Oxford. p. 290-302.

[8] Gabrielli, R.A. and G. Herdrich, Review of nuclear thermal propulsion systems. Progress in Aerospace Sciences, 2015. 79: p. 92-113.

[9] A. Boxberger, M.L., Q.H. Le, C. Syring, B. Wollenhaupt, R.A. Gabrielli, G. Herdrich, Advanced Propulsion Systems Engineering Report- Report to the European Commission, Contract No. 284081,Disruptive Technologies For Space Power And Propulsion (DiPoP) Consortium. 2012: Stuttgart, Germany.

[10] NASA. Space nuclear propulsion. Available from: https://www.nasa.gov/tdm/space-nuclear-propulsion/.

[11] Emrich Jr, W.J., Principles of Nuclear Rocket Propulsion. 2023: Elsevier.

[12] Robbins, W. An historical perspective of the NERVA nuclear rocket engine technology program. in Conference on Advanced SEI Technologies. 1991.

[13] Frisbee, R.H., Advanced space propulsion for the 21st century. Journal of propulsion and power, 2003. 19(6): p. 1129-1154.

[14] Bennett, G. Nuclear thermal propulsion program overview. in Proceedings of the Nuclear Thermal Propulsion Workshop, NASA Conf. Pub. 1990.

[15] Schreiber, R., LASL nuclear rocket propulsion program. 1956, Los Alamos National Lab.(LANL), Los Alamos, NM (United States).

[16] Schreiber, R., The LASL Nuclear Rocket Propulsion Program, LAMS-2036. 1956, Los Alamos Scientific Laboratory: Los Alamos Scientific Laboratory.

[17] Braun, R., R. Myers, and S. Bragg-Sitton, Space nuclear propulsion for human Mars exploration. NASEM Space Nuclear Propulsion Technologies Committee Report. Washington, DC: National Academies of Sciences, Engineering and Medicine, 2021.

[18] Haslett, R., Space nuclear thermal propulsion program final report. Grumman Aerospace Corporation, Bethpage, NY, 1995. 11714.

[19] NASA. Nuclear Rockets. [cited 2023; Available from: https://www1.grc.nasa.gov/historic-facilities/rockets-systems-area/7911-2/.

[20] Angelo Jr, J. and D. Buden, Space nuclear power. 1985.

[21] Finseth, J., Rover nuclear rocket engine program: Overview of rover engine tests. 1991.

[22] Humble, R.W., H.N. Gary, and W.J. Larson, Space propulsion analysis and design. (No Title), 1995.

[23] Klein, M. Nuclear Thermal Rocket—An Established Space Propulsion Technology. in AIP Conference Proceedings. 2004. American Institute of Physics.

[24] Parsley, R.C. Advanced propulsion engine assessment based on a cermet reactor. in NASA. Lewis Research Center, Nuclear Propulsion Technical Interchange Meeting, Volume 1. 1993.

[25] SEGNA, D. Reliability comparison of nuclear with chemical propulsion for Mars mission. in Conference on Advanced SEI Technologies. 1991.

[26] Szilard, L., history of fission propulsion. University of Wisconsin-Madison: University of Wisconsin-Madison.

[27] Zhang, Y., Advanced nuclear power engine: A brief overview of gas core reactor for space exploration. International Journal of Advanced Nuclear Reactor Design and Technology, 2023.

[28] Kammash, T., Fission or fusion for Mars missions: expectations and challenges. Acta Astronautica, 1994. 34: p. 17-23.

[29] Howe, S.D., Assessment of the Advantages and Feasibility of a Nuclear Rocket. 1985, Los Alamos National Lab.(LANL), Los Alamos, NM (United States).

[30] DOE. 6 Things You Should Know About Nuclear Thermal Propulsion 2021; Available from: https://www.energy.gov/ne/articles/6-things-you-should-know-about-nuclear-thermal-propulsion.

[31] Şebnem, U., Nuclear energy and international relations: outlook and challenges for newcomers. PERCEPTIONS: Journal of International Affairs, 2017. 22(2): p. 57-84.

[32] Hazmimi, K., et al., Impact of nuclear technology to the national socio-economy: technical support by Nuclear Malaysia. 2011.

[33] OECD_NEA, Government and Nuclear Energy. 2004: Nuclear Energy Agency, Organisation for Economic Co-operation and Development.

[34] Gattie, D. and M. Hewitt, National Security as a Value-Added Proposition for Advanced Nuclear Reactors: A U.S. Focus. Energies, 2023. 16(17): p. 6162.

[35] El-Genk, M., Safety guidelines for space nuclear reactor power and propulsion systems, in Space Safety Regulations and Standards. 2010, Elsevier. p. 319-370.

[36] Venturini, G., The Legal Regime of the Use of Nuclear Power Sources in Space Missions. Nuclear Non-Proliferation in International Law-Volume V: Legal Challenges for Nuclear Security and Deterrence, 2020: p. 73-91.

[37] Karimifard, H. and A. Bineshfar, THE POLITICAL EFFECTS OF NUCLEAR TECHNOLOGY TO THE ISLAMIC REPUBLIC OF IRAN NATIONAL POWER. POLITICAL QUARTERLY, 2020. 50(1): p. 271-287 (In Persian).

[38] Pishgahi-fard, Z., et al., Position of Soft Power in National Power With Emphasis on the Islamic Republic of Iran. A Quarterly Journal of Strategy, 2012. 20(4): p. 191-211 (In Persian).

[39] I.R.I._Ministry_of_Foreign_Affairs, The Joint Comprehensive Plan of Action (JCPOA) between Islamic Republic of Iran and the countries of the 5+1 group. I.R.I._Ministry_of_Foreign_Affairs, 2015 (In Persian).

[40] Zamani, M. and S.A. Niyakuei, A Survey on the Factors Affecting the Exit of the United States from the JCPOA. Research Letter of International Relations, 2019. 12(45): p. 85-110 (In Persian).

[41] Iran, E.D.C.o.I.R.o., General approvals of the system's expediency assessment regarding the system's general policies (announcement by the Supreme Leader), E.D.C.o.I.R.o. Iran, Editor. 2007: Parliament Research's Center.

[42] Revolution, S.C.o.t.C., Comprehensive document of the country's aerospace development, S.C.o.t.C. Revolution, Editor. 2013: Parliament Research's Center.

[43] Rahbar, F. and H. Hossein zadeh, Illustrating the Relation of Power, Scientific Authority and Technology of the Islamic Republic of Iran in the World with Power and National Security Based on the Principles of the Islamic Republic. Scientific Quarterly Journal of Islamic Revolution Studies, 2016. 13(44): p. 167-188.

[44] Mahdinejhad Noori, M., et al., Development an Architecture Framework for Science, Technology and Innovation In order to Achieve Scientific Authority. Interdisciplinary Studies on Strategic Knowledge, 2020. 4(13): p. 71-110.

[45] Goodarzi, G. and K. Roudi, Interpretation of scientific authority for educational institutions by applying grounded theory. Science & Technology, 2012. 4(2).

[46] Haq Dost, A., et al., A practical look at the concept of scientific authority. Iranian Journal of Culture and Health Promotion, 2019. 3(1): p. 16-23.

[47] Wagner, P., Material science experience gained from the space nuclear rocket program: Insulators. 1992, Los Alamos National Lab., NM (United States).

[48] McClure, P., Space Nuclear Power Safety and Safeguards, in Encyclopedia of Nuclear Energy. 2021.

[49] IAEA, Basic Infrastructure for a Nuclear Power Project. 2006, Vienna: INTERNATIONAL ATOMIC ENERGY AGENCY.

[50] Bordelon, W., R. Ballard, and H. Gerrish. A Programmatic and Engineering Approach to the Development of a Nuclear Thermal Rocket for Space Exploration. in 42nd AIAA/ASME/SAE/ASEE Joint Propulsion Conference & Exhibit. 2006.

[51] Allen, G.C., et al., Space Nuclear Thermal Propulsion Test Facilities Subpanel. 1993.

ICNST 2024
International Conference on Nuclear Science and Technology
6- 8 MAY 2024 | Isfahan, Iran

Navigating Saudi Arabia's Nuclear Ambitions: A Multifaceted Analysis of Regional and Global Perspectives (Paper ID : 1156)

A Balancing Act: the Kingdom of Saudi Arabia's Nuclear Strategy in the Middle Eastern region Power Grid

Sasan Karimi2, Parisa Sadat Tabatabaei Rad3*

Abstract

Saudi Arabia's nascent nuclear program has emerged as a complex and contentious issue with implications that extend far beyond its borders. Since first broaching the topic in 2006 under the GCC umbrella and independently from 2009, Saudi Arabia's nuclear ambitions have sparked concerns and dilemmas in Tehran and Washington, among other global stakeholders. This paper delves into the multifaceted dimensions of Saudi Arabia's nuclear program, considering its implications for regional dynamics and international cooperation. The United States, known for its adherence to the "Gold Standard" in nuclear cooperation, faces a dilemma in its approach to Saudi Arabia. This dilemma revolves around the dual challenge of supporting a strategic partner while being cautious about Saudi Arabia's alignment with China, a major global competitor. Furthermore, it involves preventing Saudi Arabia from emerging as a nuclear rival to Israel. Conversely, Tehran's perspective on Saudi Arabia's nuclear program is a nuanced one. On one hand, supporting Saudi Arabia's pursuit of a peaceful nuclear program with complete fuel cycle capabilities and enrichment can help normalize the idea of nuclear energy in the region. On the other hand, it underscores the rivalry between Iran and Saudi Arabia, two key regional players vying for influence and nuclear capabilities. This paper provides a comprehensive analysis of the divergent nuclear strategies employed by Iran and Saudi Arabia within the context of the international environment and relevant organizations. It explores the varied approaches taken by regional and global actors, including Saudi Arabia itself, Iran, the United States, China, Russia, France, and Israel, shedding light on the potential paths Saudi Arabia's nuclear program may traverse. By examining these intricate dynamics, this paper aims to contribute to a deeper understanding of the regional and global implications of Saudi Arabia's nuclear aspirations. Ultimately, it seeks to inform discussions on policy options and diplomatic strategies in the Middle East, where nuclear ambitions are entwined with geopolitical rivalries and security concerns.

Keywords: Saudi's nuclear program, Iran's nuclear program, China, IAEA, Gold Standard, United States, Middle East.

[2] Post-doctoral fellow and adjunct professor, Faculty of World Studies, University of Tehran, (sasan.karimi@ut.ac.ir).
*Responsible author.
[3] Master of Science student of Latin American Studies, Faculty of World Studies, University of Tehran, (parisa.t.rad@ut.ac.ir).

International Conference on Nuclear Science and Technology

6- 8 MAY 2024 | Isfahan, Iran

ICNST 2024

Saudi Arabia's Nuclear Program

2006-2007

The Persian Gulf Cooperation Council (GCC) announced a study on the peaceful use of nuclear energy.
The GCC agreed with the IAEA to cooperate on a feasibility study for a regional nuclear power and desalination program.

2009

Saudi Arabia considered a nuclear power program on its own.

2010

The King Abdullah City for Atomic and Renewable Energy (KA-CARE) was set up in Riyadh to advance the nuclear

2011

KA-CARE appointed WorleyParsons to conduct site surveys and regional analysis for the nuclear power project.

2012

The government adopted a proposal to add 23.9 GWe of renewable capacity by 2020 and 54 GWe by 2032, later pushed back to 2040.

2013

KA-CARE projected 17 GWe of nuclear capacity by 2032, with nuclear construction starting in 2016.
GE Hitachi Nuclear Energy and Toshiba/Westinghouse signed contracts with Exelon Nuclear Partners to pursue reactor construction deals with KA-CARE (King Abdullah City for Atomic and Renewable Energy).

2014

The Saudi Arabian Atomic Regulatory Authority (SAARA) was established.
KA-CARE signed an agreement with the Finnish Radiation and Nuclear Safety Authority (STUK) for assistance in recruiting and training personnel and establishing safety standards.

2015

Saudi government revised its target for 17 GWe of nuclear capacity to 2040. KAERI signed an agreement with KA-CARE to assess the potential for building at least two South Korean SMART reactors in Saudi Arabia.
INVAP from Argentina and Saudi's Taqnia set up a joint venture company, Invania, to develop nuclear technology for Saudi Arabia's nuclear power program.

2016

The government launched the Vision 2030 initiative for 9.5 GW of renewable energy by 2023.
KA-CARE signed an agreement with China Nuclear Engineering Corporation (CNEC) to build a high-temperature reactor (HTR) in the country.
KA-CARE signed an agreement with South Korea's Nuclear Safety and Security Commission (NSSC) to promote cooperation in regulating nuclear safety, safeguards, and physical protection.

2017

The Crown Prince announced the $500 billion Neom project, a city to be fully powered by renewable energy.
KA-CARE solicited proposals for 2.9 GWe nuclear capacity from South Korea, China, Russia, and Japan. A joint working group commenced a formal feasibility study for the project.
CNEC and Saudi Technology Development Corporation signed an agreement for a feasibility study on using high temperature reactors for seawater desalination. The cabinet approved the establishment of the Saudi National Atomic Energy Project (SNAEP) and new regulations for KA-CARE.
China National Nuclear Corporation (CNNC) and the Saudi Geological Survey signed agreements on cooperation on the exploration of uranium.

2018

Crown Prince Mohammed bin Salman signed an MoU with Japan's SoftBank for 150-200 GW of solar capacity by 2030, but the project was aborted six months later.
KA-CARE awarded a contract to Worley Parsons for consultancy services for the Saudi National Atomic Energy Project.

2019

The IAEA delivered the final report of its integrated nuclear infrastructure review (INIR) mission in Saudi Arabia, noting significant progress.
KA-CARE launched a program with the Jordan Atomic Energy Commission (JAEC) and the Jordan Uranium Mining Company (JUMCO) to develop Saudi expertise in uranium exploration and mining.

2021

The country committed to becoming carbon neutral and aims to produce 50% of its electricity from renewables by 2030, with the rest supplied by natural gas.
Saudi Arabia's Nuclear and Radiological Regulatory Commission (NRRC) and the UAE's Federal Authority for Nuclear Regulation (FANR) agreed to cooperate in nuclear and radiation regulatory matters.

2022

Neom launched subsidiary company Enowa for developing its energy and water systems. Saudi Arabia confirmed the establishment of the Nuclear Holding Company, which will act as the country's nuclear developer

2023

The energy minister reiterated the Kingdom's intention to build a nuclear power plant and plans to switch to a comprehensive safeguards agreement with the IAEA.
Energy minister Prince Abdulaziz Bin Salman announced plans to utilize national uranium resources for the whole nuclear fuel cycle, including the production of yellowcake, low enriched uranium, and the manufacturing of nuclear fuel for national use and for export.

Introduction

This article examines the Kingdom of Saudi Arabia's Nuclear Program (SANP) within the framework of its foreign policy and regional geopolitical ambitions. As the Kingdom of Saudi Arabia positions itself as a central player in the Middle Eastern region, its nuclear energy aspirations are analyzed in light of rivalries, especially with the Islamic Republic of Iran, and the broader implications for regional and global stability. The analysis covers the historical development of SANP, strategic partnerships with major powers such as the United States of America and the People's Republic of China, and the nuanced interplay of international nuclear energy non-proliferation treaties. This study also explores the legal and political ramifications of the Kingdom of Saudi Arabia’s nuclear energy activities, including the impact of its policies on regional power dynamics and its diplomatic relations with neighboring countries and global powers. By evaluating the motivations behind the Kingdom of Saudi Arabia's nuclear energy ambitions, this report provides insights into the potential shifts in the regional security landscape and the challenges posed to the international non-proliferation regime.

As the geopolitical landscape of the Middle Eastern region continues to evolve, the strategic decisions of its key players significantly influence the regional balance of power. Among these players, the Kingdom of Saudi Arabia's nuclear energy ambitions represent a pivotal element in understanding the kingdom's broader strategic objectives and its place in global politics. This report delves into the intricate dynamics of the Kingdom of Saudi Arabia’s Nuclear Program (SANP), exploring its implications not only within the realm of Saudi foreign policy but also in its quest for a prominent role on the international stage. By examining the historical development, strategic partnerships, and legal frameworks surrounding SANP, this analysis sheds light on the motivations behind the Kingdom of Saudi Arabia's nuclear energy pursuits and the potential ramifications for regional stability and international nuclear energy non-proliferation efforts. Through this lens, we can better comprehend how the Kingdom of Saudi Arabia navigates its relationships with global powers and regional adversaries, crafting a nuclear energy strategy that seeks to enhance its security and regional influence.

Safeguards and Other Legal Bindings of Saudi with IAEA

The Kingdom of Saudi Arabia almost did nothing significant from the GCC announcement for a while in the nuclear energy section.4 It is important to note that the Kingdom of Saudi Arabia joined the NPT in 19885, but it had no safeguard agreement with the IAEA in force until 2009.6 On 2009, it started to enforce the safeguard agreement, which was already ratified in 2005 but not implemented. This ambiguity is possible and low cost for Saudi because of its good relations with the world powers in energy, financials, global investments, and briefly, a positive balance. That is why an optimistic approach was ongoing about Saudi's delay in agreeing on the safeguard with the agency and then the implementation of it.

Saudi Infrastructure

Saudi tried to open its nuclear energy discussion to the international arena so that it becomes normalized in advance. That is why almost since the beginning of the project, or even before, they announced the founding of a city called King Abdullah City for Atomic and Renewable Energy (King Abdullah City for Atomic and Renewable Energy). As is obvious from the title, the Kingdom of Saudi Arabia didn't isolate its nuclear energy project and introduced it as a package of renewable energies. As investment in nuclear energy industries, especially when it includes enrichment, is introduced as a weird aim for the oil-rich countries without any wish to build a nuclear energy weapon, the Kingdom of Saudi Arabia tried to justify the whole case as an energy basket package to be completed.

Rumors about the People's Republic of China and Saudi Secret Facilities

There are several rumors about the secrecy of Saudi's nuclear energy project, specifically its cooperation with the People's Republic of China.7 These rumors are mostly because of the Chinese aims to cooperate with Saudi in the nuclear energy segment, which is already declared both by Saudi and the Chinese party. Some claimed that Saudi already has its nuclear energy facilities and the uranium concentrate processing.8 Postponing the finalization of the safeguard from 1988 to 2005 and putting it in force in

[4] (Nuclear Power in Saudi Arabia, 2023)g
[5] (Squassoni, 2018)
[6] (Squassoni, 2018)f
[7] (Al-Madhaji, 2023)e
[8] (Al-Madhaji, 2023)e

2009, and also not joining the additional protocol9, which is not compatible with Saudi's behavior in its foreign policy and its relations with international organizations. This incompatibility raises such ideas.

Engaging Different Parties in the Game

Saudi has not been in a hurry with its nuclear energy project. That was why it could engage different parties in its developing nuclear energy project: the the United States of America10, South Korea11, the People's Republic of China12, Argentina13, and alike.14 Together with Saudi's financial resources, which raise the cooperation will to have a piece of a big cake for each party in advance, reports, positionings, and negotiations created a "network of players and contributors" that logically normalize the entire project.

This may be counter to what happened to the Islamic Republic of Iran's nuclear energy program, which soon has been converted to an issue15 which is still in the headlines. The Islamic Republic of Iran started not from building a justification narrative in the international arena but from simple technical experiments on its soil, all of which happened at the starting phase very primary as of today capabilities. But due to the lack of any "political preamble" which justifies these measures in all economic, technologic, and political extents, that was why it has changed to an unnecessarily long-lasting issue in its foreign relations that increased its policy costs. The main two players to be the Kingdom of Saudi Arabia's nuclear energy partners are the the United States of America and the People's Republic of China; the United States of America, which is the main but not the only great partner of the Kingdom of Saudi Arabia, has its nuclear energy cooperation policy, the most sensitive article of which is called article 12316, and the ultimate version of which is called "gold standard".17 The gold standard is the type of nuclear energy cooperation that the United Arab Emirates has accepted. This standard, which is a specific format of nuclear energy cooperation with foreign countries, prohibits the destination country from

[9] (Squassoni, 2018)f
[10] 2008
[11] 2011
[12] 2012
[13] 2015
[14] (Nuclear Power in Saudi Arabia, 2023)g
[15] (Henderson & Schenker, audi Arabia's Nuclear "Asks": What Do They Want, What Might They Get?, 2023)
[16] (Atomic Enegry Act of 1954)f
[17] signed this on January 15, 2009

enriching uranium as well as other nuclear energy material on its own soil. In return, the the United States of America conveys several other parts of the nuclear energy installations and non-enrichment technologies to this country.

For the governments like the United Arab Emirates, working under such a limitation would be a feasible one to get technologies from the the United States of America or its nuclear energy partners like South Korea that never is possible to achieve by itself. But for a country like the Kingdom of Saudi Arabia, with all its ambitions as a head of the Arab Union or special position in the Islamic world, the story is different. Especially with respect to the competition the Kingdom of Saudi Arabia feels with the Islamic Republic of Iran and the possibilities this country has due to its financial sources as well as balanced established relations with several global and nuclear energy powers, it seems not that feasible and interesting to have such a cooperation draft like what the United Arab Emirates has called “Gold Standard”.

The option that Saudi can choose is basically the People's Republic of China. The People's Republic of China, with its technological power in nuclear energy industries, can easily offer Saudi a full nuclear energy cycle including enrichment and bypass the the United States of America with all its limitations which are tried to be justified as “non-proliferative effort”; what is not that much believable from the only country which already used nuclear energy weapons in the history of the globe.

Position of the People's Republic of China in This Game with Respect to the Region

The other thing that needs to be considered is that along with the the United States of America' official aim to leave the Middle Eastern region region to some extent and pivot to East Asia, the People's Republic of China is the power which tends to step into this part of the world, a big step of which is to get closer to the Kingdom of Saudi Arabia in various ways. The Kingdom of Saudi Arabia, a regional power and major player among the Islamic states, and the biggest exporter of oil in the world, which is also a close ally to the the United States of America to some extent, could play a key role for the People's Republic of China to put its foot in the region. This shows at the same time a difference in alliance nature in comparison with the Cold War era, which was the time for permanent and comprehensive alliances; the

Kingdom of Saudi Arabia can play a perfect positive balance game between different global main powers in the current post-polar world order, which is the era of interim and subject-based alliances.

The Kingdom of Saudi Arabia, looking at the People's Republic of China as a second option along with others like France, South Korea, and Argentina for different aspects of its nuclear energy project, uses it as leverage in its negotiations with the the United States of America. It seems that the first priority of the Kingdom of Saudi Arabia is to have the most modern American nuclear energy technology for the full fuel cycle including enrichment on its own soil. But if not possible, it can be a Chinese version without any similar limitation. That is how the Kingdom of Saudi Arabia presses the the United States of America to change its nuclear energy cooperation policy as per Article 123 for Saudi and make an exception for it, which is not easy.

Situation of the US with Regard to Saudi Nuclear Ambitions: Dilemma with the Islamic Republic of Iran, Israel, and the People's Republic of China

The other sensitive issue that the the United States of America faces in case of giving the full uranium enrichment cycle to the Kingdom of Saudi Arabia is the acceptance of this policy in Tel Aviv. Israel, the only regime in the Middle Eastern region who already has a nuclear energy arsenal thanks to the Western powers, is very close to its soil, giving uranium enrichment to the Kingdom of Saudi Arabia is again a breach of former policies to always stay advanced against the Arab and Islamic countries implicitly. So, the the United States of America is in a deep dilemma with the local enrichment desire from the Kingdom of Saudi Arabia: all the Islamic Republic of Iran-wise, the People's Republic of China-wise, and Israel-wise. Postponing the issue is the only way the US takes to purchase time over the years. Relations with the Kingdom of Saudi Arabia do not let the the United States of America put pressure more than a certain amount. Not balancing these relations with a similar one with the Islamic Republic of Iran makes Saudi in the position to balance the the United States of America with the People's Republic of China instead.

Dilemma of the Islamic Republic of Iran to Support This Idea or Not

The Islamic Republic of Iran, which didn’t take any serious position about the Kingdom of Saudi Arabia's nuclear energy project, is also on a similar dilemma: on one hand, the Kingdom of Saudi Arabia is its main competitor in the Islamic world and a serious regional competitor. This is why the Islamic Republic

of Iran logically should not feel relaxed if the Kingdom of Saudi Arabia reaches a domestic nuclear energy industries and enrichment capability in which the Islamic Republic of Iran is the only one in the MENA region; because it breaks the Islamic Republic of Iran's exclusivity and the relative advantage to Saudi; the same reason for which Saudi seeks to have a similar capability to the Islamic Republic of Iran and put its maximum the same limit the Islamic Republic of Iran has. On the other hand, domestic enrichment and having a full nuclear energy fuel cycle from the Islamic Republic of Iran's official position, the absolute right of any NPT member as a part of a peaceful nuclear energy program; what cannot be neglected in a specific case. Establishing such a cycle in the Kingdom of Saudi Arabia also approves the Islamic Republic of Iran's current position, and future challenging of it would be much more difficult for the opponents. Also, it is another weakening source for Israel.

Normalization with Israel

At the end, it is important to note that the Kingdom of Saudi Arabia conditioned any normalization of relations with Israel officially to three items, one of which is receiving the most modern American nuclear energy facilities and full enrichment cycle of fuel on its own soil. The other two are a fair solution for Palestinians, which is a two-state solution from Riyadh's point of view, and a high-level security treaty with the the United States of America.18 Although the Abraham Accords are not that much on the table according to the Gaza war, at least for a significant while of time.

Conclusion

the Kingdom of Saudi Arabia's strategic pursuit of nuclear energy capabilities emerges as a multifaceted endeavor, shaped by its regional rivalries, especially with the Islamic Republic of Iran, and its aspirations for enhanced global stature. The Kingdom's nuclear energy ambitions are not merely an extension of its energy policy but a calculated move within the complex chessboard of Middle Eastern regionern geopolitics. By aligning with powerful nations such as the the United States of America and the People's Republic of China, the Kingdom of Saudi Arabia not only seeks to secure advanced nuclear energy technology but also aims to position itself as a formidable player in the regional balance of power. This

[18] (Al-Madhaji, 2023)

pursuit, however, is fraught with challenges and risks, particularly in navigating the intricate web of international nuclear energy non-proliferation norms and the geopolitical interests of other regional actors, including Israel and the Islamic Republic of Iran.

As the Kingdom of Saudi Arabia continues to advance its nuclear energy agenda, it will likely remain a topic of significant international scrutiny and debate. The implications of Saudi nuclear energy capabilities extend beyond regional dynamics, potentially influencing global nuclear energy policy and the future direction of nuclear energy non-proliferation efforts. The Kingdom's nuclear energy strategy, therefore, must be understood not only in terms of national security and energy independence but also within the broader context of its diplomatic relations and regional ambitions. Ultimately, the Kingdom of Saudi Arabia's nuclear energy trajectory will significantly impact the stability and security architecture of the Middle Eastern region, posing critical questions for international policy and regional diplomacy.

Bibliography

Alberque, W., & Ibraheem, A. (2023). *Saudi Arabia's partner in pursuing civilian nuclear power: China or the US?* IISS. Retrieved November 17, 2023

Al-Madhaji, M. (2023). *Saudi Arabia's Nuclear Ambitions: US Apprehensions and China's Allure.* Wilson Center. Retrieved December 13, 2023, from https://www.wilsoncenter.org/article/saudi-arabias-nuclear-ambitions-us-apprehensions-and-chinas-allure

Borger, J. (2023). *Crown prince confirms Saudi Arabia will seek nuclear arsenal if Iran develops one.* The Guardian. Retrieved September 21, 2023

Convention on Nuclear Safety. (n.d.).

Davenport, K. (2023). *Saudi Push for Enrichment Raises Concerns.* Arms Control Association. Retrieved November 2023

Graham-Harrison, E., Kirchgaessner, S., & Borger, J. (2020). *Revealed: Saudi Arabia may have enough uranium ore to produce nuclear fuel.* The Gaurdian. Retrieved September 17, 2020

Henderson, S. (2023). *Saudi Arabia Signals It Will Accept Stricter Nuclear Inspections.* The Washington Institute for Near Easy Policy, Washington. Retrieved September 26, 2023, from https://www.washingtoninstitute.org/policy-analysis/saudi-arabias-nuclear-asks-what-do-they-want-what-might-they-get

Henderson, S., & Schenker, D. (2023). *audi Arabia's Nuclear "Asks": What Do They Want, What Might They Get?* The Washington Institute for Near East Policy, Washington. Retrieved August 15, 2023, from https://www.washingtoninstitute.org/policy-analysis/saudi-arabias-nuclear-asks-what-do-they-want-what-might-they-get

https://www.govinfo.gov/. (n.d.). Retrieved November 13, 1998, from https://www.govinfo.gov/content/pkg/COMPS-1630/pdf/COMPS-1630.pdf

Kiimballll, D. (2023). *Just Say 'No' to Uranium-Enrichment Cooperation With Saudi Arabia.* Arms Control Association. Retrieved October 2023

Nakano, J. (n.d.). *The Saudi Request for U.S. Nuclear Cooperation and Its Geopolitical Quandaries.* Center for Strategic & International Studies. Retrieved September 7, 2023

(2023). *Nuclear Power in Saudi Arabia.* London: World Nuclear Association.

(2023). *Prospects for U.S.-Saudi Nuclear Energy Cooperation.* Congressional Research Service. Retrieved May 19, 2023, from https://crsreports.congress.gov/

Schneider, T. (2023). *Saudi Arabia could convert civilian nuclear to military, Israeli expert warns.* Times of Israel. Retrieved August 2, 2023, from https://www.timesofisrael.com/saudi-arabia-could-convert-civilian-nuclear-to-military-israeli-expert-warns/

Sohal, S. (2023). *The US Position on Saudi Arabia's Civilian Nuclear Program.* Arab Center Washington DC, Washington DC. Retrieved August 16, 2023

Squassoni, S. (2018). *The Implication of Nuclear Cooperation with Saudi Arabia.* George Washington University, Elliott School of International Affairs, Washington. Retrieved March 21, 2018, from

https://docs.house.gov/meetings/FA/FA13/20180321/108057/HHRG-115-FA13-Wstate-SquassoniS-20180321.pdf

Turak, N. (2023). *Saudi Arabia announces crucial step forward in its nascent nuclear power plans.* CNBC. Retrieved September 26, 2023

ICNST 2024
International Conference on Nuclear Science and Technology
6- 8 MAY 2024 | Isfahan, Iran

An introduction to the management of small reactors development in the world from the perspective of technological innovation system (TIS) (Paper ID : 1381)

MohammadAmin Fakhimi
Parto think tank
mafakhimi@gmail.com

Abstract

Today, the issue of energy is considered as the main axis of countries development. In the meantime, countries achieving the ability to build a nuclear power plant as a complex product system (CoPS) has a double strategic importance from a technological and economic point of view. Meanwhile, "Small Modular Reactors (SMR)" is known as a "game changer" in the new paradigm of the nuclear industry due to its advantages such as greater safety, in-house manufacturing and faster installation, the ability to move to remote and sparsely populated areas. For this reason, achieving the technology of small reactors is accompanied by the serious determination of the policy makers and stakeholders of this industry, and it is necessary to make the necessary plans in order to formulate the policy model for the development of the innovation system. Considering the complexity of this technology and its high dependence on various specialized fields and industries that increase the risk of achievement, the main problem of the research is to analyze the structural and functional components of the emerging innovation system of developing small reactors in the countries of the world and identify its potential failures that Therefore, setting policy priorities in the industry should be done from a path that has a lower probability of failure. For this purpose, the research method is a combination of a systematic review of articles related to the management of small reactors development, along with thematic analysis. In the theme analysis, the structural and functional components of the innovation system of this technology are identified and its potential failures are analyzed. This research can provide a suitable basis for evaluating the possible failures of the formation of the small reactors innovation system.

Keywords: Technological Innovation System (TIS), Small Modular Reactors (SMR), Failure Analysis

Introduction

Since the nature of technological changes is not isolated and invention-oriented, but systematic, the .policymaker should provide the platform for the development and stability of the system in all aspects The prerequisite for this intervention is a precise analysis of the technological scope and forecasting the " challenges and problems of technology development and its consequences . In this regard, the technological innovation system " approach has developed significant literature around the dynamics of the transition process and can provide the possibility of analyzing system failures based on the key factors inhibiting emerging technologies. The technological innovation system approach analyzes technological developments from the perspective of institutional, organizational, economic political, and ,technical changes. This approach is based on the opinion of Carlson and Stankowitz about innovation which considers the most important driver of creation dissemination, and exploitation of technological innovations to be the systematic interactions of actors under institutional infrastructures [1] . Their definition of the technological innovation system is "a dynamic network of actors who interact with each other in an economic/industrial area under specific institutional infrastructures and participate in the production, dissemination and exploitation of technology". The literature of the innovation system introduces the problems that delay the development of the innovation system under the title of "problem", "failure" or "weakness" of the system [2]. Analyzing technological innovation system failures in complex product systems (CoPS) that has high complexity and entanglement has its own requirements. These features are not independent from each other and may have a complementary relationship with each other during the stages of its development, i.e. pre-production, conceptual and detailed design, production, delivery and installation, post-production innovations, maintenance and disposal [3].

The development of nuclear power plant technology as a complex product system (CoPS) has an effect on economic and technological growth at the national level due to its key importance in the entire industry as well as the wide connections of its subsystems with various industries of the country and technological spillovers. This issue, along with the wide benefits of nuclear industry, has attracted the attention of policy makers of countries to achieve a clean and advanced future, the evidence of which has emerged in the world of knowledge and industry. In the meantime, there are evidences of changing the

technological paradigm of the nuclear industry from large and traditional reactors to small modular reactors (SMR). Reactors are equipment that allow the exploitation of nuclear fission to produce heat and energy. According to the definition of the International Atomic Energy Agency (IAEA), being small in addition to physical dimensions means that its production power is less than 300 megawatts [4]. Modularity also means that the systems and parts are assembled in the factory and transported as a unit to the desired location for installation. Various models of these reactors and their type of cooling are being developed, including pressurized water reactors, sodium-cooled breeder reactors, and gas-cooled reactors. Small reactor technology due to advantages such as greater safety and security, manufacturing inside the factory and faster installation, less need for access to cooling water and the ability to move to remote and sparsely populated places, easier and faster decontamination, the ability to last a lifetime and eliminate the need for refueling. Periodically, the need for lower initial capital and other capabilities are known as "game changers" [5]. These advantages and more, have led to the task of providing resources for the development of small reactors in leading countries with very serious private and public investment (such as the US Department of Energy). This issue has been strengthened with the help and advice of some non-profit think tanks on how to design support policies and related grants, which shows that these non-governmental non-profit think tanks are important players in the function of guiding research and directing the innovation system in America. So far, more than 30 projects related to the design and construction of advanced reactors have been signed in America. According to the International Atomic Energy Agency, by the end of 2020, about 70 SMR reactor designs have been presented in 18 countries of the world, of which 18 designs are in the construction stage and 52 designs are in the design stage [6]. According to the future research report of reputable international institutions, the number of these small reactors in the world will experience a growth of more than 20 times by 2043. In such a way that its market share will reach from 72.4 billion dollars in 2023 to 295 billion dollars in 2043. This report shows that by that year, small reactors alone will account for more than 2% of the global energy portfolio [7].

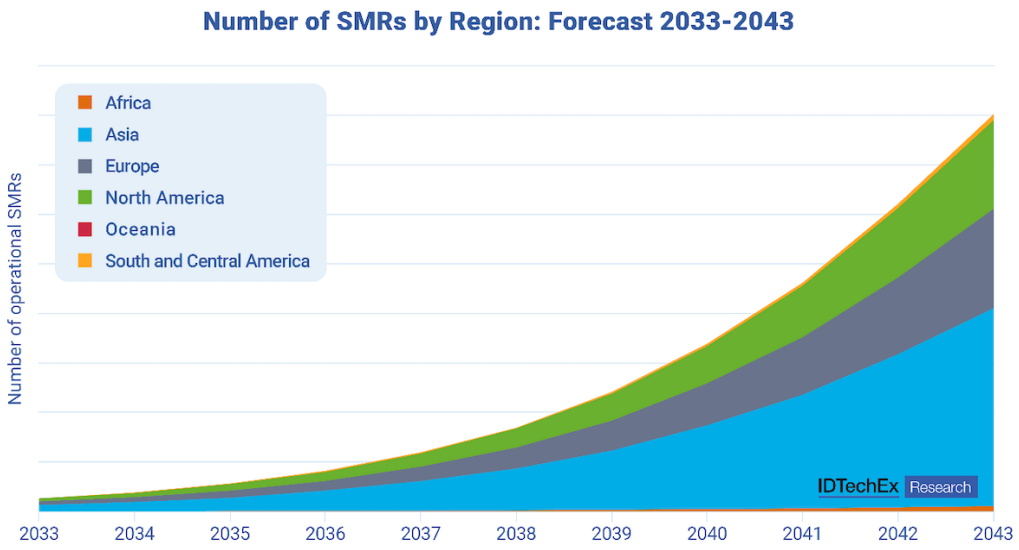

Figure 1 Forecasting the growth of the number of small reactors in the world by continent until 2043

Due to the exponential growth of the market volume predicted for Asia in the next decade, the Atomic Energy Organization also has an approved program for the development of small reactor technology in its agenda, which has been announced many times by the managers of this organization. Therefore, planning in this field requires a more detailed analysis of the paths of success and failure. The International Atomic Energy Agency is also trying to help in the field of sustainable energy production by forming networks and interactions as one of the most important structural components of the technological innovation system of small reactors. One of the international interactions for the development of nuclear innovation (with 33 countries) is the NI2050 program. Since 2015, this program guides and facilitates the technological cooperation of countries in various innovative nuclear issues, especially in the field of design and construction of small reactors [8]. Another important factor to consider in the formation of the innovation system of small reactors in the world is the formation of the market and the demand structure. For this reason, governments follow policies to facilitate demand-side innovation. In successful nuclear companies, market access has been ensured first, and the result of this assurance of the market has been the growth of the technological capabilities of private companies [5]. However, the exponential increase in costs with the prolongation of the development process has led to concerns about the failure of financing mechanisms and shaping the market, and ultimately the failure of the development innovation system of these reactors. Some researchers have stated that the long-term

nature of these projects and political instability may lead to the entry into the "valley of death" and increase the costs and investment needs, so that the continuation of the support of the public and private sectors will be stopped [9]. One of the other examples of the failure of the innovation system for the development of small reactors is the unclear division of roles between companies within the industry and the existence of parallel work and conflict between industry actors [10]. This issue can be caused by the complex nature of technologies and the tacitness of knowledge, which makes the possibility of transferring successful experiences between industries diminished and management gets confused due to the existence of diverse and complex technologies. The review of international experiences shows that, like all complex projects, paying attention to the effective interaction of the components of the technological innovation system of small reactors with each other is very key in this field and can be the factor of its success or failure. Chang et al., in a research that compares the SMART[19] Small Reactor Development Project and two other nuclear projects[20] in South Korea, show that the main factor in the success or failure of these projects is the timely formation of innovation system institutions. Considering that the Smart project has a high degree of technological innovation and there was no similar example before, it requires innovation and fundamental transformation in regulatory structures and institutional requirements. Because phenomena such as locking and path dependence caused by established technologies hinder the development of small reactor technology. This is while in the SMART project, the established regulatory regime based on large nuclear power plants, led to the creation of unnecessary and strict requirements in granting the design license to this project and caused the initial innovative design of SMART to be withdrawn and its technical capabilities reduced. found, a significant slip in the time and cost of the project will occur. This article states that in another project where the innovation system was successfully formed (APR1400 reactor), the development of the regulatory and institutional structure was carried out simultaneously and in sync with the technological development of the product, which is referred to as "institutional and technical co-evolution"[11]. Empirical analysis of the challenges and failures of the innovation system of small reactor development in countries such as America, South Korea and England that have invested in this field shows that "Analysis of the failures of the emerging innovation system of small reactor development" as an emerging technology, significant lessons learned

[19] SMART System-integrated Modular Advanced Reactor
[20] APR1400 (Advanced Power Reactor), KSTAR (Superconducting Tokamak Device)

for countries interested in this. technology will bring. This issue is the main issue of the present research. It should be noted that entering emerging and complex technologies in Iran is unprecedented. For example, entering nanotechnology in 2007 at the same time as other countries, entering quantum in 2013 and its strong growth in the country, and entering the field of nuclear radiopharmaceuticals are other examples that have faced various challenges with rapid growth. The studies from these experiences can have lessons learned for entering the field of small reactors.

Technological innovation system theory and structural and functional components:

The point of view of the technological innovation system has a systemic approach to technological changes and states that a dynamic network of agents and institutions that are under certain institutional infrastructures and participate together in the production, dissemination and exploitation of technology determine the speed and manner of achieving technology. Next, the main elements of the innovative technological system, which include structural factors and functional factors, are examined.

Structural factors:

The structural factors that are the components of an innovation system can be considered all the parts of the economic structure that somehow affect learning and research and development and include actors, networks, institutions and infrastructures. These factors can be considered nationally, sectoral or related to a specific technology.

Functional factors:

The functions of the system focus on the performance of the system components and actually on the processes that are important for the optimal performance of the innovation system. These functions are considered factors of the effective process on the development of technology. In fact, functions show the state of a specific innovation system at a specific point in time. In the latest classification of TIS functions, they are placed in seven categories, which are explained below.

Entrepreneurship:

Entrepreneurship means discovering and exploiting business opportunities based on technology and its applications. This function involves testing new technologies, applications, or markets through which a learning process occurs during new business opportunities.

Development of knowledge:

The function of knowledge development includes all the activities that can be included in the learning process. This learning can be related to various topics such as technical knowledge, market, networks and consumers. In general, this function refers to the creation of knowledge in the overall process of the system. This function is not limited to the development of knowledge through basic research and includes other types of knowledge development such as experimental development through the cycle of doing, using and interacting.

Dissemination of knowledge:

Since the dissemination of knowledge within the system is necessary to produce new products, services or processes, this function actually refers to the commercialization of ideas and knowledge produced by other system components.

Research orientation:

The function of directing the system consists of activities that select and limit the options available in relation to technologies, their application and their market at different levels. This function, in short, means choosing a specific direction for technology development and not paying attention to other technologies that are not defined in this direction. This orientation depends on national perspectives and priorities.

Shaping the market:

The set of activities that take place with the aim of making the technology competitive compared to the technologies available in the market, are in line with the realization of this function. In short, this function

expresses the necessity that a new technology should be accepted by users and consumers. In other words, a new market must be formed for new technologies to carry out the development and commercialization process of these technologies.

Mobilization of resources:

This function includes a set of activities related to the provision and coordination of the necessary inputs for the development of the innovation system in line with the realization of the resource mobilization function. In general, this function represents the recruitment and allocation of resources needed for different processes of the innovation system. These resources mainly include financial resources and human resources. In this regard, it is also possible to mention the infrastructures used by the actors of the innovation system.

Legitimization:

This function, whose main goal is to deal with the resistance to change by different actors, makes the new technology digestible and justifiable for the actors of the system through promotion, advertising and lobbying activities. The noteworthy point here is that legitimacy is not granted, but is consciously formed through the activities of institutions and individuals and seeks social acceptance.

Types of technological innovation system failures

The literature of the innovation system introduces the problems that delay the development of the innovation system under the title of "problem", "failure" or "weakness" of the system [2]. Some experts have identified systemic issues in various technologies using the technological innovation system, and each of them has presented their own classification of these issues. In their analysis of Sweden's new energy system, Jacobson and Johnson identified a number of factors inhibiting the development and diffusion of technology under actors and markets, networks and institutions. This classification is completely compatible with the classification made by Chaminad and Adquist, which includes the categories of infrastructure and investment problems, transition problems, institutional problems (hard and soft), locking problems, learning and ability problems. , problems related to the network, non-

equilibrium exploitation-discovery mechanisms and complementarity problems. Smith also names four categories of systemic "failures": failure in providing infrastructure and investment, failures related to transition, lock-in failures and institutional failures. The classification of the OECD report of system failures that was published in 1997 is: lack of interactions between actors, mismatch between basic and applied research, bad performance of technology transfer institutions and inefficiency of absorption and information on the part of business enterprises. Weber and Roracher have also classified innovation system failures under three general categories: market failure, structural failure, and transformational failure. Their innovation was to introduce a category of failures under the title of transformation, which includes directional failures, expression of demand, policy coordination and reflection [12].

research method

Considering that many qualitative data have been collected and analyzed, the most suitable method of data analysis is "thematic analysis". Thematic analysis is a way to examine and categorize existing patterns in qualitative data, where scattered data are regularly summarized and a coherent analysis is presented. This method includes identifying basic themes, categorizing these themes under organizing themes, forming comprehensive themes and finally validation by experts. Validation of the analysis with the experts makes the researcher's interpretations and the experiences of the experts to be congruent and appropriate [13], [14].

Also, considering that by reviewing several policy experiences, a summarized picture of actions and challenges is presented, the research strategy is "inductive". Based on the systematic review and content analysis of the selected sources, the initial model of challenges and solutions of other countries for the development of innovation in the nuclear industry is extracted. In the steps of "quality control and validation of findings" and "presentation of final results", a panel was held with the presence of seven experts and activists of this industry, and the research results were modified to make the findings fit with the contextual and institutional conditions of Iran.

Research findings

In this part, the results of the analysis of the failure of the technological innovation system of small reactors based on "thematic analysis" and its matching with the contextual conditions of Iran based on the "panel of experts" are stated. These results include the following four sections:

1. Obstacles to the development of innovative nuclear technologies (such as small reactors) in the world
2. Strategies and policies of countries in the development of innovative nuclear technologies (such as small reactors)
3. The challenges of establishing a platform for the development of innovative nuclear technologies (such as small reactors) in Iran (based on the results of the analysis of the above topic and validation in the panel of experts)
4. Proposed policy solutions for the development of innovative nuclear technologies (such as small reactors) in Iran

1-Obstacles to the development of innovative nuclear technologies (such as small reactors) in the world

The results of the analysis of the obstacles and challenges of the development of innovation in the nuclear industry are listed in the table below. It should be mentioned that the basic themes (codes) have been .avoided for the sake of brevity

Table1: Obstacles and challenges to the development of innovation in the nuclear industry (thematic (analysis results

Row	Organizing themes	Overarching themes	Example explanation
1	The complexity of planning and the exponential increase in costs as the process lengthens	governance system	Due to the long-term nature of these projects, the public sector can hardly maintain support due to political instability. On the other hand, even if the private sector participates in the beginning, it may not be possible to continue support with the passage of

			time and entering the "valley of death", increasing costs and investment needs[15] .
2	Weakness of regulatory institutions	governance system	Most of the countries' legislators are not promoters of nuclear technology development. Because they usually give policy support to industries that have reached maturity and have fewer challenges[16 [. Another important issue is that there are unknown gaps in new technologies such asSMR from the point of view of nuclear safety standards. Although these reactors can comply with the general standards of the Atomic Energy Agency, more lenient rules should be established according to their safety model, which has not yet been developed. Especially since these reactors can be built in a place different from the place of operation.
3	The difficulty of international technology transfer	being open	The need for a research reactor, precision instruments and special equipment on the one hand, and the fact that all facilities are not integrated in one country on the other hand, makes countries use international capacities. However, the required international licenses and safeguards and the reluctance of technology transfer by advanced countries act as a fundamental obstacle. One of the examples of this issue is the failure to transfer the main and key technologies such asRCP (reactor cooling pump) by WEC (American company) to Korea. The restrictions related to the nuclear program of Iran, Japan, Brazil and other countries, as well as the efforts made by the French companyAREVA in weakening the Korean company, are also examples of other types of these challenges[17 [.
4	The limitation of endogenous development due to the heavy dependence on the accumulation of technological and knowledge capabilities	Innovation system	The countries that have followed the path of developing the nuclear industry act the same way in preventing its spread to other countries. On the other hand, the leaders of power plant construction in the world export nuclear power plants at cheaper prices than developing countries, which diminishes its commercial advantage for developing countries [17 [.
5	Traditional management of research budgets	governance system	The main obstacle to innovation is not the lack of research funding. Rather, the main problem is the lack of ability to focus the results of this research towards market application[15] ,On the other hand . for example, some traditional institutions such asthe Nuclear Regulatory Commission (NRC) in America manage well the determination of licenses, guidelines and requirements for light water reactors, but due to the traditional view and the application of strict old requirements, they cannot meet the support needs of advanced reactors. and be new. This issue has caused some companies to leave America[16] .
6	Actor network challenges	governance system	The unclear division of roles between companies within the industry and the existence of parallel work

			and conflict between them make it difficult to manage this industry[17] .
7	Complexity of technology	Innovation system	The complex nature of the technologies of this industry makes countries unable to transfer the successful management experiences of other industries to the nuclear industry, and the management gets confused due to the existence of diverse and complex technologies[11 [.

2- Strategies and policies of countries in the development of innovative nuclear technologies (such as small reactors)

The following table is also based on the analysis of the content of the technological experience of Korea's nuclear industry, international programs, support policies and actions of different countries to develop innovation in the nuclear industry.

Table2: strategies for developing innovation in the nuclear industry (thematic analysis results)

Row	Organizing themes	Overarching themes	Example explanation
1	Policy dynamics and long-term support	governance system	In South Korea's ٥-year plans, science and technology policies are updated[18] Also, the two main wings of Korea's success . are "long-term research and development in the technical phase" and "the performance of the Korean government in the "management phase[19] .
2	Integration and integration of the main institutions of the industry		,In order to resolve the conflict between different industry units it is necessary and necessary to integrate them intelligently and separate the duties of each. The experience of separating the ,roles of two companiesKEPCO andKHNP, is an example of this, which was able to ensure the success of the main phase of .technological transformation of Korean industry in the ١٩٩٠s [11 [
3	Transferring technology in the first phase of Farassi and combining internal capabilities with changing the architecture of the dominant foreign design in the next phase of Farassi	governance system And being open	Examining the experience of nuclear technology development in three countries, China, Korea, and France, shows that the development process of this industry, due to its many complexities, does not begin except with the transfer of technology from the owner country to the recipient country[20] In Korea, this issue was accompanied by the policy of . technological self-reliance, so that the actors of this industry are not used to importing technology and are directed towards the development of internal capabilities[17 [.
4	The use of international cooperation mechanisms, especially	being open	To reduce the costs of the industry and commercialize its outputs, a single country cannot overcome all obstacles because the level of technological maturity in nuclear reactor

	among countries at the same level		in the world determines the costs of designing[21] technology and developing nuclear infrastructure. The main objective of NI2050 international initiative is innovation and market creation for this industry[15 [
5	Export oriented		Korea's ambitious plan to export ٨٠ nuclear power plants and achieve ٢٠٪ of the nuclear energy market in the world implies an export-oriented policy and benefiting from the commercial .benefits of the nuclear industry[17 [
6	A priori instead of a posteriori support	Innovation system	According to the nuclear innovation roadmap in America, the Nuclear Regulatory Commission of the Congress, the National Laboratories and the federal managers of the Department of Energy should change the support from post-project support to pre-project support[16] .
7	Removing barriers to innovation in the business model		In recent years, the business model of some nuclear companies such as)TerraPower andTerrestrial Energy has moved (towards the model of Silicon Valley companies instead of being dependent on government funding. In this way, small but international teams develop technology with the aim of gaining market acceptance[16] .

3 - The challenges of creating a platform for the development of innovative nuclear technologies (such as small reactors) in Iran (based on the results of the analysis of the above topic and validation in the panel of experts)

By presenting the initial findings to the experts and receiving their opinions about the obstacles to the formation of the nuclear innovation system in Iran and potential solutions, it became clear that according to the set of strengths and weaknesses of Iran's nuclear industry, some of the challenges and solutions for the development of nuclear innovation in the countries of the world can be adapted to Iran. and some others need to be completed. The basic obstacles to the development of the industry, based on the opinion of experts, as extracted from the review of the background of the research, were categorized under the two headings of "internal coordination of actors" and " connection with the market and external environment " . The following table shows the most important issues and challenges of the formation of .the industry innovation system

Table3 **Basic obstacles of nuclear industry innovation system (expert panel results)**

Issues and challenges facing the formation of Iran's nuclear industry innovation system

[21] technology readiness levels (TRLs)

The relationship between the industry and the market and the external environment	Internal coordination of industry stakeholders
- The existence of high uncertainty and political fluctuations in international relations and, as a result, the reluctance of foreign companies to enter into long-term technological cooperation .contracts - Weakness of information regarding the applications, spillovers and technological-economic benefits of the industry, especially in .non-energy fields and lack of public awareness - Weakness in the industry's connection with the international environment and lack of benefiting from the benefits of technological cooperation under the International Atomic Energy Agency - Absence of an upstream policy-making institution to regulate the relations between the nuclear industry and other industries such as energy, health and agriculture - Weakness in the connection between industry players and other specialized institutions of the country such as research institutes and private companies - The reluctance of some extra-organizational components of the nuclear innovation system financing institutions, research institutes and) companies) to participate in the technological projects of the industry due to the possibility of foreign sanctions	- Predominance of the political-security approach over the technological-economic approach in the industry and not facilitating the entry of private companies - - power technologies - Lack of familiarity of the industry players with the concepts of innovation management and technology policy making and as a result weakness in technology foresight and strategic .planning - Using technologies and infrastructures that are at the end of the technology life cycle - Leadership instability and the presence of politicization in the removal and installation of managers - Structural disintegration and the existence of parallel work and conflict between companies and sub-groups of the organization - Lack of attention to the attraction and retention of expert human resources and the expanding trend of employee migration - There is a gap in the value chain from the supply of raw materials and fuel to the final stages and commercialization

Conclusion

Iran's nuclear industry needs to make changes in the governance system, technology diplomacy and nuclear innovation in order to overcome two major obstacles, i.e. "weak management and internal coordination" and "weak communication between the industry and the market and the external environment". This shows that success in this industry will not be achieved only by increasing investment in specialized training, research and development and creating infrastructure facilities (physical, financial and human). In other words, things like reforming and creating credit and financial institutions, licensing system and property rights along with the use of foreign policy capacities to facilitate foreign direct investment, purchase and transfer of technology and access to the international market, a fundamental role in the development of innovation in the nuclear industry and a successful transition. It plays with developed countries. Especially for the technology of small modular reactors, the decision on the type of technology and the scale of the power plants depends on several factors such as the country's electricity

development plan and the assessment of the country's capabilities, which requires a separate study. However, the basis for making strategic decisions in this regard is to carry out institutional reforms and understand the macro environmental considerations of this technology. Some of the most important policy proposals are listed below:

Legitimization : creating public acceptance and legitimacy regarding the spillovers and technological-economic advantages of the nuclear industry, especially among knowledge-based companies ;(governance)

Development Innovation ecosystem : paying attention to agility and technological intelligence in choosing ideas and establishing credit funds and risky investments with the aim of expanding previous support for high-cost innovative projects and emerging technologies; Creating, strengthening and facilitating mechanisms for accelerating and supporting innovative businesses in the nuclear industry ;(innovation)

Preparing the upstream document : compiling the nuclear industry document and roadmap and ;determining macro goals and policies based on technological foresight (governance)

Attention to open innovation while maintaining security : separation of safety security and protection considerations of power and non-power sectorsof thenuclear industry, attracting innovators and encouraging the entry of the private sector and knowledge-based companies into the non-energy ;(governance) sector

Education and learning : providing necessary training to key industry players regarding innovation ;management and technology policy (innovation-governance)

Export-oriented targeting : development of technological relations with neighboring countries and other countries as much as possible, with a focus on establishing contracts for the export of nuclear technology ;products (diplomacy)

Capacity utilization International technological cooperation : using the technological cooperation capacities of the Atomic Energy Agency such asINPRO, NI2050 etc. programs and developing scientific ,

and research relations with nuclear laboratories, universities and related think tanks in the world by the ;Nuclear Science and Technology Research Institute (Diplomacy)

Paying attention to the requirements of the technology annex : requiring foreign companies active in the country (currently only Rosatom company in Bushehr) to cooperate in the form of joint venture companies and enter into contractsR&D Jointly with domestic companies with the aim of "adaptation and technological learning based on the announcement of technology attachment (diplomacy- "[22] ;(innovation

Creation of an independent regulatory body : integration between different policy-making bodies in the field of industry development by creating a set of regulators independent of the organization in order to create coordination between the academic sector, knowledge-based companies, the safety system and .the organization and allocate funds around priority projects (governance)

[22] Assimilation

References

[1] B. Carlsson and R. Stankiewicz, “On the nature, function and composition of technological systems,” J. Evol. Econ., vol. 1, pp. 93–118, 1991.

[2] H. Heirani, N. Bagherimoghaddam, and H. Karimian, “Dynamic structural-functional analysis of technology development process in the context of Technological innovation system; The case of Iran combined heat and power(CHP) technology,” J. Technol. Dev. Manag., vol. 2, no. 3, pp. 49–80, Nov. 2014, doi: 10.22104/jtdm.2015.181.

[3] J. Gheidar-Kheljani, A. Esna Ashari, and M. H. Karimi Gavareshki, “Triple the capability, uncertainty and complexity of complex product and system development projects,” Innov. Manag. J., vol. 9, no. 1, pp. 59–99, May 2020.

[4] “Official Web Site of the IAEA,” International Atomic Energy Agency. Accessed: Sep. 08, 2023. [Online]. Available: https://www.iaea.org/, https://www.iaea.org

[5] R. K. Lester, “A Roadmap for US Nuclear Energy Innovation,” Issues Sci. Technol., vol. 32, 2016, Accessed: Sep. 08, 2023. [Online]. Available: https://issues.org/a-roadmap-for-u-s-nuclear-energy-innovation/

[6] I. A. E. Agency, Advances in Small Modular Reactor Technology Developments: A Supplement to the IAEA Advanced Reactors Information System (ARIS). IAEA, 2014.

[7] S. Dale, “Nuclear Small Modular Reactors (SMRs) 2023-2043,” IDTechEx, Cambridge, UK, Forecasting 934, 2023. [Online]. Available: https://www.idtechex.com/en/research-report/nuclear-small-modular-reactors-smrs-2023-2043/934

[8] W. D. Magwood, “Nuclear Innovation 2050,” OECD, 2018. [Online]. Available: https://www.oecd-nea.org/ndd/ni2050/ni2050_%20brochure.pdf

[9] “Capacities and capabilities of South Korea science and technology,”).. Center for Progress and Development of Iran, 2012.

[10] C. Son and J.-Y. Choung, “Platform design and imitative innovation inside the transition black-box: Korean nuclear power plant APR1400 case,” Asian J. Technol. Innov., vol. 22, no. 1, pp. 67–85, Jan. 2014, doi: 10.1080/19761597.2014.905230.

[11] J.-Y. Choung and H.-R. Hwang, “Institutional capabilities and technology upgrading: The case of the nuclear industry in Korea,” Technol. Forecast. Soc. Change, vol. 145, pp. 284–294, 2019.

[12] K. M. Weber and H. Rohracher, “Legitimizing research, technology and innovation policies for transformative change: Combining insights from innovation systems and multi-level perspective in a comprehensive ‘failures’ framework,” Res. Policy, vol. 41, no. 6, pp. 1037–1047, Jul. 2012, doi: 10.1016/j.respol.2011.10.015.

[13] V. Braun and V. Clarke, “Using thematic analysis in psychology,” Qual. Res. Psychol., vol. 3, no. 2, pp. 77–101, Jan. 2006, doi: 10.1191/1478088706qp063oa.

[14] N. King and C. Horrocks, Interviews in qualitative research. Los Angeles: SAGE, 2010.

[15] W. D. Magwood, “Nuclear Innovation 2050,” International Atomic Energy Agency, 2018. [Online]. Available: https://www.oecd-nea.org/ndd/ni2050/ni2050_%20brochure.pdf

[16] R. K. Lester, “A roadmap for US nuclear energy innovation,” MIT Univ., 2016.

[17] C. Son and J.-Y. Choung, “Platform design and imitative innovation inside the transition black-box: Korean nuclear power plant APR1400 case,” Asian J. Technol. Innov., vol. 22, no. 1, pp. 67–85, Jan. 2014, doi: 10.1080/19761597.2014.905230.

[18] CPDI, “Capacities and capabilities of South Korea science and technology,” Center for Progress and Development of Iran, 2012. [Online]. Available: international.ut.ac.ir

[19] T. J. Lee and Y.-J. Lee, “Technological catching-up of nuclear power plant in Korea: the case of OPR1000,” Asian J. Innov. Policy, vol. 5, no. 1, pp. 92–115, 2016.

[20] M. N. Dudin, E. E. Frolova, J. A. Artemieva, N. V. Ivanovskaya, and E. V. Sitkareva, “Transfer of innovation technologies as a factor of the world nuclear power industry development,” Int. J. Appl. Bus. Econ. Res., vol. 14, no. 9, pp. 5723–5736, 2016.

ICNST 2024
International Conference on Nuclear Science and Technology
6- 8 MAY 2024 | Isfahan, Iran

Nuclear fusion propulsion and its role in futurolog\y and development of space exploration (Paper ID : 1558)

Mohammad Nikoosefat [1*], Maryam Ebrahimi [2]

[1] *Nuclear Physics Group, Faculty of Basic Science, Comprehensive University of Imam Hossein, Tehran, Iran.*

[2] *Faculty of Physics and energy Engineering, Amirkabir University of Technology, Tehran, Iran.*

** Email: mohammad.nikoosefat91@gmail.com*

Abstract

Nuclear fusion is a new and efficient way to produce energy for the present and the future. The most important advantages of nuclear fusion are cleanliness, safety, cheapness and abundance of deuterium, which is the primary fuel of fusion reactors and is present in large quantities in ocean water. Other applications of nuclear fusion include the production of radiopharmaceuticals in the diagnosis and treatment of various types of cancer, radiation therapy, materials science, nanotechnology, and nuclear fusion propulsion. During the last years there has been considerable interest in new propulsion systems. Over this time the nuclear propulsion systems have grown considerably and fusion propulsion devices are generally preferred for future space exploration. High energy density triggers (such as lasers, particle beams or antiprotons) have been considered for detonating the fusion fuel. Also fissionable material can be used to boost the performance of a fusion system. There are several challenges to realize the idea of nuclear fusion propulsion, which physicists are researching to overcome them. In this research, while expressing the latest scientific achievements in the field of nuclear fusion propulsion, the upcoming challenges in the development of this new space technology are examined. If pulse nuclear fusion propulsion can become a reality then the performance is enough to complete manned missions to the inner planets in weeks and the outer planets in months and this is a great scientific achievement for humanity.

Keywords: Nuclear fusion propulsion, Space exploration, Futurology, Upcoming challenges.

Introduction

Magnetic fusion has the potential to facilitate the efficient and extensive exploration and development of the solar system. Various theoretical fusion reactor designs suggest that magnetic fusion could be beneficial for space activities, especially propulsion in space. These designs are characterized by using the D-^{3}He fuel cycle, utilizing plasma for direct thrust, and following continuous, low-thrust trajectories. This paper outlines the general arguments supporting the use of magnetic fusion power in space, analyzes fusion fuels and setups, studies the trajectories of fusion rockets, and delves into possible missions. Thirty years ago, during the initiation of the Apollo lunar landing mission, a group of academics began to focus on exploring the other planets in the Solar System. They discovered that while chemical rockets can carry people from Earth to orbit, more advanced propulsion is needed for efficient travel to other planets. They determined that fusion energy is a promising option for space missions. Research on long-range propulsion was inactive for many years due to the U.S. and Soviet space programs concentrating on activities in Earth's orbit. President Bush's Space Exploration Initiative (SEI) has recently revitalized human efforts to expand into the Solar System. The Space Exploration Initiative (SEI), along with advancements in fusion physics and technology and the discovery of a substantial lunar reserve of 3He, a highly promising fuel for magnetic fusion energy (MFE) propulsion when combined with deuterium (D), are driving a renewed interest in utilizing fusion power in space. Two main things that are taken into account when choosing a propulsion system for a mission to another planet are the need for high thrust power per unit mass and high exhaust velocities to get the best trajectories and highest payload percentages. Chemical and nuclear-thermal rockets have great specific power but are limited to exhaust velocities below 104 m/s, which is insufficient for efficient solar system propulsion that requires velocities at least ten times higher. Nuclear-electric propulsion achieves high exhaust velocities, but with specific powers around ten times lower than those projected in hypothetical fusion reactor studies. A fusion system utilizing plasma for thrust generation achieves a significantly high exhaust velocity. When selecting a fuel cycle, specific power is the key criterion, and the considerations are notably distinct from those for a fusion reactor on Earth. Direct thrust is essential for achieving superior performance compared to nuclear (fission)-electric propulsion, as both require similar radiation shielding and power conversion. Reactions that produce a significant amount of their fusion power as neutrons or bremsstrahlung radiation are not ideal for magnetic fusion. In ICF systems, micro-explosions typically happen in a way that allows

most neutrons to escape without impacting any structure due to the space they occur in. Due to its higher power density, D-T fuel is preferred for certain geometries, even with only a 20% charged-particle power component. This makes it the ideal candidate for inertial confinement fusion (ICF), particularly when compared to D-^{3}He ICF, which necessitates very large pellet gains and, consequently, high-power lasers or beams. An issue with using D-T fuel is the necessity of incorporating a tritium-breeding 'blanket' and tritium-processing facility, which may not be feasible if neutrons escape into space. Alternatively, a separate tritium-supply source must be utilized to provide the required 2 Mg (tonnes) of tritium for a Mars mission. A limited quantity of D-^{3}He fuel will be required due to the addition of materials to the exhaust plasma to enhance thrust in D-^{3}He fuel. The ^{3}He source is expected to come from the Moon first and later from the gas giant planets. The fusion-rocket technology is envisioned for extensive space exploration and development, focusing on regular operations on the Moon and activities in the outer solar system [1, 2]. Several studies of space fusion propulsion have been performed, and an overview of these studies is provided in the next section.

Research Theories

Several investigations of space fusion propulsion have been performed, although all have been minor in scope. According to research [1], the benefits of exploring the Solar System in terms of science and economics will become apparent in the future. Efficient propulsion, which can be provided by magnetic fusion, is crucial for this endeavor. Multiple potential reactor designs seem promising, but they require significant study and development. Some fusion reactor configurations that have been studied for space applications are as: Simple mirror, Tandem mirror, Dipole, Field-reversed configuration (FRC), Colliding compact toroids, Spheromak, Spherical torus (ST), Bumpy torus, Spherically convergent ion flow (SCIF). The fuel cycle options are restricted, and it is probable that D-^{3}He fuel will be used to operate magnetic fusion propulsion reactors. Magnetic fusion technology is expected to offer favorable mission parameters, such as one to three months travel time to Mars or payload fractions ranging from 60% to 80%. These parameters could facilitate the establishment of colonies, resource acquisition, and scientific outposts [1].

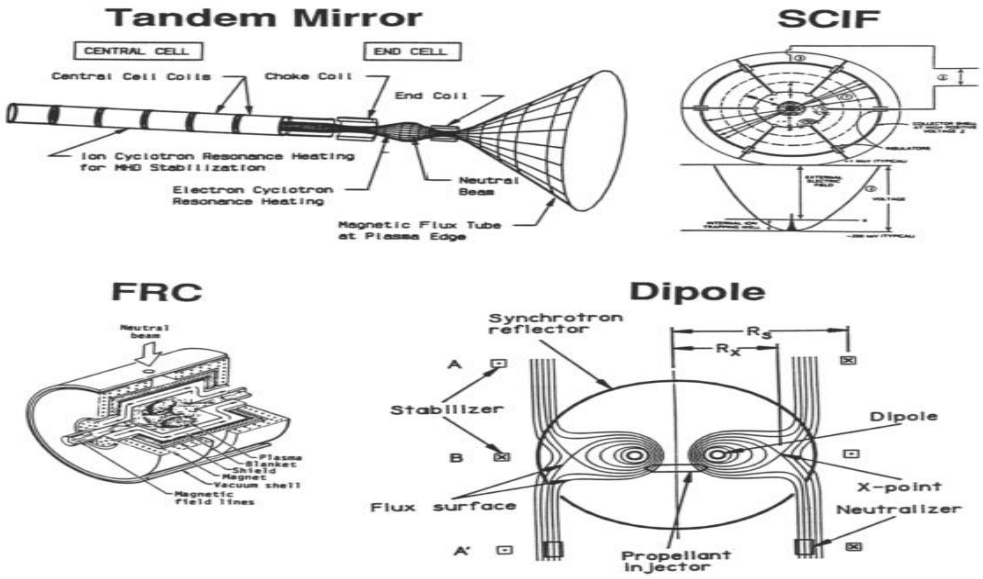

Figure 2- Some potential D-3He magnetic fusion propulsion configuration options [1].

In research [2], two distinct proposals for fusion-based space propulsion have been compared. The first proposal relies on propulsion through the hypothetical ejection of fusion products, known as the ash drive. The second concept utilizes an extra coolant to boost performance. The coolant was originally thought to be gaseous and is responsible for much of the propulsion, so the term "working gas drive" has been suggested. Propulsion properties are assessed for four fusion reactant pairs: deuterium-tritium, D-^{3}He, ^{3}He-^{3}He and ^{11}B-p. Hydrogen is the preferred coolant in operating gas motors because of its remarkable caloric and propulsive qualities. Comparative studies indicate that gas drives outperform ash drives in terms of specific impulse, although ash drives produce significantly less thrust than gas drives. A significant disadvantage of ash drives is their relatively low thrust efficiency. Most of the plasma power must be dissipated as waste heat, resulting in excessively heavy radiator masses. When thermal fusion propulsion becomes fully developed, it can significantly influence space travel. This is mostly because of the high energy density of nuclear fusion. These systems seem to facilitate astronautic trips in the Solar System. However, this pertains to the system architecture. The functional gas drive concept was found to be more promising than the ash drive technique in this study. Ash drives that rely solely on ejecting fusion products have average efficiency, high exhaust velocity, weak thrust, and, based on system mass considerations, result in massive masses that lead to minimal acceleration. A mission

simulation in progress suggests that ash drives could be beneficial for long-distance missions to locations past Neptune and Pluto, like the Haumean system, Kuiper Belt Objects, or potentially even the Oort Cloud. Based on preliminary simulations, it is estimated that a distance of 400 astronomical units may be traveled in around seven to 10 years. This can be likened to the mission outlined in reference [3], which specifies timeframes of 20 to 40 years using innovative electric propulsion. The increased mission time and reduced fuel usage make ash drives relatively intriguing for robotic exploration of the outer solar system. Ash-powered propulsion systems could expand humanity's reach within the solar system and potentially into interstellar space [2].

As mentioned in researches [2, 3, 6-13], fusion for propulsion faces challenges due to fuel temperatures of $\mathbf{10^8}$ K or higher, reaction products with MeV-range kinetic energies, large reactor sizes, and a higher neutron flux than nuclear fission. Fusion is classified based on the method used for confining the plasma, with Magnetic Confinement Fusion (MCF), Inertial Confinement Fusion (ICF), Magneto-Inertial Fusion (MIF), and Inertial Electrostatic Confinement Fusion (ICF) being the most commonly studied approaches. MCF uses strong magnetic fields to confine low-density plasma over a large spatial and temporal scale, reducing thermal losses. The primary device used for fusion confinement is the tokamak, but there are various spin-offs like spheromaks, Reversed Field Pinch (RFP), and stellarators. Polywell and Reversed Field Configuration (FRC) fusion approaches can be partially categorized as MCF, but they involve inertial aspects and differ from tokamak-type machines. ICF compresses a solid-state target using high-energy laser pulses or ion beams, usually a hollow shell with stratified layers of hydrocarbons and deuterium-tritium ice. The process can be broken into four phases: ablation, implosion, stagnation, ignition, and burn. The National Ignition Facility (NIF) is the largest scale device, with claims of breakingeven in the next few years. IEC is a method of radially confined ions using a spherical electrostatic field, simple and easy to build despite limited funding. Approaches like the Polywell concept use an external cusp field to mitigate limitations. Magneto-inertial fusion (MIF) uses a magnetic field to reduce thermal losses and enhance fuel self-heating, relying on a liner that is energetic enough to compress the target, behaves as a stable magnetic flux conserver, and confines the target long enough for the fusion yield to exceed the liner driver and target generation energies. Fission-fusion hybrid reactors have been developed for over 50 years, primarily for military applications. Theoretical developments by Winterberg involve a relativistic central electron beam, a high voltage pulse, and a surrounding liner.

The concept of thermonuclear fusion for propulsion has been around since the late 1950s, with notable works from Englert and Hilton. NASA's program dedicated to fusion energy for space propulsion and power from 1958 to 1978 focused on basic plasma physics, cryogenic and superconducting magnet development, and high temperature confinement. Alternative fuel cycles can lower costs by considering MIF-based systems and fusion fuel options, thereby reducing the overall cost of fusion propulsion..The most crucial reactions are as follows:

$D + T \rightarrow \boldsymbol{\alpha} + n$ 17.59 MeV	$D + D \rightarrow T + p$ 4.014 MeV
$D + D \rightarrow {}^{3}He + n$ 3.27 MeV	$D + {}^{3}He \rightarrow \alpha + p$ 18.35 MeV
$D + {}^{6}Li \rightarrow \boldsymbol{2\alpha}$ 22.374 MeV	$D + {}^{6}Li \rightarrow p + {}^{7}Li$ 5.026 MeV
$D + {}^{6}Li \rightarrow n + {}^{7}Be$ 3.38 MeV	$p + {}^{11}Be \rightarrow 3\alpha$ 8.68 MeV
$n + {}^{6}Li \rightarrow T + \boldsymbol{\alpha}$ 4.86 MeV	$n + {}^{7}Li \rightarrow T + \alpha + n$ -2.87 MeV

The University of Alabama (UAH) has acquired a 3 TW pulse power machine, the Decade Module 2 (DM2), from the Defense Threat Reduction Agency (DTRA) for fusion research. DM2 is a 500 kJ pulsed power facility capable of 2MA discharges at 3 TW of instantaneous power and is under construction at UAH's laboratory. Charger-1 will be a multi-purpose pulsed power laboratory for fusion propulsion experiments, including testing z-pinch diodes and pulsed magnetic nozzle experiments. The program began with the arrival of DM2 in 2012, providing a facility for producing plasmas with thermonuclear temperatures. In the first few years, the program plans to develop and test fusion diode and magnetic nozzle experiments. Due to funding volatility, the facility will be maintained and upgraded for other programs. Near-term upgrades will enable higher scale tests, but may fall short of breakeven. A breakeven facility is planned, with a potential fusion demo mission. TRL-2 is currently focused on fusion propulsion, with Charger-1 allowing proof of concept experiments to determine ignition mechanisms, fuel combinations, and expanding plasma control. TRL-3 experiments demonstrate magnetic nozzle

effectiveness and research plasma instabilities. Based on these researches, a new facility will be built as a prototype ground test facility for pulsed fusion propulsion, incorporating new technologies and potentially using linear transformer drivers (LTD) for electrical pulse conditioning [1, 4-13].

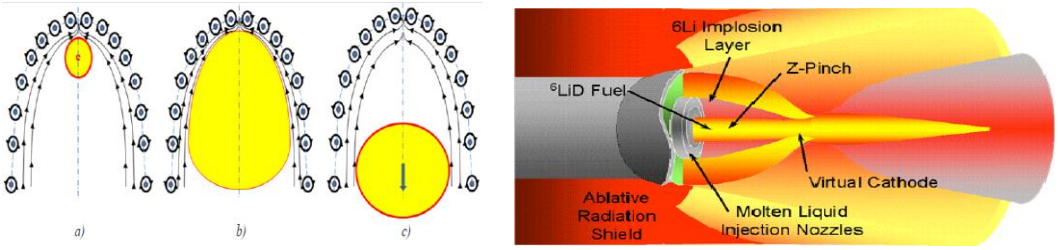

(a) (b)

Figure 3- a) Process of magnetic nozzle operation and b) The Advanced 6Li – D-6Li Fusion Propulsion concept uses fusion to vaporize and control an ablative radiation shield [13].

According to the study [5], D-^{3}He magnetic fusion offers advantages for space applications, including low radioactivity, higher specific power values, flexible impulses, net energy availability, and high energy density. The tokamak architecture is popular for thermonuclear fusion through magnetic confinement, but space applications prefer other configurations like the dipole due to their simplicity and high specific power. The dipole configuration is simpler and may produce greater specific power, but extensive experimentation is needed to assess feasibility and minimize costs. Fusion propulsion devices are large and heavy, making full-scale tests on earth challenging. Magnetic fusion reactor designs for space applications have been analyzed, calculating specific powers of 1-10 kW thrust/kg. Key features include D-3He fuel, solenoidal magnet geometry, and advanced fusion concepts. Inertial Fusion Energy (IFE) has been proposed for igniting thermonuclear micro-explosions with pulsed laser beams since 1963. The fast ignition concept (FIC) was developed to improve IFE propulsion, focusing on ultraintense and chirped lasers for producing highly directed and ultraintense beams of relativistic electrons in the MeV energy range. The nuclear pulse rocket concept has been improved by combining thermonuclear microexplosion with strong magnetic reflectors. Fission and fusion are energy sources that can be combined to minimize radioactive waste and maintain stability. Penn State University has demonstrated that a fission reaction can ignite a fusion reaction using a small number of antiprotons, making it the most efficient for manned planetary missions. NASA has determined that the Antimatter-Catalyzed Micro-Fusion/Fusion (ACMF) drive concept is the most efficient for manned planetary missions, taking 120

days and requiring approximately 140 nanograms of antimatter and 362 metric tons of propellant. Penn State University has designed a spacecraft called ICAN-II, which would use the ACMF drive for omniplanetary mission within the Solar system. The spacecraft would have a total mass of 625 metric tons, with 82 additional metric tons available for payload. The radiation from ICAN-II's ACMF engine would be intercepted by a 4 meter radius silicon carbide shell, 1.2 meters of lithium hybride to shield fuel rings from high-energy neutrons, and 2.2 meters of shileding to protect the crew modules. Antimatter-powered propulsion concepts fall into four categories: solid core, gaseous core, plasma core, and beamed core configurations. Some concepts utilize antiprotons as drivers to catalyze and initiate hybrid fission/fusion processes in compressed plasma or condensed material targets, with antimatter requirements being much lower than those of pure-antimatter systems. CERN and FNAL have developed antiproton production capabilities, including the Low Energy Antiproton Ring (LEAR) and the Antiproton Decelerator (AD).

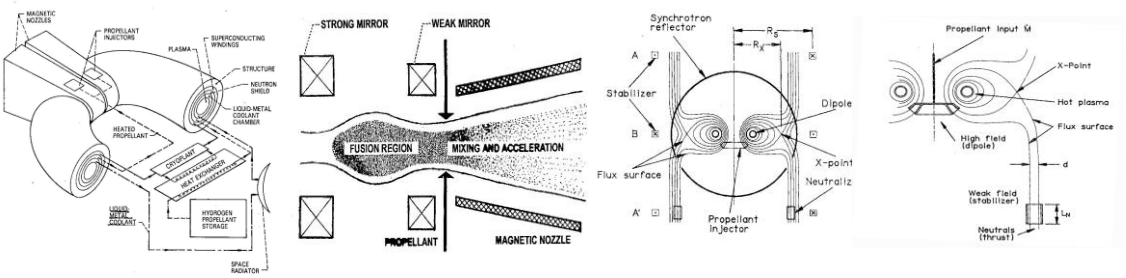

(a) (b) (c) (d)

Figure 4- a) Major subsystems of toroidal fusion rocket propulsion system b) System for direct production of thrust from open magnetic configuration c) Dipole reactor propulsion scheme d) Detail of propellant feed and thruster.

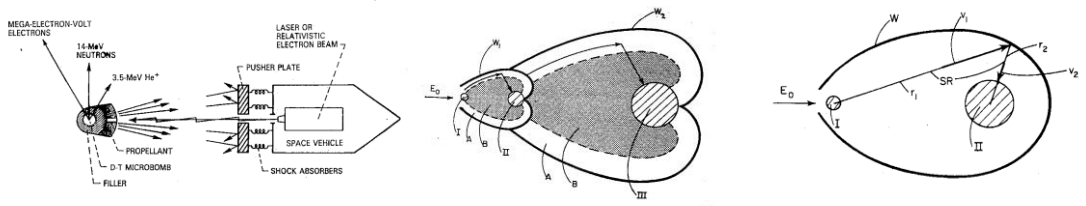

(a) (b) (c)

Figure 5- a) Inertial fusion propulsion system b) Three stage thermonuclear microexplosion target employing the explosive lens technique. I, II, III first, second and third stage; Gap A and medium B with blast velocity vA and vB; W1, W2 walls; Eo input energy to ignite I c) Shock wave mirror for two stage thermonuclear microexplosion. I first, II second stage target; W egg shaped wall; SR blast wave ray from I to II, v1 velocity of incident and v2 of relected wave; r1, r2 bipolar coordinates centred in 1 and II; Eo input energy to ignite I.

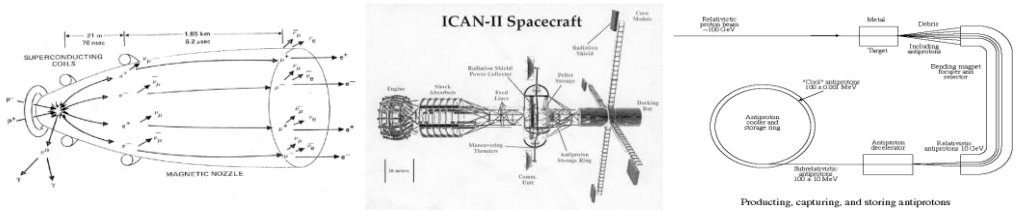

Figure 6- Schematic of an idealized antiproton rocket b) ICAN-II project c) Producing, capturing, and storing antiprotons.

Conclusions

This paper aims to advance fusion propulsion for deep space exploration, demonstrating its necessity for interplanetary space travel. It provides a motivation, justification, and highlighting the need for nuclear technology for single-stage round trip missions to Mars within two years and fusion systems for round trips of less than one year. The paper also discusses the dominance of fusion confinement approaches and the history of fusion propulsion. It suggests that the cheapest, smallest reactors will emerge from the magneto-inertial fusion (MIF) parameter space, which is a hybrid between low density magnetic confinement and beyond solid density inertial confinement. Pulsed z-pinch-based approaches have potential solutions for instabilities, and breakeven systems may require only ~60 MA of curren. Undoubtedly, development and research in the field of nuclear fusion and mastering its application in building space propulsion will be a transformative and authoritative issue for countries in the aerospace field. Nuclear fusion gives humanity the power to explore deep space with greater ability and courage, and with the development of research in this field, we will witness the prosperity of nuclear fusion propulsion technology in the near future. Of course, under the most important achievements of nuclear fusion propulsion technology, we can mention the economic efficiency, the exact explanation of which requires more research in the field of nuclear strategies.

References

[1]. Razin, Y.S., et al., A direct fusion drive for rocket propulsion. Acta Astronautica, 2014. 105(1): p. 145-155.

[2]. Gabrielli, R.A., et al., Two generic concepts for space propulsion based on thermal nuclear fusion. Acta Astronautica, 2014. 101: p. 129-137.

[3]. Poncy, J., et al., A preliminary assessment of an orbiter in the Haumean system: How quickly can a planetary orbiter reach such a distant target? Acta Astronautica, 2011. 68(5-6): p. 622-628.

[4]. Bussard, R.W., Fusion as electric propulsion. Journal of Propulsion and Power, 1990. 6(5): p. 567-574.

[5]. Deutsch, C. and N.A. Tahir, Fusion reactions and matter–antimatter annihilation for space propulsion. Laser and Particle Beams, 2006. 24(4): p. 605-616.

[6]. Gabrielli, R., et al., Two generic concepts for space propulsion based on thermal nuclear fusion. Acta Astronautica, 2014. 101: p. 129-137.

[7]. Kammash, T. and M.-J. Lee, Gasdynamic fusion propulsion system for space exploration. Journal of Propulsion and Power, 1995. 11(3): p. 544-553.

[8]. Petkow, D., et al., Comparative investigation of fusion reactions for space propulsion applications. TRANSACTIONS OF THE JAPAN SOCIETY FOR AERONAUTICAL AND SPACE SCIENCES, SPACE TECHNOLOGY JAPAN, 2009. 7(ists26): p. Pb_59-Pb_63.

[9]. Santarius, J., Magnetic fusion for space propulsion. Fusion Technology, 1992. 21(3P2B): p. 1794-1801.

[10]. Santarius, J.F. Fusion space propulsion–a shorter time frame than you think. in UWFDM-1287, presented at the 53rd Joint Army-Navy-NASA-Air Force (JANNAF) Propulsion Meeting, Monterey, California. 2005.

[11]. Wessel, F.J., et al. Colliding beam fusion reactor space propulsion system. in AIP Conference Proceedings. 2000. AIP Publishing.

[12]. Haloulakos, V. Fusion propulsion systems. in IEEE Thirteenth Symposium on Fusion Engineering. 1989. IEEE.

[13]. Cassibry, J., et al., Case and development path for fusion propulsion. Journal of Spacecraft and Rockets, 2015. 52(2): p. 595-612.

International Conference on Nuclear Science and Technology
6- 8 MAY 2024 | Isfahan, Iran

Human Resources Development in the Nuclear Power Plant: A Case Study on Education in Iran (Paper ID : 1598)

Zamani F. Correspondent[1*], Karimi Sabet J. Co-Author[2]

[1]*Nuclear engineering, shahid Beheshti University, Tehran, Iran*

[2]*Nuclear Science and Technology Research Institute, Tehran, Iran*

Abstract

Sustainable, carbon-free, and affordable electricity production is a key component of the sustainable development of countries. In 2023, nuclear power contributed only 1.1% of Iran's electricity generation, only by the Bushehr Nuclear Power Plant (BNPP). From 2011 to 2023, this plant generated 61,247 million kilowatt-hours of nuclear power, resulting in a reduction of 60,218 thousand tons of various environmental pollutants. This achievement has led to significant savings, including 15,700 million cubic meters of natural gas and 1.97 million barrels of crude oil.

The imbalance between electricity generation and the growing demand poses challenges to air pollution, emphasizing the need for the development of nuclear power plants to generate 20,000 megawatts of nuclear power according to Iran's nuclear vision. Recognizing the importance of designing, developing, and safely operating these plants to prevent potential accidents, this article analyzes and evaluates this aspect with a "Milestone Approach" to achieving the defined goal.

Given that human resources development (HRD) is a crucial topic in the field, especially focusing on education and training, this paper specifically discusses nuclear education's history, reviews the current state of education, and analyze the role of universities in the education of nuclear power human resource development in Iran.

Keywords:Human Resources Development, Education, environmental pollutants, Milestone Approach

Introduction

Today, human societies have an urgent need for energy consumption, and the amount of energy consumption of countries has a direct relationship with the level of development of countries. So that the consumption of energy in developed countries is much higher than the scale of energy consumption in

developing countries, and this shows the active economy of developed countries. Energy production often comes from fossil fuels, which causes greenhouse gas emissions. In the 21st century, greenhouse gas emissions are one of the main challenges of sustainable development and environmental security. One of the disadvantages of greenhouse gas emissions is air pollution, which causes the premature death of millions of people around the world every year. Considering the urgent need of mankind for energy consumption and the harmful effects of fossil fuel consumption, developed and developing societies have encouraged the use of low carbon fuels and clean energy sources such as wind, solar, hydro and nuclear. Among these, nuclear energy production among other low-carbon sources of energy production is of great importance due to the lack of dependencies such as dependence on geographical conditions.

Today, sustainable and low-carbon energy supply in the future of the societies of developed countries cannot be imagined and achieved without taking into account the high share of nuclear energy production in the countries' energy production portfolio. In fact, the sustainable energy production of societies is one of the main solutions to deal with climate change, moving towards increasing the share of nuclear energy in the countries' energy production portfolio. Since the Islamic Republic of Iran is one of the developing countries, it has an urgent need to produce energy for development. Iran is currently facing the challenges of energy production and air pollution caused by the consumption of fossil fuels in such a way that the continuation of this path and the consumption of this amount of fossil fuels cannot be continued not only because of the insufficient resources of fossil fuels, but also the big cities of Iran are facing challenges. It has faced major air pollution during the year. In order to overcome this problem, the Islamic Republic of Iran has included the production of 20,000 megawatts of nuclear power in the next 20 years in its 20-year nuclear vision document. Undoubtedly, it is not possible to create 20,000 megawatts of nuclear power without considering the development of human resources. In the following, after examining the agency's approach to the development of human resources, we will discuss the history of nuclear education in Iran and after examining the current situation, we will draw conclusions.[1]

Milestones Approach

The IAEA Milestones Approach enables a sound development process for a nuclear power programme. It is a phased comprehensive method to assist countries that are considering or planning their first nuclear

power plant. Experience suggests that the time from the initial consideration of the nuclear power option by a country to the operation of its first nuclear power plant is about 10–15 years.

The aim is to help Member States understand the commitments and obligations associated with developing a nuclear power programme. Countries that already have nuclear power can assess their preparedness for expansion.

The Milestones Approach splits the activities necessary to establish the infrastructure for a nuclear power programme into three progressive phases of development, with the duration of each dependent on the degree of commitment and resources applied in the country. The completion of each phase is marked by a specific “Milestone” at which progress can be assessed and a decision can be made about the readiness to move on to the next phase.[2]

The infrastructure development for supporting a nuclear power program unfolds across three distinct phases:

Phase 1: Prior to committing to a nuclear power program, thorough considerations are undertaken. A Pre-Feasibility Study aids the country in establishing a robust national stance, addressing the fundamental question: why pursue nuclear energy? This phase initiates promptly after nuclear power is integrated into the energy strategy.

Phase 2: Preparations for the contracting and construction of a nuclear power plant commence subsequent to a policy decision. This phase entails the establishment of key organizations, alongside the formulation of legal and regulatory frameworks.

Phase 3: Activities encompassing contracting, licensing, and construction of the inaugural nuclear power plant are executed.

Each phase's completion is denoted by a specific milestone, serving as a checkpoint to evaluate development progress and make informed decisions regarding the progression to the subsequent phase. These milestones are:

Milestone 1: Readiness to make an informed commitment to a nuclear power program;

Milestone 2: Readiness to solicit bids/negotiate a contract for the inaugural nuclear power plant;

Milestone 3: Readiness to commission and operate the first nuclear power plant.

As depicted in Figure 1, the Milestones approach encompasses 19 fundamental infrastructure matters necessitating precise actions across the three phases. Accomplishing the prescribed actions for each step signifies the attainment of the corresponding milestone. It's essential to note that the sequence in which these 19 infrastructure issues are presented does not imply relative importance; each one demands meticulous attention.[1]

Figure 1. Nuclear Infrastructure Issues

Three Essential Entities

The establishment of a nuclear power program involves three crucial organizations:

The government ought to establish a mechanism, such as a Nuclear Energy Programme Implementing Organization (NEPIO), to streamline the collaboration among all involved entities. The government holds the ultimate responsibility for safety.

A proficient, autonomous Regulatory Body needs to be established. It holds the responsibility for safety supervision and ensuring adherence to legal and regulatory frameworks.[2]

The Owner/Operator must demonstrate competence in operating the nuclear power plant safely and reliably while meeting regulatory mandates.

In aiding Member States with the implementation of the Milestones Approach, the IAEA has developed additional guidance documents and offers training, expert counsel, and peer review services, notably through the Integrated Nuclear Infrastructure Review (INIR). Utilizing insights from this review, the IAEA formulates tailored, country-specific integrated work plans to help newcomer States address deficiencies in their nuclear infrastructure. Additionally, the IAEA conducts subsequent reviews to monitor their advancement.[3]

One of the 19 important cases in the milestone approach is to pay special attention to the development of human resources. Without a doubt, without having skilled and specialized human resources, progress in the field of nuclear science and technology and the launch and operation of new nuclear power plants are not possible. Therefore, it is necessary to pay special attention to the development of human resources with the aim of achieving 20,000 megawatts of nuclear power in the next 20 years.[4]

Nuclear History in Iran

The history of the entry of nuclear science and technology in Iran can be seen at the same time as the first Iranian graduate in the field of physics, nuclear fundamental particles, and modern optics graduated from Sorbonne in France. In 1320, in a letter to the president of Tehran University, Dr. Mahmoud Hasabi requested the start of education in nuclear fields at the same time as the few advanced countries. After that, in 1334, with the conclusion of the CENTO Treaty between the

countries of Iran, Pakistan, and Iraq, which was one of the clauses of this treaty of cooperation in the field of nuclear education and research, it led to the promotion of nuclear education in Iran. After that, in 1335, with the signing of an atomic memorandum for peace between Iran and the United States, as well as the establishment of the Atomic Center of the University of Tehran, the Peyman Sento Center was moved from Baghdad to Tehran. With the invitation of Dr. Hasabi from Professor Compton, he visited Tehran University's Faculty of Science, which led to the equipping of Tehran University's Atomic Center with the cooperation of the United States. After that, in 1336, the National Atomic Energy Commission of Iran was established under the supervision of the then Prime Minister in 1340. Tehran University's research reactor was started to be built by America in Tehran University's Atomic Research Center; after 6 years in 1340, this reactor reached a critical state for the first time, that in 1335, with the transfer of the atomic center of the University of Tehran, the Atomic Energy Organization of Iran was established, which led to the creation of an independent governance center specific to the field of nuclear science and technology. In 1353, Tehran and Shiraz universities were the first universities to create preparatory courses related to nuclear and send students abroad for graduate studies. After the revolution in 1357, there was a gap of several years. In 1364, Sharif University of Technology started a nuclear engineering master's course, and three years later, Amirkabir University of Technology started to launch a nuclear engineering doctorate course, in the early 80s, the first nuclear engineering faculty at Shahid Beheshti University was established.[7]

Currently, this field is offered in different directions at master's and doctorate levels at the Azad University of Science and Research, Isfahan University, Shahid Beheshti University, Shiraz University, Amir Kabir University of Technology, and the Sharif University of Technology, and at undergraduate level at Islamic Azad University.[8]

The Current State of Nuclear Education in Iran

The information collected from the Higher Education Research and Planning Institute of the Ministry of Science, Research and Technology, the beginning of graduate education in Iran can be considered since 1985 with the launch of the master's course in nuclear engineering at Sharif University of Technology.[6]

The first nuclear science and technology students graduated from Sharif University of Technology in 1988; According to the graph below, the trend of graduates of this field has been growing significantly from 1988 to 20211, although the maximum number of graduates is in the academic

year of 2015, but since that year, the number of graduates in the master's degree has increased It remains almost constant and every year around 500 people graduate from universities under the supervision of the Ministry of Science, Research and Technology (**Fig 2**).

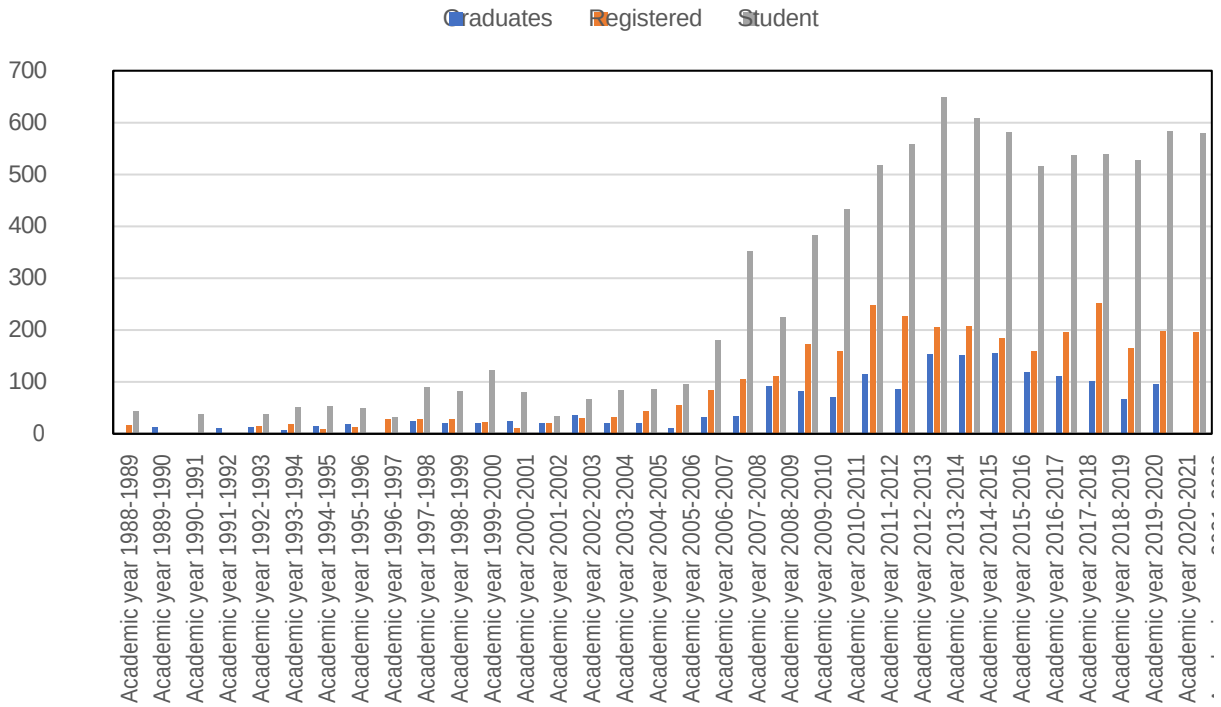

Figure 2. Survey of nuclear engineering master's statistics (Ministry of Science, Research and Technology)

According to the statistics published by the Higher Education Planning Research Institute of the Ministry of Science, Research and Technology, the number of nuclear engineering doctoral students has been increasing until today. So in the academic year 2021-2022, 220 students are studying in fields related to nuclear science and technology, while the number of graduates in this field is an average of 10 people per year for many years. The same is true in development. Iran's manpower is important in the nuclear field.[5]

In total, the number of graduates of the nuclear education system, including nuclear engineering, nuclear physics, and related fields, up to the latest statistics of the Ministry of Interior (i.e. 2022) is 4951 people, of which 85% are graduates. Masters equivalent to 4217 people and Ph.D. The share is 15% and includes 734 people (Figure 3).[8]

Ph.D (15%)

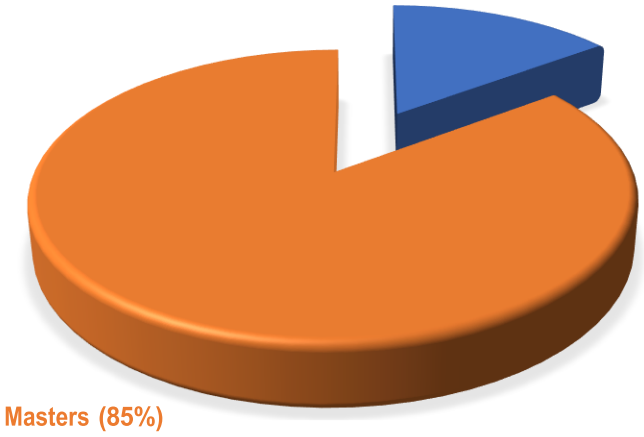

Figure 3. Graduates of nuclear education system

An important point among these is the increase in the share of female graduates since the beginning of nuclear postgraduate studies in Iran. Although women make up about 40% of Iran's postgraduate graduates, but for the first time in the history of Iran, in the academic year 2013-2014, the number of female graduates exceeded that of men, which shows gender justice in the nuclear education system. It is in Iran (Figure 4).[7]

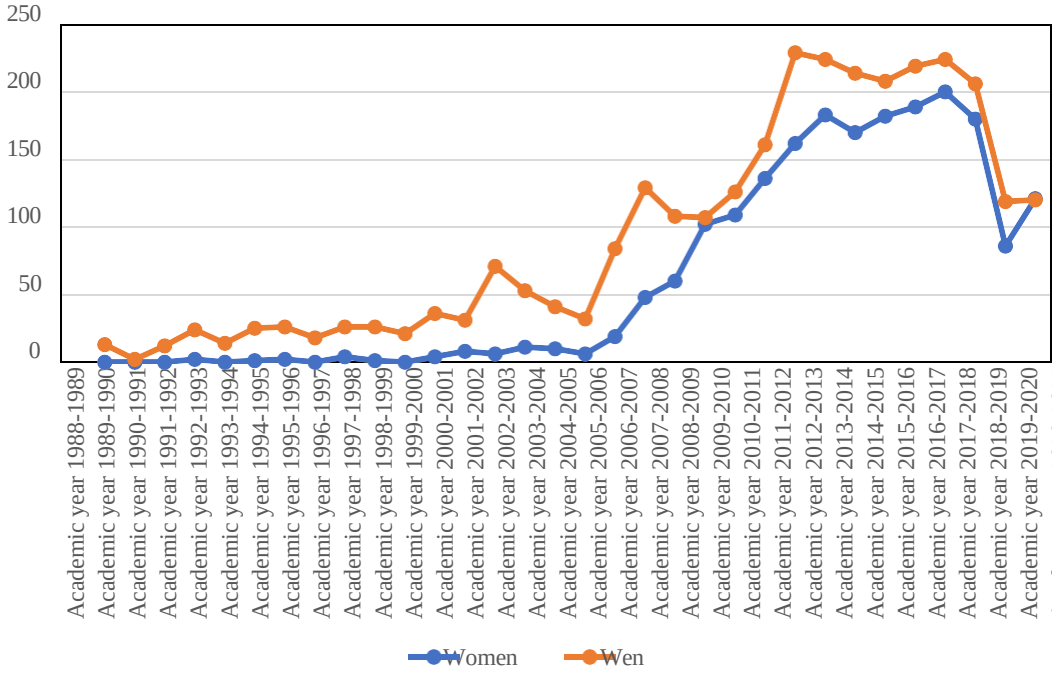

Figure 4. The number of graduates of nuclear postgraduate education by gender

Conclusion

All the developing or developed countries are facing many challenges to provide energy for their industries and human societies, including the provision of cheap energy, and the availability and cleanness of consumed fuel. Considering the great challenge of climate change the increase in temperature and the production of atmospheric pollutants due to the excessive use of fossil fuels, the world has no choice but to use clean and carbon-free fuels, and nuclear energy plays a significant role in this; In such a way that currently in the world, approximately 60 reactors are being built and 110 reactors are being designed and planned. Of these, China ranks first among other countries with 21 reactors under construction, and Asia ranks first among all continents with 39 reactors under construction.[9]

Iran is also facing the challenge of energy shortage and air pollution, and in its development plans, it has put the production of 20,000 megawatts of nuclear power on the agenda, which requires special attention in the development of human resources. By examining the statistics of the number of nuclear students and graduates in Iran, it can be concluded that higher education in this field is far from the goal set, so for the construction of each 1000 MW reactor according to international standards (which of course is country by country) According to geographical, technological, cultural, educational level, etc. conditions, approximately 3,000 workers are needed. Although 73% of this amount will be reduced after construction and in the operation phase, the number and process of entering universities is far from the amount required to realize the production of 20 thousand megawatts of nuclear power. According to the study of the human resource development program model of emerging countries in the nuclear industry such as Qatar, Turkey, Algeria, etc., Iran should first conduct an in-depth study and research on human resource needs, considering the location of the power plants in question and its infrastructure potential. and after that, with the coordination of educational centers including universities and research centers, including the Nuclear Science and Technology Research Institute, as well as the industry, formulate a long-term action plan to obtain the human resources they need. According to the figure below, the development of nuclear industries will not be possible in any country without the cooperation of universities, research institutes, industry, and most importantly, proper governance.

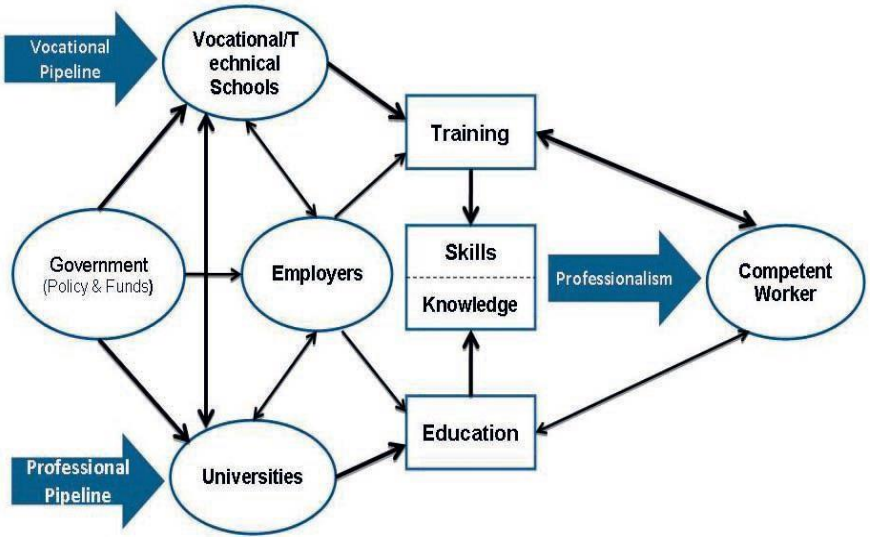

Figure 5. relationship between government, vocational schools, universities and employers[10]

References

[1] Tenaga Nasional Berhad, Annual Report 2015 (TNB, Kuala Lumpur, 2015).

[2] International Atomic Energy Agency, IAEA Nuclear Energy Series (NG-G-3.1): Milestones in the Development of a National Infrastructure for Nuclear Power (IAEA, Vienna 2007).

[3] Tenaga Nasional Berhad, Global Strategy and Domestic Considerations for Nuclear Energy in Peninsular Malaysia (TNB, Kuala Lumpur, 2010).

[4] International Atomic Energy Agency, IAEA Nuclear Energy Series (NG-T-3.10): Workforce Planning for New Nuclear Power Program (IAEA, Vienna, 2011).

[5] International Atomic Energy Agency, IAEA Nuclear Energy Series (NG-G-2.1): Managing Human Resources in the Field of Nuclear Energy (IAEA, Vienna, 2009).

[6] Nuclear Energy Department, Regulatory Economics and Planning Division, "Development of Training Modules for Potential NPP Operator," in TNB HRD Nuclear Power Program (TNB, Kuala Lumpur, 2012).

[7] Nuclear Energy Department, Regulatory Economics and Planning Division, "TNB-EDF Nuclear Roadmap", inPresentation at the TNB Review Team Briefing, Kuala Lumpur, 2014.

[8] M.F. Salim, Report on Working Visit to EDF France (TNB, Kuala Lumpur, 2014).

[9] Nuclear Planning Unit, Regulatory Economics and Planning Division, Nuclear Program Training and Development Database (TNB, Kuala Lumpur, 2015).

[10] Nuclear Energy Department, Regulatory Economics and Planning Division, Summary Development of Curriculum (DACUM) on Nuclear Power, Kajang (2013).

Stable & Radioactive Isotopes

ICNST 2024
International Conference on Nuclear Science and Technology
6- 8 MAY 2024 | Isfahan, Iran

Radiation absorbed dose estimation of 166Ho-EDTMP radiopharmaceutical in humans based on biodistribution data in Wistar rats (Paper ID : 1066)

Reza Bagheri[1,*], Hassan Ranjbar[2]

[1]Radiation Applications Research School, Nuclear Science and Technology Research Institute, Tehran, Iran
[2]Nuclear Fuel Cycle Research School, Nuclear Science and Technology Research Institute, Tehran, Iran

Abstract

Bone marrow malignancies including multiple myeloma are treated by the myeloablative radiotherapy and subsequent stem cell transplantation. Radiopharmaceuticals are used for the selective delivery of radiation absorbed dose to bone marrow. In this work, the radiation absorbed dose of various organs of the adult man from ^{166}Ho-EDTMP radiopharmaceutical was estimated based on biodistribution data in Wistar rats. The MIRD dose calculation method and the Sparks and Aydogan methodology for extrapolation of %IA of organs from animal to human were applied. The results shows that, more than 61% of injected activity is cumulated on the surface of the trabecular and cortical bones. Red marrow and osteogenic cells radiation absorbed doses were estimated to about 1.4 and 3.1 mGy/MBq, respectively. Compared to other aminophosphonate radiopharmaceuticals, ^{166}Ho-EDTMP requires a minimum activity to deliver a therapeutic dose of 25 Gy to the red bone marrow. This work indicates that ^{166}Ho-EDTMP is a promising radiopharmaceutical for bone marrow ablation in patients with multiple myeloma with low undesired dose to other normal organs.

Keywords: ^{166}Ho-EDTMP, Bone marrow ablation, Absorbed dose, MIRD method, Wistar rat.

Introduction

Bone metastases occur in many patients with solid malignant tumors and nearly half of them experience bone pain. Besides, multiple myeloma is another bone related disease that arise from malignant plasma cells in bone marrow [1]. Currently, bone-avid beta emitting radiopharmaceuticals are used for the selective delivery of radiation absorbed dose to tumor cells and bone marrow for bone pain palliation and bone marrow ablation followed by stem cell transplantation [2]. High energy beta emitting radionuclides (with beta particle range of about 50–1000 cell diameter) connected to phosphonates are utilized as bone pain palliative or bone marrow ablative conjugates.

Holmium-166 with short half-life of 1.1 day, two relatively high beta energies (1.85 MeV [51%] and 1.77 MeV [48%]), long penetration range in soft tissue (8.7 mm) and gamma ray for imaging studies (81 keV, 6.7%) is an excellent radionuclide for delivering of high dose in short period of time [3].

Various holmium-166 labeled aminophosphonic acid conjugates have been used in human and normal animal studies for bone marrow ablation including ^{166}Ho-DOTMP [1,4], ^{166}Ho-EDTMP [1,5], ^{166}Ho-PAM [6], which among them, ^{166}Ho-DOTMP is the only clinically used bone marrow ablative agent of holmium-166 [4].

A very limited number of research articles have been published about the ^{166}Ho-EDTMP radiopharmaceutical and its estimated absorbed dose. Appelbaum et al. [5] estimated total radiation absorbed dose of ^{166}Ho-EDTMP for bone marrow and some other organs of a normal beagle in a canine model. In addition, the production, quality control and pharmacokinetic studies of ^{166}Ho-EDTMP compound in Wistar rats were reported by Bahrami-Samani et al. [1].

Although, the theoretical radiation absorbed dose of this radiopharmaceutical has been reported in different animal models (a normal beagle, baboon and male BALC/c mice), no radiation absorbed dose estimation has been directly reported to human organs through the extrapolation between animals and human data.

The aim of this research is to estimate the absorbed dose to each organ of the adult man from ^{166}Ho-EDTMP radiopharmaceuticals for first time based on biodistribution data in Wistar type rats previously reported by the authors [1]. The following methods are used to reach of this goal; the Medical Internal Radiation Dosimetry (MIRD) dose calculation method and the methodology outlined by Sparks and Aydogan [7] for extrapolation of the percent of injected activity (%IA) in human organ from the percent of injected activity (%IA) in animal organ. Although the extrapolation between nonhuman primates (such as beagle, baboon, mice and rat) and human data may lead to overestimation or underestimation of absorbed dose, previously published numerous studies have justified the usefulness of these models for initial absorbed dose evaluations.

Experimental

Biodistribution studies in rats

Production and quality control of ^{166}Ho-EDTMP radiopharmaceutical have been fully-described by our previous work [1]. Biodistribution of ^{166}Ho-EDTMP was studied in normal Wistar rats (190 g) injected with 100 µL (5.55 MBq) of radioactive solution through their caudal vein. The animals were sacrificed by CO_2 asphyxiation at selected times after injection (2, 4, 24, 66 and 168 h). Three rats were killed in each time interval. After drawing blood from the aorta, the heart, liver, kidney, spleen, stomach, intestine, muscle, lung and bone tissues were removed, weighed and counted in an HPGe detector against a standard value of the injected activity. The tissues' radioactivities were stated as percent of the injected activity per gram of that tissue (%IA/g).

^{166}Ho-EDTMP's biodistribution adapted from rats to humans

In the development of radiopharmaceuticals, animal studies are performed to get first approximation of the expected human biokinetics and radiation absorbed dose. However, the biodistribution of radiopharmaceuticals in human body must as soon as possible be investigated using nuclear medicine imaging equipment as a base for the radiation absorbed dose assessments. Several investigations have previously published to extrapolate biokinetic and biodistribution data from animals to humans [7,8] in cases where there is no human data. Regarding the considerable difficulties to extrapolate biokinetic data from animals to human confirmed by Sparks and Aydogan [7], the methodology outlined by Sparks and Aydogan is applied in this study in order to have a rough approximation of radiation absorbed dose in man from ^{166}Ho-EDTMP. Based on this method, in relative organ mass scaling, the percent of injected activity (%IA) in human organ is assumed to be equal to the ratio of the fraction of the total body mass of the organ in human to the fraction of the total body mass of the organ in animal multiplied by the percent of injected activity (%IA) in animal organ:

$$\%IA\ Human\ organ = \%IA\ Animal\ organ \times \frac{\frac{Organ\ mass_{human}}{Body\ mass_{human}}}{\frac{Organ\ mass_{animal}}{Body\ mass_{animal}}} \qquad (1)$$

The weight of selected organs of the adult man and normal Wistar rats are considered according to ICRP publication 23 [9] for humans and Peters and Boyd [10] and Miller et al. [11] articles for Wistar rats. The contents of the gastrointestinal tract were removed by washing and milking before weighing for Wistar rats.

The activity of organs in any time interval after injection of A_0 Bq of ^{166}Ho-EDTMP is calculated from the following equation and the time-activity curves is generated for each source organ according to this equation:

$$A(t) = \frac{\%IA(t)}{100} \times A_0 e^{-\lambda t} \quad (2)$$

2.4. Dosimetric calculations

The radiation absorbed dose in target organs of interest was estimated using methods recommended by the Medical Internal Radiation Dose (MIRD) Committee of the Society of Nuclear Medicine. The calculations are based on the methodology described below:

$$D(r_k) = \sum_h \tilde{A}_h S(r_k \leftarrow r_h) \quad (3)$$

where, D(r_k) stated in (mGy) is the radiation absorbed dose to a target organ, r_k, from a source organs, r_h. $\tilde{A}_h$ is the cumulated activity in the source organ, r_h, and is calculated by the following equation:

$$\tilde{A}_h = \int_0^\infty A_h(t)dt \quad (4)$$

and, the S($r_k \leftarrow r_h$) expressed in [mGy/(MBq s^{-1})], is the specific absorbed fraction of energy for the target organ, r_k, per unit cumulated activity in source organ, r_h. In this study the S-values for holmium-166 are taken from the OLINDA/EXM software [12].

The cumulated activity of each source organ was calculated as the integral of the time-activity curves up to 168 h (more than 6 half-life of ^{166}Ho), plus the integral of the rest of the curve to infinity with a conservative assumption that, organs' activities decay with a physical half-life of holmium-166 (26.8 h). Considering the 168 h spent time after injection of radioactivity (more than 6 half-life of ^{166}Ho), rationality of this assumption is established, especially for organs with the rapid clearance of the radionuclide.

Results and Discussion

Biodistribution of ^{166}Ho-EDTMP in normal Wistar rats

The biodistribution of ^{166}Ho-EDTMP in different organs of Wistar rats up to 7d (168 h) after injection is given in Fig. 1.

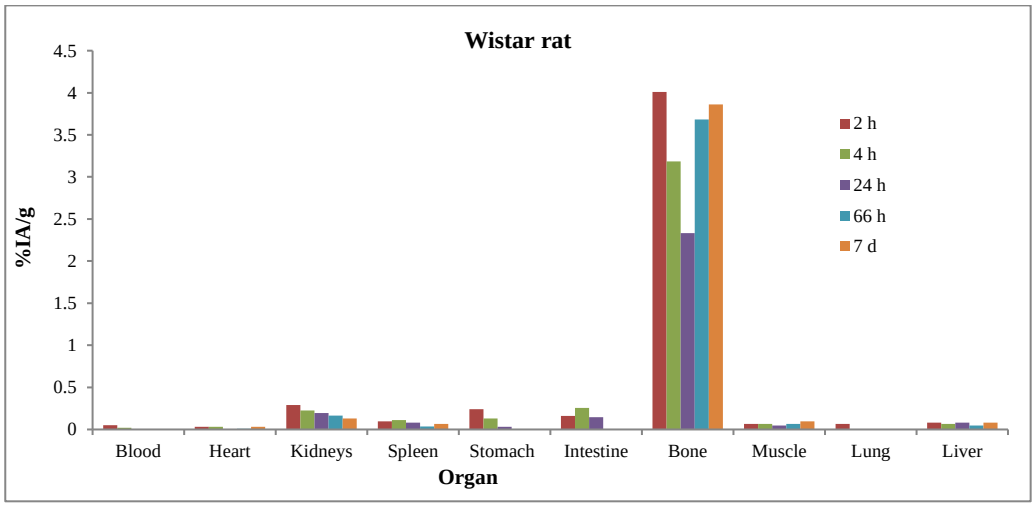

Fig. 1. Percentage of the injected activity per gram (%IA/g) of ^{166}Ho-EDTMP in normal Wistar rat organs [1]

As shown in Fig. 1, the major portion of injected activity is washed out from the blood circulation after 4 h and is rapidly taken up in bones in 2h after administration and is retained almost constant up to 7 d. Significant bone accumulation of the radiopharmaceutical is observed in average (<60%). Rapid and continuous excretion can be observed in the kidneys. ^{166}Ho-EDTMP sparsely accumulated in spleen and liver which can be a major advantage of this compound due to the possibility of increasing the maximum administered activity as a therapeutic radiopharmaceutical.

^{166}Ho-EDTMP's biodistribution adapted from rats to humans

The percent of injected activity (%IA) in human organs, extrapolated from Wistar rats' biodistribution data, are given in Fig 2. This figure shows the fraction of the decay-corrected injected activity that cumulates in each source organ in any time interval. As seen in Fig. 2, most of the activity is cumulated in bone tissue. Radiolabeled phosphonates such as ^{166}Ho-EDTMP, primarily tend to be localized uniformly on bone surfaces (Bagheri et al., 2015). In accordance with the recommendations of the ICRP, human bone surface uptake was considered as the trabecular (cancellous) and the cortical (compact) bones' surface proportion at a ratio of 62% to 38% of the total skeletal surface [13].

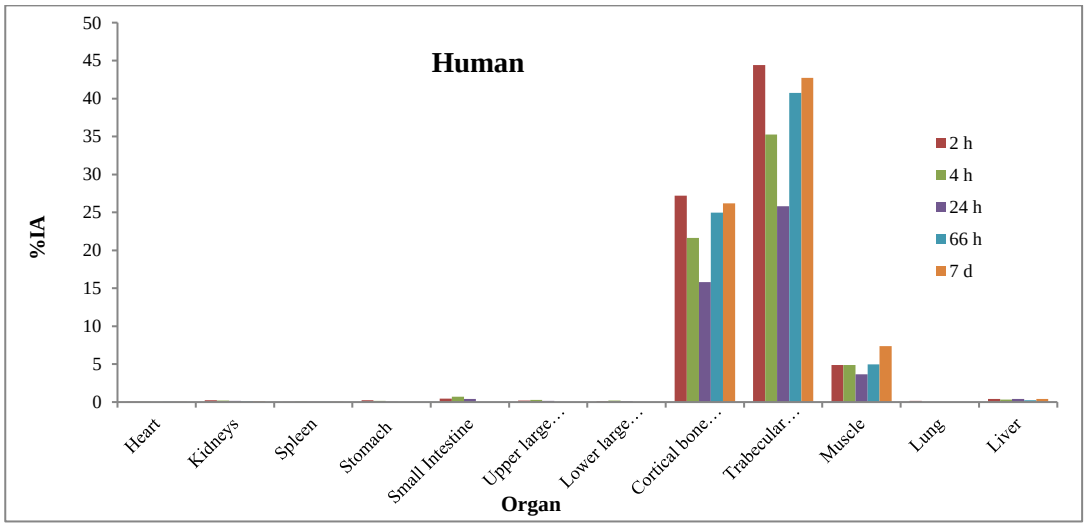

Fig. 2. Percentage of the injected activity (%IA) of ^{166}Ho-EDTMP in the adult man organs

Totally, more than 61% of injected activity is cumulated on the surface of the trabecular and cortical bones. Because of the larger surface area of trabecular bone against cortical one (10.5 m^2 vs. 6.5 m^2), contribution of the trabecular bone from activity distribution on bone is more than the cortical one (ICRP 2002). In addition, about 5% of injected activity will be deposited in muscle due to the large weight fraction of skeletal muscle in human body (about 40% of total body weight). The percent of injected activity in the remaining source organs is less than 1%.

The decay-corrected time-activity curves for source organs of human per injection of 1MBq of ^{166}Ho-EDTMP activity are given in Fig. 3. As shown there most of the activity is deposited on cortical and trabecular bone surfaces. Approximately after the 3 half-lives of ^{166}Ho radionuclide (about 80 h), there are insignificant activities in source organs except for bone tissues.

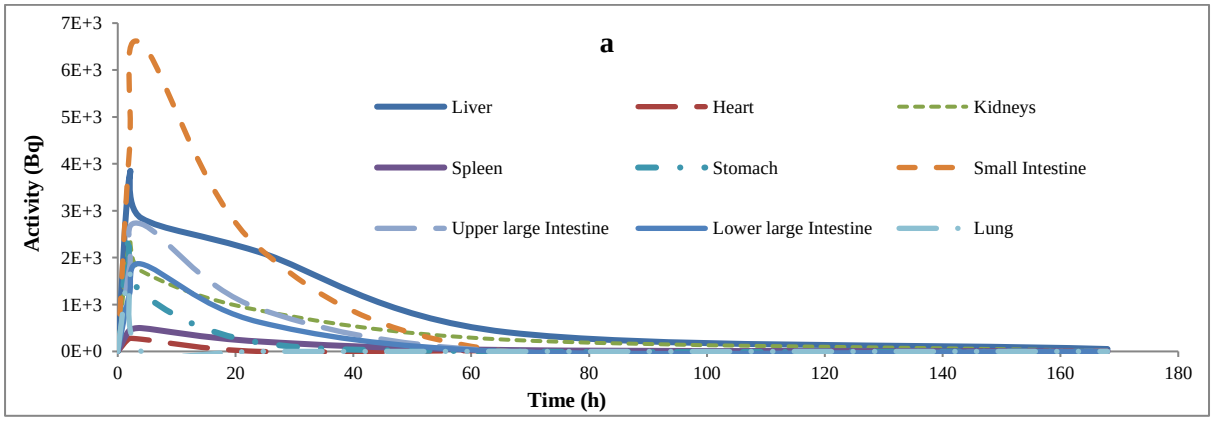

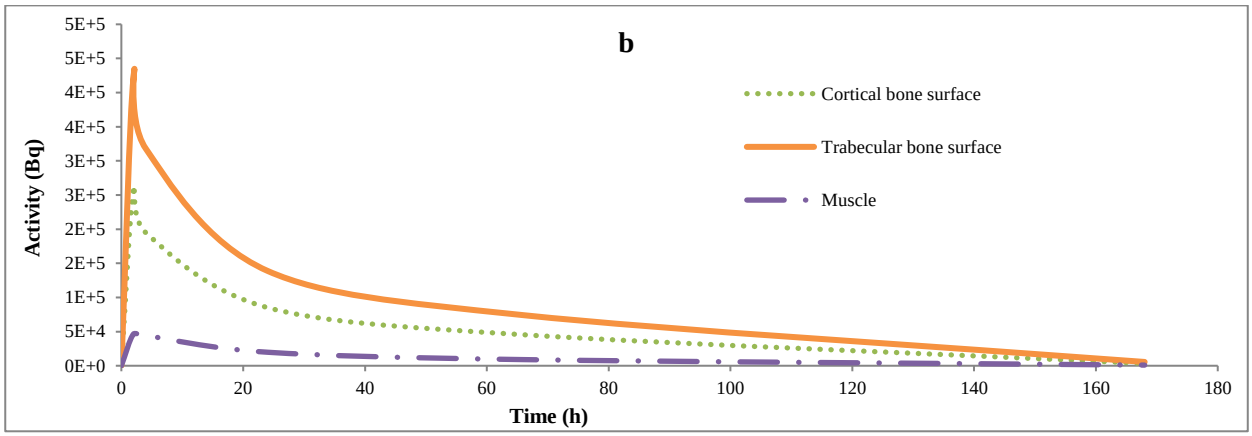

Fig. 3. The decay-corrected activity curves of ^{166}Ho-EDTMP for source organs of the adult man

Theoretical radiation absorbed dose calculations

The cumulated activity in the source organs of the adult man per injection of 1 MBq of the ^{166}Ho-EDTMP radiopharmaceutical is given in Table 1. As expected, the highest cumulated activity of ^{166}Ho-EDTMP radiopharmaceutical is observed in trabecular and cortical bones surfaces.

Table 1. The cumulated activities (MBq s/MBq) in the source organs of the adult man per injection of 1 MBq of ^{166}Ho-EDTMP

Organ	Cumulated activity	Organ	Cumulated activity
Heart	17	Lower large intestine (LLI)	152
Kidneys	250	Cortical bone surface	31477
Spleen	55	Trabecular bone surface	51357
Stomach contents	89	Muscle	6802
Small intestine contents	537	Lungs	12
Upper large intestine (ULI) contents	222	Liver	492

Estimated radiation absorbed dose of the selected target organs of the adult man per injection of 1 MBq of ^{166}Ho-EDTMP radiopharmaceutical based on biological data on Wistar rats are presented in Table 2. In addition, human organs' radiation absorbed dose from ^{166}Ho-DOTMP is given in Table 2 for comparison as the only clinically used bone marrow ablative conjugate of holmium-166 [4].

Table 2. The radiation absorbed dose (mGy/MBq) of the adult man organs per injection of 1 MBq of ^{166}Ho-EDTMP and ^{166}Ho-DOTMP radiopharmaceuticals

Organ	^{166}Ho-EDTMP	^{166}Ho-DOTMP	Organ	^{166}Ho-EDTMP	^{166}Ho-DOTMP
Adrenal	0.002	0.014	Ovaries	0.002	---
Brain	0.002	0.014	Pancreas	0.001	0.013
Breasts	0.001	0.013	Red marrow	1.435	0.517
Gallbladder wall	0.001	0.013	Osteogenic cells	3.085	0.920
Lower large intestine (LLI) wall	0.060	0.014	Skin	0.001	0.013
Small intestine	0.072	0.013	Spleen	0.034	0.013
Stomach wall	0.020	0.013	Testes	0.001	0.013
Upper large intestine (ULI) wall	0.054	0.013	Thymus	0.001	0.013
Heart wall	0.007	0.013	Thyroid	0.002	0.014
Kidneys	0.094	0.045	Urinary bladder wall	0.001	0.291
Liver	0.030	0.013	Uterus	0.001	0.013
Lungs	0.003	0.014	Total body	0.140	0.062
Muscle	0.029	0.013	Reference	This work	[4]

Due to the bone-seeking properties of phosphonates, similar to ^{166}Ho-DOTMP radiopharmaceutical, the highest radiation absorbed dose from ^{166}Ho-EDTMP was delivered to skeletal tissues too (Osteogenic cells and red marrow).

Bone and red bone marrow tissues receive radiation absorbed dose more than 100 times the dose delivered to most of the non-target organs. The kidney is the next organ with the highest radiation absorbed dose, demonstrating rapid clearance of radiopharmaceutical from the blood circulation in first few hours post-injection of ^{166}Ho-EDTMP radiopharmaceutical.

In addition, the results indicate that at injection of 1 MBq of ^{166}Ho-EDTMP, red marrow and bone surfaces would receive more radiation absorbed dose (about three times) than 1 MBq ^{166}Ho-DOTMP injection, so lower injected activities of ^{166}Ho-EDTMP would be required as a therapeutic radiopharmaceutical. This is due to the lower skeletal uptake of DOTMP (varied

from 19% to 39%) compared with EDTMP ligand (up to 70%) [4,14]. By reduction of the injected activity of ^{166}Ho-EDTMP to the one-third required for obtaining desired dose for bone marrow ablation, automatically this advantage will result in lower radiation absorbed dose of non-target organs. Gastrointestinal tract (stomach, small and large intestine), liver, spleen and kidneys would receive slightly more radiation absorbed dose from ^{166}Ho-EDTMP compared to ^{166}Ho-DOTMP radiopharmaceutical.

The maximum tolerated dose (MTD) of bone and bone marrow is about 50-70 and 1–2 Gy, respectively [15]. Radiation absorbed dose of 25 Gy to the red marrow can be considered as the ablative therapeutic dose [2,4,16]. The minimum therapeutic activity required to deliver a 25 Gy dose to the red marrow, along with the activity corresponding to the maximum tolerated dose (MTD) by bone tissue, were given in Table 3 for various bone-avid radiopharmaceuticals. For calculations of these values, bone surface and bone marrow radiation absorbed dose per injection of 1 MBq of the selected radiopharmaceuticals is given in Table 3, as well.

Table 3. The minimum activity of aminophosphonic acid radiopharmaceuticals required to deliver a therapeutic dose of 25 Gy to the red marrow

Tissue	**^{90}Y-EDTMP**	**^{153}Sm-EDTMP**	**^{166}Ho-DOTMP**	**^{177}Lu - EDTMP**	**^{186}Re-HEDP**	**^{188}Re-HEDP**	**^{166}Ho-EDTMP**
Activity (GBq) corresponding to MTD of bone	3.3	13.9	65.2	11.1	19.2	15.7	19.4
Min. activity (GBq) required for bone marrow ablation	13.9	35.7	48.4	31.2	27.2	41.0	17.4
Bone surface absorbed dose (mGy/MBq)	18	4.3	0.9	5.4	3.1	3.8	3.1
Red marrow absorbed dose (mGy/MBq)	1.8	0.7	0.5	0.8	0.9	0.6	1.4
Reference	[17]	[18]	[4]	[19]	[20]	[21]	This work

As seen in Table 3, generally EDTMP ligand conjugates demand less activities than DOTMP and HEDP ligands to deliver required dose for bone marrow ablation for a given radionuclide. This is due to the relatively high bone uptake property of EDTMP ligand (up to 70%) relative to DOTMP

and HEDP (up to 40%) ligands [14]. Among the EDTMP ligand conjugates, only the ^{90}Y-EDTMP radiopharmaceutical requires less injected activity than the ^{166}Ho-EDTMP to fulfill of 25 Gy dose for complete ablation of red bone marrow. Beta particle of ^{90}Y ($E_{\beta,av}$= 933 keV) is more energetic than ^{166}H ($E_{\beta,av}$= 673 keV), ^{153}Sm ($E_{\beta,av}$= 235 keV) and ^{177}Lu ($E_{\beta,av}$= 130 keV). It should be noted that, only the ^{166}Ho compounds (^{166}Ho-EDTMP and ^{166}Ho-DOTMP) could result in complete extirpation of bone marrow, while bone tissue dose would not exceed the MTD limit. Other radiophosphonates' required activities in order to complete red marrow ablation would exceed the MTD limit to bone tissue.

Conclusion

Theoretical radiation absorbed dose in man from ^{166}Ho-EDTMP radiopharmaceutical was estimated based on biodistribution data in Wistar rats using MIRD and Sparks and Aydogan (1996) methodologies. Biodistribution data in rats show a fast blood clearance with a major accumulation of activity in the bone tissue (up to 61 %IA in average). The results indicate that the ^{166}Ho-EDTMP would produce about 3 times more radiation absorbed dose to red bone marrow compared with ^{166}Ho-DOTMP radiopharmaceutical per unit of injected activity. The radiation absorbed dose coefficients of red bone marrow and osteogenic cells from ^{166}Ho-EDTMP were estimated to about 1.4 and 3.1 mGy/MBq, respectively. This work indicates that ^{166}Ho-EDTMP is a promising radiopharmaceutical for bone marrow ablation in patients with multiple myeloma with low undesired dose to other normal organs. However, more clinical studies in human should be seriously followed for radiation absorbed dose evaluation of organs from ^{166}Ho-EDTMP radiopharmaceutical.

References

[1] Bahrami-Samani, A., Bagheri, R., Jalilian, A.R., Shirvani-Arani, S., Ghannadi-Maragheh, M. and Shamsaee, M. (2010). Production, quality control and pharmacokinetic studies of Ho-EDTMP for therapeutic applications. Scientia Pharmaceutica, 78:423-433.

[2] Rajendran, J.G., Eary, J.F., Bensinger, W., Durack, L.D., Vernon, C. and Fritzberg, A. (2002). High-dose ^{166}Ho-DOTMP in myeloablative treatment of multiple myeloma: Pharmacokinetics, biodistribution, and absorbed dose estimation. Journal of Nuclear Medicine, 43:1383-1390.

[3] Bagheri, R., Jalilian, A.R., Bahrami-Samani, A., Mazidi, M. and Ghannadi-Maragheh, M. (2011). Production of Holmium-166 DOTMP: A promising agent for bone marrow ablation in hematologic malignancies. Iranian Journal of Nuclear Medicine, 19:12-20.

[4] Breitz, H.B., Wendt III, R.E., Stabin, M.S., Shen, S., Erwin, W.D., Rajendran, J.G., et al. (2006). ^{166}Ho-DOTMP radiation-absorbed dose estimation for skeletal targeted radiotherapy. Journal of Nuclear Medicine, 47:534–542.

[5] Appelbaum, F.R., Brown, P.A., Sandmaier, B.M., Storb, R., Fisher, D.R., Shulman, H.M., et al. (1992). Specific marrow ablation before marrow transplantation using an aminophosphonic acid conjugate ^{166}Ho-EDTMP. Blood, 80:1608-1613.

[6] Vaez-Tehrani, M., Zolghadri, M., Yousefnia, H. and Afarideh, H. (2016). Estimation of human absorbed dose for ^{166}Ho-PAM: comparison with ^{166}Ho-DOTMP and ^{166}Ho-TTHMP. The British Journal of Radiology, 89:1-7.

[7] Sparks, R.B. and Aydogan, B. (1996). Comparison of the effectiveness of some common animal data scaling techniques in estimating human radiation dose. In: Proceedings of the Sixth International Radiopharmaceutical Dosimetry Symposium, Oak Ridge, TN. Oak Ridge Associated Universities, pp. 705–716.

[8] Siegel, J.A. (2005). Establishing a clinically meaningful predictive model of hematologic toxicity in nonmyeloablative targeted radiotherapy: practical aspects and limitations of red marrow dosimetry. Cancer Biotherapy and Radiopharmaceuticals, 20:126–140.

[9] ICRP, (1975). ICRP Publication 23, Report of the task group on reference man. New York: Pergamon Press.

[10] Peters, J. M. and Boyd, E.M. (1966). Organ weights and water levels of the rat following reduced food intake. Journal of Nutrition, 90:354–360.

[11] Miller, G., Klumpp, J.A., Poudel, D., Weber, W., Guilmette, R.A. and Swanson, J. (2019). Americium systemic biokinetic model for rats, Radiation Research, 192:75-91.

[12] Stabin, M.G., Sparks, R.B. and Crowe, E. (2005). OLINDA/EXM: the Second-generation personal computer software for internal dose assessment in nuclear medicine. Journal of Nuclear Medicine, 46:1023–1027.

[13] ICRP, (2002). ICRP Publication 89, Basic anatomical and physiological data for use in radiological protection: reference values. New York: Pergamon Press.

[14] Bagheri, R., Afarideh, H., Ghannadi-Maragheh, M., Shirmardi, S.P. and Bahrami-Samani, A. (2015). Study of bone surface absorbed dose in treatment of bone metastases via selected radiopharmaceuticals: using MCNP4C code and available experimental data. Cancer Biotherapy and Radiopharmaceuticals, 30:174-181.

[15] Kassis, A.I. and Adelstein, S.J. (2003). Considerations in the selection of radionuclides for cancer therapy. In: Welch MJ, Redvanly CS (editors). Handbook of Radiopharmaceuticals, Radiochemistry and Applications. London: Wiley & Sons, 767–793.

[16] Barlett, M.L., Webb, M., Durrant, S., Morton, A.J., Allison, R. and Macfarlene, D.J. (2002). Dosimetry and toxicity of Quadramet for bone marrow ablation in multiple myeloma and other hematological malignancies. European Journal of Nuclear Medicine, 29:1470–1477.

[17] Rösch, F., Herzog, H., Plag, C., Neumaier, B., Braun, U., Müller-Gärtner, H.W., et al. (1996). Radiation doses of yttrium-90 citrate and yttrium-90 EDTMP as determined via analogous yttrium-86 complexes and positron emission tomography. European Journal of Nuclear Medicine, 23:958-966.

[18] Vigna, L., Matheoud, R., Ridone, S., Arginelli, D., Della Monica, P., Rudoni, M., et al. (2011). Characterization of the [^{153}Sm]Sm-EDTMP pharmacokinetics and estimation of radiation absorbed dose on an individual basis. Physica Medica, 27:144-152.

[19] Zaknun, J., Bal, C. and Dupont, P. (2011). Pharmacokinetics and dosimetry of the bone-seeking agent ^{177}Lu-EDTMP in patients with metastatic prostate cancer. Journal of Nuclear Medicine, 52(suppl1):1748.

[20] Lyra, M., Papanikolos, G., Phinou, P., Frantzis, A.P., Jordanou, J. and Limouris, G.S. (2003). Rhenium-186-HEDP dosimetry and multiple bone metastases palliation therapy effects. Radionuclide Ther. Oncol. Curr. Status Future Aspects 10:51-60.

[21] Liepe, K., Hliscs, R., Kropp, J., Runge, R., Knapp Jr., F.F., Franke, W.G., et al. (2003). Dosimetry of ^{188}Re-Hydroxyethylidene diphosphonate in human prostate cancer skeletal metastases. Journal of Nuclear Medicine, 44:953-960.

Measurement of absorption dose vs. distance from 241Am-Be neutron source and evaluation of different neutron interactions with soft tissue elements (Paper ID : 1092)

S.M.Khamesi[*1], M.Shayesteh[2], M.Eshghi[2], M.Salehi Barough[1]

1. *Department of Medical Radiation Engineering, Central Tehran Branch, Islamic Azad University, Tehran, Iran*

2. *Department of Physics, Imam Hossein University, Tehran, Iran*

Abstract

The 241Am-Be neutron source has many applications due to its specific neutron spectrum, storage and mobility. The aim of this study was to measure absorption dose rate at different distances from the source and evaluate the various interactions of neutrons with soft tissue elements. The results show that the absorption dose rates in the simulation and experimental methods have an average difference of less than 5% and as a result it can be said that they have a good agreement. The results of evaluation of different interactions of neutrons with soft tissue elements showed that the share of hydrogen in the total absorption dose rate in soft tissue is 91.3%. Also, the share of thermal neutron capture with nitrogen and hydrogen were 0.048 and 0.37, respectively, while the total share of fast neutron scattering with different elements was 99.58%.

Keywords: ^{241}Am-Be neutron source, Absorption dose rate, Capture interaction, scattering interaction

Introduction

Nuclei are made up neutrons and protons, and neutrons interact with nuclei through nuclear forces since they are chargeless particles. Unlike charged particles, neutrons do not have to cross the Coulomb barrier when approaching a nucleus. Therefore, neutrons have a larger probability (cross-sectional area) of nuclear interactions than charged particles [1]. Scattering and capture are two types of neutron interactions with nuclei.

The nature of the target nucleus does not change in scattering interactions; instead, it changes the neutron energy spectrum, decelerating the fast neutrons. The nature of the target nucleus, however,

changes in capture or adsorption interactions, and a neutron is added to it, leading to changes in their atomic weight. Indeed, a composite nucleus is generated in capture interaction, which is generally stimulated and soon returns to a steady position by emitting a gamma photon or rejecting a particle or a mixture of particles (neutrons, alpha or fission fragments, etc.) [2].

In comparison to other neutron sources, radioisotopic sources have a small size, a relatively long half-life, flux stability, and various shape and dimensions. The usage of (α, n) reactions is one of the radioisotopic sources of neutron generation. By mixing alpha rays emitter radionuclides with the target substance, neutrons are generated. The strongest neutron flux will be generated when the target material is beryllium [3]. The ^{241}Am-Be source is one of the alpha-beryllium sources with long half-life. This source has a specific neutron energy spectrum and gamma, which have been evaluated by a significant number of researchers using organic scintillators, flight time methods, proton recoil methods, and neutron counters [4, 5]. The studies demonstrated that neutrons from the ^{241}Am-Be source exhibit a spectrum with a mean energy of 4.5 MeV and maximum energy of 11 MeV [6, 7].

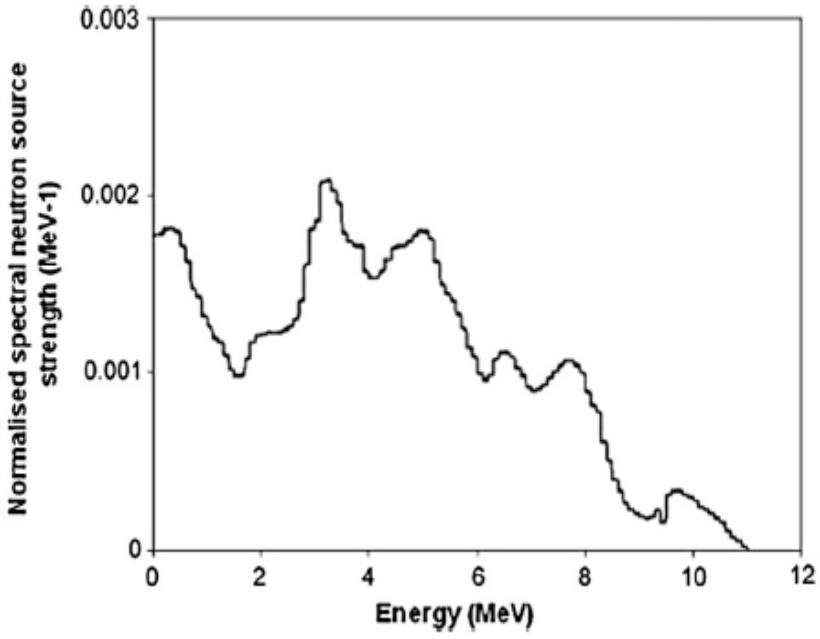

Fig.1. The spectrum of neutron source ^{241}Am-Be [7]

The neutrons emitted from ^{241}Am-Be source has a continuous spectrum of energy, spanning from thermal neutrons to fast neutrons with an energy of 11 MeV (Figure 1).

The principal mechanism of transfer of energy for fast neutrons is an elastic collision, whereas thermal neutrons can be captured and cause nuclear reactions [1, 8]. Hydrogen is the best moderator of fast neutrons because the maximum energy transfer occurs in the elastic scattering with light nuclei [8].

Nuclear interactions are unpredictable, and the likelihood of any nuclear interaction may be described by a parameter called the cross-section area. Even though the values may be found in the NNDC library [9], the cross-section area of each neutron interaction with various elements changes depending on the neutron energy.

The energy absorbed in each soft tissue element that interacts with the neutrons can be used to calculate the absorbed dose of neutrons with a specific energy spectrum. Table 1 shows the soft tissue components for radiation dosimetry.

For an isotropic scattering regarding an elastic collision with a nucleus with mass number M, the mean neutron energy transfer fraction f is equal to

$$f = \frac{2M}{(M+1)^2} \qquad (1)$$

The mean fraction of neutron energy transfer for each soft tissue element is reported in Table 1.

Table 1. Soft tissue composition for radiation dosimetry [10]

element	Mass percentage	N_i (atom/kg)	f_i
Oxygen	71.39	2.69×10^{25}	0.111
Carbon	14.89	6.41×10^{24}	0.142
Hydrogen	10	5.98×10^{25}	0.500
Nitrogen	3.47	1.49×10^{24}	0.124
Sodium	0.15	3.93×10^{22}	0.080
Chlorine	0.10	1.7×10^{22}	0.053

The equivalent dose, abbreviated as H, is a measurement of the dose received into the tissue based on its biological effects. In other words, at the same dose, the biological effects of all the beams will never be the same, but they will vary in intensity and strength based on the kind and energy of the beam. Sv or rem are the unit of dose equivalents.

$$H = D \times Q_F \qquad (2)$$

In equation (2), D and QF are the amount of absorbed dose and the quality factor for various radiations, respectively. These coefficients are shown in Table 2 for various radiations.

Table 2. Quality factor values for different radiations [10]

radiation	Q_F
Gamma rays	1
Thermal neutrons	2
Fast neutrons	10
Protons	10

The effective dose, shown as E, is a quantity that contains the biological effects of different radiations and the role of different tissues concerning the incidence of different effects in estimating the dose absorbed in the tissue. Similar to equivalent dose, the effective dose unit is Sv or rem.

$$E = W_T\, H \qquad (3)$$

H is the equivalent dose, and WT is the weighting factor of tissue T, in the equation (3). The weighting factor for the tissues tested in this investigation are listed in Table 3.

Table 3. Weighting factor of tissues [10]

Tissue or organ type	Weighting factor W_T
Breast	0.05
Prostate	0.01

In this study, an ^{241}Am-Be neutron source with 5-curie activity and 1.332×10^{7}n/s neutron intensity was employed. The amount of flux and absorption dose rate in different distance from ^{241}Am-Be neutron source was calculated experimentally (with BF_3 detector) and simulation (MCNPX), and then compared with each other.

The impact of different interactions of released neutrons from the source with different tissue elements is also explored in another section of this research, and then the contribution of these interactions in the absorbed dose of tissue is determined. Finally, the equivalent and the effective dose at the closest measured distance from the source (20 cm) , taking into account prostate and breast tissues is estimated.

Research Theories

The absorbed dose can be determined based on the kind of neutron interaction with various tissues. For fast neutrons with energies less than 11 MeV, the principal energy transfer mechanism is an elastic collision. Thermal neutrons can also be observed in the ^{241}Am-Be spectrum, which may lead to nuclear interactions through the capture mechanism [11, 12].

^{241}Am-Be neutron source

In this study, ^{241}Am-Be neutron source with 5-curie activity and 1.332×10^{7}n/s neutron intensity was employed in the shape of a cylinder with a diameter of 3.3 cm and a height of 10 cm. This neutron source is housed in a stainless steel capsule that is 3.5 cm in diameter and 10.5 cm in length (Figure2).

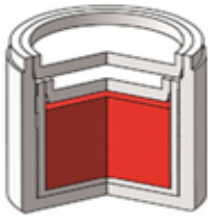

Fig.2. The shielded ^{241}Am-Be neutron source

BF_3 detector

In order to obtain experimental results, the BF_3 neutron detector made by Centronic Company has been used that its active length and diameter are 31.1 and 2.4 cm, respectively.

Experimental

Measurement of flux in experimental and simulation method

The shielded ^{241}Am-Be source is positioned in the center of an iron tank with a diameter of 95 cm and a height of 120 cm that is filled with normal water, and four cylindrical collimators each having 9cm diameter and 43cm long are placed on the four sides of the source. The BF3 detector can be placed at various distances from the source and counted the neutrons released from it. To prevent fast neutrons from leaking into the environment, polyethylene cylinders are usually placed

in these collimators (Figure 3). In the experimental method, the neutron count and flux rates are determined by removing the polyethylene cylinder from one of the collimators and inserting the BF3 detector at various distances from the source.

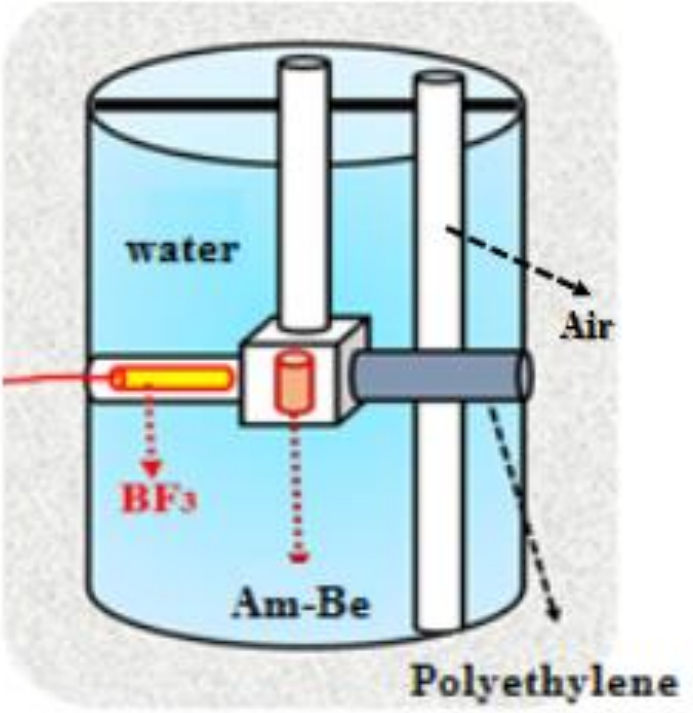

Fig.3. The position of neutron source and BF3 detector

According to the neutron flux values obtained from the ^{241}Am-Be source at different distances inside the collimator, in this study, a cylindrical phantom of soft tissue with a specific volume was placed at similar distances from the source inside the collimator and the amount of absorption dose rate in the soft tissue was calculated experimentally and then compared with that of simulation.

Additionally, neutron flux values were obtained at the same distances from the ^{241}Am-Be source using the MCNPX simulation code. In Figure 4, the results of neutron flux measurements utilizing the BF3 detector and Monte Carlo simulation are shown.

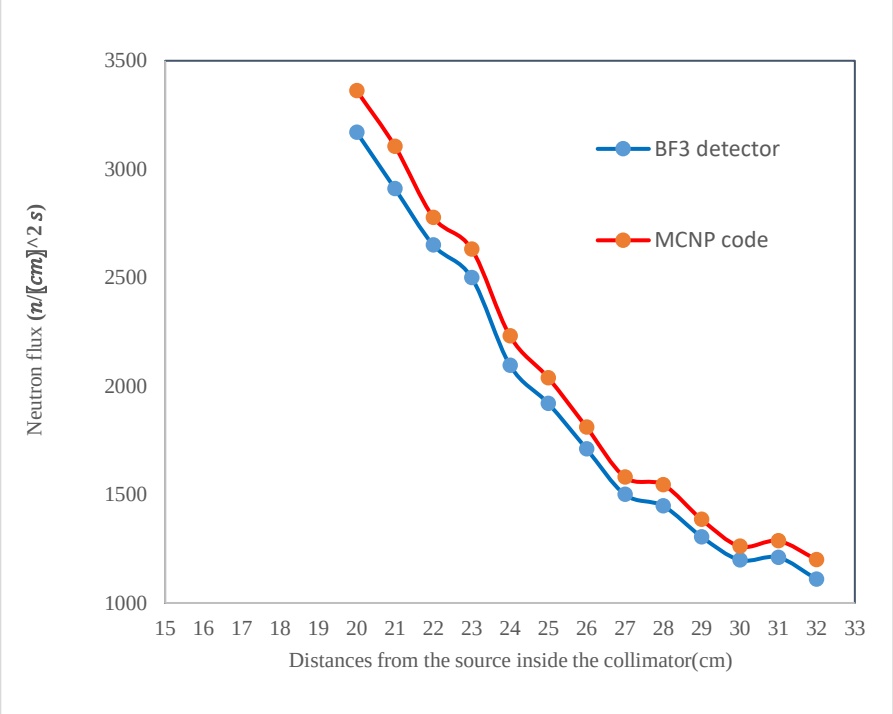

Fig.4. Experimental and simulation results of neutron flux at different distances from the source inside the collimator

Measurement of absorbed dose in experimental and simulation method

A cylinder with certain volume contain of ICRU soft tissue was created in the space inside the collimator at determined distances from the ^{241}Am-Be source to measure the absorbed dose, and the total absorbed dose was directly estimated in terms of MeV/gram using Tally F6.

The neutron flux should first be determined for various energies before the absorption dose rate are calculated under experimental conditions. The amount of flux can be estimated independently for different energies in the simulation method by defining the En card and the energy segmentation. In experimental method the calculation can be done using the spectrum of neutron source and the percentage of neutron abundance in each energy range (Figure1).

The energy transfer mechanism for fast neutrons in soft tissue is mostly through elastic scattering. In the elastic scattering, the scattered nuclei lose their energy near the interaction place. The radiation dose that is absorbed locally is calculated using the initial neutron flux. The dose rate for neutrons with energy E is obtained from the following equation [10]:

$$\dot{D_n}(E) = \frac{\varphi(E)\times E\times\sum N_i\sigma_i f_i}{1\ J/kg.Gy} \qquad (4)$$

As shown in equation4,$\varphi(E)$, E, N_i, σ, and f represent the neutrons flux with energy E (in terms of$\frac{n}{cm^2 s}$), neutron energy in joules, the number of atoms per kilogram of ith element, the scattering cross-section of ith element for neutrons with energy E (in terms of barn multiplied by 10^{-24} cm^2), and the mean energy fraction transferred from a neutron to a scattered atom due to a collision with a neutron, respectively. Since the neutrons emitted from the ^{241}Am-Be source have a continuous energy spectrum, it was calculated separately for each energy group.

Thermal neutrons in soft tissue transfer their energy mainly through N^{14} (n, p) C^{14} and H^1 (n, γ) H^2 reactions. The dose rate can be determined using the following equations [10]:

$$\dot{D_{n,p}} = \frac{\varphi\times N\times\sigma\times Q\times 1.6\times 10^{-13} J/MeV}{1\ J/kg.Gy} \qquad (5)$$

As shown in equation 5, φ, N, σ, and Q demonstrate the thermal neutron flux, the number of nitrogen atoms per kilogram of tissue (1.49×10^{24}), nitrogen adsorption cross-section (1.75 barns), and the energy released in reaction (0.63 MeV), respectively.

The H^1 (n, γ) H^2 reaction is such that since the gamma-emitting isotope is uniformly distributed throughout the body, the rate of absorption dose is computed using global gamma radiation dose-related equations [8].

$$\dot{D_\gamma} = A \times \emptyset \times \Delta \qquad (6)$$

$$A = \varphi \times N \times \sigma \qquad (7)$$

In equations 6 and 7, φ, N, σ, ∅, Δ, and A show the thermal neutron flux, the number of hydrogen atoms per kilogram of tissue (5.98×10^{25}), the cross-section of hydrogen adsorption (0.33 barn), the fraction of gamma energy absorbed into the tissue (0.278), the dose rate in the large infinite homogeneous mass from the tissue containing the uniform distribution of the radioactive isotope at a density of 1 Bq/kg, and the special activity of this distributed gamma emitter, respectively [10].

$$\Delta = 1.6\times10^{-13}\times 2.23 = 3.57\times10^{-13}\ \frac{Gy.s^{-1}}{Bq.kg^{-1}} \qquad (8)$$

The total absorption dose rate is equal to the sum of the absorption dose of a fast and thermal neutron, as calculated by the equation below.

$$\dot{D} = \dot{D_n} + \dot{D_{n,p}} + \dot{D_\gamma} \qquad (9)$$

Results and discussion

This section is divided into three parts, with the outcomes of each segment listed below. First, given the neutron flux values at different distances from the ^{241}Am-Be source in the space inside the collimator using experimental and simulation methods, the soft tissue with a certain volume was inserted into the collimator space at similar distances. (Figure2). Then the absorption dose rate in the experimental method calculated based on Equations 4, 5 and 6 and finally compared with the absorption dose rates obtained from the simulation at similar distances.

The total neutron flux multiplied by the percentage of neutron abundance per energy at a specific distance from the 241Am-Be source equals the neutron flux per energy at that distance. These values were estimated for each distance from the ^{241}Am-Be source based on the neutron flux data at that distance. For example, the neutron flux is 3170 n/cm^{2}s at a distance of 20 cm from the source ^{241}Am-Be, which is the nearest distance to the source. Consequently, φ (E) and σ (E) values can be determined (Tables 4 and 5).

Table 4. The values $\varphi(E)$ at a distance of 20 cm from the ^{241}Am-Be source

E (MeV)	percentage of neutron abundance	$\varphi(E)$ (n/cm^{2}s)
$0 < E \leq 0.01$	9.5	$3170 \times 0.095 = 301.15$
$0.01 < E \leq 0.1$	2.4	76.08
$0.1 < E \leq 0.5$	6.2	196.54
$0.5 < E \leq 1$	10	317
$1 < E \leq 2$	9	285.3
$2 < E \leq 3$	16	507.2
$3 < E \leq 4$	12	380.4
$4 < E \leq 5$	13	412.1
$5 < E \leq 6$	8.2	259.94
$6 < E \leq 7$	7.2	228.24
$7 < E \leq 8$	2.5	79.25
$8 < E \leq 9$	2.3	72.91
$9 < E \leq 10$	1.2	38.04
$10 < E \leq 11$	0.5	15.85
total	100	3170

Table 5 displays the cross-section of the scattering of different elements in the tissue for different neutron energy using the NNDC library [9].

Finally, the absorption dose rate values resulting from the interaction of neutron scattering interaction with various tissue elements were computed for all neutron energy groups using the data from Tables 4 and 5 and Equation 4. Table 4 shows that approximately 9.5 percent of neutrons are thermal and slow. Therefore, equations 5 and 6 were used to calculate the absorption dose rate from capture interaction. Finally, the total adsorption dose rate in different distances from the source is obtained by inserting the adsorption dose rate for fast and thermal neutron in Equation 9, the results of which are shown in Figure5.

Figure 5 compares the total absorbed dose rates obtained from the two approaches of experimental and simulation in terms of distance from the ^{241}Am-Be source.

Table 5. Scattering cross section of different elements in the tissue for different neutron energies [9]

E **(MeV)**	**Scatter cross section for nitrogen element (barn)**	**Scatter cross section for hydrogen element (barn)**	**Scatter cross section for oxygen element (barn)**	**Scatter cross section for carbon element (barn)**	**Scatter cross section for sodium element (barn)**	**Scatter cross section for Chlorine element (barn)**
0.1	4.41	12.74	3.64	4.40	4.29	0
0.5	2.36	6.12	4.53	3.40	3.13	0
1	2.64	4.24	8.15	2.5	2.53	2.46
2	1.50	2.90	1.57	1.6	1.66	2.63
3	1.32	2.28	1.20	1.17	1.15	2.59
4	1.44	1.89	2.03	1.93	0.91	2.29
5	0.77	1.62	0.89	1.12	0.74	1.93
6	1.05	1.41	1.67	0.87	0.66	1.68
7	0.84	1.25	0.76	0.57	0.61	1.48
8	0.862	1.12	0.53	1.35	0.583	1.32
9	0.863	1.02	0.70	0.63	0.582	1.18
10	0.87	0.93	0.73	0.65	0.584	1.06
11	0.78	0.85	0.98	0.83	0.60	0.98

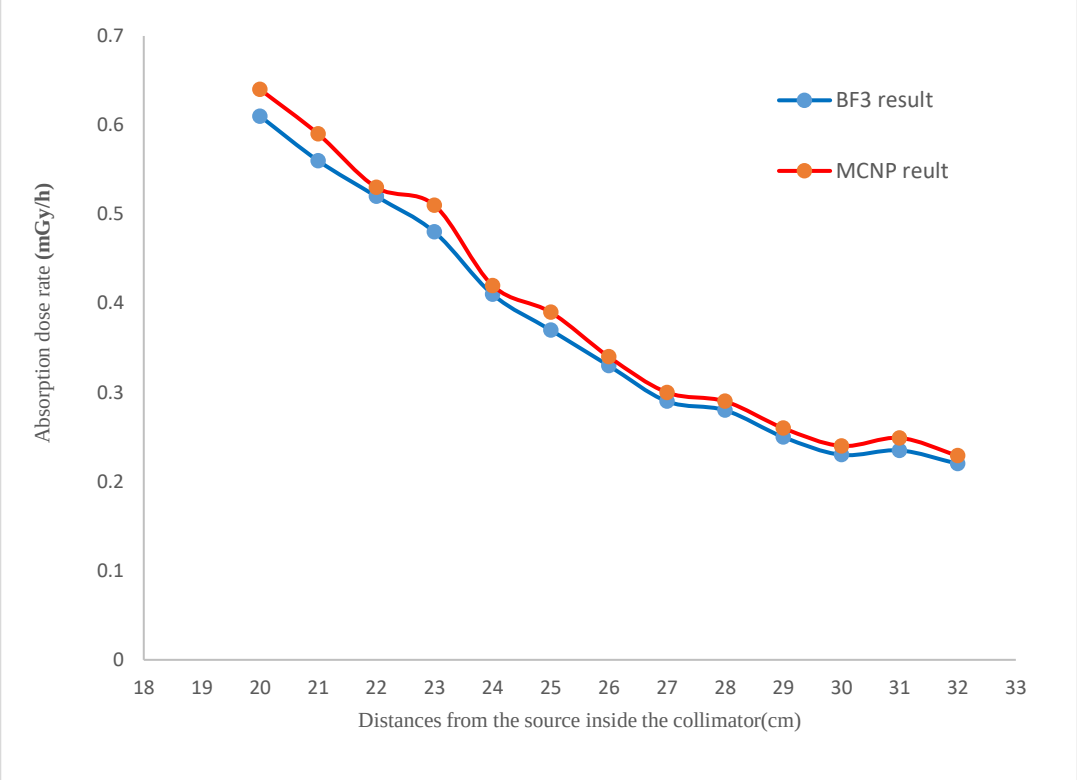

Fig. 5. Experimental and simulation results of absorption dose rate at different distances from ^{241}Am-Be source in collimat

Table 6 shows the absorption dose rate at four different distances from the source.

Table 6. Absorption dose rate from experimental and simulation methods at different distances from^{241}Am-Be source

Absorption dose rate from simulation method (mGy/h)	Absorption dose rate from experimental method (mGy/h)	distances from ^{241}Am-Be (cm)
0.67	0.6	20
0.45	0.41	24
0.31	0.28	28
0.24	0.21	32

Table7. Statistical error in experimental and simulation methods

Experimental method	Simulation method
0.012	0.01

In another part of this study assumed that the soft tissue of the prostate or breast tissues was located in 20 cm from the ^{241}Am-Be source, so the equivalent and effective doses were computed using equations 2 and 3 and Tables 2 and 3, respectively. Of course, these calculations are based only on experimental data and its values can be seen in Tables 8 and 9.

Table8. Equivalent dose obtained by experimental method at a distance of 20 cm from the ^{241}Am-Be source

Total equivalent dose rate (mSv/h)	Equivalent dose rate per thermal neutron (μSv/h)	Equivalent dose rate per fast neutron (mSv/h)	distances from ^{241}Am-Be (cm)
5.975	5.04	5.97	20

Table9. Effective equivalent dose obtained by experimental method at a distance of 20 cm from the ^{241}Am-Be source

Effective equivalent dose for prostate tissue(mSv/h)	Effective equivalent dose for breast tissue(mSv/h)	distances from ^{241}Am-Be (cm)
0.059	0.298	**20**

Conclusions

The ^{241}Am-Be source, which has a determined energy spectrum and is relatively easy to maintain and transport, has a wide applications in medicine, industry, neutron laboratories in the field of nuclear research and neutron activation [13-18]. Due to long half-life of the ^{241}Am-Be source (432 years) [19-21], proper shield designing against neutron flux is required.

Due to the distribution of neutron flux at different distances from the source (inside the collimator), in this study, the absorption dose rate was measured at similar distances. Considering the neutron flux values at different distances in the experimental method, the rate of absorption dose was calculated at different distances from the source by Equations 4, 5, and 6, which are the adsorption dose caused by scattering interaction between fast neutron and different elements of the soft tissue, and the adsorption dose resulted from thermal neutron capture in the soft tissue, respectively. Then, the absorption dose rate was calculated at different distances using the simulation method and compared with the experimental values [Figure 5 and Table 6]. The results demonstrate that the mean absorption dose rates in the simulation and experimental methods have a mean difference

less than 5%, indicating that considering the statistical error, the simulation and experimental results have an acceptable consistency.

On the other hand, since hydrogen constitutes more than 70% of soft tissue, neutrons have the maximum interaction with scattering-based hydrogen, and hydrogen accounts for 91.3% of the overall absorption dose rate in soft tissue (Table 10).

Table10. The contribution of different elements of artificial texture in the total absorption dose

The contribution of different elements of artificial texture in the total absorption dose	
hydrogen	91.3%
oxygen	5.48%
nitrogen	1.15%
Carbon	1.68%
Sodium	0.22%
Chlorine	0.17%

Moreover, as compared to the contribution of fast neutron scattering interactions, the share of thermal neutron capture interactions with nitrogen and hydrogen, which includes (n, p) and (n, γ) interactions, is very small(Table 11).

Table 11. Contribution of various interactions of emitted neutrons from the ^{241}Am-Be source with soft tissue

$\dot{D}_n$	$\dot{D}_{n,p}$	$\dot{D}_\gamma$
99.58%	0.048%	0.37%

In addition, considering the weighting factor for prostate and breast tissues, the effective equivalent dose was calculated at the distance of 20 cm from the ^{241}Am-Be source (Table 9), indicating that this value is higher in the breast tissue.

Acknowledgements

This article has been derived from a Ph.D. thesis (number: 162519957) at Department of Medical Radiation Engineering, Central Tehran Branch, Islamic Azad University (Tehran, Iran). We would like to thank the cooperation of all members of the Imam Hossain University for their assistance. This research did not receive any specific grant from funding agencies in the public, commercial, or not-for-profit sectors.

References

[1] Tsoulfanidis, N., & Landsberger, S. (2021). Measurement and detection of radiation. CRC press.

[2] H.P. gen Schieck ‹Nuclear Reactions: An Introduction. Springer 2014.

[3] Vega C, H. R., & Martinez O, S. A. (2015). Neutron spectra and dosimetric features of isotopic neutron sources: a review.

[4] Ghal-Eh, N., Rahmani, F., & Bedenko, S. V. (2019). Conceptual design for a new heterogeneous 241Am-9Be neutron source assembly using SOURCES4C-MCNPX hybrid simulations. Applied Radiation and Isotopes, 153, 108811.

[5] Ito, H., Wada, K., Yano, T., Hino, Y., Ommura, Y., Harada, M., & Ishitsuka, M. (2023). Analyzing the neutron and gamma ray emission properties of an americium-beryllium tagged neutron source. arXiv preprint arXiv:2304.12153.

[6] Croft, S. (1989). The use of neutron intensity calibrated 9Be (α, n) sources as 4438 keV gamma-ray reference standards. Nuclear Instruments and Methods in Physics Research Section A: Accelerators, Spectrometers, Detectors and Associated Equipment, 281(1), 103-116.

[7] Kluge, H., & Weise, K. (1982). The neutron energy spectrum of a 241Am-Be (Alpha, n) source and resulting mean fluence to dose equivalent conversion factors. Radiation protection dosimetry, 2(2), 85-93.

[8] Chilton, A. B., Shultis, J. K., & Faw, R. E. (1984). Principles of radiation shielding.

[9] National Nuclear Data Center (NNDC), ENDF/B-VII.1, (USA2011Web.2011) http://www.nndc.bnl.gov

[10] Cember, H. (2009). Introduction to health physics.

[11] D. Ghasemabadi. (2009). Design of Neutron Mine Detector Using 241Am-Be Continuous Neutron Sources and D-D Pulse, Master of Nuclear Physics, Imam Hossein University, Faculty of Physics. (In Persian)

[12] Thakur, V. M., Jain, A., Biju, K., Sunil, C., Anilkumar, S., Babu, D. A. R., & Sharma, D. N. (2012). Studies on optimization of Moderator thickness for BF 3 detectors used for monitoring of fissile material.

[13] Ellis, K. (1993). In vivo activation analysis: present and future prospects. Journal of radioanalytical and nuclear chemistry, 169(2), 291-300.

[14] Morgan, W. D. (2000). Of mermaids and mountains: Three decades of prompt activation in vivo. Annals of the New York Academy of Sciences, 904(1), 128-133.

[15] Zimbal, A. (2007). Measurement of the spectral fluence rate of reference neutron sources with a liquid scintillation detector. Radiation protection dosimetry, 126(1-4), 413-417.

[16] Ochbelagh, D. R., Hakimabad, H. M., & Najafabadi, R. I. (2007). The investigation of Am–Be neutron source shield effect used on landmine detection. Nuclear Instruments and Methods in Physics Research Section A: Accelerators, Spectrometers, Detectors and Associated Equipment, 577(3), 756-761.

[17] Khelifi, R., Amokrane, A., & Bode, P. (2007). Detection limits of pollutants in water for PGNAA using Am–Be source. Nuclear Instruments and Methods in Physics Research Section B: Beam Interactions with Materials and Atoms, 262(2), 329-332.

[18] Khelifi, R., Bode, P., & Amokrane, A. (2007). Flux calculation in LSNAA using an ^{241}Am-Be source. Journal of Radioanalytical and Nuclear Chemistry, 274, 639-642.

[19] Mowlavi, A. A., & Koohi-Fayegh, R. (2004). Determination of 4.438 MeV γ-rays to neutron emission ratio from a 241Am–9Be neutron source. Applied Radiation and Isotopes, 60(6), 959-962.

[20] Ghassoun, J., Chkillou, B., & Jehouani, A. (2009). Spatial and spectral characteristics of a compact system neutron beam designed for BNCT facility. Applied Radiation and Isotopes, 67(4), 560-564.

[21] Shultis, J. K., & Faw, R. E. (2010). Radiation shielding and radiological protection. In Handbook of nuclear engineering (pp. 1313-1448). Springer, Boston, MA.

Theorical investigation of electromagnetic transition (E1) and (E2) for neutron capture (Paper ID : 1181)

Khalili H. [1*], Dalvand M [1],Cheshmi S.A.
[1]*Department of Physics, Faculty of Science, Arak University, Arak 8349-8-38156, Iran*

Abstract

In nuclear astrophysics, analyzing electromagnetic transition strengths is a powerful method for studying the development of atomic nuclei, the Big Bang nucleosynthesis, and the stellar fuel cycle. Electromagnetic radiation serves as a valuable probe to investigate the intricate details of nuclear structure. Intrinsic nuclear moments, such as the magnetic dipole moment and electric quadrupole moment, are closely linked to the multipole moments derived from the probabilities of radiative transitions between nuclear states. The occurrence of E2 (electric quadrupole) and E1 (electric dipole) transitions depends on the excitation energy and spin-parity of the involved states. Within the theoretical framework of the Woods-Saxon potential model, the ground and excited states of 11B were meticulously calculated. Interestingly, both B(E2) and B(E1) coefficients, which quantify transition strengths, exhibited a monotonic increase with increasing excitation energy, regardless of the excited state spin. This observation underscores the significant influence of excitation energy on the electromagnetic properties of nuclei. This study investigates the connection between excitation energy and reduced transition probabilities for the 10B+n system using a potential model approach

Keywords: Woods-saxon Potential, Reduced transition probability, Electromagnetic Transition.

Introduction

Analogous to atomic electrons, atomic nuclei can exist in ground and excited states. During transitions between these states, nuclei can emit photons, typically at gamma-ray wavelengths. Low-order transitions (dipolar and quadrupole), classified by their "multipolarity," are the most readily observed. These transitions can be modeled as the emission of oscillating electric or magnetic multipoles. Analyses of electromagnetic transition strengths in atomic nuclei have been instrumental in the development of nuclear physics[1]. Precise knowledge of these reduced transition probabilities is crucial for understanding various nuclear models and numerous astrophysical phenomena[2]. Stellar nucleosynthesis particularly emphasizes the analysis of reaction rates. To validate these rates, studying transition strengths is essential[3]. Therefore, this

work investigates the transition strengths from various bound excited states of the ^{11}B isotope. Overall, research on 11B is an active and important field of study due to its numerous scientific and practical applications . We analyze their dependence on excitation energy and spin using an n + ^{10}B -> ^{11}B reaction. Since gamma emission accompanies this reaction, examining the electromagnetic power is crucial for understanding the process[3]. Neutron capture is a nuclear reaction where a nucleus collides and merges with one or more neutrons, forming a heavier nucleus. Neutrons, lacking an electric charge, can enter a nucleus more readily compared to positively charged protons repelled by electrostatic forces. In this work, we utilize the Woods-Saxon potential and the RADCAP model to arrive at our conclusions.

Research Theories

This investigation utilizes the RADCAP model to explore wave functions and analyze the reduction of transition probabilities. The RADCAP model calculates various quantities of interest for two-body fusion reactions of this type[٤]. The governing equation for these two-body systems is the radial Schrödinger equation, given by:

$$-\frac{\hbar^2}{2M_N}\nabla_r^2\psi(r) + (V(r) - E)\psi(r) = 0$$

(1)

The ^{10}B(n,γ)^{11}B reaction utilizes the Woods-Saxon potential within the Hamiltonian. This phenomenological choice for the one-body potential offers a convenient model for describing both bound-state and continuum properties of single-particle wave functions. The justification for this choice follows as[5]

$$V(r) = V_0(r) + V_C(r), \langle \vec{s}, \vec{l} \rangle V_S(r)$$

(2)

V_c, V_0, V_{so} are Coulomb potential between charge particles, central potential, spin-orbital potential between projectile and target particles and, respectively [6].

The operators for electric transitions of multipolarity $\lambda\,\pi$ are given by [7]:

$$\hat{O}(E\lambda) = e_{eff\,\lambda} r^{\lambda} y_{\lambda\mu}(\hat{r})$$

(3)

In the above equation, e_{eff}represents the effective charge. For nuclei with an equal number of neutrons and protons, E1 transitions between zero-isospin states do not occur. The matrix element for $J_0M_0 \rightarrow JM$ is given by[۸-9]:

$$\langle J \| O_{E\lambda} \| J_0 \rangle = (-1)^{j+I_a+J_0+\lambda} [(2J+1)(2J_0+1)]^{\frac{1}{2}} \begin{Bmatrix} j & J & I_a \\ J_0 & j_0 & \lambda \end{Bmatrix} \langle j \| O_{E\lambda} \| j_0 l_0 \rangle, \tag{5}$$

Now, using the Wigner-Eckart theorem, the matrix elements of these operators can be expressed in terms of reduced matrix elements [10].

$$\langle lj \| \hat{O}_{E\lambda} \| j_0 l_0 \rangle = \frac{e_\lambda}{\sqrt{4\pi}} (-1)^{l_0+l+j_0-j} \frac{\hat{\lambda}\hat{J_0}}{\hat{j}} \left\langle j_0 \tfrac{1}{2} \lambda_0 \middle| j \tfrac{1}{2} \right\rangle \times \int_0^\infty dr\, r^2\ u_{lj}^J(r) u_{l_0 j_0}^{J_0}, \tag{6}$$

Calculating transition strengths requires radial integrals, which necessitate the determination of radial wavefunctions. The excited and ground state radial wavefunctions can be obtained by solving the corresponding Schrödinger equation for the potential discussed previously..

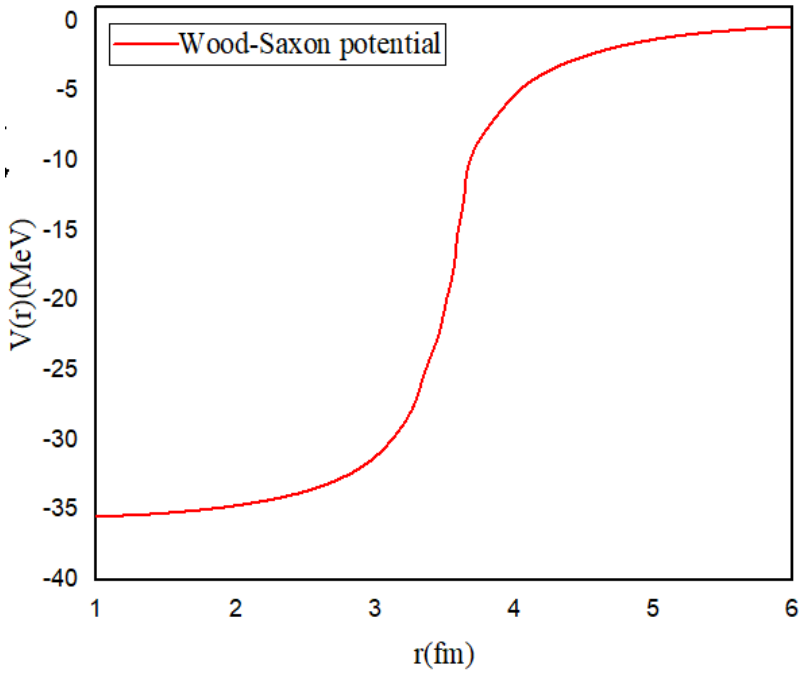

Fig. 1. The Woos-Saxon potential [V (r)] is plotted as a function of radial distance for n+ ^{11}B system

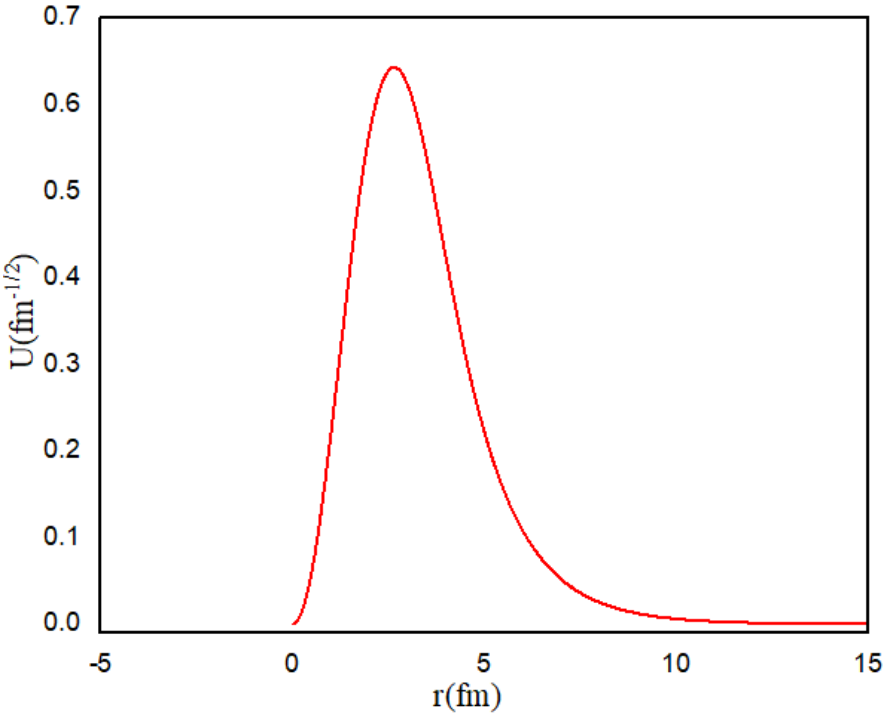

Fig.2.The radial ground state wave function

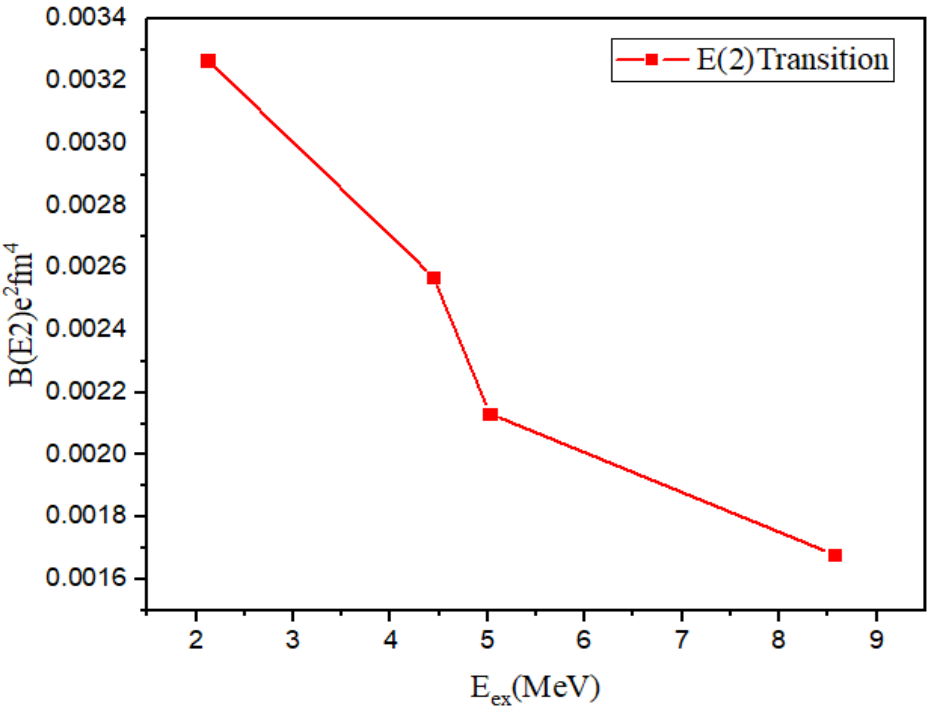

Fig.3 .Variation of B(E2) values with respect to the excitation energy of excited states

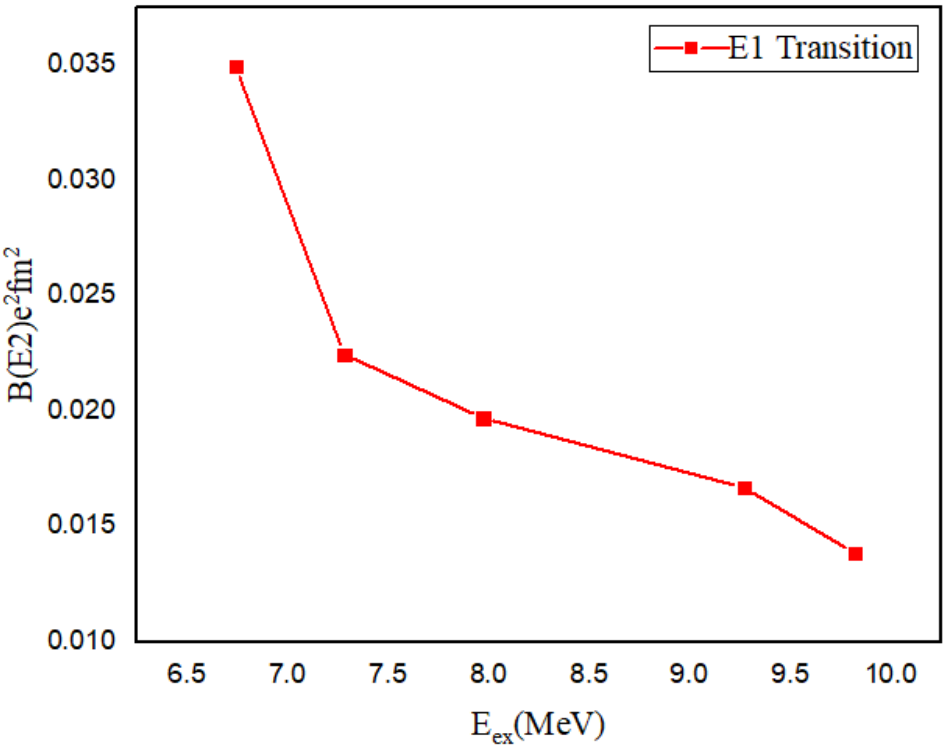

Fig.4. Variation of B(E1) values with respect to the excitation energy of excited states

Results and Discussion

This study investigated the wave function and energy of bound and excited states in the $^{10}B(n,\gamma)^{11}B$ reaction using the Woods-Saxon potential model. Fine-tuning the Woods-Saxon potential parameters allowed for the determination of the reaction's binding energy. The Q-value of the process was found to be 11.45 MeV, and the final state's spin-parity was established as $[\frac{3}{2}]^-$,The Woods-Saxon parameters for the ground state were obtained and presented in Figure 1. Additionally, Figure 2 depicts the radial wave function calculated using the potential parameters from Table 1, along with its corresponding wave function chart. Furthermore, the excitation energies and spin-parities of the excited states in ^{11}B for E1 and E2 transitions were determined and tabulated in Tables 2 and 3, respectively. Figure 3 illustrates the variation of B(E1) and B(E2) values with respect to excitation energy. This figure clearly shows a decreasing trend in B(E1) and B(E2) values as the excitation energy increases.

Table 1. The Wood-Saxon parameters for ground state ^{10}B+n reaction

E(MeV)	V_0	$R_0=R_C$	AA=AAS	V_{S0}	R_{S0}
11.45	-35.76	3.50	0.694004	-30.0586	2.19105

Table 2. The Wood-Saxon parameters for E1 tansition

Binding energy(MeV)	V0	R0=RC	AA=AAS	VS0	RS0	B(E1)
4.71	-23.28	2.42	0.75900	16.0586	2.19105	0.03494
4.17	-52.10	3.51	0.959004	13.0586	2.19105	0.2247
3.48	-30.08	4.54	0.999004	8.0086	2.03105	0.01971
2.18	-52.36	3.34	40.9004	10.9586	2.20105	0.01669
1.63	-40.02	3.50	0.659004	10.0586	2.10105	0.1386

Table3.The Wood-Saxon potential for E2 transition

Binding energy(MeV)	V0	R0=RC	AA=AAS	VS0	RS0	B(E2)
9.33	-34.04	3.08	0.70900	26.9586	2.19105	0.003267
7.01	-55.02	3.790	0.609004	34.9586	2.19105	0.002572
6.43	-30.09	4.07	0.999004	30.0586	2.19105	0.002132
2.89	-34.52	3.00	0.709004	10.0586	2.10105	0.001680

Conclusions

In conclusion, this study examined the variation of B(E1) and B(E2) transition strengths in the ^{11}B nucleus across different excitation energies and spin-parity states. Utilizing the Woods-Saxon potential model within the framework of the ^{10}B+n cluster model, we observed a strong correlation between the transition probabilities and the excitation energy. This finding highlights the significant impact of excitation energy on the electromagnetic properties of ^{11}B nuclei.

Acknowledgements

We acknowledge the support provided by Arak University in the preparation of our paper.

References

[1]Bertulani C. A., and Baur G(1986). "Electromagnetic processes in relativistic heavy ion collisions", Nuclear Physics A ,458(4), 725-744,.
[2]Ranjesh,Kharab(2018). Dependence of B(E2) and B(M1) transition strengths on energy and spin of excited states of ^{18}F. Modern Physics Letters A 33,(32) 1850188.
[3] Khalili.H,M.Dalvand et al.(2023).Numerical Study of El ectromagnetic Transitions in Proton Radiative Capture by ^{10}B . Iranian Journal of Applied Physics
[4]Khalili.H,M.Dalvand et al.(2023). Numerical study of transition rate and B(E2) transition strengths for 17O(p,γ)18F reaction.Ahvaz university.

[5] Bohr. A, Mottelson .B, (1969). Nuclear Structure,vol. I, Benjamin, New York.

[6]Dalvand.M,H.Khalili(2024)Examination of gamma radiation from10B(p,γ)11C reaction at low energies.The EUROPEAN PHYSICAL JOURNAL A.

[7] Bertulani C. A. (2003), "RADCAP. .", A potential model tool for direct capture reactions , Computer Physics Communications 156(1), 123-141.

[8] Edmonds., Alan Robert.(1996), “Angular momentum in quantum mechanics”, Vol. 4. Princeton university press.

[9] Buckner M. Q. Iliadis C.,Kelly K. J., Downen L. N., Champagne A. E., Cesaratto J. M., Howard C., and Longland R (2015). "High-intensity-beam study of 17O(p, γ)18F and thermonuclear reaction rates for O 17+ p", Physical Review C ,91(1), 015812.

[10] Bolsterli Mark (1969). "A New Exposition of Nuclear Physics: Nuclear Structure Single-Particle Motion. Aage Bohr and Ben R. Mottelson. Benjamin, New York,Science,166(3904),489-489.

ICNST 2024
International Conference on Nuclear Science and Technology
6- 8 MAY 2024 | Isfahan, Iran

Evaluation of parameters affecting the simultaneous production of rhenium-186 and rhenium-188 by experimental and numerical methods (Paper ID : 1234)

Hassan Ranjbar [1*], Reza Bagheri [2], Reza Davarkhah [1]

[1]Nuclear Fuel Cycle Research School, Nuclear Science and Technology Research Institute, Tehran, Iran
[2]Radiation Applications Research School, Nuclear Science and Technology Research Institute, Tehran, Iran

Abstract

For many years, different ligands have been combined with rhenium therapeutic radioisotopes, specifically rhenium-186 and 188, to create radiopharmaceuticals for the treatment of various illnesses. Because of the unique qualities that set each of these radioisotopes apart, they can all be used to eradicate different kinds of cancers. Large cancers can be effectively removed in 188Re thanks to the use of high-energy, long-range beta particles. However, ^{186}Re's low energy, short range beta particles are a sufficient weapon to destroy tiny tumors with a high yield and little side effects. As a result, the properties of each of these radioisotopes can only partially address the therapy on their own. Therefore, we reasoned that ^{188}Re and ^{186}Re in conjunction must provide the greatest results when treating tumors of different sizes. One possible outcome of neutron-irradiation of natural rhenium is the simultaneous production of ^{186}Re and ^{188}Re. We want to know if the natural irradiation of rhenium, together with the simultaneous synthesis of these radioisotopes, provides us with the right amounts of radioactivity to make compositional radiopharmaceuticals. This study examines the kind and quantity of impurities created, as well as the practical and theoretical evaluations of the simultaneous generation of ^{186}Re and ^{188}R to achieve compositional radiopharmaceuticals by natural rhenium irradiation in the Tehran research reactor. The outcomes demonstrated that the theoretical computations and experimental data correlate well. The data's greatest relative error has been determined to be 8%. The findings shown that ^{186}Re and ^{188}Re could be produced simultaneously with suitable and almost equal activities with irradiating natural rhenium for 4 days and considering 1 day for cooling. Also, the levels of impurities in the simultaneous manufacture of ^{186}Re and ^{188}Re using the natural rhenium irradiation technique are negligible in comparison to the primary products, and the primary products' activities are sufficient to make compositional radiopharmaceuticals.

Keywords: Simultaneous production, Radioisotope production, purity

Introduction

To date, most preclinical and clinical research has focused on harnessing beta-emitting radionuclides such as 131I, 90Y, 153Sm, 186Re and 188Re for therapeutic applications [1]. The ability of 186Re and 188Re to treat both small and large tumors makes their combined use well-suited for a range of cancers, including metastases from prostate cancer which often present as small lesions widely distributed throughout the body. Treatment plans utilizing these radionuclides are estimated to deliver absorbed doses of 30-50 Gy to tumor tissues over 1-2 weeks with limited damage to surrounding healthy organs.

Of the beta-emitting radioisotopes commonly used for treatment purposes, the two rhenium radioisotopes - 186Re and 188Re - occupy a unique position due to their additional ability to generate gamma rays for diagnostic imaging alongside their therapeutic beta emissions. This dual therapeutic and imaging capacity distinguishes rhenium from other commonly used beta emitters in nuclear medicine.

The radionuclide 186Re produces beta particles with a maximum energy of 1.07 MeV in 71% of decay events and has a half-life of 3.7 days. It also emanates γ-radiation at 137.16 keV in 9.4% of decays, permitting scintigraphic imaging during treatment. In contrast, 188Re produces high-energy beta particles with a maximum energy of 2.12 MeV in 79% of decays and has a half-life of 17 hours. Additionally, it emanates γ-radiation at 155 keV in 15% of decays, facilitating scintigraphy alongside therapy. 186Re can be produced via neutron irradiation of 185Re in a reactor according to the 185Re(n,γ)186Re nuclear reaction, or in a cyclotron utilizing reactions such as 186W(d,2n)186Re and 186W(p,n)186Re. Alternatively, 188Re can be generated either through a 188W/188Re generator system or via the 187Re(n,γ)188R nuclear reaction [2].

The high energy beta particles and long tissue penetration range of 188Re allow for high dose delivery to large tumors, suggesting it may demonstrate greater therapeutic efficacy for voluminous cancers. In contrast, 186Re's lower energy beta particles and shorter penetration convey most of its energy within small tumors, indicating it is well-suited for eradicating localized lesions. Additionally, 186Re's longer half-life of 3.7 days means it will require more time to deliver an equivalent absorbed dose compared to 188Re. As such, a mixture of these radionuclides or "cocktail" may prove more powerful, facilitating customized dosing to destroy cancers of varying dimensions [3,4]. This tailored approach could maximize therapeutic effect.

When using either radionuclide alone, the emission of shorter-lived 188Re would cease rapidly, potentially preventing full irradiation of larger malignancies. Meanwhile, administering solely the longer-lived 186Re could lead to delayed initiation of tumor damage, complicating patient management. However, combining 186Re and 188Re into a single radiopharmaceutical would allow 186Re irradiation of residual disease to continue after 188Re's radiation finished, complementing their properties. Accordingly, generating both radioisotopes at appropriate activities appears critical for developing combined formulations and optimizing targeted radiotherapy outcomes.

Naturally occurring rhenium exists as two isotopes, 185Re and 187Re. 185Re is considered a stable rhenium radioisotope, while 187Re has an extremely long half-life of approximately 4.33×10^{10} years, allowing it to also be classified as effectively stable. The abundances of 185Re and 187Re in natural rhenium are 37.4% and 62.6%, respectively. Notable for radiopharmaceutical applications, both 185Re and 187Re exhibit large thermal neutron capture cross sections (σ=112.05 barns for 185Re and 76.46 barns for 187Re), rendering them amenable to neutron bombardment for production of radioactive rhenium isotopes. Therefore, a mixture of ^{186}Re and ^{188}Re can be produced by irradiating natural rhenium.

Prior studies have generated 186Re and 188Re via reactor irradiation of natural rhenium, achieving varying isotope ratios depending on parameters such as irradiation time, cooling period, and neutron flux levels for medical application [5,6]. Some utilized only 4 days cooling, which would render the 188Re concentration trivial given its half-life, leaving 186Re as the predominant isotope in the mixture. Other works proposed 7 days irradiation followed by 1 day cooling [7-9]. Continued optimization of production methods is critically important to control the resultant ratios and tailor mixtures appropriately based on intended therapeutic use given the differences in half-lives between 186Re and 188Re. Further research aims to define optimized production protocols to generate well-characterized combinations of these radioisotopes for combined radiopharmaceutical formulations.

The objective of the present work is to determine the optimal irradiation duration for rhenium to concurrently generate 186Re and 188Re at matched, therapeutically useful radioactivity while minimizing impurity production. This will facilitate the development of well-characterized mixed

radiopharmaceutical formulations leveraging the complementary properties of these radioisotopes for maximizing therapeutic efficacy in targeted radionuclide therapy applications.

Research Theories

As previously discussed, the neutron bombardment of natural rhenium provides a means to simultaneously generate both 186Re and 188Re due to the large neutron capture cross-sections of 185Re and 187Re. Through this approach, the two radioisotopes can be produced in a coordinated manner to facilitate the subsequent formulation of mixed radiopharmaceuticals. By optimizing the irradiation parameters, 186Re and 188Re may be obtained concurrently at suitable activities, allowing expeditious development of combined radiotracers. Leveraging the complementary properties of these radionuclides could maximize therapeutic outcome. Therefore, neutron activation of natural rhenium holds promise as a method for the coordinated production of 186Re and 188Re to enable generation of compositional radiopharmaceuticals.

While the current work focused on neutron activation of natural rhenium, other production options exist that were not investigated but could be topics of future study. For example, irradiation of enriched 185Re or 187Re targets may facilitate higher yields or altered ratios of 186Re and 188Re. Additionally, alternative nuclear reactions such as 186W(p,n) could be examined for simultaneous generation of the desired radioisotopes. A broader analysis of production methods may identify additional optimized schemes.

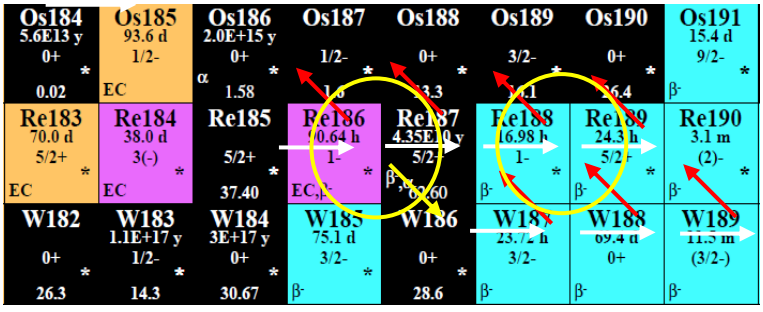

Fig. 1. Schematic diagram of possible radionuclides produced by irradiation of natural rhenium

Figure 1 depicts the neutron irradiation of natural rhenium, comprised of 185Re and 187Re, and the resultant nuclear reactions. As illustrated, the capture of neutrons by 185Re generates one of the principal radionuclides of interest, 186Re, which subsequently undergoes beta disintegration

to 186Os and electron capture to 186W. The reaction chain also involves neutron absorption by 186Re to form 187Re. Additionally, 187Re is produced via beta decay of 187W as well as originating from the natural abundance of 187Re in rhenium, both of which then capture neutrons to generate 188Re. These nuclear reactions will continue propagating as long as neutron bombardment of the rhenium target is sustained.

Analytical calculations of radionuclide activities are crucial for radioisotope production planning and optimization. Impurity generation may accompany the formation of desired products. Evaluating theoretical outcomes enables thorough examination of all production factors prior to experimental work. Notably, whilst irradiation parameters influence absolute activity levels, the relative ratios of produced nuclides and contaminants remain constant, as does the optimal irradiation time sought in this research. These findings are invariant with respect to altered irradiation conditions.

The time-dependent change in nuclear densities arising from neutron activation and transmutation can be expressed using the following system of differential equations:

$$\frac{dN_i(r,t)}{dt} = \varphi(r,t)\sum_j N_j(r,t)\sigma_{j\to i}(r) + \sum_k N_k(r,t)\lambda_{k\to i}(r) - \varphi(r,t)N_i(r,t)\sum_l \sigma_{i\to l}(r) - N_i(r,t)\sum_n \lambda_{i\to n} \quad (1)$$

Equation (1) constitutes a system of homogeneous first-order ordinary differential equations that describe the time evolution of nuclear densities in the irradiated rhenium target. The equations can be expressed in a compact matrix formulation by omitting the spatial dependence, as shown below:

$$\frac{d\mathbf{N}}{dt} = \mathbf{AN} \quad (2)$$

Computational modeling of radionuclide production was carried out using the MATLAB software environment. This allowed for the calculation of activities for radionuclides generated via neutron bombardment in the reactor system. Ultimately, implementation of the fundamental equation relating activity A to nuclear decay constant λ and number of atoms N (i.e. A = λN) enabled determination of predicted radiochemical yields [10].

Results

Precise calculation of radionuclide activities was achieved using a customized MATLAB simulation. Theoretical modeling and computational tools enable activity estimation at varying irradiation times as a function of influential parameters like neutron flux. Additionally, the decay rates of primary radioisotopes and impurities can be projected following irradiation or at intervening time points in subsequent chemical handling procedures. In this way, radionuclide purity levels over time after production cessation can be investigated. Experimental validation was performed by irradiating natural rhenium powder targets of 1 mg in an TRR research reactor with a nominal neutron flux of 5×10^{12} n/cm^2/s for 5 days. Radionuclide measurements were taken using high resolution gamma spectroscopy.

In the current work, activities of both 186Re and 188Re were simulated at different irradiation durations with the aim of obtaining matched values. A one-day cooling period was also stipulated. The calculated activities of the primary products 186Re and 188Re as a function of time are illustrated in Figure 2. This provided a means to identify suitable irradiation conditions conducive to generating the therapeutically optimized ratio of rhenium radioisotopes.

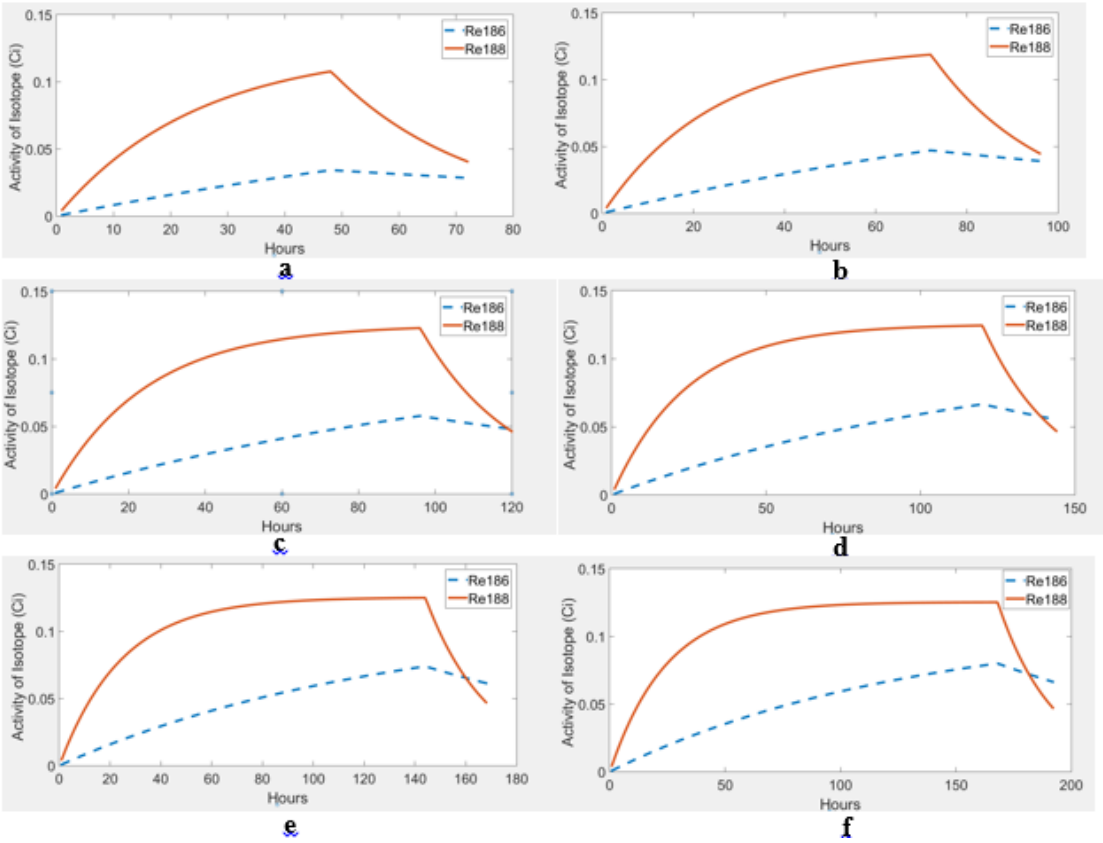

Fig. 2. Examination of activity over time under varying irradiation durations accounting for 1 day of cooling: a) sample irradiated for 2 days, b) sample irradiated for 3 days, c) sample irradiated for 4 days, d) sample irradiated for 5 days, e) sample irradiated for 6 days, f) sample irradiated for 7 days.

To enable more rigorous analysis and promote high radiochemical purity, the production kinetics of potential impurity radionuclides were also examined. Accounting for off-target radionuclides generated is critically important in radiopharmaceutical synthesis, as any residual impurities could deliver unintended radiation doses to patients. The presence of extraneous radionuclides in the irradiated target that ultimately transfer into the prepared radiotracer is an undesirable outcome. The precisely computed activities of possible impurities are displayed in Table 1. Considering such contaminant data alongside the activities of the primary radionuclides allows for thorough optimization and purification strategies to be devised, ensuring only the therapeutic radionuclides of interest are incorporated into the final pharmaceutical composition.

Table 1. Activities of impurities at the end of different irradiation time and one day cooling

Radionuclides		Irradiation time (Day)					
		2	3	4	5	6	7
^{189}Re	Activity (Ci)	1.613×10^{-7}	2.329×10^{-7}	2.777×10^{-7}	3.036×10^{-7}	3.178×10^{-7}	3.254×10^{-7}
^{187}W		4.574×10^{-8}	1.284×10^{-7}	2.559×10^{-7}	4.248×10^{-7}	6.302×10^{-7}	8.667×10^{-7}
^{187}Re		2.775×10^{-11}	2.774×10^{-11}	2.774×10^{-11}	2.773×10^{-11}	2.772×10^{-11}	2.772×10^{-11}
^{188}W		1.023×10^{-11}	4.458×10^{-11}	1.222×10^{-10}	2.606×10^{-10}	4.753×10^{-10}	7.797×10^{-10}
^{186}Os		5.915×10^{-20}	1.052×10^{-19}	1.599×10^{-19}	2.216×10^{-19}	2.892×10^{-19}	3.616×10^{-19}

As can be seen in Table 1, the calculated activities of potential impurities following 4 days of irradiation and 1 day of cooling are significantly less than those observed after 7 days of irradiation and cooling in some previous studies. This indicates that shorter irradiation durations combined with adequate decay can minimize off-target radionuclide generation, promoting highly purified final radiopharmaceutical production as needed for safe radiotherapeutic applications. The current computed results therefore suggest favorable kinetic parameters for obtaining balanced 186Re and 188Re activities with low residual impurity levels.

Discusion

As depicted in Figure 2, subfigures (a) and (b) illustrate activity curves for 186Re and 188Re that do not intersect, precluding achievement of equal activities. Meanwhile, the activity curves intersect temporarily during cooling in subfigures (d), (e) and (f), yet diverge again by cooling's conclusion.

Notably, subfigure (c) shows near convergence of the activity profiles for 186Re and 188Re at the termination of cooling. This indicates attainment of almost identical radical yields, a favorable outcome for the intended generation of combined radiopharmaceuticals. The results therefore suggest that an irradiation period of 4 days as modeled in subfigure (c) may enable coordinated production of 186Re and 188Re at matched levels that facilitate immediate formulation into an optimized therapeutic radiotracer.

Long-lived radionuclides such as 187Re (4.33×10^{10} y), 188W (69.8 d), and 186Os (2×10^{15} y) exhibit very low predicted activities compared to the principal products 188Re (17h) and 186Re (90h), allowing them to be reasonably discounted. The remaining potential impurities 189Re (24.3 h) and 187W (24 h) have half-lives closer to the target radionuclides, inevitably leading to some generation over time. However, even these activities are deemed negligible relative to 188Re and 186Re production levels.

As shown in Table 1, calculated 189Re and 187W activities are at least an order of magnitude (10 times) lower than the 186Re and 188Re activities, meeting the pre-defined threshold for acceptable residual impurity levels. Specifically, 189Re and 187W activities are below 1×10^{-6} Ci, while 186Re and 188Re activities are around 5×10^{-2} Ci after irradiation and cooling. These impurity levels are considered negligibly low and minimized compared to threshold values, as their activities are less than 0.02% of the primary radioisotopes even without additional purification steps.

In the present study, impurity activities are conclusively trivial in comparison to 188Re and 186Re. Consequently, no purification steps are warranted when utilizing the optimized 4 days irradiation and 1 day cooling production parameters. Furthermore, these trace contaminants would not be discernible via spectral analysis of irradiated rhenium targets. Overall, high radiochemical purity can be secured for the intended compositional rhenium radiopharmaceutical.

Table 2 provides a comparative analysis of experimentally and theoretically determined activities for 186Re, 188Re, 187W and 189Re at the conclusion of five days of irradiation/cooling. As shown, only minor deviations are observed between the computed and experimentally measured values. This close agreement between the theoretical modeling predictions and empirical outcomes serves to validate the precision of the computational radioisotope production simulations. The conformity exhibited suggests the theoretical approach offers a reliable means for approximately forecasting radionuclide yields prior to embarking on radiotracer generation optimization efforts.

Table 2. Activities of radionuclides produced at the end of the fifth day in experimental and theoretical method

Radionuclide	Experimental activity (Ci)	Theoretical activity (Ci)
^{186}Re	5.02×10^{-2}	4.791×10^{-2}
^{188}Re	4.87×10^{-2}	4.628×10^{-2}
^{189}Re	3.01×10^{-7}	2.777×10^{-7}
^{187}W	2.76×10^{-7}	2.559×10^{-7}

The concurrent production of 186Re and 188Re in well-defined ratios now enabled through this optimized neutron activation process holds promise for formulation of customized targeted radiotherapies. Depending on the intended application, the isotope concentrations could potentially be tuned for smaller micrometastases versus larger primary tumors. Ongoing work will focus on developing mixed radiopharmaceutical formulations incorporating these radioisotopes for preclinical validation of enhanced therapeutic efficacy against cancers of varying sizes and disease stages compared to single isotope treatments.

Conclusions

This work theoretically evaluated simultaneous production of the medically relevant radionuclides 186Re and 188Re from natural rhenium targets via neutron irradiation at varying times (2–7 days with 1 day cooling) to determine optimal yields. Calculations encompassed impurity radionuclide generation kinetics, accounting for both negligibly produced isotopes as well as more substantially formed 189Re and 187W. Results demonstrated that within 4 days irradiation/1 day cooling scheme, these two impurities exhibited markedly lower activities compared to prior studies using 7 days irradiation/cooling protocols. Considering all factors, the calculated impurity levels can reasonably be deemed inconsequential relative to the target radioisotopes. Therefore, no purification procedures would be warranted, as residual contaminants introduced during this production method would not compromise the intended radiopharmaceutical compositions. The results of this research showed, the application of theoretical modeling facilitated thorough prospective evaluation of the entire production scheme and identification of favorable parameters-demonstrating the utility of theoretical approaches for guiding experimental radiotracer engineering prior to empirical validation.

Limitations

The computational model made certain simplifying assumptions that could be expanded upon in future work. Neutron transport effects were not considered, and the model treated the reactor system as a uniform neutron flux. Additionally, only primary decay and transmutation reactions were included; secondary processes like neutron scattering and induced fission were neglected. Accounting for spatial and energy dependence of neutron flux profiles as well as additional nuclear reaction channels may improve predictive accuracy. The model also did not incorporate specific parameters of the experimental irradiation conditions and target geometry that could influence results. Overall, the model provides a useful first-order approximation but its predictive power may be enhanced in future by addressing some of these limitations.

References

[1] Chatachot, K. (2020). Evaluation of patient doses from 177lu-PSMA in metastases prostate cancer treatment at King Chulalongkorn Memorial hospital.

[2] RAMAMOORTHY, N. (2020). MEDICAL APPLICATIONS–PART II: NUCLEAR MEDICINE AND RADIOPHARMACEUTICALS. Ionising Radiation and Mankind, 53.

[3] Ranjbar, H., Bahrami-Samani, A., Beiki, D., & Ghannadi-Maragheh, M. (2017). Development of 153Sm/177Lu-EDTMP as a possible therapeutic complex. Iranian Journal of Nuclear Medicine, 25(1), 11-16.

[4] Ranjbar, H., Bahrami-Samani, A., Yazdani, M. R., & Ghannadi-Maragheh, M. (2016). Determination of human absorbed dose of cocktail of 153 Sm/177 Lu-EDTMP, based on biodistribution data in rats. Journal of Radioanalytical and Nuclear Chemistry, 307, 1439-1444.

[5] Das, T., Banerjee, S., Samuel, G., Kothari, K., Unni, P. R., Sarma, H. D., ... & Pillai, M. R. A. (2000). [186/188Re] rhenium-ethylene dicysteine (Re-Ec): preparation and evaluation for possible use in endovascular brachytherapy. Nuclear medicine and biology, 27(2), 189-197.

[6] Häfeli, U. O., Casillas, S., Dietz, D. W., Pauer, G. J., Rybicki, L. A., Conzone, S. D., & Day, D. E. (1999). Hepatic tumor radioembolization in a rat model using radioactive rhenium (186Re/188Re) glass microspheres. International Journal of Radiation Oncology* Biology* Physics, 44(1), 189-199.

[7] Kothari, K., Pillai, M. R. A., Unni, P. R., Mathakar, A. R., Shimpi, H. H., Noronha, O. P. D., & Samuel, A. M. (1998). Preparation of 186Re complexes of dimercaptosuccinic acid and hydroxy ethylidine diphosphonate", Modern Trends in Radiopharmaceuticals for Diagnosis and Therapy. In Proc. Symp. Lisbon.

[8] Kothari, K., Satpati, D., Mukherjee, A., Sarma, H. D., Venkatesh, M., & Pillai, M. R. A. (2002). Kidney uptake of 186/188Re (V)-DMSA is significantly reduced when the reducing agent is changed from stannous ion to metabisulfite. Journal of Labelled Compounds and Radiopharmaceuticals: The Official Journal of the International Isotope Society, 45(8), 675-686.

[9] Kothari, K., Pillai, M. R. A., Unni, P. R., Shimpi, H. H., Noronha, O. P. D., & Samuel, A. M. (1999). Preparation, stability studies and pharmacological behavior of [186Re] Re–HEDP. Applied radiation and isotopes, 51(1), 51-58.

[10] Evaluated Nuclear Data File (ENDF), https://www-nds.iaea.org/exfor/endf.htm.

ICNST 2024
International Conference on Nuclear Science and Technology
6- 8 MAY 2024 | Isfahan, Iran

Estimating the absorbed dose of sensitive organs in cardiac Spect (MIBI) using MIRD and conjugate view method (Paper ID : 1255)

Mahsa Firouzbakht [a], Elham Saniei [a*23] ,Mehdi Salehi Barough[a]

[a] *Facaulty of nuclear engineering, Central Tehran Branch Islamic Azad University, Tehran, Iran*

Abstract

Cardiac scan is one of the common scans in nuclear medicine centers in order to diagnose heart diseases and coronary artery blockages. The purpose of this study was to calculate the absorbed dose of liver, heart and thyroid organs in cardiac scintigraphy with 99mTC-MIBI radiopharmaceutical. In this study, the radiopharmaceutical 99mTC-MIBI was first injected into the patient in the stress phase. And then the scan images were obtained by gamma camera in 15, 30, 60, 150 minutes after injection. Then, the activity value was calculated by the inoculation method, and finally, the absorbed dose was calculated by the MIRD method. Finally, the values of absorbed dose per prescribed activity for heart, liver, and thyroid organs were 4.4, 6.74, and 0.99 millicuries in the stress phase, respectively, and 3.4, 7.6, and 1.01 millicuries in the resting phase, respectively. According to this study, the liver received the maximum absorbed dose and the thyroid received the minimum absorbed dose.

Introduction

One of the uses of radioactive materials is the diagnosis and treatment of diseases (1) in nuclear medicine, the diagnosis and treatment of diseases is done by radiopharmaceuticals. (2 and 3) Nuclear medicine images are very valuable because they collect physiological data (4)

The radiopharmaceutical investigated in this study was 99mTC-MIBI. 99mTC-MIBI is injected intravenously and has a high volume of distribution. (5) This radiopharmaceutical causes an internal dose in the patient's body. (6) In fact, there are several methods for measuring the internal dose of radioactive substances in nuclear medicine. In this study, the MIRD method, which is one of the most reliable internal dosimetry methods in nuclear medicine, has been used. (7, 8) The purpose of this study is to measure the absorbed dose of the liver, thyroid and heart

[23] * Corresponding Author. Tel.: +98-912-430-6819.

E-mail address:El.saniei@iau.ac.ir

organs after the injection of 99mTC-MIBI radiopharmaceutical in the stress phase using spect images.

Data preparation

This study was conducted on 20 patients who referred to the nuclear medicine department of Baath Hospital in Tehran province. In this study, the resting stage was performed on one day and the stress stage on the next day, and in each stage, 20 millicuries of radiopharmaceutical 99mTC-MIBI were injected into the patient.

Material and methods

Gamma camera (Dual-Head) was set on photopic 140 kev with a window width of ±20% for 99mTC to scan patients. Then, each patient was asked to lie down on the bed of the gamma camera, and then the collimators of the gamma camera were set at a suitable distance from the patient. Then 99mTC-MIBI radiopharmaceutical was injected into the patient, and 15 minutes later, imaging was started in the anterior and posterior regions, and then images were obtained at 30, 60, and 180 minutes from each patient in a period of one minute in the anterior and posterior views. Then, the amount of absorbed activity in each of the organs at different times of 2, 30, 60, 180 minutes after injection was obtained from equation (1) .(9)

$$A = \sqrt{\frac{I_A \times I_p}{e^{-\mu t}}} \times \frac{f}{c} \quad (1)$$

where t was the thickness of the patient's body in the area of the organs studied in this research in cm, which was calculated through the lateral images obtained from the patients. The correction factor is linear. C is the system calibration factor obtained from studies for a given activity value under the same imaging conditions of the patient in air by activity counting for 99mTC. IA and Ip were the counts per minute in the anterior and posterior views, respectively, and were calculated in this way, which was initially using the scan images obtained on the gamma camera monitor at 15, 30, 60, and 150 minutes in each of the anterior and posterior views. A ROI was manually drawn for each organ in the organ anatomy area, and the number of counts per minute as well as the number of pixels in the desired area were calculated in the ROI area drawn by the gamma camera software. And then outside the anatomical region of each organ in the side margin to get the field count on the images obtained from the ROI scan. It should be noted that in order to obtain the field count, it should not be drawn in the area of

another organ where the count is high. For field counting, the number of counts per minute as well as the number of pixels were calculated by the software for the drawn area. And finally, according to the following formula, IA and Ip counts per minute were calculated in the anterior and posterior regions, respectively, by applying background correction (Relation 2). (10)

$$I_A=I_{ROI\ Source}\text{-}I_{ROI\ background}\times S_{sorce} \qquad (2)$$

$$I_p=I_{ROI\ Source}\text{-}I_{ROI\ background}\times S_{sorce}$$

After calculating the activity for each of the liver, heart and thyroid organs at different times of 15, 30, 60, 150 minutes, the activity curve was drawn according to time, and then by calculating the area under the graph, the cumulative activity value was calculated and finally according to the relation (3) the amount of absorbed dose was calculated. (11, 12, 13).

$$D = \tilde{A}\times S \qquad (3)$$

In this regard, the cumulative activity of the target organ is the absorbed dose in the organ, which is calculated using equation 4.

$$S = \Phi \times \frac{\Delta}{m} \qquad (4)$$

where the fraction of energy emitted from the source organ that is absorbed in the target organ is the equilibrium dose constant, which is considered equal to 0.256 for the set of rays emitted from technetium in terms of gram rad per microcurie per hour. (14)

Results

By drawing the ROI on each of the organs during the times studied in this research and calculating the count per unit of activity time in each of the organs, as well as calculating the activity using the method of integration and finally entering the data into Excel software. The average activity was obtained for each organ. After the calculations related to the activity, the graph of the average activity in terms of time was drawn for each of the organs, and the results of the average of the liver, heart, and thyroid in the stress and resting stages are shown in Figure 1 and 2, respectively.

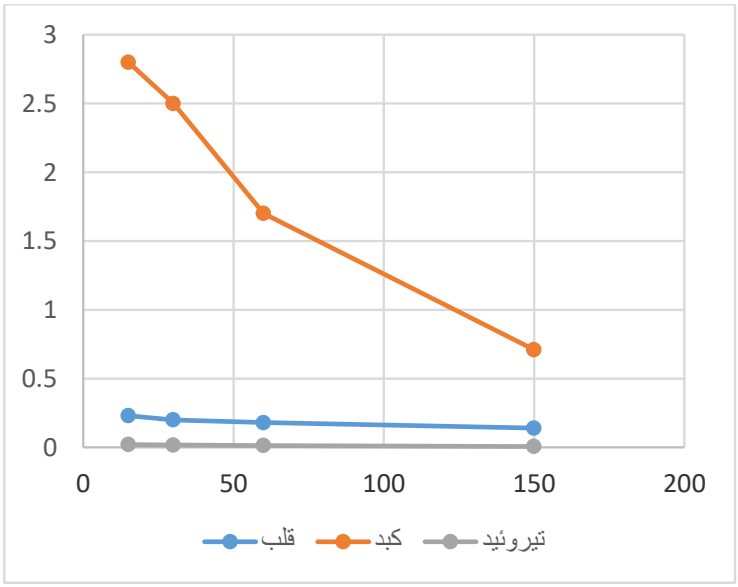

Figure 1: Graph of the average activity in terms of time for the organs of the heart, liver, and thyroid during the stress stage

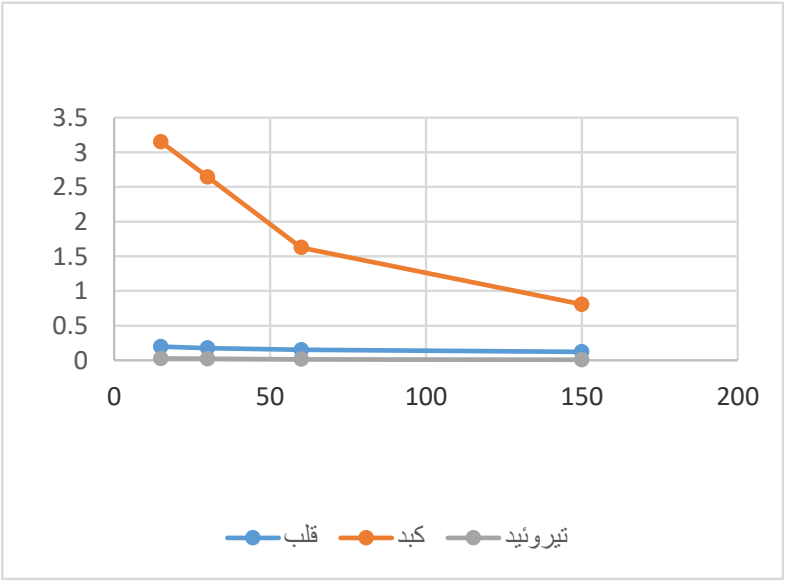

figure 2:. The graph of the average activity in terms of time in the fasting stage in the heart, liver and thyroid

As can be seen, the liver, heart and thyroid have a descending graph. According to the results of this research, we see that the activity of these organs decreases with the passage of time after the administration of radiopharmaceuticals. And after this step, by calculating the area of activity in

terms of time, the amount of cumulative activity was calculated for each of the organs. The results of this section are given below.

At the end, the absorbed dose was calculated, and the results related to the absorbed dose of the liver, heart and thyroid organs in the stress and rest phase are given in Table 1.

Table 1: The average amount of absorbed dose for liver, heart and thyroid organs in stress and resting stage

Rest stage	Stress stage	Absorption dose of organs
۰,۰۰۳٤	۰,۰۰٤٤	Heart
۰,۰۰۷٦	۰,۰۰٦۷	Liver
۰,۰۰۱	۰,۰۰۰۹۹	Thyroid

Conclusion

In this study, it was seen that in the first minutes after the injection of MIBI radiopharmaceutical, the activity of the injected radiopharmaceutical in the final organs of the heart, liver, and thyroid reached its maximum level and decreased with the passage of time. The absorbed dose of the liver is the highest and the absorbed dose of the thyroid is the lowest.

The results obtained in this research showed a good agreement with the results reported in the report of Stabin and his colleagues (16). This match shows that this method can be a suitable method for calculating the absorbed dose of organs in nuclear medicine centers, and considering that this method does not require special equipment, it can be used as a simple method for specialists in this department.

Reference

(1) Passante NP. Essentials of Nuclear Medicine Imaging. American Journal of Roentgenology. 2013;200(1):W89-W.

(2) . Zaidi H, Erwin WD. Quantitative analysis in nuclear medicine imaging. Journal of Nuclear Medicine. 2007;48(8):1401.-

(3).Chandra R. Nuclear medicine physics: Wolters Kluwer Health/Lippincott Williams & Wilkins; 2012.

(4).Gupta TK. Instrumentation and Its Applications in Nuclear Medicine. Radiation, Ionization, and Detection in Nuclear Medicine: Springer; 2013. p. 451-94.

(٥). Verbruggen AM ND, Van Nerom CG, Bormans GM, Adriaens PJ, De Roo MJ. . Technetium-99m-L, L-ethylenedicysteine: a renal imaging agent. I. Labeling and evaluation in animals. Journal of nuclear medicine: official publication. Society of Nuclear Medicine 1992; ;33(4):551-7.

(٦). Prvulovich EM BJ, Waddington WA, Rudrasingham P,

Verbruggen AM, Ell PJ. . Clinical evaluation of technetium-99m-L, L-ethylenedicysteine in patients with chronic renal failure. Journal of nuclear medicine: official publication, Society of Nuclear Medicine. 1997;;38(5):809-14.

(٧). Chu KH LY, Hsu CC, Chen CY, Pan LK. Evaluation of effective dose for a patient under Ga-67 nuclear examination using TLD, water phantom and a simplified model. Journal of radiation research. 2012;;53(6):989-98.

(٨). Stabin MG, Sparks RB, Crowe E. OLINDA/EXM: the second-generation personal computer software for internal dose assessment in nuclear medicine. Journal of Nuclear Medicine. 2005;46(6):1023-7

(٩). McParland BJ. Nuclear medicine radiation dosimetry: advanced theoretical principles: Springer Science & Business Media; 2010.

(١٠). Pereira J ,Stabin M, Lima F, Guimarães M, Forrester J. Image quantification for radiation dose calculations–limitations and uncertainties. Health physics. 2010;99(5):688.

(١١). Liu B, Kuang A, Huang R, Zhao Z, Zeng Y, Wang J, et al. Influence of vitamin C on salivary absorbed dose of 131I in thyroid cancer patients: a prospective, randomized, single-blind, controlled trial. Journal of Nuclear Medicine. 2010;51(4):618-23.

(١٢).Wegst AV. Methods of calculating radiation absorbed dose. International Journal of Radiation Applications and Instrumentation Part B Nuclear Medicine and Biology. 19.٧١-٢٦٩:(٣)١٤;٨٧

(۱۳). ICRP. Radiation dose to patients from radiopharmaceuticals. Addendum 3 to ICRP Publication 53. ICRP Publication 106;197, 38; 2008

(۱٤). Weber DA, Makler PT, Watson EE, Coffey JL, Thomas SR, London J. Radiation absorbed dose from technetium-99m-labeled bone imaging agents. Journal of Nuclear Medicine. 1989;30(6):1117-22.

(۱٥).James H.Thrall.Harvey A.Ziessman.Nuclear Medicine The Requisites.1996

(۱٦). Stabin MG. Fundamentals of nuclear medicine dosimetry: Springer; 2008.

Quasi-linear model of cryogenic distillation for 13C isotope separation (Paper ID : 1266)

Younes Amini*, Fatemeh Mansourzadeh, Valiallah Ghazanfari, Mohammad Mahdi shaman

Nuclear Fuel Cycle Research School, Nuclear Science and Technology Research Institute, Tehran, Iran

* Corresponding author: y_amini@alum.sharif.edu, yamini@aeoi.org.ir

Abstract

This paper presents a model and simulation of cryogenic (^{13}C) isotope separation in a column. Utilizing the two-film theory, we established the isotopic mass transfer rate and derived the system of quasi-linear differential equations governing the evolution of the ^{13}C isotope during separation. The dynamics of the column are represented by quasi-linear model, dependent on time and spatial coordinates. Numerical analysis and simulation were conducted using the finite-differences method, validated by the Delf model. The results confirmed the reference data, revealing that after 60 hours, the ^{13}C concentration reached 2.7% and depleted ^{13}C contained 0.5%, with a maximum relative error of ±4.9% and an average relative error of ±2.4%. This quasi-linear PDE model serves as a valid approach, offering a foundation for future studies in modeling and process control.

Keywords: Quasi-linear model, Isotope separation column, Mathematical modeling, Carbon-13, Cryogenic distillation

Introduction

Today, stable isotopes are widely used in various industrial, research and medical fields. Due to the ever-increasing market demand and the fields of application of these isotopes and as a result of the significant increase in the price of these products, different countries have a special view on the production, separation and enrichment of these valuable isotopes [1-3].

Carbon element has two stable isotopes ^{12}C and ^{13}C. Carbon-13 has many uses in organic chemistry studies, biology, archeology, oil and gas, space and ocean studies, and in medical diagnosis in carbon monoxide-based breathing tests, and therefore the isolation of this isotope is very important in the industry [4-6].

Among the different separation methods, centrifugation and distillation methods are more likely to be industrialized because of their outstanding features. In the centrifuge method, the separation

factor depends on the mass difference (Δm) along with the mass of the isotopes, so it is mainly used to separate heavy isotopes. But in the distillation method, the separation factor depends on the relative mass difference of the isotopes (Δm/m) and because the relative mass difference of the components is much higher in light isotopes compared to heavy isotopes, the distillation method is suitable for the separation of light isotopes on a large scale. For example, it is very easy to separate hydrogen isotopes (^{1}H and ^{2}H) with a relative mass difference of 100% with the help of distillation [7].

Conventional isotopic enrichment distillation columns are very tall. Recently, the use of refrigeration distillation technology for isotope separation has been considered by researchers. Generally, in isotope separation systems, the input feed to the distillation column is a gas, and because in the distillation operation, there must be two phases of liquid and gas in the system. So, if the input feed to the column is a gas with a very low boiling temperature, for example, oxygen or methane (with boiling temperatures of 90 to 110 K), in order to create a liquid phase in the system, the temperature of the column needs to be below the boiling point of the input feed. Come. The process of distillation at very low temperatures is called cryogenic distillation. In fact, cryogenic distillation is similar to normal distillation, except that this method is used to separate the components of a gaseous mixture (under standard conditions). Therefore, it is necessary to carry out the process at low temperatures according to the boiling points of the components [8, 9]. Until 1940, the main method of enriching stable isotopes was using the clathron apparatus (EMIS) of the American Oak Ridge Laboratory. The high cost of this method made researchers focus on more economical methods such as centrifugation and distillation. The theory of multistage isotope separation was developed by Cohen in 1951 and the concepts of holdup, enrichment and equilibrium time were defined for ideal and real cascades. Centrifuges with parallel and non-parallel flow and evaporation were investigated [10]. Cohen also briefly discussed the behavior of gas-liquid inhomogeneous flow in chemical exchange columns and emphasized that this theory is the same for all isotope separation methods. In 1974, a complete and in-depth review of laboratory methods and theoretical work done on isotope effects with an emphasis on isotope vapor pressure was presented by Janso [11].

Carbon isotope separation through CO distillation technology is about 50 years old. Various semi-industrial (pilot) units have been developed in different countries and in different periods of time. The first production chains were put into operation in Great Britain, the Soviet Union and the United States. Because of this long history, it can be said that today, CO refrigeration distillation

is a well-known and reliable process for carbon isotope separation. Interest in this method for separating carbon isotopes was first created based on laboratory results (Table 3 1). According to the information presented in this table, it can be seen that one of the distinctive characteristics of the CO distillation process is relatively small HETP values of 2 to 3 cm. The interest in this separation method (distillation of carbon monoxide) in addition to the maximum separation coefficient between the components present in the system, is also related to the suitability of the HETP range related to CO distillation [12].

In this research article, a model and simulation of cryogenic (13C) isotope separation present in a column. Utilizing the two-film theory, we established the isotopic mass transfer rate and derived the system of quasi-linear differential equations governing the evolution of the ^{13}C isotope during separation. The dynamics of the column are represented by quasi-linear model, dependent on time and spatial coordinates. Numerical analysis and simulation were conducted using the finite-differences method, validated by the Delf model. The results confirmed the reference data, revealing that after 60 hours, the ^{13}C concentration reached 2.7% and depleted 13C contained 0.5%, with a maximum relative error of ±4.9% and an average relative error of ±2.4%.

Mathematical modeling and Simulation

Figure 1 shows the cryogenic distillation column of carbon-13 separation. The mail flow on the figure as below:

The feed flow rate (F);

Concentration (Nf) (mole fraction);

The waste flow rate (W);

Concentration (Nw) (mole fraction);

The product flow rate (P);

Concentration (NP) (mole fraction).

The mass-flow equilibrium is given by the equation:

$$F=P+W \text{ [moles/sec]} \quad (1)$$

The (^{13}C) isotope balance gives:

$$F.N_f=P.N_p+W.N_w \quad (2)$$

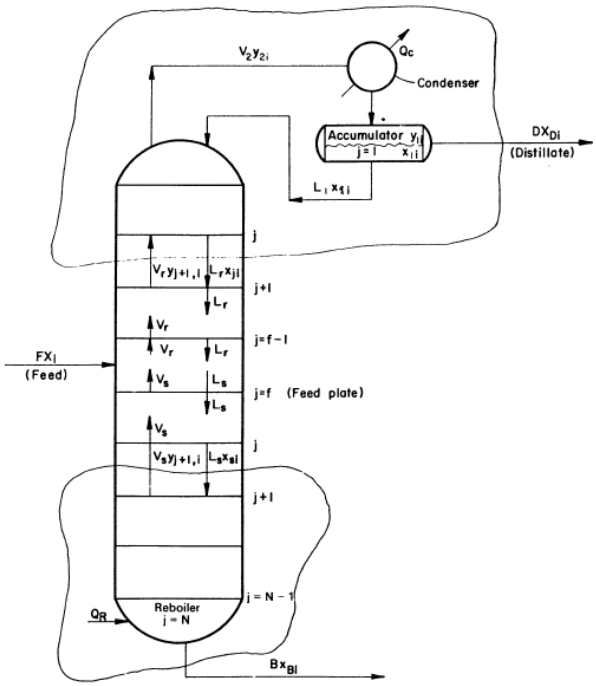

Figure 1: schematic of the separation column

For P=0, the column operates at "infinite reflux" (or "total reflux"). To separate the (^{13}C) isotope with the mole-fraction of (NP), at the flow rate P (mole/sec), the required feed flow rate is given by the equation:

$$F=(Np-Nw)/(Nf-Nw).P=(Np-Nw)/(N0-Nw).P \quad (3)$$

resulting in a "waste" flow rate:

$$W=(Np-Nf)/(Nf-Nw).P=(Np-N0)/(N0-Nw).P \quad (4)$$

Dedicated equipment is necessary to ensure the important operation condition W=F (for P=0). In order to define the main variables, it is useful to divide the operating variable into two categories: qualitative variables and quantitative variables. Because the feeding carbon dioxide flow rate has high purity, the main qualitative variable is the (^{13}C) isotope concentration (mole fraction) in different points of the column, but, more importantly, in the final product (P, Np). The quantitative variables refer to the hydrodynamic equilibrium and to the thermal equilibrium. Both the quantitative and qualitative variables maybe divided into input and output variables.

If (T, k) is the transfer speed and constant of the isotope exchange , the general equations of COHEN (Cohen, 1951) are, for a level (coordinate, z) in column:

$$H\frac{\partial N}{\partial t} + L_l\frac{\partial N}{\partial z} = +T \quad (5)$$

$$h\frac{\partial n}{\partial t} + L_g\frac{\partial n}{\partial z} = -T \quad (6)$$

where (N) is the mole fraction of (^{13}C), (n) is the mole fraction of (^{12}C), (H, h) are the carbon atoms accumulated (hold-up) in a specific volume in column, (Ll, Lg) are the acid (liquid) and oxides (gaseous) flow in counter-current expressed in atoms of carbon and (T) is given by the equation:

$$T=-k[N(1-n)-\alpha(1-N)] \quad (7)$$

Using Matlab, the author solved the nonlinear differential equations 5 and 6 for $\frac{\partial N}{\partial z} = 0$ and $\frac{\partial n}{\partial z} = 0$, with initial conditions N(t=0)=n(t=0)=1.1 given by the natural abundance of ^{13}C

$$H\frac{\partial N}{\partial t} = -k[(N-\alpha n)+n, N(\alpha-1)] \quad (8)$$

$$h\frac{\partial n}{\partial t} = +k[(N-\alpha n)+n, N(\alpha-1)] \quad (9)$$

The volumetric overall mass transfer coefficient

The volumetric overall mass transfer coefficient is related to physical properties like molecular diffusivity and vapor and liquid phase film thickness, which are very difficult to measure [13, 14]. However, in the following we will estimate the value of the mass transfer coefficient, based on the plant parameters by referring to the isotopic mass balance relations and to the rate of transfer per unit volume defined.

The overall volumetric mass transfer coefficient K may now be determined, written for the boundary condition (z = Zc), and it is equal to:

$$\mathrm{K} = \frac{\mathrm{L}}{(\alpha-1)\mathrm{Z_c}}\frac{\ln(\mathrm{N(Z_c)}/(1-\mathrm{N(Z_c)}))}{\mathrm{N_0}/(1-\mathrm{N_0})} \quad (10)$$

The isotope separation partial differential equations

The system of PDEs (8) and (9) can be solved in terms of the ^{13}CO liquid mole fraction (N), by describing the ^{13}CO vapor mole fraction (n) as:

$$\mathrm{n} = \frac{((\mathrm{H_l}/\mathrm{K})(\partial^2\mathrm{N}/\partial\mathrm{t}^2) + (\mathrm{L}/\mathrm{K})(\partial\mathrm{N}/\partial\mathrm{z}) + \mathrm{N})}{1+(\alpha-1)(1-\mathrm{N})} \quad (11)$$

and computing its partial derivatives with respect to time and height:

$$\frac{\partial\mathrm{n}}{\partial\mathrm{t}} = \frac{((\mathrm{H_l}/\mathrm{K})(\partial^2\mathrm{N}/\partial\mathrm{t}^2) + (\mathrm{L}/\mathrm{K})(\partial^2\mathrm{N}/\partial\mathrm{t}\,\partial\mathrm{z}) + (\partial\mathrm{N}/\partial\mathrm{t}))\mathrm{A} + (\partial\mathrm{N}/\partial\mathrm{t})(\alpha-1)\mathrm{B}}{\mathrm{A}^2} \quad (12)$$

$$\frac{\partial n}{\partial z} = \frac{((H_l/K)(\partial^2 N/\partial t^2) + (L/K)(\partial^2 N/\partial^2 z) + (\partial N/\partial z))A + (\partial N/\partial z)(\alpha - 1)B}{A^2} \quad (13)$$

Where:

$$A = [1 + (\alpha - 1)(1 - N)] \qquad B = \frac{H_l}{K}\frac{\partial N}{\partial t} + \frac{L}{K}\frac{\partial N}{\partial z} + N$$

Due to the small enrichment factor (ε =0.0069), the concentration changes along the length of the column are very slow, and after several days it reaches a stable condition. For this reason, the second time derivative can be omitted.

Since the distillation operation works under full reflux conditions, the intensity of the liquid and vapor flows will be equal to each other, and as a result, L=V. Due to the fact that the accumulation of gas in the column is very small compared to the liquid, it can be ignored and we have: $H_t=H_l$.

To further simplify the equation with similar assumptions, the combined derivative and the terms including ∂N/∂t (α-1) and ∂N/∂z (α-1)B can be ignored. did After simplifying and introducing Ψ=L-V as the current intensity of the bottom product of the column of equation, it will be as follows:

$$(H_l + H_v)\frac{\partial N}{\partial t} = \left(\frac{LV}{K}\right)\frac{\partial^2 N}{\partial z^2} - \frac{\partial N}{\partial z}[\Psi + L(\alpha - 1)(1 - N)] \quad (14)$$

Numerical analysis

The obtained quasi-linear equations should be solved by numerical methods by applying initial and boundary conditions. For shapes that have a simple geometry, the finite difference method is the most suitable option for solving these quasi-linear equations. Finite difference methods have high flexibility for nonlinear problems.

It should be mentioned that in this work, the explicit method is used to solve the quasi-linear equations. If we denote the mole fraction of ^{13}CO in the liquid phase N(z,t) by u(i,j), then the forward, backward and central derivatives of the quasi-linear equations will be as follows:

$$\frac{\partial N}{\partial z} = u_z(i\ j) \approx \frac{u(i+1\ j) - u(i\ j)}{\Delta z} \quad \text{forward} \quad (15)$$

$$\frac{\partial N}{\partial t} = u_t(i\ j) \approx \frac{u(i\ j+1) - u(i\ j)}{\Delta t} \quad \text{forward} \quad (16)$$

$$\frac{\partial^2 N}{\partial z^2} = u_{zz}(i\ j) = \frac{u(i+1\ j) - 2u(i\ j) + u(i\ j-1)}{\Delta z^2} \quad \text{central} \quad (17)$$

$$\frac{\partial^2 N}{\partial z\,\partial t} = u_{zt}(i\ j) = \frac{u(i\ j+1) - u(i-1\ j-1) - u(i\ j) + u(i-1\ j)}{\Delta z \Delta t} \quad z: \text{backward} \quad t: \text{forward} \tag{18}$$

By performing mathematical operations, the quasi-linear PDE equation (55-5) will be simplified as follows:

$$u(i\ j+1) = \frac{1}{A}\left[(A-2B)u(i\ j) + Bu(i+1\ j) + Bu(i-1\ j) + Cu(i\ j)^2 - Cu(i+1\ j)u(i\ j)\right] \tag{19}$$

Where:

$$a\Delta z^2 = A \qquad b\Delta t = B \qquad c\Delta t\Delta z = C$$

Results and Discussion

The results of the simulation for the quasi-linear model are shown in the figure below. Figure 2 shows the distribution of ^{13}C concentration with respect to time and place for the quasi-linear model. As can be seen in the figure, at zero time, the concentration in all points is equal to the natural concentration of ^{13}C (1.11%). With the passage of time, the concentration of ^{13}C in the upper and lower parts of the column decreases and increases, respectively. The course of increasing the concentration of ^{13}C after 4 days from the start of the experiment can be seen in all points of the column.

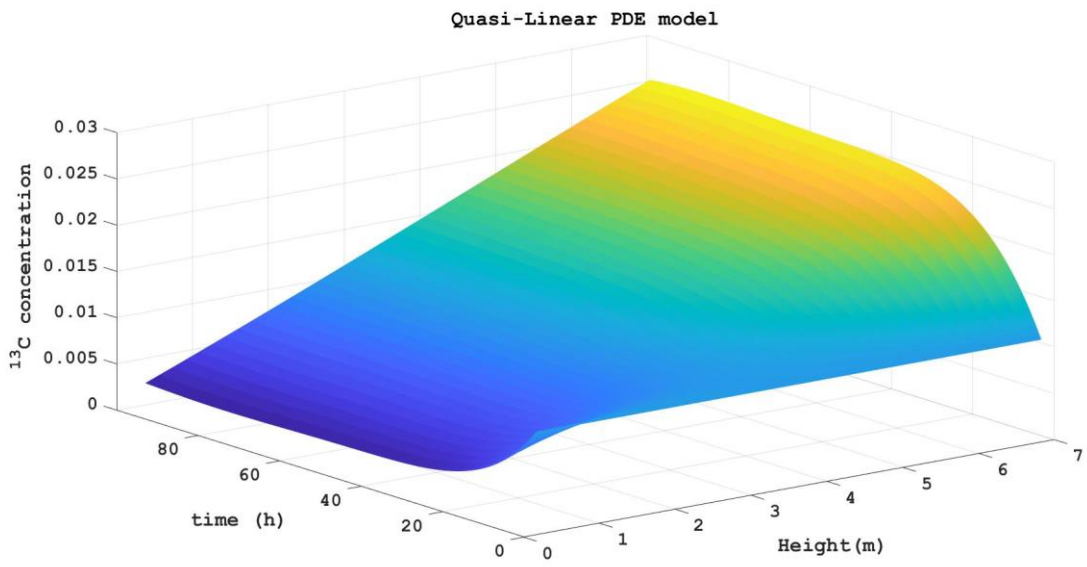

Figure 2: Distribution of ^{13}C concentration according to space and time for quasi-linear model

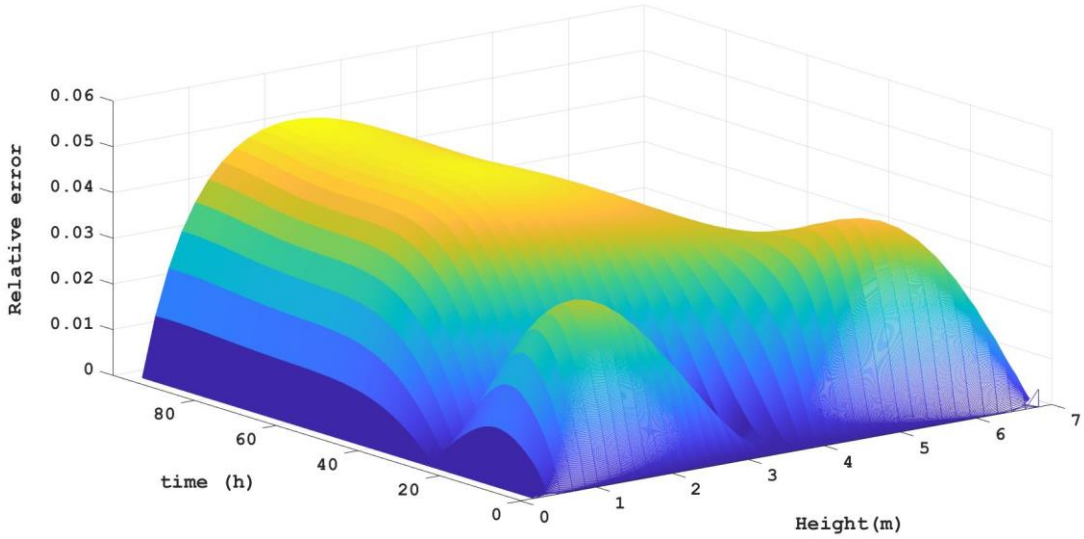

Figure 3: The relative error of the quasi-linear model compared to the fully nonlinear model

By plotting the relative error of the quasi-linear model compared to the linear model in terms of space and time for Δt=144sec and Δx=0.04m, which can be seen in Figure 3, the relative error of the quasi-linear model is low in all points of the column. From this low error value, it can be concluded that the simplifying assumptions for converting the nonlinear model into a quasi-linear model have little effect on the final calculations.

Conclusions

In this work, a model for simulating ^{13}C refrigeration distillation was presented using a comprehensive structure. Since isotopic distillation is performed in columns with a small diameter, therefore, with a good approximation, the penetration in the radial direction can be ignored. By using two-film theory and mass balance for the heavy component in liquid and gas phase as well as other governing relationships, a system of quasi-linear equations was presented based on the mole fraction of 13C. Then, the quasi-linear equation was solved by using the explicit method and using the appropriate step length for time and place. By removing the combined derivative, and the terms including $\partial N/\partial t$ $(\alpha-1)$ and $\partial N/\partial z$ $(\alpha-1)B$, the nonlinear model was transformed into a

quasi-linear model. It was observed that these simplifying assumptions cause slight changes in the final solution of the quasi-linear model compared to the non-linear model.

References

[1] B.M. Andreev, Separation of isotopes of biogenic elements in two-phase systems, Elsevier2006.
[2] J. BIGELEISEN, Isotope separation practice, ACS Publications1969.
[3] Y. Amini, J. Karimi-Sabet, M. Nasr Esfahany, M. Haghshenasfard, A. Dastbaz, Experimental and numerical study of mass transfer efficiency in new wire gauze with high capacity structured packing, Separation Science and Technology 54(16) (2019) 2706-2717.
[4] D.E. Armstrong, A.C. Briesmeister, B. McInteer, R.M. Potter, Carbon-13 production plant using carbon monoxide distillation, Los Alamos Scientific Lab., 1970.
[5] B.M. Andreev, A. Polevoi, Separation of Sulphur Isotopes by Physicochemical Methods, Russian Chemical Reviews 52(3) (1983) 213.
[6] M. Ahmadi-Motlagh, Y. Amini, J. Karimi-Sabet, Experimental study of nitrogen isotope separation by ion-exchange chromatography: Effect of process factors, Journal of Radioanalytical and Nuclear Chemistry 331(1) (2022) 309-315.
[7] P.S. BAKER, Stable isotope preparation and applications, Survey of Progress in Chemistry, Elsevier1968, pp. 69-125.
[8] J.A. Mandler, Modelling for control analysis and design in complex industrial separation and liquefaction processes, Journal of process control 10(2-3) (2000) 167-175.
[9] Y. Amini, J. Karimi-Sabet, M.N. Esfahany, Experimental and numerical study of multiphase flow in new wire gauze with high capacity structured packing, Chemical Engineering and Processing: Process Intensification 108 (2016) 35-43.
[10] K. Cohen, G.M. Murphy, The Theory of isotope separation as applied to the large-scale production of U235, (No Title) (1951).
[11] G. Jancso, W.A. Van Hook, Condensed phase isotope effects, Chemical Reviews 74(6) (1974) 689-750.
[12] H. London, F. Phil, Separation of Isotopes George Newnes Limited, London: Tower House (1962).

[13] D.C. Dumitrache, B. De Schutter, A. Huesman, E. Dulf, Modeling, analysis, and simulation of a cryogenic distillation process for 13C isotope separation, Journal of Process Control 22(4) (2012) 798-808.

[14] D.C. Dumitrache, I. Inoan, B. De Schutter, An analytic model for a C13 isotope separation process by cryogenic distillation, Journal of Process Control 24(5) (2014) 463-474.

ICNST 2024
International Conference on Nuclear Science and Technology
6- 8 MAY 2024 | Isfahan, Iran

Appropriate Design of Iridium- 192 Target for Industrial Radiography Source (Paper ID : 1386)

Dehghan M, Kashi S*, Behzadi M, Norouzi A

Advanced technologies of IRAN Company, Tehran, Iran

Corresponding Author: skashi@aeoi.org.ir

Abstract

One of the most important radioactive sources in the field of industry and medicine is Ir^{192}. This radioisotope is produced by (n,γ) reaction in a nuclear reactor under neutron flux. Then Ir^{192} is transformed into stable Pt^{192} by emitting beta and gamma particles with maximum energy of 0.672 MeV and 0.604 MeV. Half-life of this radioisotope is 74.2 days. The Ir^{192} is used in medicine as brachytherapy and in the treatment of breast, tongue, prostate and brain tumors due to its relatively low energy gamma emission 0.412 MeV. Also, Ir^{192} is used in the industrial radiography for diagnosing welding defects. In this article, the Appropriate design of a target for production of a radiography source of Ir^{192} has been followed. Due to the self-shielding effect and high absorption cross-section, the amount of specific activity of Ir^{192} depends on the density and geometric dimensions of the target. according to the performed Calculations by Monte Carlo method with MCNP-2.6 code, by reducing the density and thickness of the target, a higher specific activity is obtained.

Keywords: Iridium-192, Radioisotope, Specific activity, Radiography, stable isotope

1. Introduction

The production technology of radiopharmaceutical sources is considered to meet the increasing demand of radioactive isotopes for newer and more specialized applications. In medicine, the iridium-192 radioisotope is commonly used for brachytherapy to treat malignant diseases and in industry, widely for non-destructive testing (NDT), radiation processing, process control systems and analysis. At this article, the production of iridium-192 radioactive source in the form of disks is investigated. As seen in Figure 1 iridium-192 is produced by (n,γ) reaction on iridium in a nuclear reactor. Iridium-192 decays into stable Pt^{192} and Os^{192} with a half-life of 74.2 days and emits beta particles with maximum energy (46%) of 0.672 Mev and gamma rays with energy of

0.604, 0.468 and 0.308 Mev. The production of compact disks with high specific radioactivity of iridium-192 is facing problems due to the characteristic of neutron self-shielding caused by the high absorption cross section of neutrons. The Mcnp-2.6 code is used to simulate Ir-192 production.

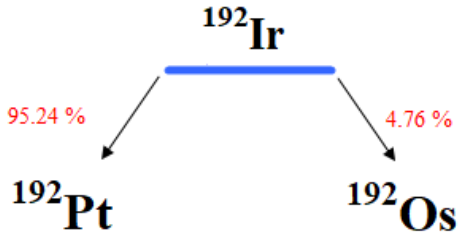

Fig 1. The decay scheme of Ir-192

Figure 2 shows the iridium-192 capsule which is used in industrial radiography can. [1]

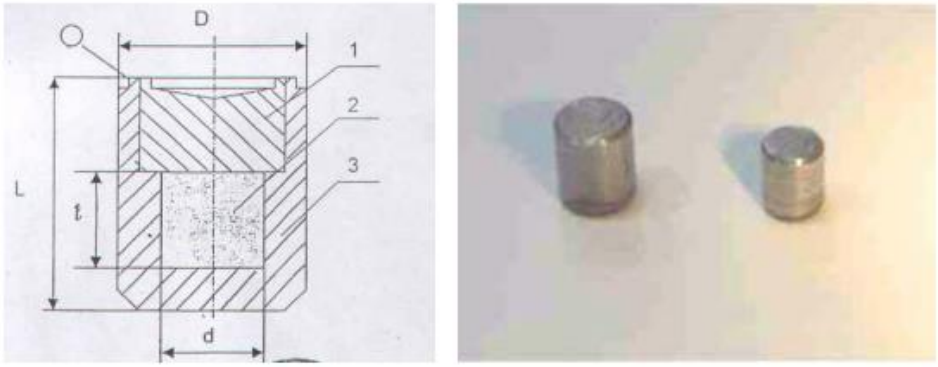

Fig.2. Industrial ^{192}Ir source: 1 - plug, 2 -active core, 3 – capsule

The detection of welding defects on carbon steel with a thickness of less than 4 mm by iridium-192 radiography is shown in Figure 3. [1]

Fig.3. ^{192}Ir industrial radiography performance test

The diameters of capsules in welding points are correspond with the technical specification for sources (4 mm for GI192M54 and 5 mm for GI192M55) (Table 1); the heights of capsules are corresponding with the technical specification for sources (4 mm for GI192M54 and 5 mm for GI192M55) (Table 1). [1]

Table.1. Specifications for industrial sources.

Source type	Dimensions, mm				Gamma dose rate at a distance of 1m, A/kg	Equivalent activity (estimated value) Bq(Ci)
	Source		Active Core			
	Diameter D	Length L	Diameter d	Length L (max)		
GI192M51	$4_{-0.022}$	5±0,15	0.5	0.5	(1,7-3,3) 10^{-8}	(1,8-3,7)x10^{10} (0,5-1)
GI192M52			1.0	1.0	(0,6-2,4) 10^{-7}	(0,7-2,6)x10^{11} (2-7)
GI192M53			1.5	1.5	(2,7-7,3) 10^{-7}	(3,0-8,0)x10^{11} (8-21)
GI192M54			2.0	2.0	(0,8-1,6) 10^{-6}	(0,9-1,7)x10^{12} (25-45)
GI192M55	$5_{-0.022}$	6±0,15	2.5	2.5	(1,8-2,6) 10^{-6}	(2,0-2,8)x10^{12} (55-75)
GI192M56			3.0	3.0	(2,8-4,2) 10^{-6}	(3,1-4,6)x10^{12} (85-125)
GI192M56-1			2.0		(0,8-1,7) 10^{-6}	(0,9-1,7)x10^{12} (25-45)
GI192M56-2			1.5		(2,7-7,3) 10^{-7}	(3,0-8,0)x10^{11} (8-21)
GI192M57	$6_{-0.022}$	7±0,15	3.5	3.5	(4,6-5,6) 10^{-6}	(5,0-6,1)x10^{12} (135-165)
GI192M58			4.0	4.0	(0,6-1,0) 10^{-5}	(0,7-1,1)x10^{13} (200-300)

Two types of high-dose iridium-192 sources (1.1 mm and 4 mm diameter) have been investigated for medical applications. A laser welding system consists of a laser welding machine and an automatic welding machine for making fountains. A 4mm fountain with an activity of (370 GBq) 10 Ci will be supplied to domestic hospitals to test the fountain as brachytherapy fountains. Iridium-192 source has received a great deal of attention recently for this purpose because it has advantages of relatively smaller size and lower emission energy. Since this source has a 380 keV energy level and 1.1 ~ 1.6 mm in diameter, it can be used for the treatment of blood vessels or bile ducts that have a narrow space. Hence, miniaturized iridium-192 sources have also been developed for remote after loading systems.

2. Research Theories

2.1. Theoretical study of iridium-192 production

To produce iridium-192 using neutron activation method, iridium-192 is irradiated with a neutron flux in a reactor. The production reaction is carried out according to the Equation 1.

$$Ir^{191} + n \rightarrow Ir^{192} + \gamma \quad (1)$$

$$\sum_a^{191} \varphi = \sigma_a N^{191} \varphi \quad (2)$$

$$\frac{\partial N^{191}}{\partial t} = -\sum_a^{191} \varphi = -\sigma_a N^{191} \varphi \quad (3)$$

$$N^{191} = N_0 e^{-\sigma_a \varphi t} \quad (4)$$

Since the product radioisotope starts decaying with its own half-life, the changing rate of Ir-192 can be written as:

$$\frac{\partial N^{192}}{\partial t} = \sum_a^{191} \varphi - \lambda N^{192} \quad (5)$$

$$N^{192} = \frac{\sum_a^{191} \varphi}{\lambda^{192}} (1 - e^{-\lambda t}) \quad (6)$$

Equation 7 can be solved to determine the value of activity per gram at time 't', as follows:

$$S = \frac{0.6\sigma\varphi}{A}\left(1 - e^{-\lambda t}\right) \ \frac{Bq}{g} \quad (7)$$

Where:

φ, is the flux in n/cm^2.s,

T, is the time of irradiation,

λ, is the decay constant = 0.693/T ½.

A, is atomic weight of target element

N, is atom density

The specific activity of the irradiated sample should be more than 16.8-18.5 TBq/g (450-500 Ci/g). The activity of the iridium-192 complex should be greater than 370 GBq (10 Ci) for effective treatment. Also, in Table 2, the energy characteristics and cross-sectional area of iridium-192 are reviewed. [2]

Table.2. Specifications of ^{192}Ir

Thermal cross section (Barn)	Beta energy (MeV)	Gamma Energy (MeV)
954± 10	0.259	0.604
	0.539	0.468
	0.675	0.3084

2.2. Simulating the production of iridium-192 using MCNP-2.6 code

The geometry of disks in Equation 7 is irrelevant, but the activity that results is influenced by their geometrical dimensions. For more precise results, the value of $(\sigma\varphi)$ in equation7 is calculated using the MCNP code[3]. The iridium-192 disks with 99.99% enrichment in different dimensions and densities are simulated by MCNP code in condition of Tehran research reactor. The results of calculations are shown in tables 3 and 4. The dimensions of disks with a diameter of 3 mm and a length of 0.15 mm are considered as reference dimensions. ,the specifications of iridium disk are listed in Table 3. [4]

Table.3. Specifications of Iridium source (reference sample)

parameter	**value**
$T_{1/2\ (Ir\text{-}192)}$	74.2 day
Target Diameter	3 mm
Target thickness	0.15 mm
Density	23.5 gr/cm^3

The disks are placed on a can which is model by MCNP code in Figure 4. In order to improve the thermal neutron flux for irradiation, the central fuel assembly is removed and two cans, including iridium disks, are replaced. The Figure 5 shows the position of two cans in the center of the core of the Tehran reactor and the calculated thermal and fast neutron fluxes by MCNP code are given in Table 4.

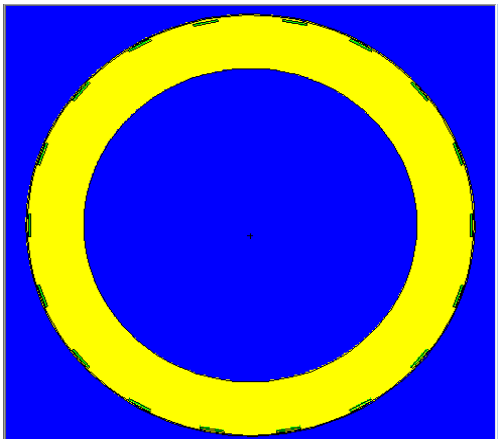

Fig.4. Iridium disks on a can (modeled by the MCNP code)

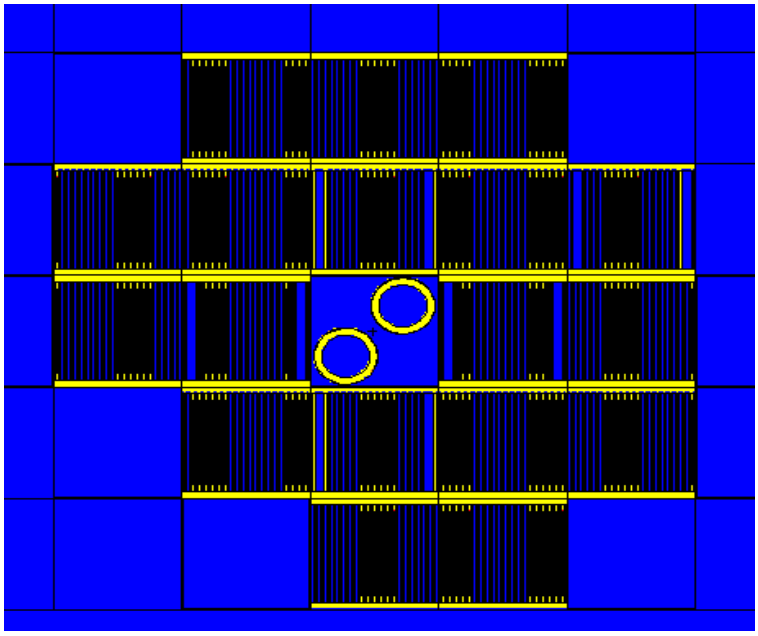

Fig.5. Tehran reactor core with iridium cans

Table.4. thermal and fast fluxes of Tehran reactor

Thermal flux (#/cm^2.s)	Fast flux (#/cm^2.s)
6.3E+13	1.38E+14

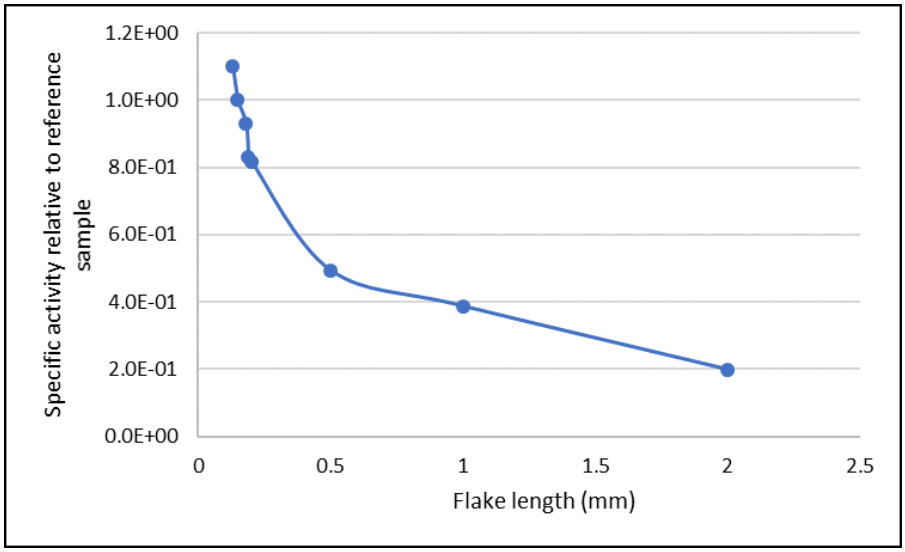

Fig.6. Comparison of specific activity for disks with different thickness

According to the results of Figure 6, The specific activity (A/gr) decreases when the thickness of disk increases. This effect is because of geometrical dimension effect due to self-shielding of Iridium.

Also, the effect of density on activation was investigated. The density of iridium in the form of metal is 23.5 gr/cm^3, but the disks which are produced from the iridium powder in the method of Spark Plasma Sintering, SPS, may have various density in range of 14-23 gr/cm3. it is necessary to calculate the appropriate density and investigate the sensitivity analysis on density.

According to the results of Figure 7, disk sample by lower density can reach to a higher specific activity due to the lower Self-shielding effect.

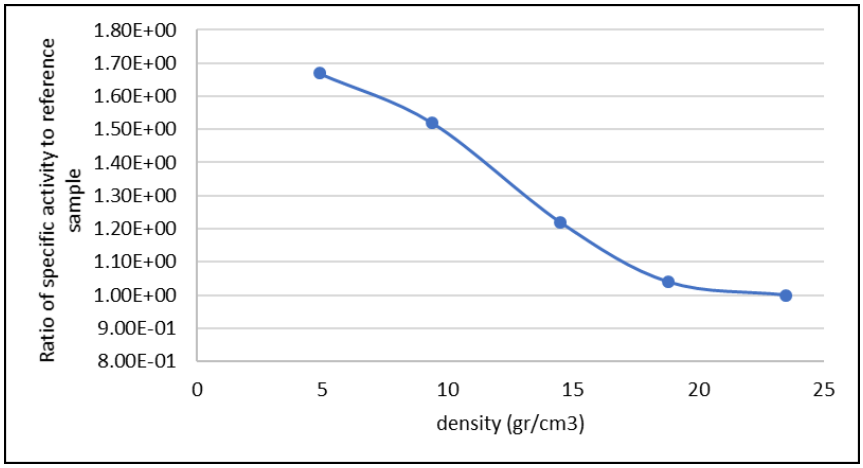

Fig.7. Comparison of specific activity for disks with a length of 0.15 mm and different densities.

The rate of changing of iridium 191 and192 can be seen in Figure 8.

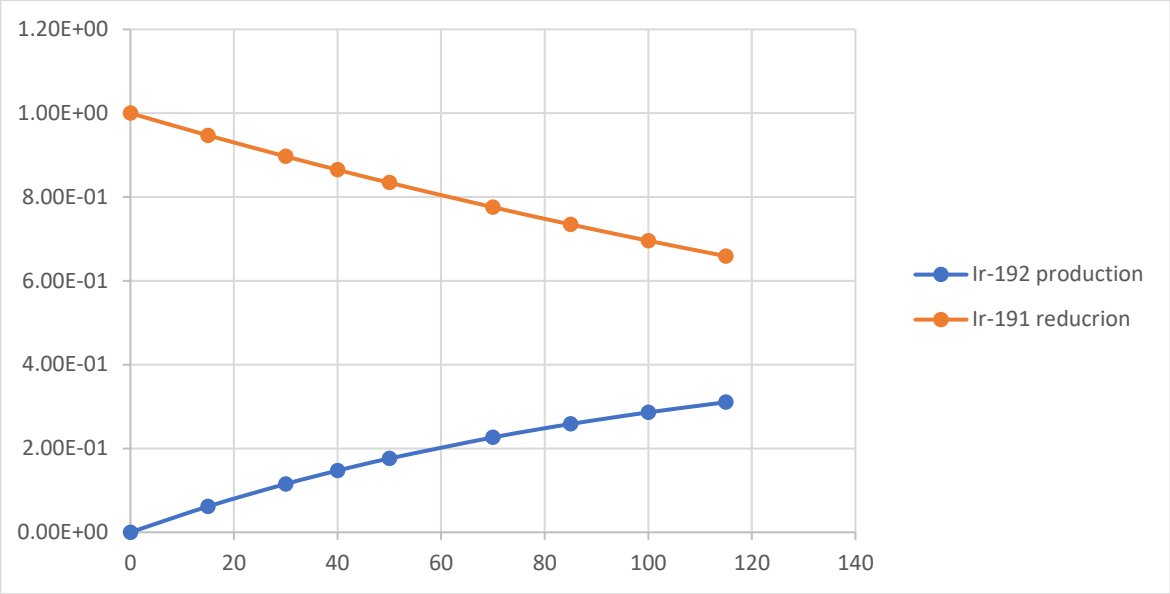

Fig.8. The change rate of iridium 192 and the consumption rate of iridium 191

5- Conclusions

According to the calculations, due to the Self-shielding effect and the high absorption cross-section of iridium-191 the specific activity value depends on the density and the geometrical dimensions of the disks. Higher specific activity is the result of lower density and smaller geometric dimensions. Since the iridium is an expensive material and by considering the limitation of construction a disk with thin layer about 0.15 mm and low density about 16 gr/cm^3 is proposed as appropriate design.

6- References

[1] Production techniques and quality control of sealed radioactive sources of palladium-103, iodine-125, iridium-192 and ytterbium-169 Final report of a coordinated research project 2001–2005.

[2] Rajko P.Dobrijević, Jurij L.Vučina Laboratory for Radioisotopes, Vinca Institute of Nuclear Sciences 11001 Belgrade, P.O.Box 522, Yugoslavia.

[3] Nick T. Thomopoulos, Essentials of Monte Carlo Simulation Statistical Methods for Building Simulation Models, springer,(2013).

[4] TRR FSAR. Introduction and general description of the facilities, Chapter 1.

ICNST 2024
International Conference on Nuclear Science and Technology
6- 8 MAY 2024 | Isfahan, Iran

Calculations of technetium-99m radioisotope production using cyclotron and neutron activation methods (Paper ID : 1395)

Rahmani A[1], Naserbegi A[1*], Kashi S[1], Norouzi A[1]

[1]Advanced technologies Co. of Iran, Tehran, Iran
**Corresponding Author: a_naserbegi@sbu.ac.ir*

Abstract

One of the most important and widely used nuclear medicine radioisotopes for diagnostic imaging is Technetium-99m. This radioisotope is produced from decay of molybdenum-99 isotope and can be achieved from neutron activation methods in the reactor, cyclotron, and nuclear fission reaction. To produce technetium-99 using neutron activation, Mo-98 is irradiated via neutron flux in reactor, then molybdenum-99 is produced. Mo-99 decays to Tc-99m with a half-life of 66 hours. In the present work, due to the increasing demand of technetium-99m production for diagnostic imaging, both calculations for technetium-99m production by neutron activation of Mo-98 and cyclotron with Mo-100 have been done. Then the results of this calculation have been compared. For the neutron activation method, the Monte-Carlo-method with MCNP-2.6 is applied.Evaluation of parameters such as neutron flux, proton beam, absorption cross sections, and time required for the production of this radioisotope shows that cyclotron production method for technrtium-99m is more beneficial.

Keywords: Technetium-99m, Neutron activation, Cyclotron, Nuclear medicine

1. Introduction

Technetium element with atomic number 43 is a synthetic element that has no stable isotope in nature. As a result, the standard atomic mass is not defined for it. The first discovered isotopes of this element were Technetium -97 and Technetium -99, which were produced and traced for the first time in 1936. Technetium-99m is a widely used radioisotope in nuclear medicine. This radioactive substance is a kind of nuclear isomer of Tc-99 isotope, which tries to reach a stable state by isomeric transition (radiation of gamma rays or internal transition). The isotope Tc-99m with special nuclear properties such as short half-life and single-energy gamma ray (140 Kev) is used to diagnose diseases and study the structure and function of the body organs of living organisms [1].

There are various methods to produce Tc-99m including nuclear fission, neutron activation and cyclotron production. In the fission process of uranium-235 with neutron radiation in nuclear reactors, molybdenum-99, iodine-131, and xenon-133 many other fission products produce. After that, Mo-99 can be converted into Tc-99m using a generator system. The production of technetium-99m using neutron activation involves a multi-step process that begins with Mo-98. Mo-98 is irradiated with thermal neutrons, which are absorbed by Mo-98 and convert it into Mo - 99. Then, by using a generator, Mo-99 turns into Tc-99m. Radionuclide generators produce a short-lived medical radionuclide by decay of a longer-lived radionuclide. Regular generators for the production of Tc-99 are made based on a chromatography column using alumina adsorbent and are milked at certain time intervals to achieve the required activity [2]. Fig 7 display the main components of a generator along with the diagram of activity changes during milking time.

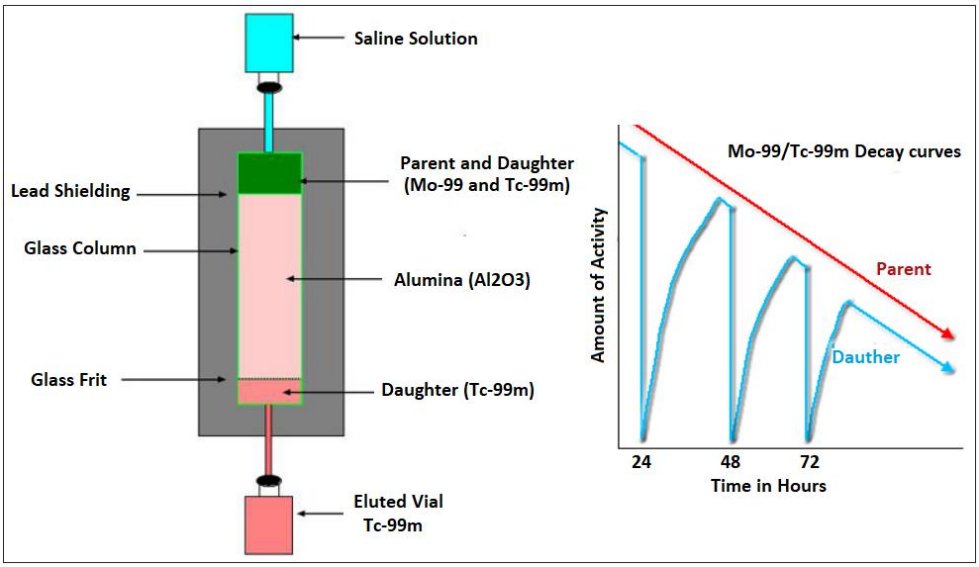

Fig 7. Main components of a generator along with the diagram of activity changes during milking time for Mo-99/Tc-99m

The decay scheme of Mo-99 and its conversion to Tc-99m, in a generator based on column chromatography has been shown in Fig .

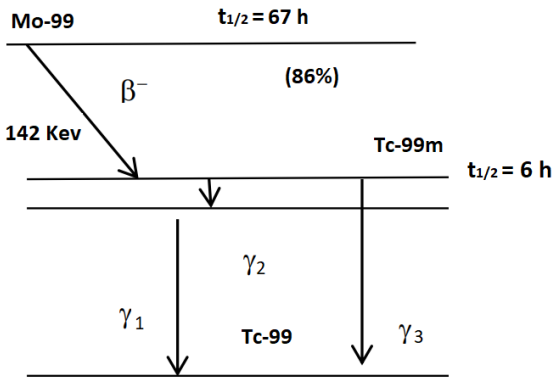

Fig 8. The decay scheme of Mo-99

The third way to produce Tc-99m is to use a cyclotron. Cyclotron is a charged particle accelerator that accelerates charged particles in the center of a cylinder using an oscillating electric field and a strong magnetic field. The type of accelerated particles such as neutrons and deuterons, their energy and the target materials all affect the nuclei that are produced. The cyclotron portions for radionuclides synthesis and acceleration of charged particles has been illustrated in Fig 9. Several different nuclear interactions are available to produce Tc-99m in cyclotrons using Mo as the target material. Among these reactions, the production route of Mo-100(p, 2n)Tc-99m is more profitable and is used more often [3].

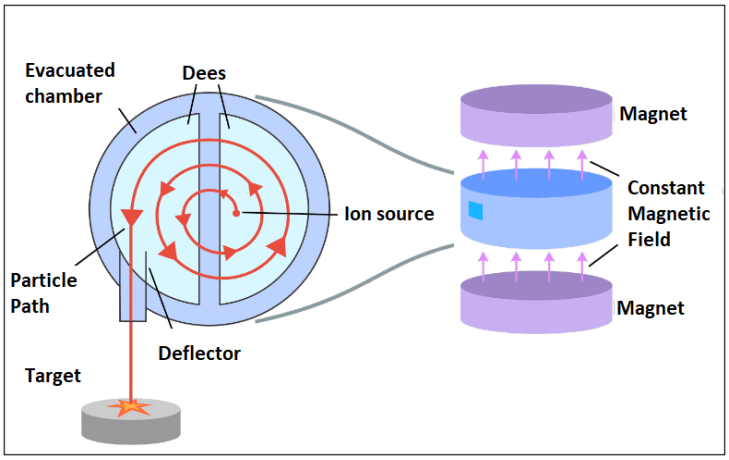

Fig 9. Cyclotron portions for acceleration of charged particles

So far, many research has been done in the field of how to produce and consume the radiopharmaceutical technesim-99m. In 2017 Clanton et al. investigated the production of Mo-99/Tc-99m via photo neutron reaction using natural molybdenum and enriched Mo-100. The results of their calculations showed that the specific activity at end of cycle for a single disk of

Mo-natural and enriched Mo-100 is 42 and 442 GBq g^{-1} mA^{-1} (1.13 and 11.89 Ci g^{-1} mA^{-1}) for a nominal 3-day irradiation [4]. Spectral analysis of proton-irradiated natural MoO_3 relevant for technetium-99m radionuclide production has been done by Imam et al. In this research, a solid natural MoO3 target has been irradiated using 11-MeV proton beams at variable proton doses. The experimental results of their work indicated that as much as 75.71% of Tc-99m radioactivity was directly generated via a Mo-100(p, 2n)Tc-99m nuclear reaction [5].

In the present work, the efficiency of cyclotron reaction and neutron activation methods for the production of Tc-99m has been compared. Calculations of the production rate in the neutron activation method have been performed using MCNP-2.6 and then validated using theoretical calculations. Also, theoretical and experimental equations reported in other researches have been used to calculate the production rate of Tc-99m in cyclotron.

2. Research Theories

2.1. Theoretical study of molybdenum-99 production using neutron activation

To produce Mo-99 using neutron activation method, Mo-98 is irradiated with a neutron flux in a reactor. The production reaction is carried out according to the Equation 1.

$$^{98}Mo + n \rightarrow \gamma + {}^{99}Mo \qquad (1)$$

After the production, Mo-99 decays to Tc-99m through beta decay with a half-life of 66 hours. Equation 2 shows the available values of parent Mo-99 and daughter, Tc-99m, at any time in terms of initial values and decay constants. In this equation, α is the percentage of decay of Mo-99 that turns into Tc-99m.

$$N_{^{99m}Tc} = \frac{\alpha\lambda_{^{99}Mo} N_{0^{99}Mo}}{\lambda_{^{99m}Tc} - \lambda_{^{99}Mo}} (e^{-\lambda_{^{99}Mo}t} - e^{-\lambda_{^{99m}Tc}t}) + N_{0^{99m}Tc} e^{-\lambda_{^{99m}Tc}t} \qquad (2)$$

To produce Mo-99 in a reactor using the neutron activation method, as mentioned, Mo-98 is placed in a reactor in front of a neutron flux. When a target is irradiated in a reactor, the amount of radioactive atoms at a time "t" is calculated as $\frac{Bq}{g}$ according to Equation 3 [6]:

$$s = \frac{0{,}6\sigma\varphi}{A} \left(1 - e^{-\lambda t}\right) \qquad (3)$$

Where σ is the neutron absorption cross-section leading to the production of radioisotope of attention in barn, φ is the flux in n/cm2/s, t is the time of irradiation, λ is the decay constant, and A is the atomic weight of target element.

When t$\gg T_{1/2}$, the saturation activity is obtained as $\frac{Bq}{g}$ according to equation 4.

$$S = \frac{0,6\sigma\varphi}{A} \qquad (4)$$

Equation 4 shows that the activity in an irradiated target grows exponentially and reaches a saturation value limited by the neutron flux in the reactor. Table 1 shows the abundance percentage of molybdenum isotopes in a natural sample [6].

Table 1. The abundance percentage of molybdenum isotopes in a natural sample

Isotope	Abundance, %
^{92}Mo	14.84
^{94}Mo	9.25
^{95}Mo	15.92
^{96}Mo	16.68
^{97}Mo	9.56
^{98}Mo	24.13
^{100}Mo	9.63

2.2. Production simulation of Tc-99m using MCNP-2.6 code

MCNP is a multi-purpose code that is used for particle transport calculations such as electrons, protons, neutrons, heavy charged particles, photons, etc. For the neutron activation of molybdenum-98 target, Tehran Research Reactor (TRR) has been used as a neutron source in MCNP-2.6 code. TRR is a pool-type reactor with light water as a moderator and coolant, which is used for research purposes, training and production of radioisotopes. Currently, Tehran reactor fuel is U_3O_8-Al plate with enrichment of about 20%. The MoO_3 target in solid form insert to a stand and replaced with one of the fuel assembly of this reactor, then it is irradiated by thermal neutrons. So neutron flux in the reactor will be 8.13×1013 n/cm2.s, which produces 5 Mwth energy. The schematic geometry of molybdenum trioxide arrangement which is simulated with MCNP-2.6 code is shown in Fig 10. After the core simulation, the neutron flux was calculated at the irradiation positions [7].

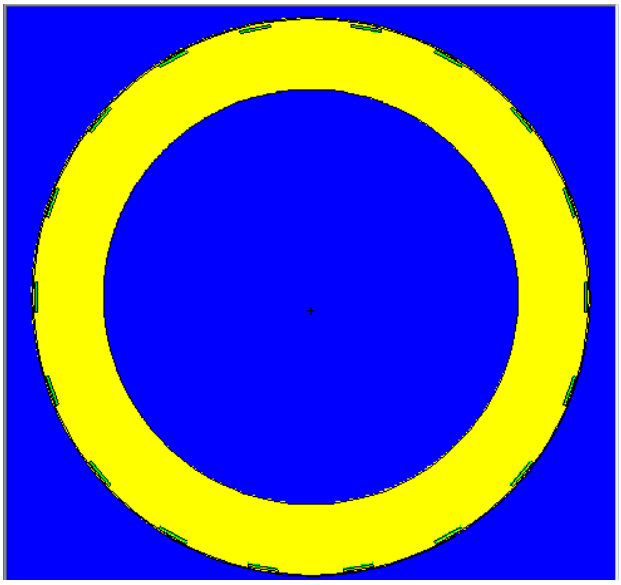

Fig 10. Schematic of MoO3 arrangement geometry in MCNP-2.6 code

2.3. Calculation of theoretical production of Tc-99m in cyclotron

There are several different methods for producing technetium-99 in cyclotron that can be investigated in terms of production feasibility. These interactions are listed in Table 2.

Table 2. Cyclotron reactions for Tc-99m production

NO.	Reaction
1	^{100}Mo(p,2n)^{99m} Tc
2	^{98}Mo(p, γ)^{99m} Tc
3	^{nat}Mo(p, x)^{99m} Tc
4	^{100}Mo(d, 3n)^{99m} Tc
5	^{98}Mo(d, n)^{99m} Tc
6	^{97}Mo(d, γ)^{99m} Tc

According to the amount of available energy in cyclotrons, reaction number 1 can have the highest rate of efficiency among other reactions. In addition, the calculation of cross sections at different energies showed that reaction number 1 has the highest cross section for the production of Tc-99m in cyclotron. The production gain for a cyclotron reaction in a certain range of energy is calculated according to equation 5.

$$\gamma = \frac{N_L H}{M} I(1 - e^{\lambda t}) \int_{E_1}^{E_2} \frac{\sigma(E)}{S_P(E)} dE \qquad (5)$$

In this equation, γ is production yield, N_L is Avogadro's number, H is target isotope abundance, M is target element mass number, $\sigma(E)$ is cross section in the certain energy range, I is proton beam current, $S_P(E)$ is target stopping power of target isotope, λ is decay constant, and t is irradiation time by proton beam in the target example. The target is used in the form of a metal plate of molybdenum powder with a mass of 620 mg. To perform the theoretical calculations, it is assumed that the target is irradiated with protons of 9 - 19 Mev and a current of 50µA for 1 hour. Calculations to measure the amount of activity obtained from 1 gram of molybdenum are presented in the results section [8].

3. Results and discussion

3.1. Theoretical neutron activation result

The activity of Tc-99m versus time has been shown in Table 3. According to equation 2, if the initial value of Tc-99m is considered to be zero, the variation of Tc-99m activity versus time are according to Fig 11.

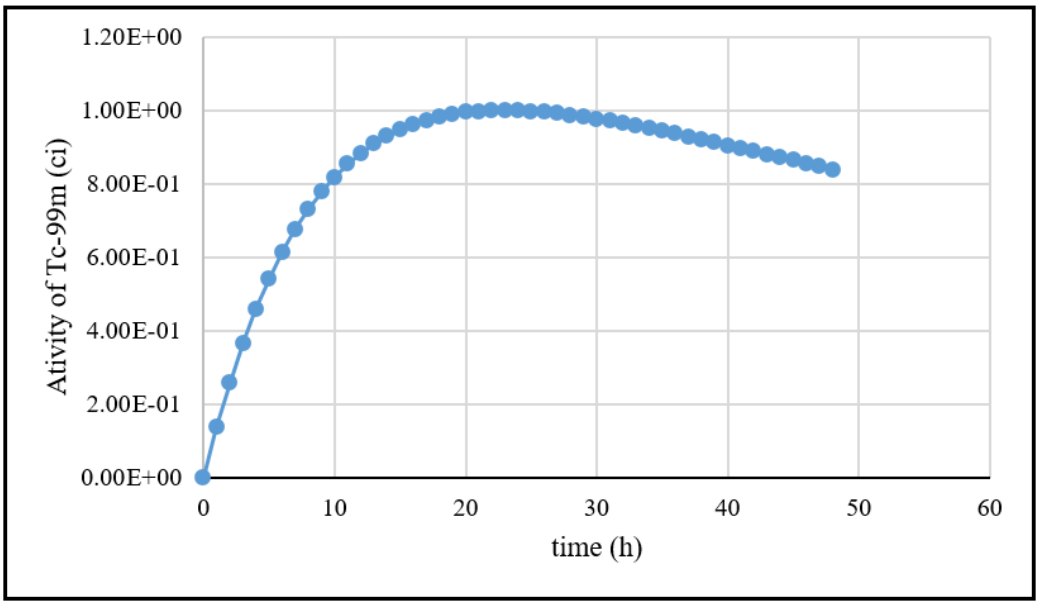

Fig 11. Tc-99m activity versus time

Table 3. Activity of Tc-99m

Time, h	Activity, Ci
0.0002	0.00E+00
5	5.42E-01

10	8.18E-01
15	9.47E-01
20	9.95E-01
25	9.97E-01
30	9.77E-01
35	9.44E-01
40	9.05E-01
45	8.64E-01
48	8.39E-01

According to equation 3, the amount of Mo-99 produced from 1 gram of Mo-98 that has been irradiated with a neutron flux of 8.13×10^{13} and absorption cross-section of $\sigma_a = 0.13\ barn$ can be calculated as follows:

$$s = \frac{0.6 \times 0.13 \times 8.13 \times 10^{13}}{98} = 6.46 \times 10^{10} \qquad \left(\frac{Bq}{gr_{Mo-98}}\right) \qquad at, t = 0$$

This initial amount is equal to 3.6 μg of Mo-99. As a result, to Produce 3.04 μg of Mo-99 (1 curie of Tc-99m), 0.85 grams of Mo-98 are needed. The activity of Mo-99 versus time of irradiation has been presented in Table 4.

Table 4. Activity of Mo-99

Time, day	Activity, Ci
7	1.45
17	1.72
27	1.74
37	1.75
47	1.75
57	1.75
67	1.75
77	1.75
83	1.75

Fig 12 shows the variation in the activity of Mo-99 and as can be seen, after about 19 days, the activity of Mo-99 will reach saturation (1.75 Ci).

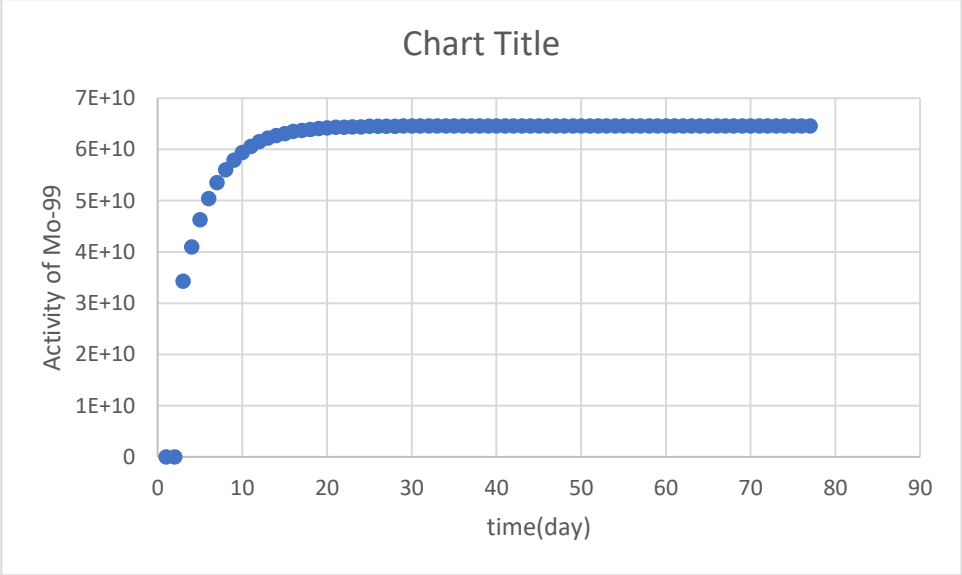

Fig 12. Mo-99 activity versus time

3.2. MCNP neutron activation result

To estimate the amount of activity that resulted from the activation of Mo-99, the MCNP-2.6 code has been used. The target used in the simulation is molybdenum trioxide (MoO3) with a density of 4.69 g/cm3, which is placed in standard aluminum stands with 22mm diameter & 44mm height. As mentioned before, this target is irradiated via thermal neutron flux of 8.13×10^{13} n/cm^2.s in TRR. According to Reference [6], the amount of activity that is produced from MoO3 target is 2.35 Ci/grMo-98 .Although the amount of activity that is calculated from the equation 3 with neutron flux of 1.6×10^{14} n/cm2.s is 2.85 Ci/grMo-98 [6]. Total flux resulting from MCNP-2.6 is 8.13×10^{13} n/cm2.s. The amount of activity that is created from MoO3 target calculated by MCNP-2.6 is 2.01 Ci/grMo-98. To properly compare the results, the activity values obtained from the MCNP-2.6 and calculated from equation 2 were normalized to the neutron flux reported in reference 6 (1.6×10^{14}). The results (Table 5) showed that for one gram of molybdenum 98 which is under the neutron flux, the yield are close to the analytical and experimental results with a good approximation. As a result, the decay of 2.01 curies of Mo-99, the maximum activity of 1.375 curies Tc-99m will be obtained.

Table 5. Results of activity

Activity, Ci/grMo-98

MCNP-2.6 run with MoO3 target	2.01
Calculated from equation 2	2.85
Yield of MoO3 target according to Reference 3.	2.38

3.3. Cyclotron production result

In the production method of Tc-99m using a cyclotron, after irradiating the targets, the target remains in its coating for 2 hours for the decay of short-lived radionuclides such as Tc-100 and Tc-96m. Then the cover is opened, and to remove some impurities the irradiated tablet is heated to a temperature of 60±5°C. The average yield reported for the production of Tc-99m using 620 mg of Mo-100, 356 MBq/μAh was measured. According to the above result, the amount of activity obtained from 1 gram of Mo-100 is calculated according to the following equation under the conditions used by the cyclotron of Karaj Nuclear Research Centre for Medicine and Agriculture:

$$1gr\ Mo^{100} \times \frac{356\frac{MBq}{\mu Ah}\ Tc^{99m}}{620\times10^{-3}grMo^{100}} \times \frac{10^{6}Bq}{1MBq} \times \frac{50\mu Ah}{1h} \times \frac{1Ci}{3{,}7\times10^{10}Bq} = 0{,}776\ Ci\ Tc^{99m}$$

The results show that if 1 gram of Mo-100 is placed in a cyclotron, after chemical purification, 0.776 curies of Tc-99m are produced. The direct production of Tc-99m and the need for less time for irradiation are the advantages of this method.

4. Conclusions

The main goal of this study is to evaluate the amount of molybdenum-99 production by various methods to produce technetium 99, which plays a significant role in the field of medicine. In this research, the activity of Mo-99 obtained from irradiated M0-98 was calculated and compared with the activity value obtained from a real sample. The results showed that for one gram of molybdenum 98 which is under the neutron flux, the results are close to the analytical and experimental results with a good approximation. Finally, the production rate of Technicium 99 was directly calculated in a cyclotron. The advantage of using the cyclotron method over other methods is less time for activation and direct conversion of Mo-100 to Tc-99m. The comparison between the activity obtained from the cyclotron and neutron activation method shows that higher

activity of Tc-99m(0.7 Ci for 1hour of Mo-100 irradiation) than the neutron activation method (maximum activity of Tc-99m is 0.08 Ci for 1week of 1g-Mo-98 irradiation) will be achieved.

References

[1] Mausolf, Edward J., Erik V. Johnstone, Natalia Mayordomo, David L. Williams, Eugene Yao Z. Guan, and Charles K. Gary. (2021). Fusion-based neutron generator production of Tc-99m and Tc-101: a prospective avenue to technetium theranostics. Pharmaceuticals, 14(9): 875.
[2] Schaffer, P., F. Bénard, A. Bernstein, K. Buckley, A. Celler, N. Cockburn, J. Corsaut et al. (2015). Direct production of 99mTc via 100Mo (p, 2n) on small medical cyclotrons. Physics Procedia, 66: 383-395.
[3] IAEA (2014). Cyclotron Based Production of Technecium-99m Radionuclides, IAEA Radioisotopes and Radiopharmaceuticals Series Publications, IAEA,Vienna.
[4] Martin, T. Michael, Talal Harahsheh, Benjamin Munoz, Zaher Hamoui, Ryan Clanton, Jordan Douglas, Peter Brown, and Gamal Akabani. (2017). Production of 99 Mo/99m Tc via photoneutron reaction using natural molybdenum and enriched 100 Mo: part 1, theoretical analysis. Journal of Radioanalytical and Nuclear Chemistry, 314: 1051-1062.
[5] Johnstone, Erik V., Natalia Mayordomo, and Edward J. Mausolf. (2022). Discovery, nuclear properties, synthesis and applications of technetium-101. Communications Chemistry, 5(1): 131.
[6] IAEA (2003). Manual for reactor produced radioisotopes, IAEA Radioisotopes and Radiopharmaceuticals Series Publications, IAEA, Vienna.
[7] Kelsey, I. V., T. Charles, Sergey D. Chemerizov, Gregory E. Dale, James T. Harvey, Peter Tkac, and George R. Vandegrift III. (2011). MCNPX simulation of photonuclear Mo-99 production experiments. Los Alamos National Lab. (LANL), Los Alamos, NM (United States).
[8] Gagnon, Katherine, François Bénard, Michael Kovacs, Thomas J. Ruth, Paul Schaffer, John S. Wilson, and Steve A. McQuarrie. (2011). Cyclotron production of 99mTc: experimental measurement of the 100Mo (p, x) 99Mo, 99mTc and 99gTc excitation functions from 8 to 18 MeV. Nuclear medicine and biology, 38 (6), 907-916.
[9] Thomopoulos, Nick T. (2012) . Essentials of Monte Carlo simulation: Statistical methods for building simulation models. Springer Science & Business Media, springer.
[10] TRR FSAR. Introduction and general description of the facilities. Chapt

Investigating the Separation of 15N in Ammonium Hydroxide solution using the Ion Exchange Chromatography (Paper ID : 1414)

MokhtarJozani F.[1], Karimisabet J.[2], Outokesh M.[2], Mansourzadeh F.[2*], AhmadiMotlagh M.[2]

[1]Nuclear Fuel Cycle Research School, Nuclear Science and Technology Research Institute, Tehran, Iran.
[2]Sharif University of Technology, Tehran, Iran

Abstract

Nitrogen has two stable isotopes, ^{15}N and ^{14}N, with abundances of 0.366% and 99.634%, respectively. ^{15}N has many applications in agriculture and organic chemistry studies as a non-radioactive tracer, as well as in nitrid fuels of fast breeder reactors (FBR). One of the practical techniques in ^{15}N isotope separation is ion exchange chromatography. In this research, a chromatographic system including two consecutive columns (with an inner diameter of 1.5 cm and bed length of 80 cm) was used, which were filled with DOWEX 50W x2 strong cation exchange resin.
Investigations were carried out for ammonium hydroxide feed with a concentration of 0.3 M and a flow rate of 2.5 ml/min. The ammonium adsorption band formed in the first column is eluted by sodium hydroxide solution with a concentration similar to the concentration of the feed solution. The isotope ratio in each sample was determined using an isotope ratio mass spectrometer (IRMS). The ^{15}N isotopic percentage in the last sample reached 0.56%, which is more than the results reported in the References for DOWEX 50W x8 resin with 0.2 M ammonium hydroxide feed and 1.5 ml/min eluent flow rate. The results show that the high concentration of the feed solution and the low flow rate of the eluent solution are more suitable for the separation process.

Keywords: Isotope separation, Ion exchange, Chromatography, Nitrogen Isotopes.

Introduction

^{15}N is used as a tracer in environmental studies, for evaluating new fertilizer and its economical application, in nuclear field and in biotechnologies studies, however, the price of its labeled compounds has been the limiting factor for extensive application in the world, due to the high costs of the isotopic separation processes.[1]

So far enriched ^{15}N has been commercially produced by two major processes of NITROX (chemical exchange between HNO_3 and NO) and the low temperature distillation (cryogenic

distillation) of NO molecules. Ion exchange is another process for isotope separation based on the chemical exchange that is used for small quantities.[2]

The ion exchange chromatography displacement technique is an efficient process for obtaining enriched stable isotopes in a wide enrichment range and its versatility allows to obtain different labeled compounds in the same ion exchange columns. Separation and concentration of a stable isotope from an isotopic mixture with natural occurrence is a very complex problem, and it is impossible to obtain good results only with a simple separation step. In addition, the natural concentration and isotopic separation coefficients are usually very low. In such conditions long working times are necessary to reach the steady state. In this sense, commonly the multi-elementary separation steps have been carried out in circuits of columns. Hydrodynamic factors must also be considered if the process is wanted to be efficient, so the ammonium band should be displaced as fast as possible to obtain the maximum transport per unit time, but not so fast that band boundaries become diffuse or the HETP excessively large, in this sense the resin particle size plays an important role as well as the selected flow rate.[1]

The separation factor of nitrogen stable isotopes using a dilute ammonium hydroxide solution and cationic high cross-linkage degree resin DOWEX 50-X12 was obtained by SPEDDING[3], although, a high isotopic effect is possible to obtain using a resin with lower percent of divinylbenzene, as well as to increase the mass transfer process in the solid phase.[3] In 1988, Park et al. studied on the separation of nitrogen via displacement band chromatography using sulfonated styrene–divinylbenzene resins. They found that HETP and separative power dependent on the operating parameters such as superficial velocity, concentration and also resin characteristics (size, crosslinking)[4]. In 2021 Ahmadi-Motlagh et al. investigated the effect of initial feed concentration and migration distance on the efficiency of nitrogen isotope separation using a set of 10 columns filled with the ion-exchange resin DOWEX- 50 W X8 with 1 cm I.D. and 100 cm height. They obtained the maximum enrichment of 6.616% ^{15}N with 70 m migration distance. They also found that by increasing the number of columns and consequently increasing the length of the displacement, higher enrichment of the ^{15}N is expected to be possible.[5]

The aim of this work is to study the separation process of nitrogen stable isotopes by ion exchange chromatography. The separation process was carried out using a set of 2 columns filled with DOWEX 50W-x2 strong cation exchange resin.

Experimental

materials

The DOWEX 50W-x2 ion exchange resin used as stationary phase is a cationic, strongly acidic, polystyrene-divinylbenzene exchanger. The other chemicals used, were NH_4OH, HCl and NaOH were purchased from Merck co. and distilled water was used as the solvent for reagents and for stripping the columns.

Apparatus

A set of 2 chromatographic columns was used for isotopic enrichment. The columns were prepared using Pyrex glass pressure tube and were connected in series (with an inner diameter of 1.5 cm and bed length of 80 cm). A peristaltic pump was used for feeding and stripping the columns and regeneration of the resin. (Fig. 1)

Fig. 13. A peristaltic pump connected to solution containers.

Methods

When the resin was uniformly packed into the column, it's washed with 1 M HCl to remove the impurities in the ion exchange resins and then was washed with distilled water to remove free H^+ ions from the bed. This process continues until the output current from the end of the column has

a neutral pH. Then ammonium hydroxide feed solution 0.3 M was introduced continuously through the first column until complete saturation of the resin. Then the column is eluted with an eluent of NaOH. The ammonium band is displaced down to the next column by a NaOH solution of 0.3 M at a rate of 2.5 ml/min. this displacement of the band continues until the total ammonium enters the second column. At this stage when the rear boundary of the ammonium adsorption band enters the next column, the first column was separated from the connection system and eluted by HCl for regeneration. During this process, the ammonium concentration profile moves down the bed and then replaces the cation H^+ once more. Due to the multi-elementary steps of adsorption–desorption and the difference in the adsorption capacity of ^{14}N and ^{15}N in the resin beds, the isotopic exchange reaction takes place. At the end of the migration, sampling is performed from the end of the column for isotopic analysis. During isotopic runs, and to trace the chromatographic profiles of feed materials, it was very important to know the location of the band boundaries in a column. So, an electric conductivity meter for monitoring the band boundary was set at the bottom of each column.[5] The conductivity cell is shown in Fig. 2.

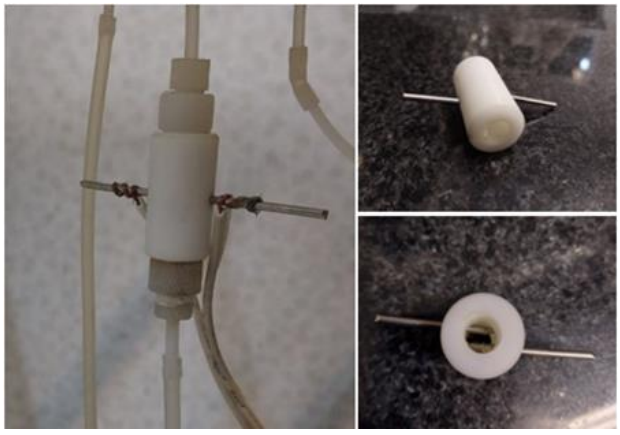

Fig. 14. conductivity cell.

The ion exchange resin pre-saturated with H^+ is converted to the ammonium form, according to the reaction (1) as a neutralization acid–base reaction:

$$NH_4OH + RH \leftrightarrow RNH_4 + H_2O \quad (1)$$

where R is the fixed resin phase. The elution of this ammonium band occurs continually and the formation of neutral species of NH_3 takes place (2)[6]:

$$NaOH + RNH_4 \leftrightarrow RNa + NH_4OH \quad (2)$$

the separation of nitrogen isotopes by means of cation-exchange resin is based on the isotopic fractionation between ammonia in aqueous solution and ammonium ion in the ion exchange resin as shown below:

$$R^{14}NH_4^+ + {}^{15}NH_3 = R^{15}NH_4^+ + {}^{14}NH_3 \quad (3)$$

Where R represents the fixed anion in the resin.[7] The figure 3 shows this process:

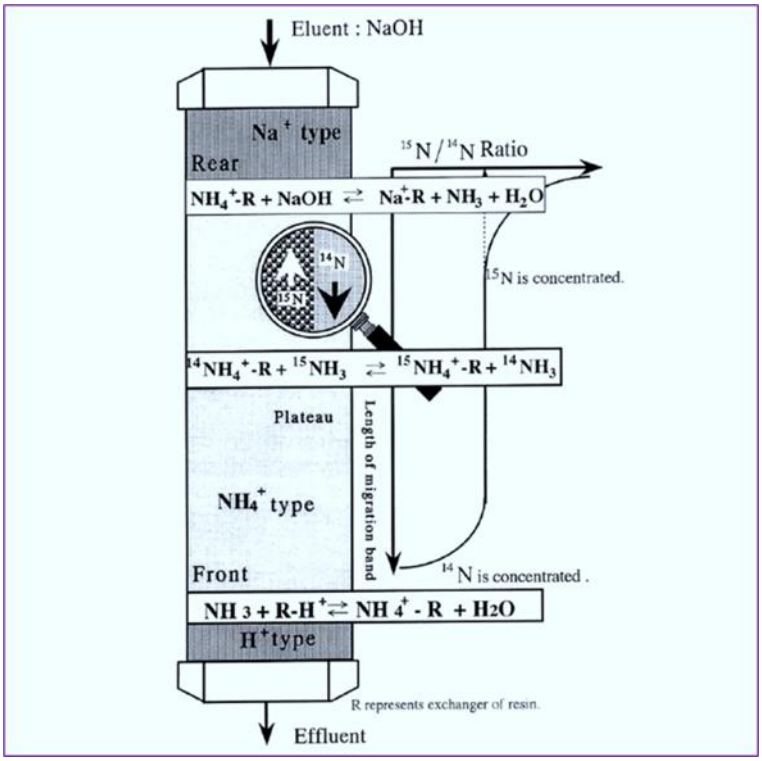

Fig. 15. The diagram of the displacement band chromatographic process for nitrogen isotope separation.[7]

The temperature of the column was kept constant at 298 K by temperature-controlled water through a water jacket. Migration of adsorbed band along the resin bed could also be observed visually by its color difference.

Analysis

At the bottom of the column, the effluents were collected. In order to prevent the NH_4OH samples from de-gassing, certain volumes of excess HCl solutions were added in the collection tubes prior to the samplings.[7] For every 10ml of NH_4OH solution, 5ml of HCl was added in the collection tubes. The $^{15}N/^{14}N$ isotopic abundance ratio in each sample was determined using an Isotope Ratio Mass Spectrometer (IRMS). The Isotope Ratio Mass Spectrometer (IRMS) available in Misbah

Energy Company in Arak city was used for isotope analysis. The accuracy of the measurement is -0.15‰ .

Results and Discussion

The determined ^{15}N isotopic abundance of 5 samples collected from the chromatographic column are listed in table1.

Table 6. results of IRMS.

Sample	δ ^{15}N (%) vs Air	^{15}N% (atom%)
1	42.1	0.38
2	64.9	0.39
3	173.7	0.43
4	367.2	0.50
5	534.9	0.56

Therefore, the isotope distribution curve can be as Fig.4:

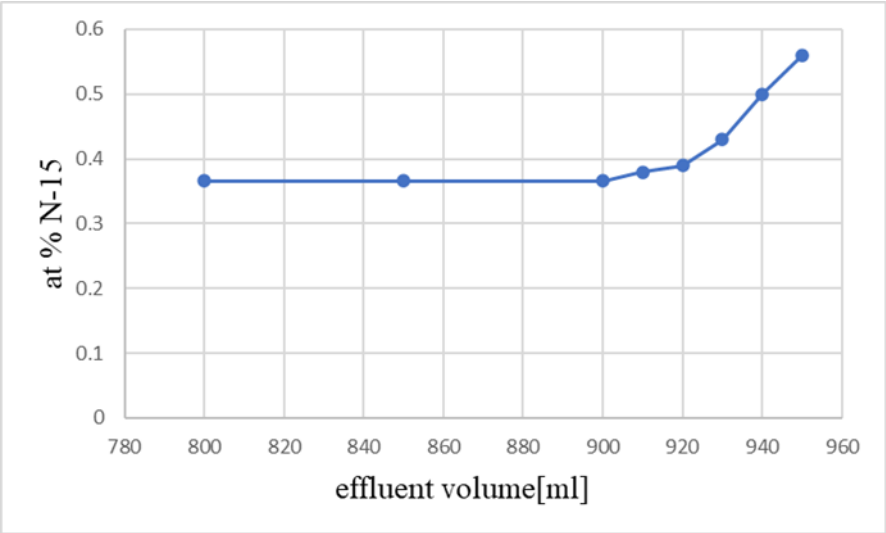

Fig. 16. isotopic abundance ratio at the rear boundary region.

Separation factor and HETP are used to evaluate the performance of the chromatographic column in enriching process of ^{15}N. The separation coefficient ε is defined by

$$\varepsilon = \frac{\sum C_i V_i (R_0 - R_i)}{Q R_0 (1 - R_0)} \quad (4)$$

Where C_i and V_i are ammonium concentration and volume of the ith sample, respectively. In addition, Q shows the total exchange capacity of the resin, R_0 and R_i are the isotope concentration of ^{15}N in the feed and ith sample. Then the equilibrium constant is related to the isotope separation factor by the equation below:

$$k = \varepsilon + 1 \tag{5}$$

The HETP of the chromatographic column for the non-steady separation is calculated using equation below:

$$H = \frac{\varepsilon}{k} \times \left\{1 + \frac{R_0}{\exp(\varepsilon k R_0 L) - 1}\right\} \tag{6}$$

In this equation, H denotes HETP, ε is the separation coefficient, L is the migration length, R_0 represents the natural abundance of nitrogen isotopes and k is the slope coefficient, which could be obtained from the slope of the equation below:

$$\ln(R - R_0) = k(L - x) \tag{7}$$

Where (L-x) is the distance from the boundary to the position x in the adsorption band.[2]

The determined HETP is plotted in Fig. 5.

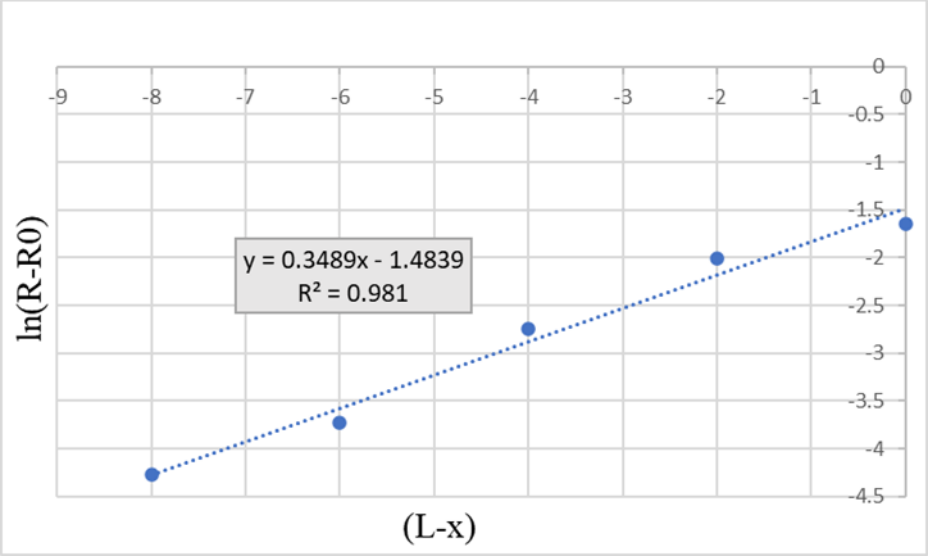

Fig. 17. Slope of isotopic distribution.

According to the figure 5, the k value is 0.3489 (the slope of equation plotted in Fig. 5.)

According to the equation number 7 and drawing Ln(R-R0) based on (L-X), intercept is -1.48393.

From equation number 6 and figure 5, the value of HETP is obtained 0.0988 cm.

Conclusions

Nitrogen isotope separation was studied using polystyrene-divinylbenzene DOWEX 50 W-X2 resin. It is found that a sharp band boundary is obtained. Therefore, the potential of displacement chromatography methods for enriching nitrogen stable isotopes was confirmed, and good results were obtained using the DOWEX 50 W-X2 cation exchange resin. The last number in the resin name indicates the percentage of cross-linking. High cross-linking means an increase in the amount of divinylbenzene in the resin structure, and this means that the percentage of the ion exchange functional group has decreased in the same amount of resin. Therefore, high crosslinking means low exchange capacity and is not desirable for the separation process, and it is better to use resins with a lower percentage of crosslinking. In this work, the ^{15}N isotopic percentage in the last sample after 160cm migration distance reached 0.56%, which is more than the results reported in the References for DOWEX 50W x8 resin with 0.2 M ammonium hydroxide feed and 1.5 ml/min eluent flow rate. In addition, by increasing the concentration of the feed solution and decreasing the flow rate of the eluent solution, higher enrichment of the ^{15}N is expected to be obtained.

References

[1] Y. Aguilera, R. Consuegra, A. Abreu, F. Baldassarre, and M. Rendueles, “Fractionation of nitrogen stable isotopes by ion exchange chromatography,” *Radioanalytical and Nuclear Chemistry*, vol. 258, pp. 93–99, 2003.

[2] H. Ohtsuka, M. Ohwaki, M. Nomura, M. Okamoto, and Y. Fujii, “Nitrogen isotope separation by means of cation exchange resin, (I) effects of eluent concentration,” *J Nucl Sci Technol*, vol. 32, no. 10, pp. 1001–1007, 1995, doi: 10.1080/18811248.1995.9731808.

[3] “A LABORATORY METHOD FOR SEPARATING NITROGEN ISOTOPES 6125.”

[4] W. K. Park and E. D. Michaels, “Separation of nitrogen isotopes by displacement band chromatography,” in *Separation Science and Technology*, Oct. 1988, pp. 1875–1889. doi: 10.1080/01496398808075669.

[5] M. Ahmadi-Motlagh, Y. Amini, and J. Karimi-Sabet, “Experimental study of nitrogen isotope separation by ion-exchange chromatography: effect of process factors,” *J Radioanal Nucl Chem*, vol. 331, no. 1, pp. 309–315, Jan. 2022, doi: 10.1007/s10967-021-08079-y.

[6] C. Y. Aguilera, S. R. Consuegra, D. A. Abreú, and M. Rendueles, “Separation of stable nitrogen isotopes by ion exchange chromatography,” *Solvent Extraction and Ion Exchange*, vol. 20, no. 6, pp. 777–791, Nov. 2002, doi: 10.1081/SEI-120016079.

[7] M. Ohwaki, Y. Fujii, and M. Hasegawa, “Flow-rate dependence of the height equivalent to a theoretical plate in nitrogen isotope separation by displacement chromatography,” 1998.

ICNST 2024
International Conference on Nuclear Science and Technology
6- 8 MAY 2024 | Isfahan, Iran

Spallation and activation of the body of International Space Station (ISS) by cosmic oxygen, proton and neutron rays (Paper ID : 1419)

Riahi A*, Heydarizade Y, Rezaie M R

Department of Nuclear Engineering, Faculty of Sciences and Modern Technologies, Graduate University of Advanced Technology, Kerman, Iran

Abstract

The International Space Station (ISS) is constantly exposed to space radiation. High fluxes of cosmic rays can affect humans and space components. The cosmic rays can change the material of ISS body by activation and spallation processes. This process causes decompose the elements or causes stop the charged particles and generating secondary particles. In this way, radioactive isotopes can be produced that called cosmogenic nucleotides. In this research, the spallation of the body of the Destiny module of the ISS by cosmic oxygen, proton and neutron rays is simulated using the MCNPX code that based on Monte Carlo method. Measuring the abundance of cosmic radionuclides with long half-lives in the atmosphere and terrestrial reserves is a very important tool for studying atmospheric processes and the interaction between different reservoirs. As a result of this simulation, radioisotopes of ^{7}Be, ^{10}Be, ^{14}C, ^{22}Na, ^{24}Na and ^{26}Al are commonly produced in the body of space station by cosmic neutron, oxygen and proton rays that ^{24}Na , ^{15}N and ^{27}Al have the most production yield respectively

Keywords: International Space Station (ISS), Spallation, Cosmic Oxygen, Cosmic Neutron, Cosmic Proton, MCNPX Code

Introduction

The International Space Station (ISS) is an orbital research center and the only space station operated by astronauts on long-term missions and the space shuttle crew on shorter visits [1]. According to a 2018 paper, Feldman et al. Used radiation transfer codes to study the interaction of galactic cosmic rays (GCRs) with interplanetary matter. In celestial bodies that do not have a large atmosphere, GCRs can strike the body and produce neutrons and protons rapidly by spallation interaction [2]. Thus spallation interaction changes the nature of the material and must be considered for high energy particle interaction. In this research, spallation and activating the body of the Destiny module of the ISS by cosmic oxygen, proton and neutron sources with the Monte

Carlo particle transport method implemented in the MCNPX toolbox has been investigated. The MCNPX code is a Monte Carlo nanoparticle code that can be used to transmit neutrons, photons, electrons, or neutron / photon / electron coupling. Its application includes radiation and dosimetry protection, radiography, medical physics, etc [3].

Cosmic rays include various rays that protons, neutrons, and oxygen are the most probability of them. Different galaxies evolve chemically at different speeds, which causes galaxies to be more scattered. Galactic winds with different efficiencies can also play a significant role in the dispersion of metals in irregular galaxies. The abundance of oxygen in interstellar gas is commonly used as a metal detector in galaxies. For irregular galaxies, the amount of oxygen is related to the total mass of the galaxy, meaning that the higher the total mass, the higher the heavy element content. The abundance of oxygen is also affected by the mass exchange between the galaxy and its environment [4].

Cosmic-ray neutrons are produced by two kinds of reactions. Fast neutrons made by direct interactions of high-energy cosmic rays are called knock-on neutrons and have energies from about 1 MeV to 1 BeV or more. A larger source of neutrons is the spallation or evaporation process. Neutron emission is the most probable de-excitation reaction when nitrogen and oxygen are excited to energies above about 8 MeV by cosmic rays [5]. when a neutron strike with a material, it only interacts with the nuclei due to the lack of electric charge. Capture of neutrons by a nucleus often results in the formation of a radioisotope [6]. Spallation also refers to nuclear reactions that occur when high-energy neutron interacts with an atomic nucleus [7].

Neutrinos, gammas, and also very energetic protons. Only about 3% of the decay particles are nucleons, mostly protons. These protons in turn interact with the cosmological radiation background. [8]

Previously research was shown that the primary and secondary cosmic rays interact together with spallation processes and generate ionizing radiation that mimics the space radiation environment. [9] but there is any report for spallation interaction of cosmic rays with international space station body. Therefore, in this research was tried to investigate spallation interaction of cosmic rays with international space station body.

simulation

To calculate neutron activation and oxygen and proton spallation of the body of ISS space station, a section of the geometry of Destiny module of space station is defined in an input file of the MCNPX code. The body of the space station is made of materials with different densities, which should be defined in the section of the cell card [10]. In the data card, cosmic source of oxygen, neutrons and protons are defined, then activation and spallation are calculated using the F8 and FT8 tallies. The interaction of high-energy particles with the target nuclei causes produce many new nuclei remaining. The produced nuclei remaining can be registered via F8 Tally if using the FT8 command [11]. The geometry of the code is a cylinder with a radius of one centimeter on the z-axis as a section of the Destiny module of the ISS [12]. Figure 1 shows a section of the components of the body of space station. The first layer is 0.2032 cm thick aluminum and the second layer is MLI thermal insulation, the third layer consists of 6 Nextel layers and the fourth layer contains 6 Kevlar layers and the last layer is 0.4775 cm thick aluminum, there is a vacuum between the layers.

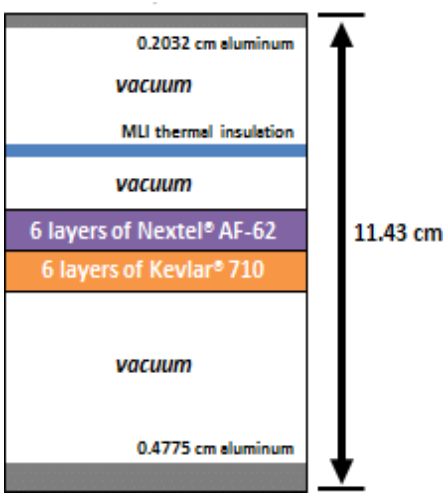

Fig. 1. Arrangement of metals in the body of the ISS space station [13].

Definition of the source in the data card: For each of the three sources, a plate with an area of 1*1 square centimeters is defined as parallel beams so that the surface of the source is in front of the section of the Destiny module and the beams strike the module uniformly. The energy range of the cosmic oxygen source is from 25 MeV to 4500 GeV [14]. The energy range of the proton is from the minimum energy of about 2 MeV to 100 GeV [15]. Neutron energy is from 60 keV to 50 MeV [16].

Results

For validation of Monte Carlo simulation, the spallation of a tungsten target by protons with an energy of 1 GeV was studied. A comparison between the FT8 output and the experimental of produced isotopes showed that this command could be used to study the spallation process [17]. after validation of Monte Carlo simulation by FT8 command in MCNPX code, the radionuclide production in the body of ISS space station by cosmic ray such as neutrons, oxygen and proton was down. In the interaction of materials with neutrons at low and high energies, the neutron activation process was observed and no nuclei resulting from the spallation process were observed. Therefore, the activation process is used for neutron interaction and the spallation process is used for oxygen and proton interaction. Table 1 also shows the produced nuclei by the neutron activation process of the Destiny module of the ISS space station that Radioisotope ^{24}Na has the highest production gain. Tables 2 and 3 show the results from spallation of the components of the body of ISS space station due cosmic oxygen and protons rays. Each of these radioisotopes is produced with a specific gain that is the mass produced by the radioisotope relative to the mass of the irradiated material. In cosmic oxygen and proton spallation, ^{15}N and ^{27}Al radioisotopes have the highest production gain, respectively.

Table 1. The results of cosmic neutron ray activation in simulation of the Destiny module of the ISS space station

Produced isotopes	Production gain	Produced isotopes	Production gain	Produced isotopes	Production gain	Produced isotopes	Production gain
^{2}H	1.06E-06	^{9}Be	1.14E-04	^{14}C	2.49E-05	^{24}Na	3.88E-04
^{4}He	4.37E-06	^{10}Be	3.45E-06	^{13}N	5.26E-07	^{25}Mg	1.74E-05
^{6}He	7.00E-07	^{10}B	4.69E-05	^{14}N	5.13E-06	^{26}Mg	8.13E-05
^{6}Li	2.30E-06	^{11}B	6.18E-05	^{15}N	3.18E-05	^{27}Mg	3.43E-04
^{7}Li	1.53E-04	^{12}B	7.89E-06	^{16}N	1.55E-05	^{26}Al	1.43E-04
^{8}Li	2.00E-07	^{13}B	1.32E-07	^{15}O	4.75E-06	^{27}Al	1.52E-07
^{9}Li	1.00E-07	^{12}C	7.98E-06	^{17}O	1.82E-10	^{28}Al	2.63E-05
^{7}Be	2.00E-07	^{13}C	9.15E-05	^{20}F	5.92E-08		

Table 2. The results of cosmic oxygen ray spallation in simulation of the Destiny module of the ISS space station

Produced isotopes	Production gain	Produced isotopes	Production gain	Produced isotopes	Production gain	Produced isotopes	Production gain
^{2}H	*7.90E-09*	^{12}C	*3.94E-03*	^{15}F	*3.25E-06*	^{26}Na	*1.62E-06*
^{6}He	*8.54E-04*	^{13}C	*1.94E-03*	^{16}F	*3.25E-06*	^{35}Na	*1.62E-06*
^{8}He	*6.82E-05*	^{14}C	*1.16E-03*	^{17}F	*4.06E-05*	^{20}Mg	*1.14E-05*
^{6}Li	*5.93E-03*	^{15}C	*3.25E-06*	^{18}F	*6.01E-04*	^{21}Mg	*1.14E-05*
^{7}Li	*3.11E-03*	^{16}C	*4.87E-06*	^{19}F	*4.48E-04*	^{22}Mg	*3.74E-05*
^{8}Li	*4.77E-04*	^{12}N	*3.09E-05*	^{20}F	*1.45E-04*	^{23}Mg	*1.66E-04*
^{9}Li	*1.02E-04*	^{13}N	*1.08E-03*	^{21}F	*6.01E-05*	^{24}Mg	*1.48E-03*
^{11}Li	*3.25E-06*	^{14}N	*3.61E-03*	^{22}F	*1.46E-05*	^{25}Mg	*2.01E-03*
^{7}Be	*3.60E-03*	^{15}N	*8.05E-03*	^{23}F	*6.50E-06*	^{26}Mg	*4.37E-03*
^{8}Be	*3.90E-05*	^{16}N	*3.31E-05*	^{17}Ne	*9.74E-06*	^{27}Mg	*8.84E-05*
^{9}Be	*8.21E-04*	^{17}N	*2.11E-05*	^{18}Ne	*9.74E-06*	^{22}Al	*9.74E-06*
^{10}Be	*4.01E-04*	^{18}N	*3.25E-06*	^{19}Ne	*1.59E-04*	^{23}Al	*1.95E-05*
^{11}Be	*8.12E-06*	^{19}N	*8.12E-06*	^{20}Ne	*1.00E-03*	^{24}Al	*1.79E-05*
^{14}Be	*4.87E-06*	^{20}N	*1.62E-06*	^{21}Ne	*6.63E-04*	^{25}Al	*3.12E-04*
^{8}B	*7.60E-04*	^{13}O	*7.47E-05*	^{22}Ne	*5.83E-04*	^{26}Al	*3.69E-03*
^{9}B	*4.87E-06*	^{14}O	*1.16E-03*	^{23}Ne	*1.15E-04*	^{27}Al	*3.47E-03*
^{10}B	*1.54E-03*	^{15}O	*7.77E-03*	^{24}Ne	*3.74E-05*	^{28}Al	*1.07E-06*
^{11}B	*2.12E-03*	^{16}O	*1.45E-03*	^{19}Na	*8.12E-06*	^{25}Si	*4.87E-06*
^{12}B	*1.01E-04*	^{17}O	*2.27E-04*	^{20}Na	*2.76E-05*	^{26}Si	*2.44E-05*
^{13}B	*1.10E-04*	^{18}O	*1.01E-04*	^{21}Na	*7.96E-05*	^{27}Si	*2.92E-05*
^{14}B	1.62E-06	^{19}O	2.11E-05	^{22}Na	5.83E-04	^{28}Si	1.14E-05
^{9}C	1.40E-04	^{20}O	1.79E-05	^{23}Na	8.38E-04		
^{10}C	1.49E-04	^{21}O	1.62E-05	^{24}Na	3.98E-04		
^{11}C	1.43E-03	^{22}O	3.25E-06	^{25}Na	3.74E-04		

Table 3. The results of cosmic proton ray spallation in simulation of the Destiny module of the ISS space station

Produced isotopes	Production gain	Produced isotopes	Production gain	Produced isotopes	Production gain	Produced isotopes	Production gain
^{6}He	*3.93E-04*	^{10}C	*3.40E-05*	^{17}O	*2.30E-05*	^{20}Na	*2.70E-05*
^{8}He	*1.48E-04*	^{11}C	*1.97E-04*	^{18}O	*7.00E-06*	^{21}Na	*4.80E-05*
^{6}Li	*1.44E-03*	^{12}C	*1.77E-03*	^{19}O	*1.00E-05*	^{22}Na	*1.01E-04*
^{7}Li	*1.42E-03*	^{13}C	*1.54E-04*	^{20}O	*1.50E-05*	^{23}Na	*1.47E-04*
^{8}Li	*2.12E-04*	^{14}C	*2.50E-05*	^{21}O	*8.00E-06*	^{24}Na	*6.60E-05*
^{9}Li	*3.30E-05*	^{15}C	*1.00E-06*	^{22}O	*3.00E-06*	^{25}Na	*2.50E-05*
^{11}Li	*5.00E-06*	^{17}C	*2.00E-06*	^{17}F	*7.00E-06*	^{26}Na	*1.00E-06*
^{7}Be	*9.10E-04*	^{18}C	*1.00E-06*	^{18}F	*6.40E-05*	^{35}Na	*4.00E-06*
^{8}Be	*9.20E-05*	^{12}N	*5.00E-06*	^{19}F	*4.70E-05*	^{20}Mg	*3.50E-05*
^{9}Be	*2.53E-04*	^{13}N	*3.40E-05*	^{20}F	*1.50E-05*	^{21}Mg	*2.50E-05*
^{10}Be	*7.70E-05*	^{14}N	*4.08E-04*	^{21}F	*2.70E-05*	^{22}Mg	*3.80E-05*
^{11}Be	*3.00E-06*	^{15}N	*1.07E-04*	^{22}F	*2.00E-05*	^{23}Mg	*5.20E-05*
^{14}Be	*1.00E-06*	^{16}N	*5.00E-06*	^{23}F	*1.40E-05*	^{24}Mg	*1.95E-04*
^{8}B	*2.22E-04*	^{17}N	*4.00E-06*	^{17}Ne	*1.70E-05*	^{25}Mg	*1.64E-04*
^{9}B	*2.20E-05*	^{18}N	*6.00E-06*	^{18}Ne	*1.30E-05*	^{26}Mg	*1.75E-04*
^{10}B	*3.35E-04*	^{19}N	*3.00E-06*	^{19}Ne	*2.20E-05*	^{27}Mg	*3.00E-06*
^{11}B	*3.15E-04*	^{20}N	*5.00E-06*	^{20}Ne	*1.08E-04*	^{22}Al	*2.00E-05*
^{12}B	*2.00E-05*	^{21}N	*1.00E-06*	^{21}Ne	*8.30E-05*	^{23}Al	*1.00E-05*
^{13}B	*4.00E-06*	^{13}O	*1.00E-05*	^{22}Ne	*7.50E-05*	^{24}Al	*1.60E-05*
^{15}B	*3.00E-06*	^{14}O	*2.90E-05*	^{23}Ne	*3.60E-05*	^{25}Al	*1.80E-05*
^{17}B	*1.00E-06*	^{15}O	*3.00E-05*	^{24}Ne	*1.80E-05*	^{26}Al	*2.00E-04*
^{9}C	*3.20E-05*	^{16}O	*7.13E-04*	^{19}Na	*1.50E-05*	^{27}Al	*9.62E-03*

Conclusion

Because the body of space station is constantly exposed to cosmic neutron, oxygen and proton particles, it causes spallation of the components of the body of space station. The results of this study show that the spectrum of nucleation produced by the activation and spallation process in the space station is a wide range, Between them, the ^{7}Be, ^{10}Be, ^{14}C, ^{22}Na, ^{24}Na and ^{26}Al nuclei can be seen. The production of these nuclei increases over time and to discuss radiation protection, the aggregation of these nuclei must also be considered. Therefore, considering the neutron activation and spallation of oxygen and protons, it can be concluded that the body of the space station, which is mainly made of aluminum; It is exposed to material change and radioactivity, and thus can affect the performance of space station electronics.

Reference

[1] T. Ersmark et al., "Geant4 Monte Carlo Simulations of the Galactic Cosmic Ray Radiation Environment On-Board the International Space Station/Columbus," IEEE Trans. Nucl. Sci., vol. 54, no. 5, pp. 1854–1862, Oct. 2007,
[2] "Benchmarking Geant4 for Simulating Galactic Cosmic Ray Interactions Within Planetary Bodies - Mesick - 2018 - Earth and Space Science - Wiley Online Library."
[3] "Los Alamos National Laboratory: MCNP Home Page.
[4] L. S. Pilyugin, T. X. Thuan, and J. M. Vílchez, "On the maximum value of the cosmic abundance of oxygen and the oxygen yield," Mon. Not. R. Astron. Soc., vol. 376, no. 1, pp. 353–360, Mar. 2007,
[5] W. N. Hess et al., "Cosmic-Ray Neutron Demography" Journal of GEOPHYSICAL RESEARCH, 1961
[6] "Neutrons - an overview | ScienceDirect Topics."
[7] "Spallation Physics Gary J. Russell ,1990
[8] Peter L Biermann., "The origin of the highest energy cosmic rays" 1996.
[9] Jeffery C. Chancellor et al., "Targeted Nuclear Spallation from Moderator Block Design for a Ground-Based Space Radiation Analog " 2017
[10] "NASA Ames Space Settlement Contest" Constantinescu Mihaela, Cosma Bianca-Maria,2018.
[11] J. S. Hendricks et al., "MCNPX EXTENSIONS VERSION 2.5.0," p. 65.
[12] "ISS.User.Guide.R2,2004.
[13] J. Fogel, M. Thangavelu, and N. Turner, "A Proposed Photoelasticity-Based Enhanced Visual Inspection Tool for Astronaut EVA," Oct. 2015.
[14] simulations of the secondary neutron ambient and effective dose equivalent rates from surface to suborbital altitudes and low Earth orbit," Life Sci. Space Res., vol. 6, May 2015,
[15] S. El-Jaby and R. Richardson, "Monte Carlo simulations of the secondary neutron ambient and effective dose equivalent rates from surface to suborbital altitudes and low Earth orbit," Life Sci. Space Res., vol. 6, May 2015,
[16] M. Smith et al., "Measurements of the neutron dose and energy spectrum on the International Space Station during expeditions ISS-16 to ISS-21," Radiat. Prot. Dosimetry, vol. 153, Jul. 2012,
[17] F. S.a.h, G. Z, and T. C, "INVESTIGATION OF THE OPTIMAL MATERIAL TYPE AND DIMENSION FOR SPALLATION TARGETS USING SIMULATION METHODS," vol. 8, no. 1, pp. 1–11, Jan. 2014.

ICNST 2024
International Conference on Nuclear Science and Technology
6- 8 MAY 2024 | Isfahan, Iran

Source term evaluation and radioisotope inventory estimation of irradiated LEU targets (Paper ID : 1453)

Kiyani A.[1*], Bahrami Samani A.[2], Pourimani R.[1], Miremad S. M.[2]
[1]Nuclear Physics, Arak University, Arak, Iran
[2] Nuclear Science and Technology Research Institute (NSTRI), Tehran, Iran

Abstract:

The Tehran Research Reactor (TRR) must irradiate miniature plates of low-enriched uranium (LEU) to produce molybdenum-99 (^{99}Mo). To do this, scientists need to have a good understanding of the radiation that these sources give off, which is made up of different radioisotopes. The irradiated LEU target serves as a source of radioactivity, producing various actinides, fission products, and activation products during the irradiation process. In addition, the radioisotope changes that occur during cooling and decay will determine the final composition of the hot target. Using radiochemical processes on targets containing ^{235}U and irradiated in reactors is a practical and effective way to produce ^{99}Mo. These targets, featuring low (LEU) or high (HEU) uranium abundances, come in diverse dimensions and chemical formulations. The main goal of this study is to figure out the source term and radioisotope inventory of native targets used to make molybdenum-99. These targets have a miniature plate geometry and the chemical formula U3O8Alx. We evaluate parameters such as radioactivity, source strength, decay heat, isotopic production, burnup, and gamma emission spectrum post-irradiation in the Tehran Research Reactor. To calculate these parameters, the ORIGEN 2.1 code can estimate the inventory of the hot target and the gamma radiation spectrum. These findings are then used to design shielding for production equipment, transportation containers, hot cells, and building dose mapping.

Keywords: LEU target, Source term, ORIGEN 2.1 code, Tehran research reactor

1. Introduction:

The need for nuclear drugs based on the meta-stable technetium-99 radioisotope (^{99m}Tc) to be used in diagnostic methods for some diseases is increasing daily. Most of the ^{99m}Tc required by medical centers is obtained due to the radioactive decay of molybdenum-99 (^{99}Mo) [1]. Therefore, to meet the demand for ^{99m}Tc for medical use, the production ^{99}Mo is of special importance. Studies show that uranium-235 fission (^{235}U(n,f) reaction) in reactors will be most efficient for ^{99}Mo production [2, 3]. Fig.1 shows the chain of production by the largest companies supplying the world markets

[4, 5]. To comply with non-proliferation guidelines, the IAEA has been promoting the use of low-enriched uranium (LEU) targets for several years to minimize human use of high-enriched uranium (HEU) targets. Based on this, domestically produced LEU plates, or miniature plates, will be used in Iran's production plan for molybdenum-99 by fission method.

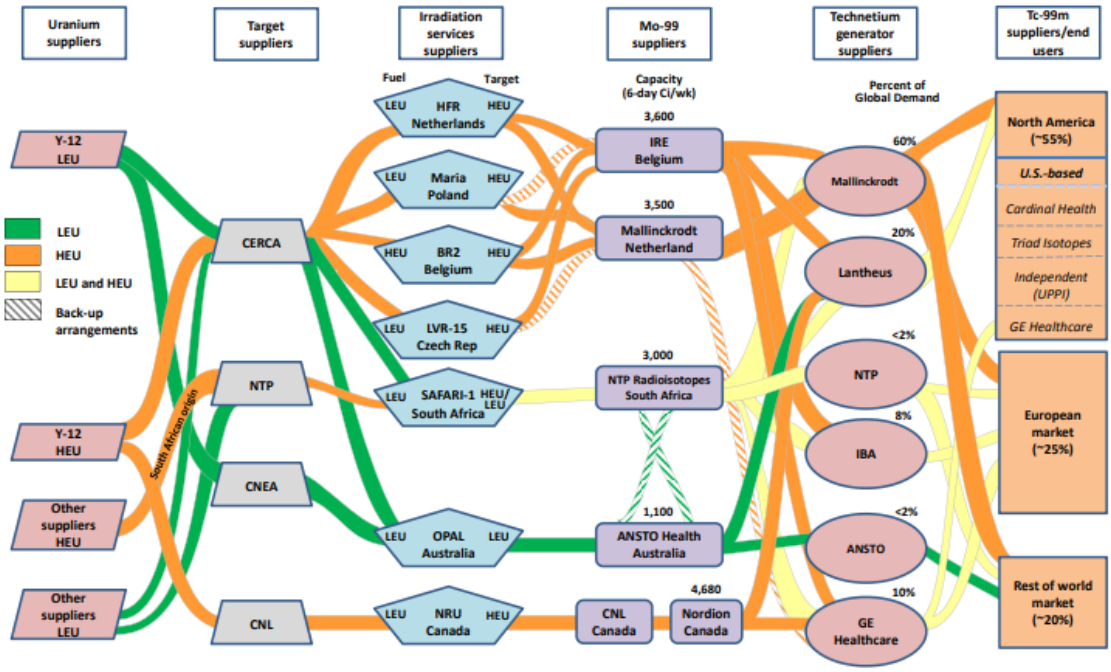

Fig. 1. Molybdenum-99 production chain in the world

These plates are irradiated in Tehran's research reactor, and after cooling, they are transferred to a laboratory equipped with a process chamber to carry out the radiochemical process to obtain 99Mo. The target of irradiated LEU is a source of radiation consisting of some actinides, fission products, and activation products produced during irradiation. In addition, the radioisotope changes that occur during cooling and decay will determine the hot target's final composition. Each of the radioisotopes present in the hot target emits one or more gamma rays with different frequencies. Depending on the hot target's existence in different conditions and times, it is possible to estimate the spectrum of the emitted gamma radiation. In fact, independent of the radioactive source's physical form in different stages of production, the type, number, and activity of the gamma-emitting radioisotopes in that source determine its nature. For this purpose, the ORIGEN code can be used to estimate the hot target inventory and the spectrum of gamma radiation [6-8].

In this article, the ORIGEN 2.1 computing code was used to determine some characteristics of a hot LEU batch in the local ^{99}Mo production facility, like the decay heat changes after irradiation, source term, and gamma spectrum before the radiochemical process was started. The study also evaluated the biological effects that the release of radioactive elements caused. The results are useful for codes like MCNP to design hot cells and transport containers.

2. Materials and Method:

2.1. LEU batch of local 99Mo Production facility

Each batch transferred to the hot cells consists of a holder with 9 grooves and 9 LEU-mini plates. To determine the source of radiation of a batch transferred to the hot cells after irradiation and cooling, it is necessary to have the specific composition of the mini plate and the holder before irradiation, in addition to their irradiation history. Figure 2 shows the drawing of the holder and LEU mini-plate (One batch). The material composition of the mini plate and holder is presented in Table 1 and Table 2.

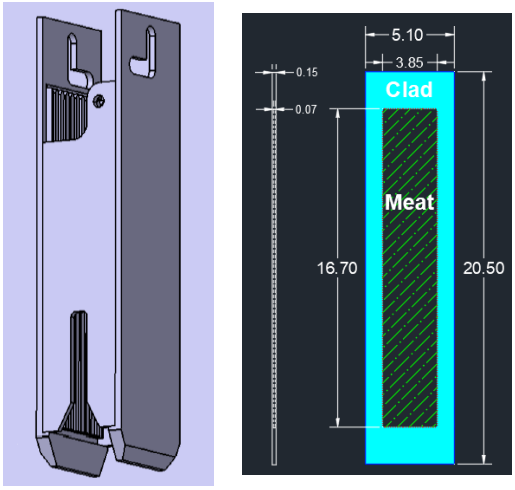

Fig. 2. A) Mini-Plat holder drawing B) LEU Mini-Plat (dimensions in cm)

Table 1. Nuclide Composition of LEU-Mini Plate

Material	Isotope	Mass (g)
LEU-Mini Plate U_3O_8-Al	U-235	3
	U-238	12.21
	O	2.79
	Al	5.2

Table 2. Nuclide Composition of Aluminum-6061

Material	Isotope	Weight Fraction (%)
Aluminum-6061	Si	6.000E-03
	Fe	7.000E-03
	Cu	2.750E-03
	Mn	1.500E-03
	Mg	1.000E-02
	Cr	1.950E-03
	Zn	2.500E-03
	Ti	1.500E-03
	Al	9.668E-01

2.2. Method

To produce a specific radioisotope using the fission method, the activity of that isotope in the hot target must reach an acceptable value. In addition to target characteristics and reactor parameters (power, fuel arrangement, selected position, etc.), irradiation and cooling time determine the desired amount of radioisotope in the hot target. These times should be chosen in such a way that the desired amount of the selected radioisotope is produced in the target. The irradiated target inventory includes actinides, fission products, activation products, and isotopes that are present in their decay chain. So, the first step to accurately knowing the hot target and estimating the radioisotopes produced in nuclear reactors is to burn up calculations. The differential equation device expresses the time-dependent burn-up equation of the i-th substance in the reactor's core at any given time, and these equations are also known as Bateman burn-up equations. In order to solve Bateman's equations, the microscopic cross-sections for all the desired nuclei and the distribution of the neutron flux in the system must be determined. As a result of uranium-235 fission, about 410 radionuclides with different abundances are produced [9-11]. The general differential equation of time changes of the amount of desired radioisotope governing the decay chain based on parameters such as flux and neutron absorption cross-section, density of uranium-235 in the target sample, irradiation time, cooling time, composition, and geometry of the sample is as follows: (1).

$$\frac{dN_i}{dt} = \gamma_i N_f \, \varphi \, \sigma_f + \sum_{i \neq j} y_i \ (\sigma_i \ \varphi + \lambda_i) N_j - (\sigma_i \, \varphi + \lambda_i) N_i \qquad (1)$$

The indices i, j, and f are related to the desired isotope, mother isotope, and fission of uranium, respectively. φ is the flux, σ is the cross-sectional area, γ is the fission yield, λ is the decay yield, and N is the atomic density. Since, in reality, we are dealing with neutrons with an energy range from thermal to fast, we must integrate over different energy intervals to solve equation 1. Therefore, solving Bateman's equations for such cases is complicated, so it is better to use the ORIGEN 2.1 code.

The ORIGEN 2.1 code calculations provide the spectrum of gamma radiation in 18 energy groups; Table 3 provides the lowest and upper boundaries of these groups [12, 13].

Table 3. Photon Energy Group Structure Used in ORIGEN 2.1 Code

Group No.	Group Energy (MeV)			Group No.	Group Energy (MeV)		
	Lower Boundary	Upper Boundary	Average		Lower Boundary	Upper Boundary	Average
1	0.00E+00	2.00E-02	1.00E-02	10	7.00E-01	1.00E+00	8.50E-01
2	2.00E-02	3.00E-02	2.50E-02	11	1.00E+00	1.50E+00	1.25E+00
3	3.00E-02	4.50E-02	3.75E-02	12	1.50E+00	2.00E+00	1.75E+00
4	4.50E-02	7.00E-02	5.75E-02	13	2.00E+00	2.50E+00	2.25E+00
5	7.00E-02	1.00E-01	8.50E+00	14	2.50E+00	3.00E+00	2.75E+00
6	1.00E-01	1.50E-01	1.25E-01	15	3.00E+00	4.00E+00	3.50E+00
7	1.50E-01	3.00E-01	2.25E-01	16	4.00E+00	6.00E+00	5.00E+00
8	3.00E-01	4.50E-01	3.75E-01	17	6.00E+00	8.00E+00	7.00E+00
9	4.50E-01	7.00E-01	5.75E-01	18	8.00E+00	1.10E+01	9.50E+00

Currently, the amount of ^{99}Mo needed by the country for medical purposes is estimated at about 100 to 120 Ci (6 days) per week. To meet this need and taking into account how ^{99}Mo is made through fission, we can say that the activity of ^{99}Mo in the set of cooled targets should be at least 834 Ci at the start of a one-day radiochemical process that works about 70% of the time. In fact, we must carefully determine the irradiation and cooling time to ensure that the hot target set's radioisotope inventory contains the mentioned amount at the start of the process. Calculations show that to achieve this value, the following conditions are needed for radiation. We simulated a miniature LEU target number containing uranium-235 in channel D6 using the MCNP code for the balanced core of the Tehran research reactor. We found the average power value to be 3.30E-02 MW. We then entered this value into the ORIGEN2.1 code. This method's calculation of the average power yields an accurate estimate of the radioisotope inventory of the hot target during short-term cooling. Table 4 presents the irradiation scenarios for the mini plate and holder.

Table 4: LEU-Mini Plate Irradiation The scenario

The variable	The value
Irradiation through TRR Channel	D6
Time of Irradiation (day)	6.0
TRR Pool Cooling Off Time (day)	1.0
Power in LEU-Mini Plates (MW)	0.033

3. Results and discussion:

Decay heat of the residual heat generated by a batch of hot target over different periods of time after the cessation of the fission process (cooling durations). The radioactive decay of fission products and actinides within the fuel material produces decay heat. Understanding how decay heat evolves over time is critical for assessing nuclear fuel's thermal behavior and designing safety measures for handling and storage. This aspect focuses on evaluating the potential health and safety risks associated with irradiated targets and their surroundings. It involves assessing factors such as radiation exposure levels, contamination risks, and potential pathways for radioactive release. We can implement measures to safeguard the health and safety of personnel, the public, and the environment near irradiated targets and facilities by understanding and mitigating these risks. Fig 3 illustrates the decay heat of one batch at various cooling durations following irradiation.

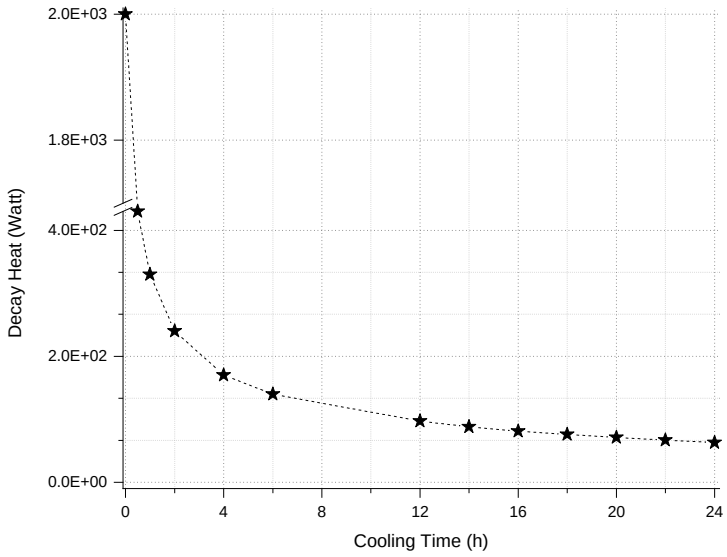

Fig. 3. Decay heat of one batch at various cooling durations

This article specifically mentions the nuclide concentration, which represents the inventory of nuclide mass in the fissionable material. From the radiation protection and shielding perspective, the concentration of nuclides after shutdown is important. During the cycle, we only assess the behavior of these nuclides. Fig 4 provides an estimate of the depletion of particular isotopes.

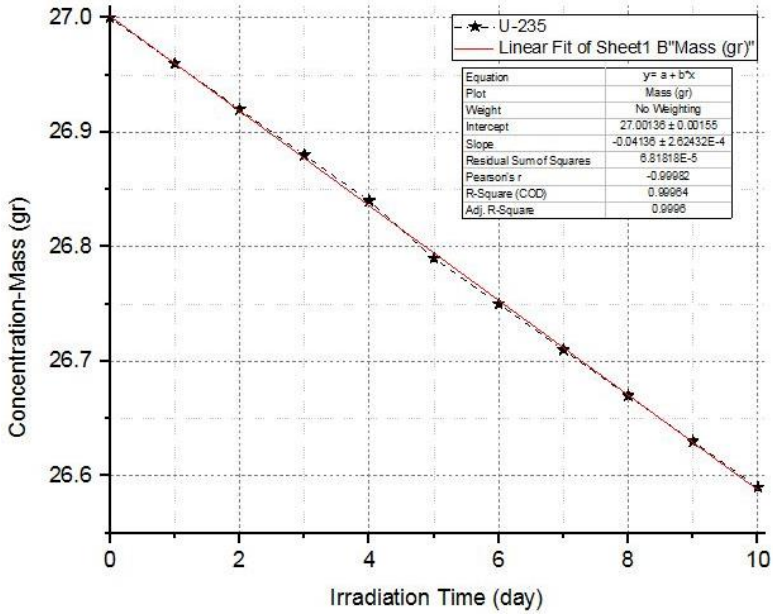

Fig. 4. Concentration (Mass) of uranium isotopes

In the Tehran reactor, activation products are produced in the sheath, aluminum used in the native target structure of the reactor and also in the impurities in the target. Additionally, the neutron capture of the target's isotopes, particularly ^{238}U, and the decay of their products primarily produce actinides. Table 6 presents the radiation source of one batch, which includes a holder and nine mini plates, and the radiation source of one mini plate and a holder at various periods following irradiation. Table 7 shows the nuclide's radioactivity after a specific period of irradiation for a group of samples. Indeed, one can determine the radioactivity of a nuclide after a specific amount of time by considering the nuclide's half-lives. Also, the nuclide Actinides and Activation Products radioactivity after irradiation time is presented in Table 8.

The gamma source strength and radioactivity (gamma spectrum) of one batch after 24 hours cooling time is presented in Table 9:

Table 6: Radiation source of a single batch at various decay times (gamma source strength (photon/s))

E_{mean} (MeV)	Discharge	1.0 h	2.0 h	5.0 h	12.0 h	24.0 h	36.0 h	48.0 h	60.0 h	72.0 h	96.0 h	120.0 h
1.000E-02	2.005E+15	5.356E+14	4.209E+14	2.943E+14	1.856E+14	1.187E+14	9.100E+13	7.543E+13	6.535E+13	5.823E+13	4.863E+13	4.221E+13
2.500E-02	4.973E+14	1.542E+14	1.240E+14	9.215E+13	6.631E+13	4.928E+13	4.125E+13	3.605E+13	3.219E+13	2.913E+13	2.440E+13	2.084E+13
3.750E-02	4.003E+14	1.459E+14	1.264E+14	1.040E+14	8.341E+13	6.670E+13	5.676E+13	4.959E+13	4.403E+13	3.955E+13	3.274E+13	2.780E+13
5.750E-02	4.358E+14	1.142E+14	9.133E+13	6.509E+13	4.210E+13	2.745E+13	2.106E+13	1.727E+13	1.472E+13	1.286E+13	1.030E+13	8.612E+12
8.500E-02	3.131E+14	8.993E+13	7.163E+13	5.323E+13	3.938E+13	3.106E+13	2.745E+13	2.512E+13	2.334E+13	2.184E+13	1.932E+13	1.719E+13
1.250E-01	3.082E+14	1.189E+14	9.949E+13	8.272E+13	7.032E+13	5.951E+13	5.217E+13	4.628E+13	4.133E+13	3.710E+13	3.025E+13	2.500E+13
2.250E-01	7.661E+14	2.259E+14	1.831E+14	1.453E+14	1.143E+14	8.259E+13	6.253E+13	4.966E+13	4.103E+13	3.485E+13	2.639E+13	2.070E+13
3.750E-01	4.732E+14	1.153E+14	7.636E+13	4.925E+13	3.545E+13	2.831E+13	2.523E+13	2.327E+13	2.178E+13	2.056E+13	1.859E+13	1.697E+13
5.750E-01	7.881E+14	3.855E+14	3.256E+14	2.570E+14	1.969E+14	1.405E+14	1.092E+14	8.906E+13	7.527E+13	6.533E+13	5.200E+13	4.331E+13
8.500E-01	8.305E+14	3.577E+14	2.633E+14	1.618E+14	1.158E+14	8.646E+13	7.063E+13	6.029E+13	5.293E+13	4.738E+13	3.946E+13	3.392E+13
1.250E+00	5.746E+14	2.088E+14	1.453E+14	8.240E+13	3.953E+13	1.852E+13	1.166E+13	8.608E+12	6.922E+12	5.825E+12	4.397E+12	3.443E+12
1.750E+00	1.708E+14	7.254E+13	5.681E+13	3.797E+13	2.662E+13	2.227E+13	2.124E+13	2.091E+13	2.071E+13	2.050E+13	1.997E+13	1.928E+13
2.250E+00	1.148E+14	4.512E+13	2.902E+13	1.160E+13	2.830E+12	1.074E+12	8.236E+11	7.239E+11	6.592E+11	6.080E+11	5.255E+11	4.586E+11
2.750E+00	4.813E+13	1.597E+13	9.270E+12	2.861E+12	8.780E+11	7.607E+11	7.678E+11	7.724E+11	7.723E+11	7.683E+11	7.518E+11	7.278E+11
3.500E+00	2.986E+13	4.320E+12	2.500E+12	6.483E+11	4.544E+10	7.123E+09	6.270E+09	6.268E+09	6.273E+09	6.248E+09	6.126E+09	5.940E+09
5.000E+00	1.609E+13	6.292E+10	4.224E+10	1.884E+10	3.392E+09	1.811E+08	9.673E+06	5.166E+05	2.758E+04	1.473E+03	4.202E+00	1.198E-02
7.000E+00	1.300E+11	1.360E-08	3.619E-11	3.631E-11	3.635E-11	3.635E-11	3.635E-11	3.635E-11	3.635E-11	3.636E-11	3.636E-11	3.636E-11
9.500E+00	2.561E+07	2.283E-12	2.289E-12	2.296E-12	2.298E-12	2.299E-12	2.299E-12	2.299E-12	2.299E-12	2.299E-12	2.299E-12	2.300E-12
Total	7.772E+15	2.590E+15	2.025E+15	1.440E+15	1.019E+15	7.331E+14	5.918E+14	5.030E+14	4.410E+14	3.945E+14	3.277E+14	2.805E+14
MeV/s	3.240E+15	1.212E+15	8.975E+14	5.700E+14	3.768E+14	2.667E+14	2.162E+14	1.859E+14	1.653E+14	1.501E+14	1.284E+14	1.129E+14

Table 7: Fission products radioactivity (Bq)

Nuclide	Radioactivity	Nuclide	Radioactivity	Nuclide	Radioactivity	Nuclide	Radioactivity	Nuclide	Radioactivity
Br-83	3.253E+12	Kr-91	1.245E+13	Zr-97	4.914E+10	Zr-103	2.364E+10	Te-131	1.415E+12
Kr-83m	3. 248E+12	Rb-91	1. 634E-09	Nb-97	4.914E+10	Nb-103	2.289E+10	Te-131m	2.548E+08
Se-84	6.179E+12	Sr-91	2.680E+12	Nb-97m	1.278E+09	Mo-103	1.510E-15	I-131	2.187E+12
Br-84	9.916E+12	Y-91	1.851E+11	Sr-98	9.276E+11	Tc-103	4.694E+00	Ba-139	4.544E-13
Se-85	5.723E+12	Y-91m	3.453E+13	Y-98	8.614E+11	Ru-103	4.548E+08	Ba-140	1.992E+13
Br-85	1.012E+13	Kr-92	1.416E+13	Zr-98	1.506E+11	Rh-103m	1.669E+13	La-140	2.176E+13
Kr-85m	1.002E+13	Rb-92	1.521E+13	Nb-98	2.572E+11	Nb-104	1.368E+13	La-141	4.081E+04
Se-86	9.725E+12	Sr-92	2.650E+13	Y-99	1.186E+11	Mo-104	1.507E-10	Ce-141	1.030E+13
Br-86	7.223E+12	Y-92	4.470E+13	Zr-99	3.752E-06	Tc-104	6.154E+11	La-142	2.771E-10
Br-86m	8.032E+12	Rb-93	1.559E-16	Nb-99	4.599E+11	Mo-105	5.028E+12	Ce-143	4.762E+12
Se-87	8. 287E+12	Sr-93	2.534E-15	Mo-99	2.042E+12	Tc-105	1.594E+09	Pr-143	1.994E+13
Br-87	1.073E+13	Y-93	1.186E+12	Tc-99m	1.067E+13	Ru-105	4.329E-18	Ce-144	1.295E+12
Kr-87	1.209E+13	Rb-94	2.879E+12	Y-100	2.515E+13	Rh-105	1.477E+13	Pr-144	1.295E+12
Br-88	1.295E+13	Sr-94	3.798E-11	Zr-100	2.591E+13	Rh-105m	1.262E+13	Pr-145	3.607E+07
Kr-88	2. 464E+13	Y-94	1.590E+11	Nb-100	7.370E+04	Sb-127	4.851E+11	Nd-147	7.803E+12
Rb-88	2.987E+13	Rb-95	3.762E+12	Nb-100m	4.396E+05	Te-127	5865E+11	Nd-149	1.478E-08
Br-89	9.253E+12	Sr-95	2.234E+10	Zr-101	3.072E+13	Sn-128	7.257E+09	Pm-149	2.223E+12
Kr-89	2. 562E+13	Y-95	2.544E+10	Nb-101	3.265E+13	Sb-128m	1.625E+12	Pm-151	2.278E+11
Rb-89	2.195E+13	Zr-95	2.974E+10	Mo-101	1.454E+12	Sb-129	7.561E-18	Sm-153	2.833E+11
Sr-89	2.149E+12	Nb-95	1.578E+09	Tc-101	1.840E+03	Te-129	6.851E-05	Total	1.544E+15
Br-90	1.085E+13	Sr-96	5.236E+11	Zr-102	1.671E+06	Sn-130	4.283E+12		
Kr-90	2.103E+13	Y-96	6.612E+11	Nb-102	3.157E+12	Sb-130m	1.187E+10		
Rb-90	2. 578E+13	Sr-97	1.587E+11	Mo-102	1.352E+13	Sn-131	4.425E+08		
Rb-90m	7.190E+12	Y-97	1.562E+11	Tc-102	2.160E+11	Sb-131	3. 068E+12		

Table 8: Activation products and actinides radioactivity (Bq)

Activation Products		Actinides	
Nuclide	**Radioactivity (Bq)**	**Nuclide**	**Radioactivity (Bq)**
Na-24	6.490E+11	**U-235**	2.060E+06
Mg-27	3.073E+12	**U-236**	5.450E+05
Al-28	9.655E+13	**U-238**	1.090E+06
Cr-51	3.817E+10	**Np-239**	3.537E+13
Mn-54	1.681E+08	**Pu-239**	9.295E+06
Mn-56	4.858E+12	**Pu-240**	1.797E+05
Fe-59	4.461E+08		
Co-60	1.228E+06		
Zn-69	1.373E+11		

Table 9: Gamma source Strength (photon/s)

E(mean) (MeV)	Fission Products (FP)	Activation Products (AP)	Actinides	Total
1.000E-02	1.187E+14	1.473E+10	4.949E+13	1.682E+14
2.500E-02	4.928E+13	3.063E+09	6.547E+11	4.994E+13
3.750E-02	6.670E+13	1.991E+09	4.381E+11	6.714E+13
5.750E-02	2.745E+13	2.832E+09	1.335E+12	2.879E+13
8.500E-02	3.106E+13	1.685E+09	8.831E+12	3.989E+13
1.250E-01	5.951E+13	1.075E+09	2.539E+13	8.490E+13
2.250E-01	8.259E+13	1.367E+09	1.761E+13	1.002E+14
3.750E-01	2.831E+13	4.926E+08	1.694E+12	3.000E+13
5.750E-01	1.405E+14	1.753E+08	7.285E+09	1.405E+14
8.500E-01	8.646E+13	1.880E+09	2.577E+08	8.646E+13
1.250E+00	1.852E+13	4.653E+10	1.613E+08	1.857E+13
1.750E+00	2.227E+13	6.881E+04	2.905E+05	2.227E+13
2.250E+00	1.074E+12	1.799E+03	4.360E-01	1.074E+12
2.750E+00	7.607E+11	4.215E+10	2.513E-01	8.029E+11
3.500E+00	7.123E+09	2.887E+07	2.223E-01	7.152E+09
5.000E+00	1.811E+08	3.001E+05	9.446E-02	1.814E+08
7.000E+00	3.635E-11	0.000E+00	1.075E-02	1.075E-02
9.500E+00	2.299E-12	0.000E+00	1.228E-03	1.228E-03
Total	7.331E+14	1.180E+11	1.055E+14	8.387E+14
MeV/s	2.667E+14	1.771E+11	9.132E+12	2.760E+14

4. Conclusions:

The Tehran research reactor uses LEU targets after irradiation and cooling to produce molybdenum-99 through the fission method. The hot target changes into a complex radioactive source as it goes through the decay chain. It makes different types of actinides, fission products, activation products, and other isotopes. Using the ORIGEN2 code, we evaluated the source term and calculated the isotope inventory. Estimating the radioisotope inventory and determining the source term at each stage of the molybdenum-99 production process will lead to estimating the gamma radiation spectrum. The nuclear shield designer's task is to determine the radioisotope inventory, the activity of each component, the spectrum of gamma radiation involved, and the strength of the source in each stage. Table 6 calculates the radiation source for a hot batch at various decay times. These calculations are used to design equipment shielding and prepare building dose mapping. We calculated the amount of reactivity of fission, activation, and actinide products in Tables 7 and 8. Finally, we use these results to evaluate the radiological effects caused by the release of radioactive elements and as input to codes like MCNP, CAP, PC-Cream, and others.

References:

[1]. Bradley, E., *Non-HEU production technologies for Molybdenum-99 and Technetium-99m*. 2013: International Atomic Energy Agency.

[2]. Lee, S.-K., et al., *Development of fission 99Mo production process using HANARO.* 2020. 52(7): p. 1517-1523.

[3]. Sciences, N.A.o., et al., *Opportunities and approaches for supplying molybdenum-99 and associated medical isotopes to global markets: proceedings of a symposium.* 2018.

[4]. Sciences, N.A.o., et al., *Molybdenum-99 for medical imaging.* 2016.

[5]. Tabasi, M., et al., *Assessment of Mo-99 radioisotope supply chain using LEU in Iran.* 2021. 42(3): p. 104-110.

[6]. Abrefah, R., P. Essel, and H.J.P.i.N.E. Odoi, *Estimation of the dose rate of nuclear fuel of Ghana Research Reactor-1 (GHARR-1) using ORIGEN-S and MCNP 6.* 2018. 105: p. 309-317.

[7]. Miremad, S., et al., *Dose rate estimation of gamma-rays emitted from a LEU miniature plate*. 2023. 44(4): p. 85-92.

[8]. Gholamzadeh, Z., et al., *ThO2 spent fuel assembly's gamma dose rate dependency to burnup and cooling time.* 2020. 1(3): p. 43-48.

[9]. Rabinovich, V.A., et al., *Thermophysical properties of neon, argon, krypton, and xenon.* 1988.

[10]. TANAKA, T. and S.J.T. NI, Japan, on assignment to Oak Ridge National Laboratory, Oak Ridge, Tennessee, personal communication, *Japan Atomic Energy Research Institute.* 1993.

[11]. Duderstadt, J.J. and L.J. Hamilton, *Nuclear reactor analysis*. 1976: Wiley.

[12]. Croff, A.G., *User's manual for the ORIGEN2 computer code*. 1980, Oak Ridge National Lab.

[13]. Croff, A.G.J.N.T., *ORIGEN2: a versatile computer code for calculating the nuclide compositions and characteristics of nuclear materials.* 1983. 62(3): p. 335-352.

ICNST 2024
International Conference on Nuclear Science and Technology
6- 8 MAY 2024 | Isfahan, Iran

The stable 129-Xenon isotope as a contrast agent MRI for lung imaging (Paper ID : 1559)

Somayeh Akbari-Karadeh[1], Amir Kazemi[2], Samira Rezaei[3*], Ali Norouzi Aghbash[4], Bakhtiar Azadbakht[4], Seyed Mahmoud Reza Aghamiri[1]

[1]Department of Medical Radiation Engineering, Shahid Beheshti University, Tehran, Iran
[2] Department of Medical Radiation Engineering, University of Science and Research Branch, Tehran, Iran
[3] Department of Reactor Engineering, Shahid Beheshti University, Tehran, Iran
[4]Iran Advanced Technologies Company, Atomic Energy Organization of Iran

Abstract

Nuclear medicine scanning and single-photon emission computed tomography (SPECT) are now the established methods for functional imaging of patients with lung disease. The FDA has granted approval for the use of ^{129}Xenon hyperpolarized (HP) magnetic resonance imaging (Xe-MRI) specifically for imaging the lungs. It offers comparable functional lung imaging with greater spatial resolution than scintigraphy and SPECT. The hyperpolarized ^{129}Xe functions as a contrast agent, enhancing the quality of MRI outcomes. The patient may breathe hyperpolarized ^{129}Xe, which enables the capture of sharp images of the lungs and trachea using a typical MRI scanner. Moreover, Xenon gas has the ability to dissolve in the blood circulation, allowing for the visualization of the circulatory system using imaging techniques. Thus, the objective of the study is to review recent research on the use of the ^{129}Xe stable isotope in lung MRI imaging.

Keywords: MRI Contrast agent, Lung disease, ^{129}Xenon, Stable Isotope

Introduction

Lung cancer is the leading cause of death worldwide, more so than any other type of cancer. According to the most recent GLOBOCAN estimates, lung cancer incidence and mortality in Asia are the highest compared to Europe and the United States, with 60% of new lung cancer cases reported in Asia alone in 2020. Approximately half of lung cancer patients receive a diagnosis after the disease has spread to other areas, which typically renders lung cancer treatment unfeasible at the time of diagnosis. For this reason, early detection of lung cancer in the early stages of the disease is a way to treat it on time and thus reduce the mortality rate [1]. The chest's computed tomography (CT) provides high-resolution images of the airway, parenchymal structure, and anatomy. Furthermore, because chest CT protocols are available in

imaging centers, CT of the chest is considered the imaging modality of choice for non-invasive assessment of chronic lung diseases [2].

Compared to magnetic resonance imaging and nuclear imaging, chest computed tomography is considered the reference standard for lung anatomical imaging due to its superior spatial and temporal resolution. However, cases such as obstructive disease and interstitial changes in the lung parenchyma are less clear on CT images and therefore rarely diagnosed. Therefore, to date, there are validated methods for visualizing regional ventilation in the context of acute and chronic pulmonary embolism diagnosis and preoperative planning of lung volume reduction surgery (LVRS) in COPD (chronic obstructive pulmonary disease). However, low resolution, long times, and, most importantly, the use of ionizing radiation limit nuclear imaging methods [3, 4].

Magnetic resonance imaging (MRI) is a technique for imaging soft tissue in very fine detail. MRI is based on protons (the nucleus of the ^{1}H atom) that are found in the body as water, and due to the lack of water molecules in lung tissue, there are limitations in lung tissue imaging, including low-contrast images of the same tissue [5, 6]. Magnetic resonance imaging uses hyperpolarized (HP) noble gases, such as ^{129}Xe and ^{3}He, to examine changes in the lungs' microstructure associated with diseases [7]. HP isotopes of noble gases (^{3}He, ^{129}Xe) increase the contrast and improve the resolution of MRI images by several orders of magnitude due to their degree of polarization close to 1 [8]. Compared to ^{3}He, ^{129}Xe has a relatively low gyromagnetic ratio, but due to the relatively large chemical change of the lines at the molecular level and different environments (~250 ppm), as well as excellent solubility in blood and tissues, it has become a suitable contrast agent for MRI imaging. In addition, ^{129}Xe has a higher relative abundance than ^{3}He (26.44, 1.37×10^{-4}, respectively), so ^{129}Xe can compensate for the effects of ^{3}He shortages around the world [9, 10].

HP ^{129}Xe -MRI is known as a promising tool for evaluating regional ventilation heterogeneity. As a result, ^{129}Xe ventilation imaging has been thoroughly investigated to improve the performance of pulmonary function tests (PFTs). To evaluate lung disease, the clinical standard includes PFTs, which only examine lung function in general and are not sensitive to diagnosing lung disease in the early stages and subtle changes in lung function. For early diagnosis and complete evaluation of heterogeneous lung diseases, it is necessary to use sensitive, accurate, and reproducible methods that provide regional information about lung structure and function.

HP ^{129}Xe MRI has been evaluated in a wide range of patients with airway obstruction problems, has been found to be significantly associated with PFT results, and can provide high sensitivity in the accurate identification of subtle airway obstruction and further examination of distal organs [10, 11].

Albert et al. performed the first MRI imaging using hyperpolarized ^{129}Xe in the mouse lungs in 1994, and Ebert et al. and MacFall et al. reported the first hyperpolarized MRI images of human lungs using ^{3}He in 1996 [12-14]. Also in 1997, the first results of imaging using ^{129}Xe, together with the ^{129}Xe spectrum of the human chest and head, were evaluated by Mugler et al. [15]. This review will focus on hyperpolarized ^{129}Xe MRI applications.

Physical Properties of ^{129}Xe

Stable isotopes are non-radioactive nuclei of elements that have similar chemical properties but have different atomic masses due to the difference in the number of neutrons. Xenon is a noble gas that has nine natural isotopes from ^{124}Xe to ^{136}Xe, but only two of the naturally abundant isotopes, ^{129}Xe (26.44% with 75 neutrons and I = -1/2) and ^{131}Xe (21.18% with 77 neutrons and I = +3/2), are suitable for magnetic resonance imaging because they have non-zero spin. The ^{129}Xe isotope is preferred because of its higher relative sensitivity compared to ^{131}Xe (Table 1). Due to the presence of a very large electron cloud in the internal structure of xenon, its spectral range reaches 8000 ppm, and as a result, it has a high polarization. The lattice spin relaxation time in the ^{129}Xe core reaches several minutes (T1 up to 4.1 hours), which can be greatly reduced by using ^{129}Xe hyperpolarization. ^{129}Xe is used to study many systems, from organic polymers, liquid crystals, and porous materials to large biomolecular materials [16-18].

Table 1. Properties of nuclei used in MRI [10].

Properties	^{129}Xe
Isotope abundance (%)	26.44
Nuclear spin	½
Gyromagnetic ratio (MHz/T)	-11.78
Spin density (10^{19} atoms/cm^3)	2.37
Chemical shift range (ppm)	~250
Self-diffusion coefficient (cm^2/s)	0.062
Free diffusion coefficient (in air) (cm^2/s)	0.14
Ostwald solubility in water	0.083–0.093
Ostwald solubility in blood	0.137–0.222

FDA Approved

Polarean Imaging plc performed the first clinical scan using the hyperpolarized ^{129}Xe technology under the brand name XENOVIEW at Cincinnati Children's Hospital Medical Center in the United States on May 11, 2023. The US Food and Drug Administration has approved XENOVIEW as the only hyperpolarized contrast agent for use with magnetic resonance imaging to evaluate lung ventilation in adults and pediatric patients 12 years of age and older. XENOVIEW can provide pulmonologists, surgeons, and other respiratory professionals with regional maps of ventilation in patients' lungs to help them manage the disease [2]. The recommended target dose of XENOVIEW is 75 mL to 100 mL dose equivalent (DE) of hyperpolarized ^{129}Xe for adults and pediatric patients 12 years of age and older. Furthermore, the cost of conducting a ^{129}Xe MRI scan is approximately $300 per scan [19].

^{129}Xe Polarization

Thermally polarized ^{129}Xe can be used for an MRI scan, but the low density of the gas produces a very weak signal that is not useful for MRI imaging. The hyperpolarization process can enhance the MRI signal by increasing the nuclear polarization by a factor of ten times the thermal equilibrium polarization. As a result, the MRI signal increases with the use of hyperpolarized ^{129}Xe gas, making MRI diagnosis easier. Spin exchange optical pumping (SEOP) can polarize ^{129}Xe up to 50% [10, 16]. Through alkali metal optical pumping, the SEOP process produces highly polarized noble gases. The SEOP process consists of two steps. The first step involves vaporizing an alkali metal, such as rubidium (Rb), and subjecting it to optical pumping using

circularly polarized light. This process transfers the electron spin polarization to the alkali metal. The next step involves transferring the alkali metal electrons' spin polarization to the desired noble gas nucleus (^{129}Xe), resulting in the generation of ^{129}Xe HP. Then ^{129}Xe HP is transferred to a portable storage tank and used for medical applications [8, 20].

Gas Phase Pulmonary ^{129}Xe MRI

^{129}Xe hyperpolarized inhalation MRI is a non-invasive, radiation-free imaging technology. Initially, Mitchell Albert et al. were trying to investigate the effects of anesthesia on brain function and used ^{129}Xe to directly scan it, but they did not obtain acceptable polarization. Therefore, Mitchell Albert et al. used 129Xe for lung MRI imaging. Gas-phase hyperpolarized xenon MRI provided accurate 3D images of the ventilated airspaces of the lungs, enabling the calculation of the ventilation defect percentage (VDP) [12].

To detect regional ventilation, ^{129}Xe MRI imaging can calculate VDP. Ventilation imaging using ^{129}Xe revealed ventilation heterogeneity and higher VDP in patients with chronic obstructive pulmonary disease, asthma, cystic fibrosis (CF), and lung cancer. ^{129}Xe MRI offers a reliable and accurate method to observe the distribution of pulmonary ventilation, even in individuals whose spirometry fails to detect airway dysfunction [21-23]. Thomen et al. conducted a study on cystic fibrosis patients and healthy subjects, using the gold standard for forced expiratory volume (FEV_1) and comparing the results with VDP measured by ^{129}Xe. Their studies revealed that the ^{129}Xe HP method is much more sensitive than FEV_1 in diagnosing pulmonary CF [24]. Stewart et al.'s study showed that patients with non-small cell lung cancer (NSCLC) exhibit a heterogeneous distribution of ventilated airspaces in the lung region. The study also demonstrated that the majority of COPD patients experienced severe ventilation problems. All these studies demonstrated that ^{129}Xe hyperpolarized MRI can detect regional functional ventilation defects before the disease has a heterogeneous distribution of ventilated airspaces in the lung region. It can also detect progression in patients with lung diseases that other imaging techniques cannot detect, enabling timely treatment [25].

HP ^{129}Xe MRI in Patients with Long COVID-19

Chest radiography is the most common imaging method for diagnosing acute COVID-19 pneumonia, and hospitalized patients repeat imaging 3 months after acute infection. If there is concern about a lung injury associated with COVID-19, a chest CT is done to further investigate.

Observations have shown lung abnormalities caused by turquoise after COVID in a number of patients, and reports indicate that the CT findings in these individuals are either normal or nearly normal. Also, the rest of the pulmonary tests usually show values in the normal range [26, 27].

In a study of patients hospitalized with post-COVID-19 conditions (PHC) 3 months after hospital discharge, Grist et al. concluded that it is possible to detect abnormalities of alveolar gas transport using ^{129}Xe MRI, even when the results of CT scans and pulmonary function tests were nearly normal. HP ^{129}Xe MRI enables the evaluation of ventilation and gas transfer from the entire alveolar epithelium to the red blood cells, as well as the identification of lung abnormalities that are not evident on a CT scan As a result, respiratory problems are identified in people with the disease post-COVID-19, and it helps to relieve shortness of breath in them [28, 29].

The role of HP ^{129}Xe MRI for treatment planning in thoracic radiation therapy

Radiation therapy plays an important role in the treatment of lung cancer. Radiation-induced lung injury (RILI) is a common occurrence in patients with lung cancer who are undergoing radiation therapy. In 2019, a report found that 25% of patients receiving radiation treatment for lung cancer developed lung radiation pneumonitis (RP), typically occurring several weeks post-treatment. In acute cases, chronic pneumonitis can develop into fibrosis [3, 30]. It is difficult to plan and evaluate radiation therapy treatments as well as predict and prevent RILI. Based on the assumption of homogeneous lung tissue, several studies have investigated which lung volume in computed tomography (CT) is the best predictor for the development of radiation pneumonitis. Chronic obstructive pulmonary diseases (COPD) are prevalent in most lung cancer patients, indicating heterogeneous lung function.

Single photon emission computed tomography (SPECT) imaging is used to provide lung function information. The images provided by SPECT in the radiation treatment design showed the appropriate values to minimize lung function radiation. However, the low resolution of SPECT images limits their application to the lung. A CT scan works well for obtaining anatomical information about the lung. Radiation oncology also uses four-dimensional CT (4DCT) to extract information about target or organ movement. In addition, new imaging techniques such as dual-energy CT (DECT) can provide information on lung ventilation and perfusion. But currently, DECT is not available in all clinical places, and CT and SPECT expose patients to ionizing radiation.

A study by Ding et al. showed that performance-based radiotherapy planning based on HP ^{129}Xe MRI was feasible in ten patients with NSCLC and showed that this treatment plan was able to reduce radiation exposure in highly ventilated areas of the lung. This study demonstrated that the HP ^{129}Xe MRI can examine lung physiology, such as gas exchange and pulmonary blood perfusion, in order to aid lung radiation therapy. Moreover, ^{129}Xe offers unique simultaneous monitoring of pulmonary ventilation, perfusion, and direct gas exchange, without exposing the patient to radiation. Recent advances in MRI techniques make it possible to obtain three-dimensional images of ^{129}Xe in the lung parenchyma, blood, and alveoli during a breath hold. Below, we present a 3D view of HP ^{129}Xe MRI images superimposed on MRI images. ^{129}Xe MRI images clearly display ventilation heterogeneity [31, 32].

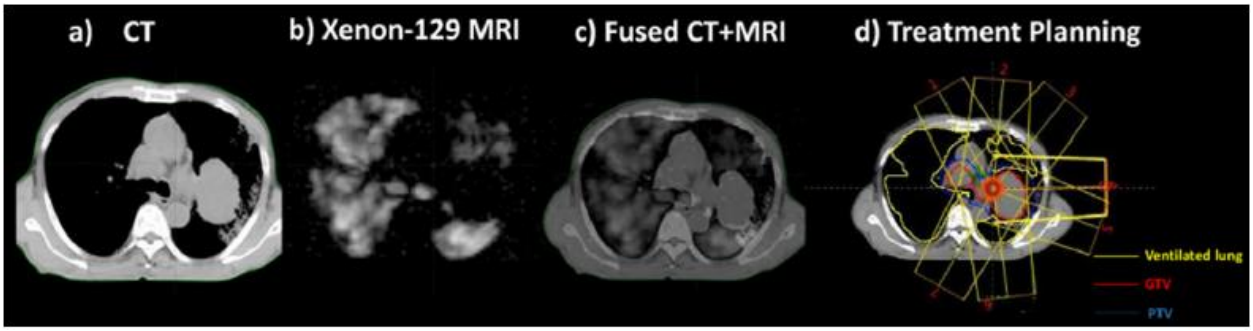

Representative images from patient P1 (age: 60, male, T3N3M0, Stage III C, AJCC Version 8). From left to right, showing: (a) simulation CT image for treatment planning; (b) HP ^{129}Xe MRI images from the corresponding location with the CT image; (c) Fused CT and MRI images; (d) Beam arrangement for radiotherapy treatment planning, with the yellow contours showing the well-ventilated lung areas [31].

Brain ^{129}Xe MRI

Researchers have developed Xenon's ability to image the brain in recent years. Swanson and colleagues demonstrated the first spectrum of animal brains using ^{129}Xe in vivo, but the image resolution was poor due to the low xenon polarization. Wakai et al. studied the brain spectra of healthy mice by increasing xenon polarization [33]. Mugler et al. showed the first in vivo spectra of the human brain using dissolved phase ^{129}Xe [15]. Also, by studying three healthy humans, Rao et al. showed the possibility of imaging the human brain using hyperpolarized ^{129}Xe.

Furthermore, since inhaled ^{129}Xe crosses the blood-brain barrier and enters extravascular tissue compartments, this study was able to directly image perfusion [34]. Zhou et al. investigated the first in vivo ischemic stroke imaging using ^{129}Xe [35]. A study by Rao et al. using hyperpolarized ^{129}Xe proved the clinical effectiveness of the brain MRI of a person suffering from a stroke due to occlusion of the left internal carotid artery [36]. ^{129}Xe MRI is an excellent method for imaging the developing brain because it is safe to inhale, has a wide solubility, and has a characteristic range of chemical changes in specific tissues. ^{129}Xe -based imaging is capable of providing fast and direct perfusion imaging even at low field with SNR equivalent to ASL (arterial spin labeling) perfusion imaging [37]. In addition, considering the capacity of xenon to penetrate the surface of the blood-brain barrier (BBB), the understanding of the BBB area and changes in permeability and transmission of the barrier is increased [38, 39].

Conclusion

This study aims to present a comprehensive analysis of the different uses of ^{129}Xe MRI in clinical trials. It also suggests the possible future use of MRI for disease diagnosis using ^{129}Xe as a contrast agent. This could potentially improve patients' treatment outcomes and disease management.

The Iran Advanced Technologies Company, a subsidiary of the Atomic Energy Organization of Iran (AEOI), is involved in various activities, including the production of stable isotopes such as tellurium-130 and xenon-129. In the near future, the company intends to provide ^{129}Xe for the designated purposes.

References

[1] D. C.-L. Lam *et al.*, "Lung Cancer screening in Asia: an expert consensus report," *Journal of Thoracic Oncology,* vol. 18, no. 10, pp. 1303-1322, 2023.

[2] R. L. Eddy and G. Parraga, "Pulmonary xenon-129 MRI: new opportunities to unravel enigmas in respiratory medicine," *European Respiratory Journal,* vol. 55, no. 2, 2020.

[3] Y. Ding *et al.*, "A pilot study of function-based radiation therapy planning for lung cancer using hyperpolarized xenon-129 ventilation MRI," (in eng), *J Appl Clin Med Phys,* vol. 23, no. 3, p. e13502, Mar 2022, doi: 10.1002/acm2.13502.

[4] L. Ebner, J. Kammerman, B. Driehuys, M. L. Schiebler, R. V. Cadman, and S. B. Fain, "The role of hyperpolarized 129xenon in MR imaging of pulmonary function,"

European Journal of Radiology, vol. 86, pp. 343-352, 2017/01/01/ 2017, doi: https://doi.org/10.1016/j.ejrad.2016.09.015.

[5] J. T. Singh, "Polarization and Delivery System for Xenon-129," 2000.

[6] T. B. R. H. R. Institute. "Hyperpolarized Noble Gas MRI Detection of Radiation-Induced Lung Injury." (accessed.

[7] J. P. Mugler, 3rd and T. A. Altes, "Hyperpolarized 129Xe MRI of the human lung," (in eng), *J Magn Reson Imaging*, vol. 37, no. 2, pp. 313-31, Feb 2013, doi: 10.1002/jmri.23844.

[8] A. S. L. G.Y. Grigoriev, "Methods for obtaining polarized xenon for magnetic resonance imaging. Review," 2022.

[9] P. Nikolaou *et al.*, "Near-unity nuclear polarization with an open-source 129Xe hyperpolarizer for NMR and MRI," (in eng), *Proc Natl Acad Sci U S A*, vol. 110, no. 35, pp. 14150-5, Aug 27 2013, doi: 10.1073/pnas.1306586110.

[10] H. Marshall, N. J. Stewart, H.-F. Chan, M. Rao, G. Norquay, and J. M. Wild, "In vivo methods and applications of xenon-129 magnetic resonance," *Progress in Nuclear Magnetic Resonance Spectroscopy*, vol. 122, pp. 42-62, 2021.

[11] L. Ebner *et al.*, "Multireader Determination of Clinically Significant Obstruction Using Hyperpolarized (129)Xe-Ventilation MRI," (in eng), *AJR Am J Roentgenol*, vol. 212, no. 4, pp. 758-765, Apr 2019, doi: 10.2214/ajr.18.20036.

[12] M. S. Albert *et al.*, "Biological magnetic resonance imaging using laser-polarized 129Xe," *Nature*, vol. 370, no. 6486, pp. 199-201, 1994/07/01 1994, doi: 10.1038/370199a0.

[13] J. R. MacFall *et al.*, "Human lung air spaces: potential for MR imaging with hyperpolarized He-3," *Radiology*, vol. 200, no. 2, pp. 553-558, 1996.

[14] M. Ebert *et al.*, "Nuclear magnetic resonance imaging with hyperpolarised helium-3," *The Lancet*, vol. 347, no. 9011, pp. 1297-1299, 1996.

[15] J. P. Mugler III *et al.*, "MR imaging and spectroscopy using hyperpolarized 129Xe gas: preliminary human results," *Magnetic resonance in medicine*, vol. 37, no. 6, pp. 809-815, 1997.

[16] B. Fan, S. Xu, Y. Wei, and Z. Liu, "Progresses of hyperpolarized 129Xe NMR application in porous materials and catalysis," *Magnetic Resonance Letters*, vol. 1, no. 1, pp. 11-27, 2021.

[17] K. Ramanpreet, S. Matt, and A. Ouriadov, "Imaging Perfusion Using Hyperpolarized 129Xe MRI and [15O]-Water PET: Current Status and Future Clinical Applications," *Open J Clin Med Images,* vol. 3, no. 2, p. 1128, 2023.

[18] W. Makulski, "129Xe and 131Xe nuclear magnetic dipole moments from gas phase NMR spectra," *Magnetic Resonance in Chemistry,* vol. 53, no. 4, pp. 273-279, 2015.

[19] B. May. "129Xe MRI Offers Detailed View of Pulmonary Function and Huge Clinical Potential."

[20] A. S. Khan *et al.*, "Enabling clinical technologies for hyperpolarized 129Xenon magnetic resonance imaging and spectroscopy," *Angewandte Chemie International Edition,* vol. 60, no. 41, pp. 22126-22147, 2021.

[21] L. Ebner *et al.*, "Hyperpolarized 129Xenon magnetic resonance imaging to quantify regional ventilation differences in mild to moderate asthma: a prospective comparison between semiautomated ventilation defect percentage calculation and pulmonary function tests," *Investigative radiology,* vol. 52, no. 2, pp. 120-127, 2017.

[22] M. Kirby *et al.*, "Hyperpolarized 3He and 129Xe MR imaging in healthy volunteers and patients with chronic obstructive pulmonary disease," *Radiology,* vol. 265, no. 2, pp. 600-610, 2012.

[23] M. He, B. Driehuys, L. G. Que, and Y.-C. T. Huang, "Using hyperpolarized 129Xe MRI to quantify the pulmonary ventilation distribution," *Academic radiology,* vol. 23, no. 12, pp. 1521-1531, 2016.

[24] R. P. Thomen, L. L. Walkup, D. J. Roach, Z. I. Cleveland, J. P. Clancy, and J. C. Woods, "Hyperpolarized 129Xe for investigation of mild cystic fibrosis lung disease in pediatric patients," *Journal of Cystic Fibrosis,* vol. 16, no. 2, pp. 275-282, 2017.

[25] N. J. Stewart *et al.*, "Comparison of 3He and 129Xe MRI for evaluation of lung microstructure and ventilation at 1.5 T," *Journal of magnetic resonance imaging,* vol. 48, no. 3, pp. 632-642, 2018.

[26] X. Han *et al.*, "Six-month follow-up chest CT findings after severe COVID-19 pneumonia," *Radiology,* vol. 299, no. 1, pp. E177-E186, 2021.

[27] F. Pan *et al.*, "Chest CT patterns from diagnosis to 1 year of follow-up in patients with COVID-19," *Radiology,* vol. 302, no. 3, pp. 709-719, 2022.

[28] J. T. Grist *et al.*, "Hyperpolarized 129Xe MRI abnormalities in dyspneic patients 3 months after COVID-19 pneumonia: preliminary results," *Radiology*, vol. 301, no. 1, pp. E353-E360, 2021.

[29] J. T. Grist *et al.*, "Lung abnormalities detected with hyperpolarized 129Xe MRI in patients with long COVID," *Radiology*, vol. 305, no. 3, pp. 709-717, 2022.

[30] A. N. Hanania, W. Mainwaring, Y. T. Ghebre, N. A. Hanania, and M. Ludwig, "Radiation-induced lung injury: assessment and management," *Chest*, vol. 156, no. 1, pp. 150-162, 2019.

[31] Y. Ding *et al.*, "A pilot study of function-based radiation therapy planning for lung cancer using hyperpolarized xenon-129 ventilation MRI," *Journal of Applied Clinical Medical Physics*, vol. 23, no. 3, p. e13502, 2022.

[32] K. Qing *et al.*, "Regional mapping of gas uptake by blood and tissue in the human lung using hyperpolarized xenon-129 MRI," *Journal of magnetic resonance imaging*, vol. 39, no. 2, pp. 346-359, 2014.

[33] A. Wakai, K. Nakamura, J. Kershaw, and I. Kanno, "In vivo MR spectroscopy of hyperpolarized Xe-129 in rat brain," in *International Congress Series*, 2004, vol. 1265: Elsevier, pp. 139-143.

[34] N. J. Abbott, L. Rönnbäck, and E. Hansson, "Astrocyte–endothelial interactions at the blood–brain barrier," *Nature reviews neuroscience*, vol. 7, no. 1, pp. 41-53, 2006.

[35] X. Zhou *et al.*, "MRI of stroke using hyperpolarized 129Xe," *NMR in Biomedicine*, vol. 24, no. 2, pp. 170-175, 2011.

[36] M. R. Rao, G. Norquay, N. Stewart, N. Hoggard, P. Griffiths, and J. Wild, "Assessment of brain perfusion using hyperpolarized 129Xe MRI in a subject with established stroke," *Journal of Magnetic Resonance Imaging*, vol. 50, no. 3, pp. 1002-1004, 2019.

[37] Y. Shepelytskyi *et al.*, "Hyperpolarized 129Xe imaging of the brain: Achievements and future challenges," *Magnetic Resonance in Medicine*, vol. 88, no. 1, pp. 83-105, 2022.

[38] M. R. Rao, G. Norquay, N. J. Stewart, and J. M. Wild, "Measuring 129Xe transfer across the blood-brain barrier using MR spectroscopy," *Magnetic Resonance in Medicine*, vol. 85, no. 6, pp. 2939-2949, 2021.

[39] Y. Friedlander *et al.*, "Hyperpolarized 129Xe MRI of the rat brain with chemical shift saturation recovery and spiral-IDEAL readout," *Magnetic Resonance in Medicine*, vol. 87, no. 4, pp. 1971-1979, 2022.

ICNST 2024
International Conference on Nuclear Science and Technology
6- 8 MAY 2024 | Isfahan, Iran

Modeling and Optimization of Distillation Column for Separation of Oxygen-18 Isotope with Mathematical Model (Paper ID : 1574)

Rahgoshay M. Correspondent[1*], Ahmadi H. Co-Author[2], Heydarinasab A

[1] *Department of Nuclear Engineering, Faculty of Engineering, Science and Research Branch, Islamic Azad University, Tehran, Iran*

[2] *Department of Nuclear Engineering, Faculty of Engineering, Science and Research Branch, Islamic Azad University, Tehran, Iran*

[3] *Department of Chemical Engineering, Faculty of Petroleum and Chemistry Engineering, Science and Research Branch, Islamic Azad University, Tehran, Iran*

Abstract

Positron emission tomography (PET) is an advanced imaging tool for the diagnosis and staging of cancer tumors. This method is based on the detection of increased glycolytic activity in malignant cells, in which cells glucose is concentrated due to an increase in membrane glucose transporters, as well as an increase in some key enzymes, such as Hexokinase, which are responsible for Glucose phosphorylation. Therefore, for this type of imaging, drugs containing Glucose are needed. On the other hand, with the expansion of the use of PET imaging devices, the need for drugs for this type of imaging method (Fluoro Deoxy Glucose drug) has also increased significantly. Fluorine Deoxy Glucose, abbreviated as FDG, is a drug tracer used in the medical imaging technique of positron emission tomography (PET). The production of Fluorine Deoxy Glucose requires the production of Fluorine-18 and, as a result, reaching Oxygen-18 with a richness of more than 95%. There are various methods to produce Oxygen with high richness. Among these methods, using a distillation column is a suitable method to produce Oxygen, which has low efficiency and high production cost. In the cryogenic distillation method in a long column, the system or the distillation column can be under vacuum or pressure and the gaseous composition entered into the distillation column is turned into a liquid at very low temperatures and the Oxygen-18 isotope or other isotopes using a slight difference in the points boiling or vapor pressure difference of isotope compounds are separated. This distillation column is filled with fillers, which increase the surface of the two-phase interface. These packages are small in size and usually made of Pyrex (unbreakable glass). The material of the distillation column is better to be insulated; like glass or plastic materials. These materials have less thermal expansion and contraction and less thermal shock than other materials. Optimization of the distillation column can reduce the cost of producing high-rich Oxygen. Numerical methods are one of the useful techniques for optimization. In this study, the distillation column has been

modeled using mathematical models, and then by changing the amount of inputs, including items such as height of the pipes. Results show that the maximum separation of the desired isotope concentration in the distillation tower depends on the type of isotope desired and the condition of the device, and is independent of the type of feed. Also, the input feed has no effect on the concentration distribution.

Keywords: Oxygen separation, distillation column, Fluorine Deoxy Glucose, PET imaging

Introduction

Positron emission tomography (PET) is a diagnostic imaging technique that allows the identification of biochemical and physiological changes in tumors. In this imaging method, the positron produced in the radio pharmaceutical enters into a pair of annihilation interaction with an electron and produces two photons. Therefore, positron emitting isotopes are used in this imaging method. FDG compound is formed from Oxygen-18 and then used in PET scan. In the radio-pharmaceutical industry, water enriched with hydrogen is bombarded and the ions produced in a linear accelerator are synthesized into FDG and injected into the patient. One of the positron-emitting isotopes that is used in combination with FDG to label this drug and establishes a good chemical bond is the Fluorine-18 isotope.

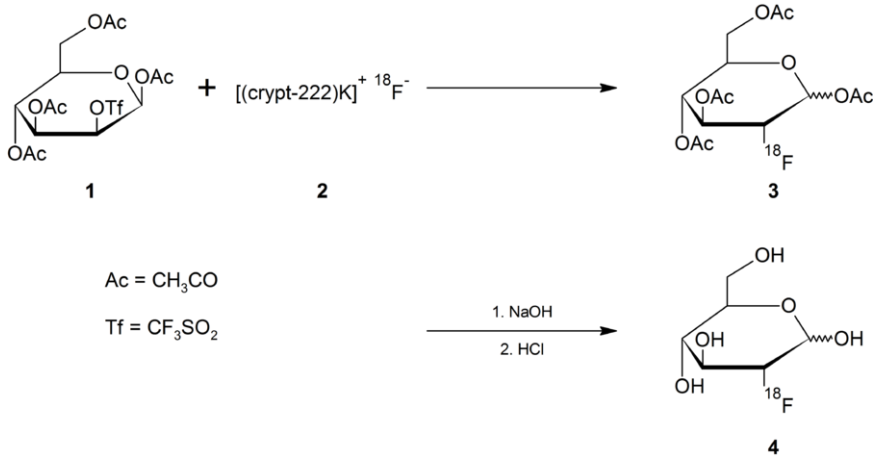

Fig 18 Chemical reaction between FDG and Fluorine-18 isotope [1]

F18 is a positron-emitting radioisotope with a half-life of 109 minutes, emitting a positron with an energy of 0.63 MeV. Two important features of this radioisotope compared to other positron

emitting isotopes, i.e. relatively long half-life and the lowest positron emission energy, have caused the use of this radioisotope to increase day by day [2]. Among the radio pharmaceuticals that are prepared using F18 are potassium fluoride [3], Fluorothia Heptadecanoic Acid (FTHA) [4, 5], Sodium Fluoride [6, 7] and FDG [8].

The use of PET with Fluoro Deoxy Glucose significantly improves the accuracy of tumor imaging [9]. In terms of oncological applications, FDG has gained wide acceptance in early stages of cancer, management of recurrent cancer, and monitoring response to therapy [9]. With conventional imaging methods, the size criterion is used to distinguish benign or malignant disease in the lymph nodes. Conversely, the PET method is based on the identification of basic aspects of tumor metabolism. FDG uptake in tumors is proportional to the metabolic rate of living cells (healthy cells and tumors) that have an increased demand for glucose [9, 10]. In fact, cells with a higher metabolism have a higher absorption of the drug, and because tumor cells have a higher metabolism, their absorption is higher compared to healthy cells. An overview of the use of FDG is shown in Figure 2.

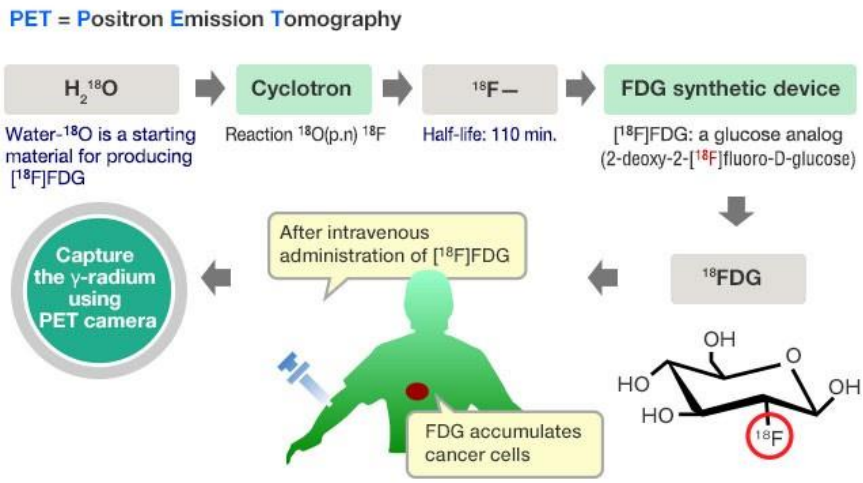

Fig 19 Overview of the production of FDG molecules by Oxygen-18 [11]

Fluorine production methods are different. In the study conducted by Abdi et al., different methods of Fluorine 18 isotope production have been investigated [12]. Among all investigated reactions, the 18O(p,n)18F and 20Ne(d,α)18F processes are more suitable. In recent years, of the above two methods, the 18O(p,n)18F method has been widely used [2, 12]. Therefore, to reach the Fluorine 18 isotopes, you must first access the Oxygen-18 isotopes. Based on this method, water enriched with the Oxygen-18 isotopes can be used as a target in proton bombardment,

which will lead to the production of isotopes. In order to achieve a high percentage of Fluorine-18 isotope, it is necessary to increase the level of Oxygen-18 in enriched water to more than 95%. Meanwhile, the Oxygen element naturally has three stable isotopes (isotopes 16-17-18). In addition, isotopes with mass numbers 12 to 24 are all unstable, among which isotope 15 with a half-life of 122.24 seconds is the most stable and 12 with a half-life of $58*10^{-24}$ seconds is the most unstable of all of these isotopes. Natural Oxygen is a mixture of three stable isotopes and the natural percentage of Oxygen isotopes is equal to 18 (0.205%), 17 (0.038%), and 16 (99.757%).

Oxygen isotopes can be separated using the following methods of distillation, thermal diffusion, chemical exchange, membrane diffusion, gaseous diffusion, electrolysis, freezing, laser, and cyclotron [13, 14], which leads to the separation of the Oxygen-18 isotope. Among these methods, the distillation method is the most important method used industrially. In the distillation method, three substances, Nitric acid (NO), Oxygen molecule (O_2) and water (H_2O) are used as the input feed of the distillation column, where the isotopic separation process is carried out using the processes in the distillation column. Isotope separation techniques are based on the isotopic effects of different compounds. In fact, in this method, the difference in the nuclear properties of isotopes is used to increase the percentage of separation of the desired isotope [15]. Isotope separation techniques depend on the properties of the element or chemical compound involved, the cost of the process, and the various applications that use different concentrations. Due to the large relative mass difference between different isotopes of light elements such as Boron, Carbon, Nitrogen or Oxygen, a practical isotope separation method for these elements is distillation based on the isotope effect of vapor pressure [16]. Distillation processes are based on the concept of relative volatility, which is a comparative measurement of the vapor pressure of the components of a mixture. Relative volatility is a quantity used to measure the tendency of two substances in a mixture to evaporate and turn into the vapor phase. This quantity is a dimensionless quantity and can be defined as follows:

$$\alpha = \frac{\left(\frac{y_i}{x_i}\right)}{\left(\frac{y_j}{x_j}\right)} \quad (1)$$

In this regard,

α is equal to the relative volatility of the most volatile component i compared to the most volatile component j.

y_i is the mole fraction of component i in the vapor phase.

x_i is the mole fraction of component i in the liquid phase.

y_j is the mole fraction of component j in the vapor phase.

x_j is the mole fraction of component j in the liquid phase.

By using the principles governing the operation of a distillation column, a distillation column can be modeled, and its mathematical model can be used for optimization.

The Procedure

Distillation is done in a tray column or in a packed column. In order to optimize the distillation column, mathematical models of the distillation column have been used. In a study, Dumitrache et al. [17] modeled the distillation column with mathematical models. The model used in the study of Dumitrache et al. [17] is as follows:

$$H_l + H_V \frac{\partial N}{\partial t} = \left(\frac{LV}{K}\right)\frac{\partial^2 N}{\partial z^2} - \frac{\partial N}{\partial z}\left[\psi + L(\alpha - 1)\right] \quad (2)$$

In this equation, *l* represents the liquid phase and *v* represents the vapor phase. *H* represents the stop in unit volume. *N* represents the mole fraction in the liquid phase. *L* and *V* represent the molar flow rate of liquid and vapor per unit area. Ψ represents product production rate and α represents relative volatility. These equations are considered in the following geometric form.

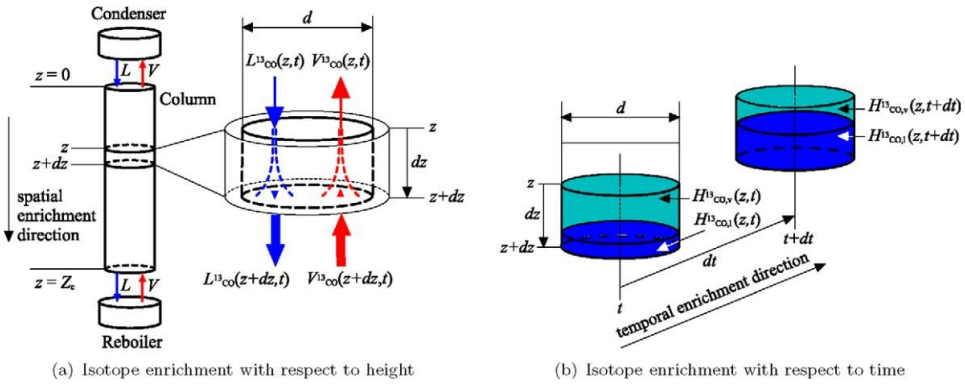

Fig 20 Schematic of distillation column according to height and separation time (a) isotopic separation according to height and (b) isotope separation according to time [17]

This equation was obtained using scientific principles and mathematical rules in the study of Dumitrache et al. [17], which is beyond the discussion. In the continuation of this mathematical model, differential equations have been solved using numerical methods and output rate optimization has been done considering different conditions.

Numerical Solution

In order to numerically solve the differential equation, the finite element method has been used. To obtain a finite element system of differential equations or ordinary differential equations for the numerical solution of a partial differential equation (PDE), methods such as finite difference methods, finite elements, finite volume, or weighted-residual methods can be used [18, 19]. In the case of a problem with simple geometry, finite differences and spectral methods are suitable options [18]. For problems with complex geometry or complex boundary conditions, finite element or finite volume methods can be chosen [20]. Since the main advantage of finite difference methods is flexibility in dealing with nonlinear problems and, in addition, they are easy to implement [21], the finite difference method is used in this study. As it is known, for a numerical method, stability and convergence are the most important aspects. As a reminder, a finite difference equation is consistent if the truncation error approaches zero (this is usually the case for finite difference approximations derived from Taylor series), stable if the error remains uniformly bounded, and if converges, the solution approaches the partial differential equation as the grid size approaches zero [21]. In this study, the liquid mole fraction function ($N(z,t)$) related to the desired substance is defined by $u(i,j)$. Two integer indexes i and j represent the evaluated quantity and are related to Cartesian coordinates as described in the following equations:

$$z(i) = z_0 + iz \quad (3)$$

$$t(j) = t_0 + jt \quad (4)$$

The grid has a fixed mesh spacing *z* in the height direction and a fixed mesh *t* in the time direction. Considering the Taylor series expansion around a point *z(i), t(j)*, the forward difference approximation for *∂N/∂t* and *∂N/∂z* in coordinates *z(i), t(j)* is. It is defined as follows:

$$\frac{\partial N}{\partial z} = u_z(i,j) \approx \frac{u(i+1,j) - u(i,j)}{\Delta Z} \quad (5)$$

$$\frac{\partial N}{\partial t} = u_t(i,j) \approx \frac{u(i,j+1) - u(i,j)}{\Delta t} \quad (6)$$

Where *z* and *t* represent the grid size in height and time dimension. The backward difference approximation for *∂N/∂t* is defined as follows:

$$\frac{\partial N}{\partial t} = u_t(i,j) \approx \frac{u(i,j) - u(i,j-1)}{\Delta t} \quad (7)$$

The second order differential for $(\partial^2 N)/(\partial z^2)$ and $(\partial^2 N)/(\partial t^2)$ is determined by the following equation:

$$\frac{\partial^2 N}{\partial z^2} = u_{zz}(i,j) \approx \frac{u(i+1,j) - 2u(i,j) + u(i-1,j)}{\Delta z} \quad (8)$$

$$\frac{\partial^2 N}{\partial t^2} = u_{tt}(i,j) \approx \frac{u(i,j+1) - 2u(i,j) + u(i,j-1)}{\Delta t} \quad (9)$$

Finally, the mixture derivative approximation $(\partial^2 N)/\partial z \partial t$ is obtained as follows:

$$\frac{\partial^2 N}{\partial z \partial t} = u_{zt}(i,j) \approx \frac{(u(i,j) - u(i-1,j) - u(i,j-1) + u(i-1,j-1))}{\Delta t \ \Delta z} \quad (10)$$

By merging formulas 6, 7, 8 and 9 in formula 1, this formula is obtained as a recursive relationship.

$$H_l + H_V\left(\frac{u(i,j+1) - u(i,j)}{\Delta t}\right) = \left(\frac{LV}{K}\right)\left(\frac{u(i+1,j) - 2u(i,j) + u(i-1,j)}{\Delta z}\right) - \left(\frac{u(i+1,j) - u(i,j)}{\Delta Z}\right)[\psi + L(\alpha - 1)] \quad (11)$$

The above equation is a linear equation that is solved by finite difference method. It is not possible to solve the above equation for the depleted and enriched part simultaneously because the boundary conditions are different in the two cases. In order to implement the modeling of the

equation related to the simulation of the distillation column, MATLAB software version 2015[24] has been used. For the purpose of modeling, boundary conditions have been used, which are explained below. Considering the boundary conditions, the concentration value can be calculated in terms of time and height.

The boundary conditions used for the equations are considered as follows.

1) At the place where the gas enters the environment, the concentration of the isotope is equal to the concentration of the isotope in the state of natural separation.

2) At time zero *(t=0)*, the concentration along the entire length of the column is equal to the concentration of the isotope in the state of natural separation.

3) At the end of the column, the third boundary condition has been obtained using the method of solving the Laplace equation.

The first and second conditions depend on the type of desired isotope to enrich the concentration. The third condition is in the form of an exponential distribution between the concentration value in the natural richness and the maximum concentration. The maximum amount of concentration depends on the length of the distillation column and the type of isotope, which is obtained by the following formulas:

$$\lim_{t\to\infty} N(Z_r, t) = N_0\, e^{2\theta_r Z_r} \qquad (12)$$

Using the diagram in Figure 4, to obtain the value at the initial points, we must obtain the formula of the diagram in order to calculate the value of the points using a software[25] and enter these points into the origin code. This program fits the points together and an exact function is obtained, which we use to obtain the exact value of the third boundary condition.

[24] The software which was available during our research and we mastered.
[25] xyExtract

$$\lim_{t\to\infty} N(Z_s,t) = N_0\, e^{2\theta_s Z_s} \tag{13}$$

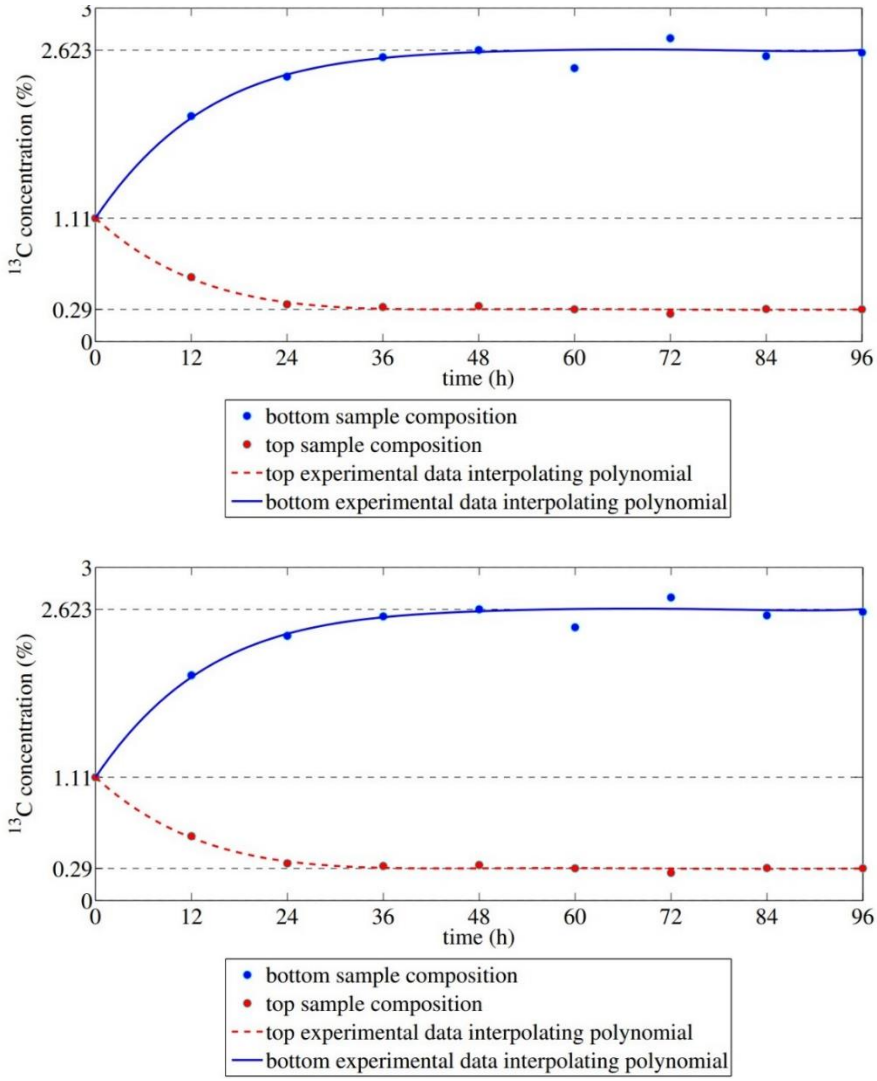

Fig 21 Carbon 13 isotope concentration distribution in infinite time (very long time) at the end of the distillation column in the depletion and separation sections

The equations mentioned in formulas 12 and 13 are obtained from the limit state of the following formulas:

$$N(z=Z_r,t) = N_0 e^{2\,\theta_r Z_r} + \sum_{j=2}^{n} \frac{N_0 2\,\theta_r}{S_j\left[\frac{\eta_r Z_r}{2} - \frac{\eta_r \theta_r}{2\left(\gamma(s_j)\right)^2}(1-\theta_r Z_r)\right]}\, e^{S_j t} \tag{14}$$

$$N(z=Z_s,t) = N_0 e^{2\,\theta_s Z_r} + \sum_{j=2}^{n} \frac{N_0 2\,\theta_s}{S_j\left[\frac{\eta_s Z_s}{2} - \frac{\eta_s \theta_s}{2\left(\gamma(s_j)\right)^2}(1-\theta_s Z_s)\right]}\, e^{S_j t} \tag{15}$$

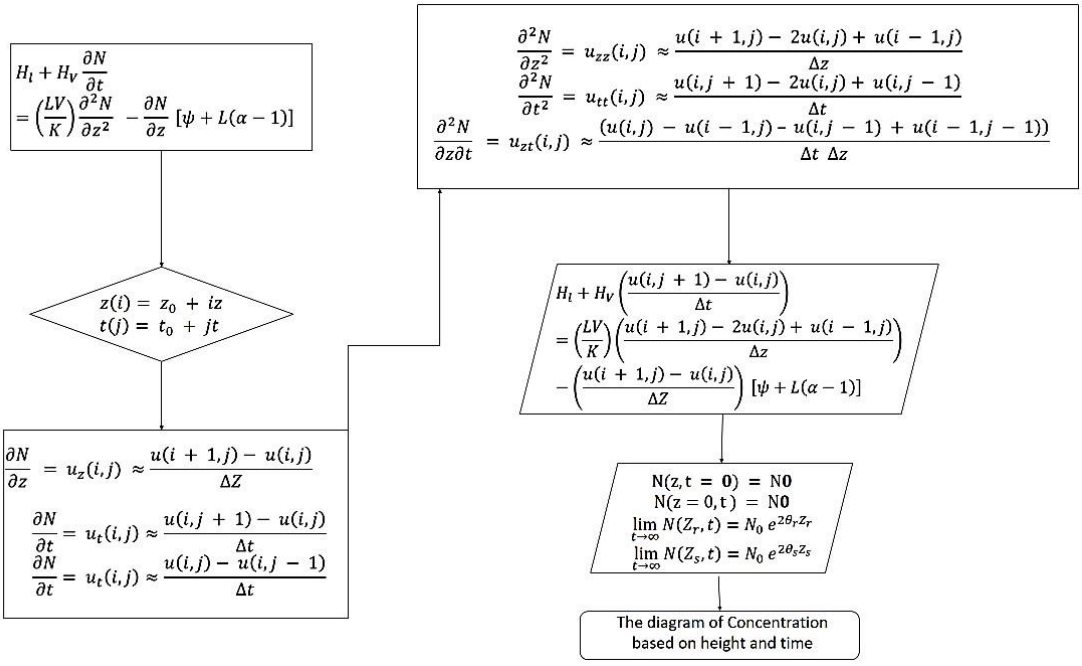

Fig 22 The flowchart of the solution

Validation

In order to validate the program written in the MATLAB environment, first the distillation column related to the Carbon Monoxide gas separation was simulated. The stated coefficients and boundary conditions were used based on the coefficients and boundary conditions presented in the study of Dumitrache et al.[17]

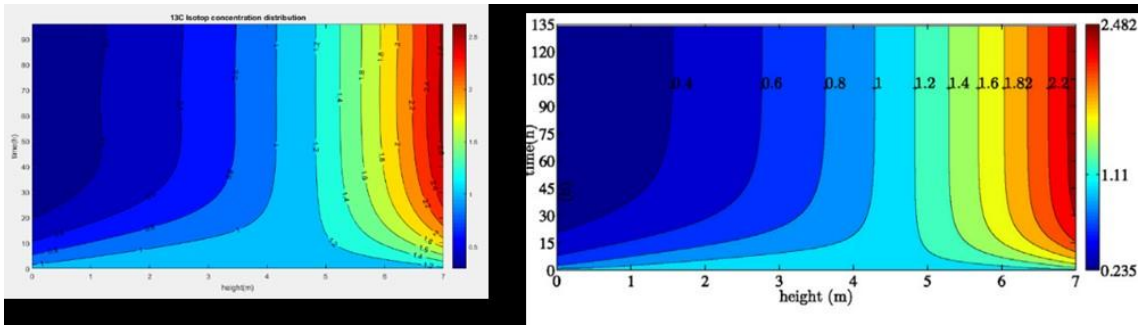

Fig 23 Comparison of the results obtained from the study of Dumitrache et al. (left figure) and the results obtained sent study (right figure)

First, the graphs related to the depleted and enriched parts were calculated, and then the results of the two parts of the column were merged and the final result was obtained. Comparison of the results shows that the graph obtained in the present study is in very good agreement with the results obtained from the study of Dumitrache et al.[17]

Modeling of Oxygen-18 Isotope Separation

The highest concentration of Oxygen isotopes is related to Oxygen-16 (99.759%) and then Oxygen-18 (0.204%). The concentration of Oxygen-17 in distillation column and equations has been omitted because it is insignificant. Therefore, in this study, the values and data related to Oxygen-18 are used. Modeling the Oxygen-18 isotope separation process needs to have parameters related to Oxygen gas. In this study, three gases, Nitric acid (NO), Oxygen (O_2) and water vapor (H_2O) are used as inputs.

Table 1 Characteristics of the materials used as input feed for the distillation column

GasValid temperature range	**Chemical Formula**	**α**	**The relationship between α and temperature**	**Valid temperature range**
Nitric acid	NO	1.0632	$\exp\left(\frac{4{,}4684}{T} - 21{,}03 \times 10^{-3}\right)$	**110-118 K**
Oxygen	O_2	1.0066 1.0062 1.0059 1.0055 1.0053 1.0052 1.0049 1.0063 1.0052 1.004	According to the following table: 76.8 78.8 80.4 82.2 84.8 86.4 88.0 83.2 90.6 98.5	**76.8-98.5 K**
Water	H_2O	1.0078	323	**323-373 K**

GasValid temperature range	Chemical Formula	α	The relationship between α and temperature	Valid temperature range
		1.0068	333	
		1.0063	343	
		1.0058	353	
		1.0053	363	
		1.004	373	

Also, the natural percentage of Oxygen-18 isotope is considered equal to 0.200. After applying different inputs of Oxygen gas, three graphs are obtained as follows. The results related to three different gases used as distillation column feed are given below.

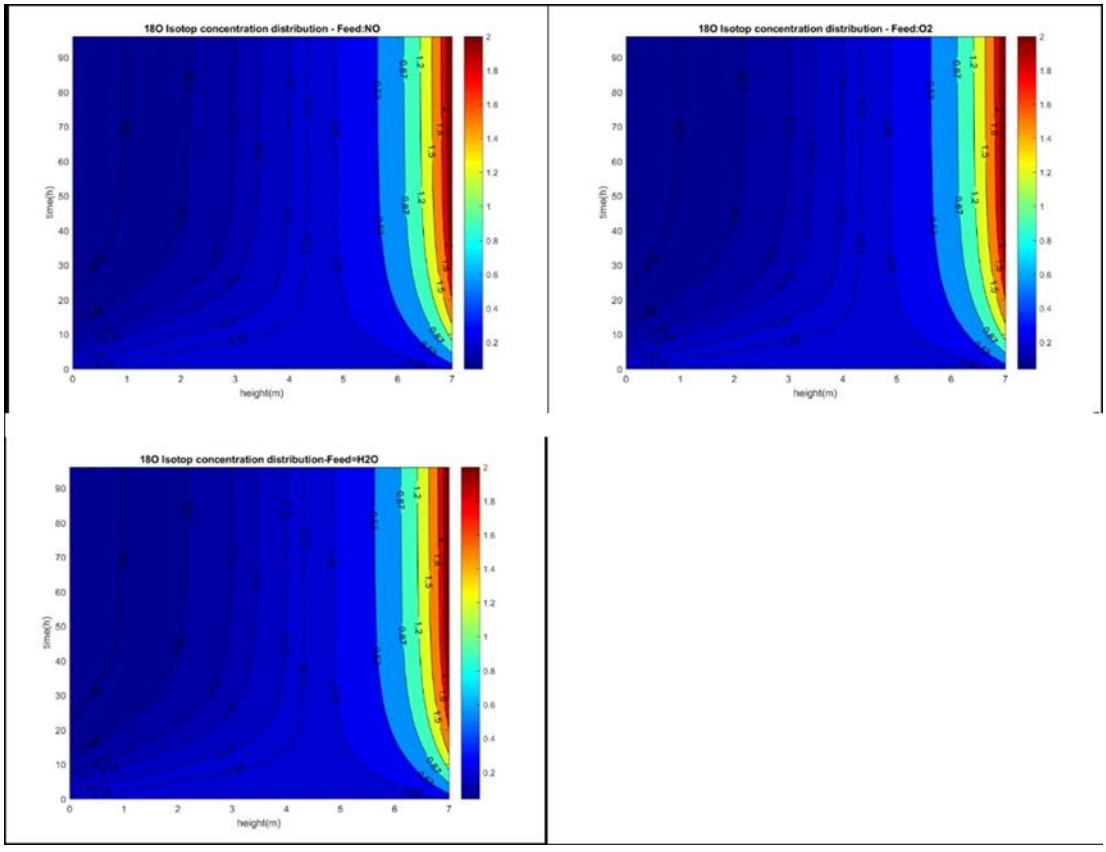

Fig 24 Distribution of Oxygen-18 isotope concentration according to time and altitude for three different substances: Nitric acid (NO) - Oxygen (O_2) and water (H_2O)

Results and discussions

Information about different gases was presented in the previous section. In this table, it is shown that the α coefficient is related to Oxygen in the temperature range of 110-118 K. This is while Oxygen and water gases work at a temperature close to room temperature. Therefore, using Nitric acid gas requires more cost for separation. From the point of view of the highest possible separation, the desired isotope concentration value is determined by the following equation:

$$\lim_{t\to\infty} N(Z_r, t) = N_0\, e^{2\theta_r Z_r} \quad (16)$$

$$\lim_{t\to\infty} N(Z_s, t) = N_0\, e^{2\theta_s Z_s} \quad (17)$$

In these relationships, θ is equal to:

$$\theta_s \equiv \frac{K_s(\alpha-1)}{2\,V_s} \quad (18)$$

$$\theta_r \equiv \frac{K_r(\alpha-1)}{2\,V_r} \quad (19)$$

And K is the total volumetric mass transfer coefficient and V is the molar flow rate of steam per unit area, which is dependent on the desired isotope gas type and device and are constant under the same conditions. Therefore, the maximum separation of the desired isotope concentration in the distillation tower depends on the type of isotope desired and the condition of the device and is independent of the type of feed (inlet gas). Nitric acid (NO) - Oxygen (O_2) and water (H_2O) are not dependent, and the concentration distribution is the same for all three substances in this study, considering that the conditions of the distillation tower are considered constant and the desired isotope for separation. The maximum amount of Oxygen-18 isotope separation does not differ. This can also be seen in Figure 4. Therefore, considering that the input feed has no effect on the concentration distribution, therefore, if NO is used as a cryogenic compound to separate Oxygen-18, it has disadvantages, which can be mentioned as follows. 1- Corrosiveness and toxicity of this compound 2- In order to maintain the temperature during the work, there is a need for proper thermal insulation As a result, water vapor is more suitable compared to Nitric acid and Oxygen gas because its operating temperature is close to room temperature. It should be regarded that all the equations in this study has been used to verify the concentration of Oxygen-

18 in various combinations such as NO, O_2 and H_2O which show that the maximum concentration is independent of gas compound. However, it depends on the type of isotope and device conditions.

References

[1] Joana s.Fowler and Tatsuo Ido. (2002). Initial and subsequent approach for the synthesis of FDG. Seminars in nuclear medicine. 32 (1):6.

[2] E. Hess, et al. (2001). Excitation function of the 18O (p, n) 18F nuclear reaction from threshold up to 30 MeV. Radiochimica Acta. 89 (6*)*:357.

[3] G. Cook, et al. (2002). Quantification of Skeletal Kinetic Indices in Paget's Disease Using Dynamic18F-Fluoride Positron Emission Tomography. Journal of Bone and Mineral Research. 17 (5): 854.

[4] M. Inubushi, et al. (2003). Positron-emission tomography reporter gene expression imaging in rat myocardium. Circulation. 107 (2): 326.

[5] M.P. Chandler, et al. (2002). Increased nonoxidative glycolysis despite continued fatty acid uptake during demand-induced myocardial ischemia. American Journal of Physiology. Heart and Circulatory Physiology. 282 (5): H1871.

[6] N. Tse, et al. (1994). Positron emission tomography diagnosis of pulmonary metastases in osteogenic sarcoma. American Journal of Clinical Oncology. 17 (1): 22.

[7] Gary J.R Cook and I. Fogelman. (2001). The role of positron emission tomography in skeletal disease. Seminars in nuclear medicine. 31 (1): 50.

[8] N. Satyamurthy, et al. (2002). Tantalum [18O] water target for the production of [18F] fluoride with high reactivity for the preparation of 2-deoxy-2-[18F] fluoro-D-glucose. Molecular Imaging and Biology. 4 (1): 65.

[9] L. Kostakoglu, H. Agress Jr, and S.J. Goldsmith. (2003). Clinical role of FDG PET in evaluation of cancer patients. Radiographics. 23 (2): 315.

[10] C. Love, et al. (2005). FDG PET of infection and inflammation. Radiographics. 25 (5): 1357.

[11] What is FDG in pet scan? And Use of water Oxygen-18 as a precursor for the production of FDG molecules to diagnose cancer, Mesbah Energy, https://www.irisotope.com, (current as of Feb. 17, 2011)

[12] Z. Abdi, et al. (2017). Investigation of 18F and 13N Radioisotopes Production Using Cyclotron Recirculating Liquid Target. Journal of Nuclear Science and Technology (JONSAT). 37 (4): 56.

[13] P.A. De Groot, Handbook of stable isotope analytical techniques. (2004). Vol. 1. Chapter 20. p.1025. Elsevier.

[14] A. Vértes, et al. (2003). Handbook of nuclear chemistry: Instrumentation, separation techniques environomental iusses. Vol. 5. Springer Science & Business Media.

[15] J.J.S Bigeleisen. (1965). Chemistry of Isotopes: Isotope chemistry has opened new areas of chemical physics, geochemistry, and molecular biology. Science. 147 (3657): 463.

[16] G. Dickel and H. London, Separation of Isotopes, Wiley Online Library; https://onlinelibrary.wiley.com/doi/abs/10.1002/bbpc.19620660324.

[17] D.C. Dumitrache, et al. (2012). Modeling, analysis, and simulation of a cryogenic distillation process for 13C isotope separation. Journal of Process Control. 22 (4): 798.

[18] H.-X. Li and Qi. C.J.J.o.P.C. (2010). Modeling of distributed parameter systems for applications—A synthesized review from time–space separation. Journal of Process Control. 20 (8): 891.

[19] H.-X. Li and Qi. C.J.J.o.P.C and Yu.Y.J.J.o.P.C. (2009). A spatio-temporal Volterra modeling approach for a class of distributed industrial processes. Journal of Process Control. 19 (7): 1126.

[20] D.S.J. Burnett. (1988). Finite element analysis: from concepts to applications. Numerical methods in engineering. 26 (8): 1908.

[21] J.H. Mathews and K.D. Fink. (2004). Numerical methods using MATLAB. Vol. 4. Pearson prentice hall Upper Saddle River. NJ.

ICNST 2024
International Conference on Nuclear Science and Technology
6- 8 MAY 2024 | Isfahan, Iran

Use of the electron paramagnetic resonance method to analyze the isotopic abundance of 97Mo and 98Mo (Paper ID : 1591)

Hosseini R.[1], Karimi sabet J.[2], Janbazi M.[2], Sharbatdaran M.[2], Ashjari M.[1]

[1]Department of Chemical Engineering, University of Kashan, Kashan, Iran
[2]Nuclear Sciences and Technology Research Institute, Tehran, Iran

Abstract

Molybdenum has seven stable isotopes of ^{92}Mo, ^{94}Mo, ^{95}Mo, ^{96}Mo, ^{97}Mo, ^{98}Mo, ^{100}Mo with natural abundances of 14.84, 9.25, 15.92, 16.68, 9.55, 24.13 and 9.63, respectively. Since the stable isotopes of ^{97}Mo and ^{98}Mo have various applications in different fields such as nuclear medicine and nuclear reactors. ^{97}Mo is used as a target material for the production of the medical radioisotope ^{99m}Tc and ^{98}Mo is used as a neutron absorber to control the rate of fission reactions. In this research, enrichment of molybdenum-97 and molybdenum-98 were performed successfully by electromagnetic method. Since the different isotopes have different nuclear spins and hyperfine coupling constants (HFCC) which cause a fundamental change in the paramagnetic resonance spectrum of the electron, they can be used in the analysis of different isotopes. A new method of electron paramagnetic resonance is used to analyze the isotopic abundance of ^{97}Mo and ^{98}Mo after separation from the electromagnetic method.

Keywords: Molybdenum Isotopes, Electron Paramagnetic Resonance, Electromagnetic Isotope Separator

Introduction

The investigation and utilization of the electromagnetic isotope separator system to acquire stable and enriched molybdenum isotopes is motivated by the requirement for such isotopes in order to manufacture radioisotopes. Their production plan was prioritized due to the significance of radiopharmaceuticals derived from molybdenum isotopes, the availability of an electromagnetic separation system for generating stable isotopes, and cyclotron and reactor accelerator systems for conducting nuclear reactions. With atomic number of 42, atomic mass of 95.94, and a density of 2.10 g/cm^3, molybdenum is an element with seven stable isotopes: ^{92}Mo, ^{94}Mo, ^{95}Mo, ^{96}Mo, ^{97}Mo, ^{98}Mo, and ^{100}Mo. Its melting and evaporation temperatures are 2610 °C and 5560 °C, respectively. The respective percentages of natural abundance are as follows: 14.84, 9.25, 15.92, 16.68, 9.55, 24.13 and 9.63 [1]. Worldwide, ^{99m}Tc is the most extensively utilized medical isotope among all radioisotopes. It is utilized in 80 to 85 percent of the estimated 30 million

nuclear medicine diagnostic procedures conducted annually. It is a daughter isotope of ^{98}Mo. The radiopharmaceutical's beneficial properties, including a favorable disintegration mode, half-life, adequate penetration power, and minimal biological damage induced by absorbed concentrations, render it a valuable tool in numerous diagnostic procedures [2]. Further uses for ^{99m}Tc include the detection of lung cancer, imaging of the heart, spleen, and liver. One illustration of the application of sodium percontate ($Na^{99m}TcO_4$) is in the scanning of the gastric mucosa, thyroid, secretory glands, and lacrimal ducts [3]. Additionally, direct or indirect production of ^{99m}Tc is possible with ^{100}Mo and ^{98}Mo. ^{100}Mo and ^{98}Mo are radioactive decay-resistant and stable. They therefore can be transported and stored similarly to conventional products, thereby reducing a number of the supply chain issues that are currently associated with ^{99m}Tc production methods [2]. In fact, one of the methods for producing ^{99m}Tc radioisotopes is by using ^{98}Mo isotopes in the reactor; all of these molybdenum isotopes can be collected and separated in a single phase using an electromagnetic separator system. This research describes the chemical refining process utilized to purify molybdenum 98 and 97 that were extracted using an electromagnetic isotope separator system. The chemical purity of the isotopes was examined using an Inductively Coupled Plasma (ICP). The enriched molybdenum 98 isotope underwent physical quality control using a Thermal Ionization Mass Spectrometer (TIMS). Ultimately, Electron Paramagnetic Resonance (EPR) was employed to verify the quality of the molybdenum 98 and 97 isotopes.The EPR method is used to detect compounds that possess unpaired electrons. The EPR method has diverse uses in molecular structure detection [4], ion beam dosimetry [5], and medicine [6]. This article presents a novel approach where molybdenum isotopes, specifically molybdenum 97 and 98, were utilized to examine their abundance. The study demonstrates that this method is effective in determining isotopic abundance by observing the variations in intensity and position of the EPR spectrum peaks.

Experimental

The electromagnetic isotope separator method is a technique that can simultaneously produce isotopes with an exceptionally high degree of purity. An electromagnetic isotope separator comprises the following primary components: an ion source, a collector, a vacuum chamber, an electromagnet, a power supply, and vacuum and cooling systems. The mechanism by which isotopes are separated using an electromagnetic separator system is predicated on the motion of

an active ion within the magnetic field. In order to sustain stable discharge and profuse ion formation, it is imperative to carefully choose a heat transfer system and feed material that can generate pressure in the plasma region (10^3 torr). The raw material is inserted into the caltron ion spring crucible and transformed from solid to vapor using an electric arc chamber and furnace. By means of electron impact, the material vapor within the electric arc chamber of the ion source is ionized via electron bombardment by the heated cathode. Following their exit from the ion source, the beams are subjected to a consistent magnetic field. At the collector located in the opposite section of the vacuum tank, they follow a circular trajectory of varying radius based on their mass. Upon reaching the collector, the isotopes are segregated with each isotope occupying its corresponding graphite envelope.The isotopes are individually contained within graphite pockets. The magnetic field deflects the ions, making it necessary for the electromagnetic isotope separation system to have highly accurate magnetic field configurations in order to concentrate the beams onto the collector. This phenomenon is accomplished through the utilization of precisely defined iron shims, often positioned within the vacuum chamber. The force exerted on a charged particle in a magnetic field is determined using the following equation:

$$F = qv \times B \quad \textbf{(1)}$$

where B denotes the magnetic field perpendicular to F, q signifies the charge of the particle, and v signifies the speed of the charged particle, which is also dependent on the particle's mass.

Ions are generated within the ion source and propelled by a high voltage before entering the vacuum chamber with significant velocity. Typically, the equation below is used to determine the radius of the beam path for ions that have the same energy concentrated at a specific point:

$$\begin{cases} F_m = Bev/c \\ F_c = mv^2/R \end{cases} \Longrightarrow Bev/c = mv^2/R \Longrightarrow v = \sqrt{2eV/m} \therefore R \simeq \frac{144.5\sqrt{MV}}{B} \quad \textbf{(2)}$$

The equation provided includes the following variables: R: The radius of the ion's path, measured in centimeters. B: The intensity of the magnetic field, measured in gauss. V: The voltage of the accelerator, measured in volts. M: The mass number of the ions.

The ions entering the chamber from the ion source have the same mass and initially diverge at an angle from the center beam. The dispersed beam diverges from the core beam at an angle $\pm\alpha$, resulting in a lack of concentricity with the center ray. In order to converge (bring together the isotopes at a single location), the center beam can be intensified while the lateral beams can be weakened. To achieve this objective, iron magnet shims are inserted between the polar surfaces. This provides a non-uniform magnetic field that enhances the strength of the central beam while

weakening the side beam. Consequently, the divergent beam is focused more effectively along with the central beam.

Eventually, the accumulated data is subsequently subjected to recycling and chemical refining procedures to eliminate elemental impurities from the desiccants. Typically, the final product is molybdenum trioxide isotope. Isotopes derived from the graphite surfaces of the envelopes, which were subsequently refined and recycled on the ^{97}Mo and ^{98}Mo envelopes, were investigated using a glass piece and a mixture of metallic molybdenum and graphite powder. After transferring this mixture to a porcelain crucible, it was positioned within an electric furnace's quartz tube, which was filled with an oxygen atmosphere. By maintaining a temperature of 850°C for an hour (the temperature was increased for one hour, and it was cooled for additional five hours), in addition to blowing oxygen gas into the tube at all times, the 450 °C conversion of graphite to CO_2 and its subsequent removal from the furnace were accomplished. After increasing the temperature, the metallic molybdenum transformed into molybdenum trioxide, and after leaving the porcelain crucible, it accumulated in the cold areas of the quartz tube, particularly in the cold trap area [7]. By employing a hot and concentrated ammonia solution, the collected molybdenum trioxide was extracted from the internal surfaces of the quartz tube, porcelain crucible, and cold trap. Subsequently, the apparatus was heated until it reached the drying stage [8]. A paper filter was utilized to isolate the Fe(III) contaminant, which was derived from Fe(II) and transformed into a brown Fe(III) hydroxide precipitate via heating by adding water [9,10]. The pH of the remaining solution was adjusted to a range of 0.7 to 1.2 by adding sulfuric acid. To recover molybdenum, the solution a 2% solution of alpha-benzoin oxime in an alcoholic solvent was added at a weight ratio of 10:1 to the original molybdenum. The precipitation of the molybdenum organometallic complex occurred as a result of the subsequent reaction [11].

$$\mathbf{MoO_2^{+2} + 2C_{14}H_{13}NO_2 \rightarrow MoO_2[C_{14}H_{12}NO_2]_2 + 2H^+}$$

The molybdenum complex was filtered and heated in an electric furnace at 500°C for 3 h. Molybdenum trioxide was produced as a result of decomposition of the organometalic complex at this temperature.

Electromagnetic isotope separator system model CI-140, mass spectrometer model LZD-207, inductively coupled plasma atomic emission spectrometer model JY-124, Atbin vacuum furnace

model ATU(10-100) and ultrasonic bath were among the devices used in this research work, which were in the Nuclear Science and Technology Research Institute in Karaj were placed.

Theory

Refining molybdenum 97 and 98 stable isotopes in a furnace generates a vacancy defect and an unpaired electron in the crystal structure of MoO_3. An external magnetic field interacts with the electron's magnetic moment, resulting in a Hamiltonian of the interaction equal to **B. μ**.

If the equation $\mathbf{B}_{ext}$ = Bk is true, then the potential provided to the electron will be equal to:

$$E = -\boldsymbol{\mu}.\boldsymbol{B}_{ext} = -\mu_z B_z = \frac{eB}{2m_e C} BS_z \qquad (3)$$

The variables involved in this equation are the charge of the electron (e) measured in coulombs, the mass of the electron (m_e), the speed of light($C=3\times10^8$ m/s), the external magnetic field(B_{ext}), and the spin of the electron along the z axis(S_z). So, if an atom or molecule has an unpaired electron, putting magnetic field on it causes that it can stay on two level of energy(Figure 1).

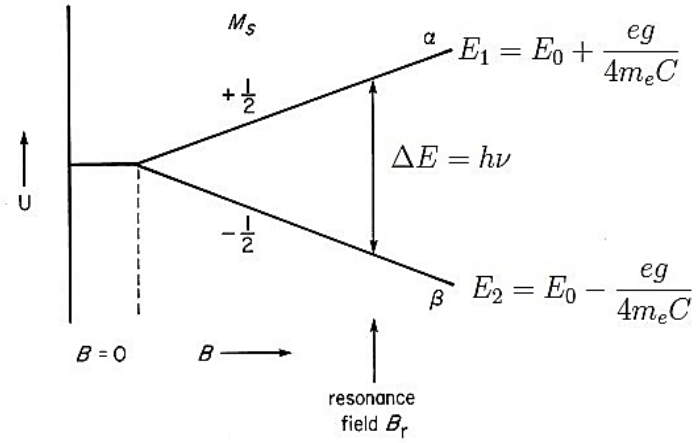

Fig. 1. Primary energy level splitting into two levels

However, if the energy of the incoming photon matches the energy between two energy of electron states, the electron will absorb the photon and transition from a lower state to a higher state when exposed to an electromagnetic wave, often in the microwave region. The system transitions to a state of elevated energy, namely, where the incoming microwave is absorbed, thus satisfying the resonance requirement:

$$B' = \frac{h\nu}{g\ \beta_e} \qquad (4)$$

The symbols ν, h, and g represent the microwave frequency, Planck's constant, and the Zeeman effect, respectively. The magnitude of the Zeeman effect varies depending on the crystal structures and isotopes involved. In equation 3 states that a resonance condition in the magnetic field leads to the formation of an energy peak. Figure 4(a) shows the EPR spectrum for molybdenum 98. The peak with the most energy is isotope 98, and the peak with the less energy is the small amount of isotope 100 that is in the crystal structure of MoO_3. If a crystal structure contains nuclei with a spin of 1/2, such as molybdenum 97, EPR absorption splits to two distinct signals. There are two potential transitions that can occur in the magnetic fields depicted in Figure 2.

$$B_k = \frac{h\nu}{g\beta_e} - \frac{A}{2g\beta_e} \quad (M = -\frac{1}{2})$$
$$B_m = \frac{h\nu}{g\beta_e} + \frac{A}{2g\beta_e} \quad (M = +\frac{1}{2}) \qquad (5)$$

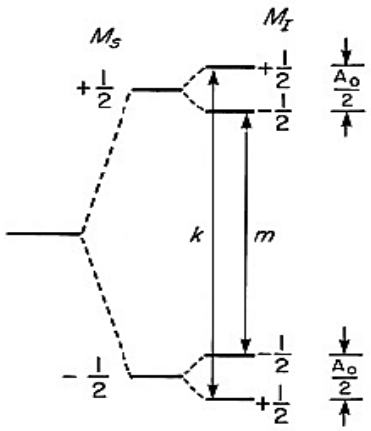

Fig. 2. Radical energy level splitting with a nucleus with spin ½

Figure 4(b) displays the EPR spectrum for molybdenum 97, which consists of two peaks of equal intensity. Both peaks correspond to isotope 97.

It is important to note that factors such as the quantity of nuclei, their equivalence or non-equivalence, the spin quantum number of the nucleus (**I**= 1/2, 1, 3/2, 2, ...), and the isotropic frequency of the nucleus influence the EPR spectrum. Consequently, the number of recorded EPR signals varies [12]. We can use the EPR spectrum to examine the percentage abundance of isotopes, considering factors such as the abundance of each isotope, the spin number of the isotope nucleus, and the coupling constant of the fine structure.

Quantum chemistry calculations are necessary for a thorough study. The current process entails calculating EPR parameters, such as the Zeeman effect and the fine structure's coupling constant. The MATLAB program, currently under development, then simulates the EPR spectrum. (The fundamental variables of a MATLAB program consist of laboratory parameters, such as microwave frequency, laboratory temperature, and EPR parameters). Various EPR parameters, including the Zeeman effect, the HFCC and the number of nuclei with equivalent and non-equivalent, determine the intensity and position of the EPR peaks. These parameters influence the resonant magnetic field, leading to changes in the EPR peaks and disrupting the spectrum. Considering the abundance of the isotope in the modeling of the EPR spectrum also leads to a modification in the intensity of the peaks.

Results and Discussion

The Inductively Coupled Plasma was utilized to ascertain the chemical impurity of molybdenum trioxide. The results, which are displayed in Table 1, indicate that the quantities of zinc, nickel, iron, and copper atoms present as impurities are exceedingly minute. As a result, the chemical treatment that was executed is suitable. The enriched molybdenum 98 isotope underwent physical quality control using a Thermal Ionization Mass Spectrometer, with a standard sample derived from nature serving as the basis the results of which are shown in the graphs of Figure 3. The isotopic abundance percentage of ^{98}Mo and natural molybdenum sample (standard) is shown in Table 2.

Table 1. The results of the elemental analysis of the molybdenum trioxide

Elements	Mo	Zn	Ni	Co	Fe	Cu
Concentration (%)	97.44	0.102	Neg.*	0.019	2.14	Neg.*

*
The values that have been measured fall below the device's detection limit (negligible)

Table 2. Natural and enriched molybdenum isotopic abundance

Molybdenum isotopes	Isotopic abundance of ^{98}Mo (calculated %)	Isotopic abundance of natural molybdenum (calculated %)	Isotopic abundance of natural molybdenum based on the valid tables (%)
^{92}Mo	0.75	15.50	15.86
^{94}Mo	0.73	9.27	9.12
^{95}Mo	0.9	15.61	15.70
^{96}Mo	1.84	16.30	16.50
^{97}Mo	1.6	9.51	9.45
^{98}Mo	80.12	23.86	23.75
^{100}Mo	14.06	9.95	9.62

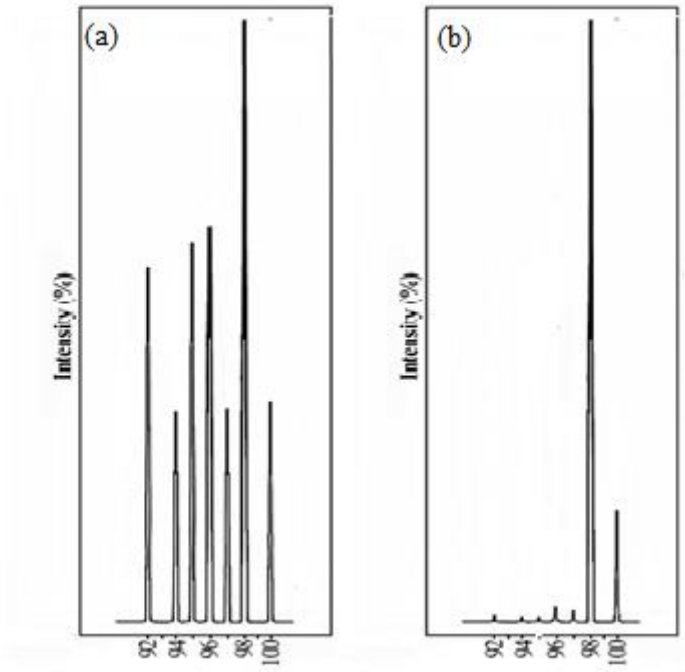

Fig. 3. Mass spectrum of (a) natural molybdenum(standard), (b) enriched molybdenum 98

As depicted in figures 4 Electron Paramagnetic Resonance was additionally employed to verify the quality of molybdenum 97 and 98 isotopes. As illustrated in the figures, distinct isotopes exhibit variations in the number, location, and intensity of peaks in the electron paramagnetic resonance spectrum, which can be attributed to their distinct microstructure constants. In regard to isotopes 97 and 98, we demonstrated that isotope 97 exhibits two peaks with the intensity of 0.8 and isotope 98 possesses a single peak with the intensity of 2. The contrasting positions of

the peaks can be attributed to the fact that the electron paramagnetic resonance parameters for the two isotopes of 97 are distinct 98. Also, it has been demonstrated that the paramagnetic resonance spectra of isotopes contain only one paramagnetic resonance peak for isotope 98, which has not HFCC, and two paramagnetic resonance peaks for isotope 97, which has HFCC with a nuclear spin of 1/2.

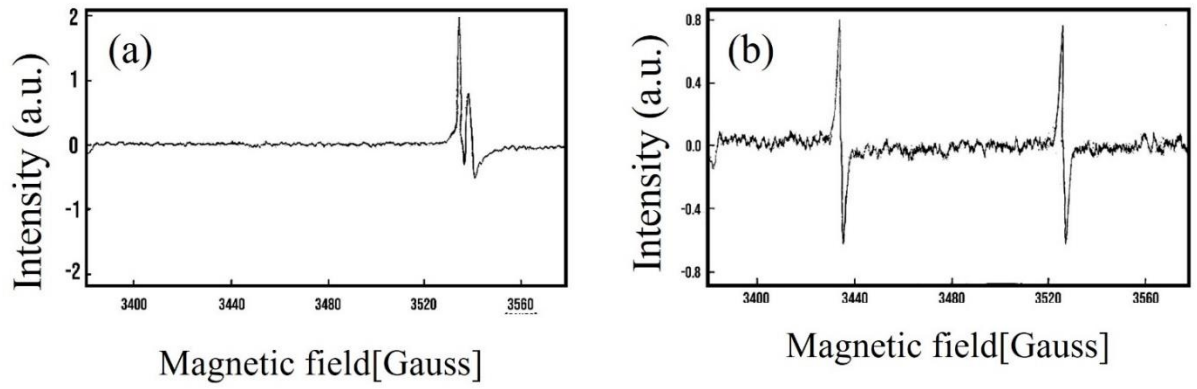

Fig. 4. Electron Paramagnetic Resonance (EPR) spectrum of (a) ^{98}Mo, (b) ^{97}Mo

Consequently, the quantity of isotopes 97 and 98 is negligible in two isotopes 98 and 97, respectively, and the lack of additional peaks originating from other molybdenum isotopes indicates that the existence of such isotopes is also negligible in these two isotopes. It is important to mention that the analysis and precise determination of isotopes in the paramagnetic resonance spectrum require additional molybdenum isotopes. This indicates that the existence of such isotopes within the aforementioned pair of isotopes is negligible.

Conclusions

Although produced in the range of grams and milligrams in quantity, electromagnetic separation of isotopes is a technique for enriching isotopes of elements with a high degree of isotopic purity. The present study achieved effective separation of molybdenum isotopes. It was demonstrated that the chemical purification procedure effectively separated atomic impurities that entered the solution during the isotope separation and mechanical scouring processes. Furthermore, isotopic quality control demonstrates that the electromagnetic procedure achieves an isotope separation of over 95%. The isotopic enrichment of the molybdenum 98 isotope by over 80% and its chemical purity by over 97% were verified. Furthermore, the novel Electron Paramagnetic Resonance method was employed to conduct quality control on the molybdenum 98 and 97

isotopes. The lack of more peaks originating from different molybdenum isotopes indicates that the existence of such isotopes is negligible for two isotopes of 97 and 98. In order to analyze and precisely determine isotopes in the paramagnetic resonance spectrum, quantum chemistry calculations are required. Currently, these calculations are in progress.

Acknowledgements

The financial support from Nuclear Science and Technology Research Institute and (NSTRI) Kashan University is gratefully acknowledged.

References

[1] Johnson, C. M., Beard, B. L., & Albarède, F. (Eds.) (2018). Geochemistry of non-traditional stable isotopes (Vol. 55). Walter de Gruyter GmbH & Co KG.

[2] Hasan, S. , & Prelas, M. A. (2020). Molybdenum-99 production pathways and the sorbents for ^{99}Mo/^{99m}Tc generator systems using (n, γ) 99Mo: a review. SN Applied Sciences, 2(11), 1782.

[3] Rathmann, S. M., Ahmad, Z., Slikboer, S., Bilton, H. A., Snider, D. P., & Valliant, J. F. (2019). The radiopharmaceutical chemistry of technetium-99m. Radiopharmaceutical chemistry, 311-333.

[4] Roessler, M. M., & Salvadori, E. (2018). Principles and applications of EPR spectroscopy in the chemical sciences. Chemical Society Reviews, 47(8), 2534-2553.

[5] Rech, A. B., Kinoshita, A., Donate, P. M., Nascimento, O. R., & Baffa, O. (2022). Electron spin resonance dosimetry studies of irradiated sulfite salts. Molecules, 27(20), 7047.

[6] Eaton, G. R. (2018). EPR imaging and in vivo EPR. S. S. Eaton, K. Ohno, & C. R. C. Press (Eds.). Boca Raton, FL: CRC press.

[7] Weaver, B. (1955). Chemical refinement procedures in the electromagnetic separation of isotopes (No. ORNL-1952). Oak Ridge National Lab. (ORNL), Oak Ridge, TN (United States).

[8] Cotton, F. A., Wilkinson, G. and Gaus, P. L. (1995). Basic inorganic chemistry. John Wiley & Sons.

[9] Vogel, A. (1996). Quantitative inorganic analysis, Longman 5th edition, 611.

[10] Anderson, N. J., Kolarik, L. O., Swinton, E. A. and Weiss, D. E. (1982). Colour and turbidity removal with reusable magnetic particles—III immobilized metal hydroxide gels. Water Research, 16(8), 1327-1334.

[11] Wu, D., Landsberger, S., Buchholz, B. A. and Vandegrift, G. F. (1994). Processing Of Leu Targets For Mo-99 Production--Testing And Modification Of The Cintichem Process. In 1995 International Meeting on Reduced Enrichment for Research and Test Reactor, paris. France sep (pp. 18-21).

[12] Weil, J. A., & Bolton, J. R. (2007). Electron paramagnetic resonance: elementary theory and practical applications. John Wiley & Sons.

ICNST 2024
International Conference on Nuclear Science and Technology
6- 8 MAY 2024 | Isfahan, Iran

Automating analysis on Windows environment with optimized software and hardware for thermal ionization mass spectrometry (MAT-260) (Paper ID : 1606)

Moeini M.[1*], Hosseini M.[2], Sayyad Jafari f.[2], Mohammadi S.[2]

[1]Nuclear of fuel cycle research School, Nuclear Science and Technology Research Institute, Tehran, Iran
[2]Ahmadi Roshan complex, Natanz, Iran

Abstract

Thermal Ionization Mass Spectrometry (TIMS) is an important tool for measuring the isotope ratio in the nuclear industry. This instrument can measure the isotope ratio in elements of the lanthanide and actinide groups. It is widely used in mineralogy and sedimentology studies of igneous and sedimentary rocks. This device at the Nuclear Science and Technology Research Institute has been optimized by upgrading the software and hardware to meet the isotope measurement needs of the nuclear industry. An attempt was made to upgrade the data collection system from manual to automatic using software, but the results were not satisfactory. To improve the system, the Advantech communication card was installed to automate the device in the data acquisition, processing, and magnet control section. The system was run using LabVIEW software. Additionally, the data processing software developed by the experts of Ahmadi Roshan complex was utilized. The device was adjusted and corrected to enable analysis using software and magnet control through the Hall effect sensor. As a result, the device detected the expected mass location of the peak of natural uranium isotopes, including 238U and 235U. TIMS was successfully optimized in terms of both software and hardware. This allowed the computer to receive data within the Windows operating system and apply the necessary settings to collect data optimally. Afterward, the computer performed isotope ratio measurement calculations.

Keywords: Thermal Ionization Mass Spectrometry, MAT-260, Automating Analysis, Isotope Ratio

Introduction

Mass and isotope analysis is done in different ways, including optical spectroscopy, mass spectrometry, and neutron activation. The mass spectrometry method is widely used due to the

accuracy of the results and analysis under controllable conditions. The results obtained from measuring the abundance of isotopes containing lanthanides and actinides are used in various sciences including nuclear, geology and agriculture.

Thermal Ionization Mass Spectrometer(TIMS-MAT260) of Nuclear Science and Technology Research Institute is used to measure isotope ratios of various environmental and laboratory samples. Due to its old age, this instrument has created limitations in its operation, which based on the planning carried out, its improvement and optimization in various departments, such as the automation of data acquisition units, data processing, and magnet control, have been considered. Is. In this device, isotopic measurement calculations were done manually, and fast data acquisition and processing and accurate and sensitive control were not applied simultaneously on the magnetic field. In modern devices, all software and hardware aspects, including user interfaces corresponding to automatic data collection, processing control, filament control, vacuum, and magnetic field control, are provided through a digital system, and calculations related to isotope ratio measurement also correspond to They are done with high accuracy and speed.

A limited number of practices can be found in various laboratories around the world, based on which TIMS instruments have been updated and upgraded to achieve better capabilities. Among these cases in 2008 was the upgrade of the software and high voltage part of a TIMS device in the Department of Earth Science, University of Bergen, Norway [1]. During another project in 2010, the development of a TIMS device in the electronics, control, and software department was done in Savanah River Nuclear Solutions in the state of Carolina, USA. In a part of the update report of this device, it is stated: "The ability to upgrade these valuable analytical tools and extend their useful life is a cost-effective option." [2]. In this regard, no instructions or other reports of such updating measures were found, which may be due to the importance and classification of information related to them.

In this article, the process of optimizing and automating the TIMS-MAT260 device under the new software in the Windows 7 operating system environment with the help of Advantech communication card using LabVIEW software is described. During this action, a computer with a processor: Core i5 2.8GHz was replaced by the previous computer. Also, to match the hardware infrastructure with the software, the new software was designed by the experts of Ahmadi

Roshan complex, which is suitable for analyzing U and Re elements. This software can manage the operation of data acquisition and control of the magnet and perform the necessary processing to perform the calculations. The Hall Effect sensor of the device was also repaired and the defect was fixed in this project.

Research Theories

The thermal ionization mass spectrometer MAT-260 consists of three main parts (Fig. 1) including: (i) ion source that can ionize the samples using the heat created on the rhenium filaments. (ii) Magnetic sector that allows the separation of isotopic rays and (iii) a very accurate and sensitive detection system consisting of a Faraday cup ion collector and a secondary electron multiplier (SEM) detector.

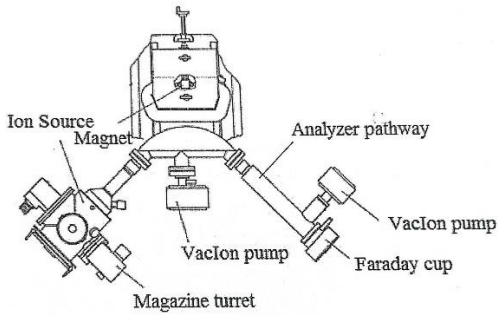

Fig. 1. The Scheme of MAT260

The samples were placed on a rhenium strip with a thickness of 0.04 mm, a width of 0.7 mm, and a purity of 99.98 as filaments that were welded on special bases as liquid drops with a concentration of 500 to 1000 ppm and by an electric current that It heats the filaments and dries them evenly. In the next step, the prepared bases are mounted on the sample magazine and placed inside the instrument. The target filament for analysis is placed in front of the ion source by the magazine turret and is ready for analysis.

The measurement of isotope ratio was done in a TIMS device in high vacuum, where a rotary pump, a turbo molecular pump, a cryo pump, and two VacIon pumps provide the necessary vacuum in this device. A high-voltage source with a voltage of 10 kV is used to accelerate the ions produced in the ion source. The magnetic field is adjusted to precisely separate the ion beams by the electromagnet in the range of one tesla. The measurement of isotope ratio in the

TIMS device is performed by calculating the ratio of mass to charge ($\frac{m}{z}$). The output signal of the Faraday cup is immediately amplified and de-noised by a pre-amplifier and amplifier unit and is observed and recorded on the output of the software as an isotope peak at the corresponding mass location.

Methodology

Due to the lack of automatic data collection and digital output, the TIMS-MAT260 device recorded the results on paper with a recorder, and its calculations were measured manually and also used manual potentiometers to adjust the magnetic field. These items are modified in the project and done automatically by the software.

To automate the analysis with the device and ease and increase the figures of merit related to the calculation of the isotope ratio, a new software (Fig. 2) was designed by the experts of Ahmadi Roshan complex in the LabVIEW software environment. This software established the connection between the device and the computer through an Advantech communication card.

The designed software has two parts:

a) The scan section where settings related to the start and end point of the scan in terms of mass (amu) can be made. Also, parameters such as scan speed (picking and collecting data), Gain (amplification factor of each signal), Reset (possibility of erasing the previous graph and performing a new scan) and Mass Adjust (possibility of determining the exact location of the peak according to the target mass) provides that the peak is placed on the mass and calibrated.) Another option designed in this section is Enable Repeat, which can repeat the analyzed range several times. This option is very suitable for checking the repeatability of peaks.

b) The analysis section, where it is possible to perform isotopic ratio calculations of two elements, uranium and rhenium, is designed. This section is being completed for other elements. The data related to the peak location from the scan section is entered in the tables of this section and by re-analyzing the necessary data for calculations, the exact location of the peak of each peak is collected. After collecting the necessary data, the information is transferred to the Analyze tables section, and calculations are performed based on comparison with the analyzed standard sample (single standard analysis) after performing the necessary calculations, the result

is reported by determining the relevant RSD. Also, in the Save Result section, all data can be output as an Excel file, and the generated file can be saved in the relevant folder after naming it.

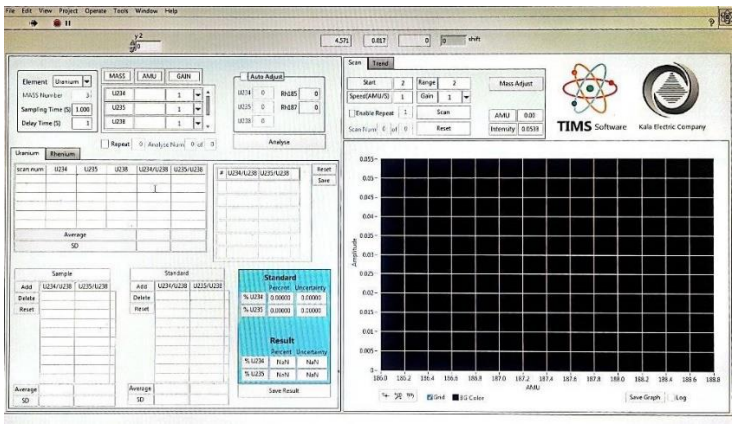

Fig. 2. The Scheme of software

Since the calibration steps and the completion of the calculation parts of the software are being completed, the output data cannot be presented in this article and will be presented in the next reports after the completion of the steps.

Conclusions

In this project, the automation operation of the TIMS-MAT260 device under the Windows 7 operating system was successfully performed. During this work, by adding an Advantech communication card, the device was connected to the computer, and a magnet card connection was also provided to the computer through an interface. The new software designed for scanning and analysis and fast and online calculations of isotope ratio was used and during an analysis of natural ^{238}U and ^{235}U, peaks were also observed. Determining the exact location of each peak as well as collecting data on the designated locations to perform analysis using a single standard method was successful in this work. In this project, additional upgarades are in progress and will be presented in the next reports.

Acknowledgments

In this project, the cooperation of the research and development department of the Ahmadi Roshan Complex is appreciated.

References

[1] https://www.uib.no/en/geo/111637/tims-laboratory

[2] Cordaro, J. V. , Johnson, S. R. , Holland, M. K. And Jones, V. D. (2010). Savannah River Nuclear Solutions, Aiken, South, Carolina 29808